Characterization of the Amyloidogenic Peptides Amylin & $PAP_{248-286}$

by

Kevin Hartman

A dissertation submitted in partial fulfillment
of the requirements for the degree of
Doctor of Philosophy
(Chemistry)
in the University of Michigan
2012

Doctoral Committee:

Professor Ayyalusamy Ramamoorthy, Chair
Professor Robert Kennedy
Professor Ari Gafni
Assistant Professor Mi Hee Lim

To my parents and family and friends who supported me through my entire education. To those who I have worked with, past and present who always inspired me to continue to pursue a career in science.

ACKNOWLEDGEMENTS

I would firstly like to thank my advisor and mentor, Ayyalusamy Ramamoorthy, who inspired me to excel in the laboratory and in the field of scientific research. His passion for science and his encouragement throughout graduate school has helped me a great deal as I have learned so much from his example, and who has always motivated me to do my very best. I would also like to thank my committee, Prof. Robert Kennedy, Prof Ari Gafni and Asst. Prof. Mi Hee Lim, for their guidance and direction in the preparation of my dissertation. Also to all the labs in which I have collaborated with on this work: The Kennedy Lab, The Gafni Lab, The Ono Lab, and The Chapman Lab.

I would also like to thank all those whom I have worked with in the Ramamoorthy lab during my time in graduate school, in particular Dr. Jeffery Brender, who continually helped me in the lab, and was always there with his expansive knowledge of amyloids. My fellow lab mate and cohort member Stephanie Le Clair who has been there through the good and bad times of research, and all of my friends and colleagues in the Rams lab, Rui Huang, Wencheng Ge, Yuki Abe, Dr. Pieter Smith, Dr. Ravi Nanga, Dr. Jaidi Xu, Dr. Ronald Soong, Dr. Shivani Ahuja, Dr. Nataliya Popovych, Dr. Kazutoshi Yamamoto, Dr. Michele Sciacca, Dr. Vivekanandan Subramanian, Dr. Nicole Jahr, Dr. Janarthanan Krishnamoorthy, Dr. Neil MacKinnon, Dr. Kamal Mroue, Dr. Manoj Pandey, Dr. Bagganahalli Somashekar, Dr. Pratima Tripathi and Dr. Dong-kuk Lee. I would also like to thank all of the undergraduates who I have worked with, Jeff Barry, Michelle Fritz, Dan Youngstrom, Samer Salamekh, Austin McHenry, Melissa

Gildenberg, Sharonne Temple, Jenn Chen, and Anna Jones. All those I have worked with in the lab have been amazing researchers and amazing friends.

I would also like to specially thank Dr. Nancy Kerner whom I worked with as both a graduate student instructor and as a graduate student mentor. I learned so much from her passionate teaching and in working with her; I was able to hone my teaching skills and continue to do something that I find enjoyment in, which is teaching others. I would also like to thank all of the staff associated with the general chemistry lab course Chem 125/126, over the years as we went through the craziness of teaching over a thousand students each fall semester.

I want to thank everyone in my 2007 cohort. We have been together since the beginning, regardless of where in the country we actually were. To all of my friends in the department, especially those who enjoyed coming tailgating before the home football games. Those are the times that I feel I will miss the most after graduate school. Everyone has helped me grow and learn throughout my time here at the University of Michigan, and I wouldn't trade this experience for anything.

I would finally also like to thank those who worked with prior to entering into graduate school, my friends from Saginaw Valley State University and the chemistry club, and my undergraduate research advisor, Dr. David Karpovich. Also I want to thank my fellow employees at The Dow Chemical Company in Building 1897. Tom and Marabeth Hofelich, Tim Elwell, Amy Tesolin-Gee, Dave Frurip, Karen Griffin, Andy Pazstor and everyone who worked with me in my first lab and research setting and who inspired me to start my graduate school career and to continue to pursue chemistry and science as a whole.

TABLE OF CONTENTS

LIST OF FIGURES

LIST OF ABBREVIATIONS

Aβ – Amyloid β

AIDS – Acquired Immune Deficiency Syndrome

ATR-FTIR – Attenuated Total Reflectance Fourier Transform Infrared Spectroscopy

CD – Circular Dichroism

CSI – Chemical Shift Index

DiPOPE – Dipalmitoyl-2-oleoyl-sn-glycero-3-phosphoethanolamine

DMPC – 1,2-dimyristoyl-sn-glycerol-3-phosphocholine

DMPG – 1,2-dimyristoyl-sn-glycero-3-phospho-(1'rac-glycerol)

DMSO - Dimethylsulfoxide

DPC – n-dodecylphosphocholine

DOPC – 1,2-dioleoyl-sn-glycero-3-phosphocholine

DOPG – 1,2-dioleoyl-sn-glycero-3-[phosphor-rac-(1-glycerol)]

DSC – Differential Scanning Calorimetry

EDTA – Ethlyenediaminetetraacetic Acid

EGCG – Epigallochatechin-3-gallate

FRET – Fluorescence Resonance Energy Transfer

GC - Gallochatechin

GFP – Green Fluorescent Protein

HFIP – Hexafluoroisopropanol

HIV – Human Immunodeficiency Virus

hIAPP – human Islet Amyloid Polypeptide

HPLC – High Pressure Liquid Chromatography

HSQC – Heteronuclear Single Quantum Correlation Spectroscopy

IAPP – Islet Amyloid Polypeptide (Amylin)

LUV – Large Unilamilar Vesicles

MALDI-MS – Matrix Assisted Laser Desorption Ionization Mass Spectrometry

NMR – Nuclear Magnetic Resonance

NOE – Nuclear Overhauser Effect

NOESY – Nuclear Overhauser Effect Spectroscopy

PAP – Prostatic Acid Phosphatase

POPC 1-palmitoyl-2-oleoyl-sn-glycero-3-phosphocholine

POPE – 1-palmitoyl-2-oleoyl-sn-glycero-3-phosphoethanolamine

POPG – 1-palmitoyl-2-sn-glycero-3-phospho-(1'-rac-glycerol)

POPS – 1-palmitoyl-2-oleoyl-sn-glycero-3-phospho-L-serine

rIAPP – rat Islet Amyloid Polypeptide

SDS – Sodium Dodecyl Sulfate

SEVI – Semen-derived Enhancer of Viral Infection

SUV – Small Unilamilar Vesicles

TEM – Transmission Electron Microscopy

TFA – Trifluoroacetic Acid

TFE – Trifluoroethanol

ThT – Thioflavin T

TOCSY – Total Correlation Spectroscopy

ABSTRACT

CHARACTERIZATION OF THE AMYLOIDOGENIC PEPTIDES AMYLIN AND $PAP_{248-286}$

by

Kevin Hartman

Chair: Ayyalusamy Ramamoorthy

Many diseases in the aging population are associated with a class of peptide that aggregates to form amyloidogenic fibers through a misfolding from random coil, to cross β-sheet fibrils. Diseases such as Alzheimer's disease, Parkinson's disease, type II diabetes, and transmission of viral infection are shown to be linked to different amyloidogenic peptides. In two different projects within the amyloid field, we have chosen to study or amylin, in relation to type II diabetes, as well as a fragment of prostatic acid phosphatase (PAP248-286) whose fibrils have been termed a semen-derived enhancer of viral infection (SEVI).

In relation to the amylin peptide, different aspects of the physiological storage conditions were probed. High concentrations of the peptide have proven very disruptive

to membranes and very prone to aggregation *in vitro*, however in the secretory granule it is stored in mM concentrations. The three unique conditions to the granule are the relatively low pH (~6.0) and very high zinc (~14mM) and insulin (~4x amylin) concentrations. Here it is seen that separately, all three of these variables cause decreased membrane disruptive ability of amylin, and decreased ability to aggregate into amyloid fibers. Disruption of this environment such as lowered zinc concentrations could facilitate amylin's membrane disruptive ability and further the progression of type II diabetes.

We also characterized the relatively unstudied PAP248-286 peptide also an amyloid, and its interaction with model membrane systems to show that the peptide itself causes lipid aggregation and induces vesicle fusion, as would be the case for a peptide which facilitates the transmission of a virus. Yet while the monomeric shows fusiogenic activity, only the fibrillar form enhances viral transmission. The formation of these fibers is then critical to viral transmission. We see that the green tea compound EGCG can be used to both inhibit and disaggregate the amyloid fibers of SEVI due to its polyphenolic nature, while preformed fibrils of the *E. coli* produced curlin protein are seen to enhance the formation of SEVI. Cofactors such as the SEVI fibers could explain why HIV is weak *in vitro*, yet AIDS continues to be a global pandemic.

CHAPTER 1

INTRODUCTION TO AMYLOIDS AND THE ISLET AMYLOID POLYPEPTIDE AND PROSTATIC ACID PHOSPHOTASE PEPTIDES

1.1 Amyloid Peptides

As a result of better healthcare and better standards of living throughout the globe, the average life span of a person has been extended greatly over the last century *(1)*. As a result of this, there are a number of aging related diseases that are now becoming more prevalent that were relatively rare before. These aging diseases have proven to be very closely associated with amyloidogenic peptides. Alzheimer's disease, Type II diabetes, Parkinson's disease, Huntington's disease, Creutzfeldt-Jakob disease, and even the enhancement of viral transmission are all linked by being related to amyloidogenic peptides *(2-7)*.

An amyloidogenic protein is any peptide or protein that undergoes a misfolding to the tertiary structure of a cross-β-sheet fiber *(8, 9)*. The peptides generally appear as random coil in solution and undergo a misfolding process where the secondary structure is changed into an α-helical intermediate prior to a conformational change into a β-sheet structure, which aggregates to form elongated fibers as can be seen in the schematic in Figure 1.1. The diseases associated with amyloid proteins have been difficult to understand, as the triggering of this misfolding is different for each disease and each

protein and in most cases, is generally believed to be caused through hydrophobic interactions within the peptide. A number of things are known to alter the kinetics of amyloid fiber formation, fluorinated solvents, fluorine labeling, metals, cellular and model membranes, surface type, and air/water interfaces *(10-16)* many times through initiating or triggering the formation of a thermodynamically unfavorable nucleus.

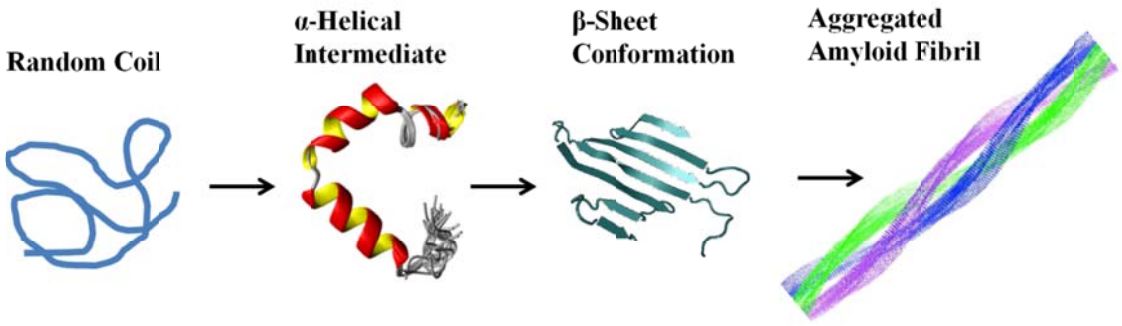

Figure 1.1 The general formation of an amyloid fiber. The majority of amyloid peptides begin as a random coil conformation in solution, after which they undergo conformational change to an α-helix before aggregating into a cross β-sheet amyloid fibril

The process of amyloid formation can generally be separated into two distinct times, the induction time, and the elongation time, and generally follows a sigmoidal growth curve as seen in Figure 1.2. The formation of the nucleus by which fiber formation is triggered is the rate limiting step of fiber formation. The monomeric peptide slowly aggregates into this unfavorable nucleus, and after with there is a very fast elongation of the fibers, as monomer subunits are continually attached to the growing fiber. Many times, the stabilization of an intermediate can either inhibit or enhance the formation of amyloid fibers, depending on the extent of stabilization. Fluorinated solvents are known to stabilize the α-helical intermediate of amyloid peptides *(12)*. In

small concentrations, these fluorinated solvents can push the peptide into its unfavorable intermediate thus beginning the process of fiber formation faster, yet with a larger concentration of solvent, the α-helical intermediate is completely stabilized and unable to continue into an amyloid fiber. In other cases such as with metals, while the intermediate is stabilized and fiber formation beginning at an earlier time point, fiber formation is inhibited as there is now a greater barrier to monomer addition with the intermediate being more stable *(13-16)*.

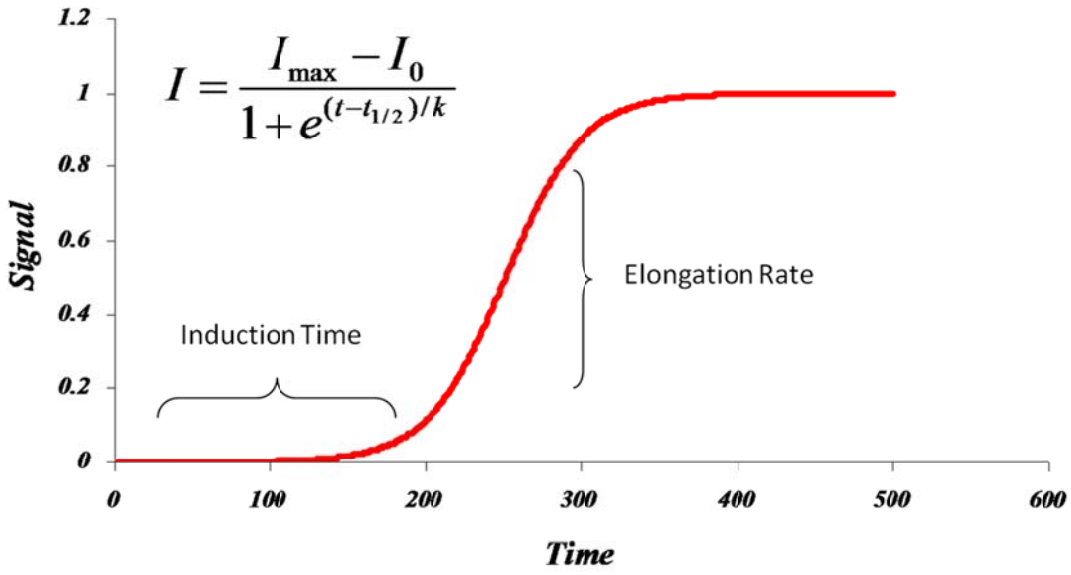

Figure 1.2 Standard sigmoidal growth curve for the formation of amyloid fibers. After an initial induction time period and the formation of a nucleus, the growth of the fibers is given by an elongation rate where monomers are added to the nucleus.

Membrane systems are also seen to alter the kinetics of amyloid formation, when binding to a cellular or model membrane surface, many amyloids will adopt an α-helical structure, which is a key conformation on the way to amyloid formation *(17, 18)*. While this is an enhancement in the first step of amyloid formation and initiate fiber formation in some peptides *(19-21),* the overall stability of this α-helix may be enhanced and therefore the continuation of the fiber formation process may be inhibited in other peptides. In addition to changes in on the peptide induced by membranes, there is a large amount of research being done on the changes in membranes induced by peptide.

1.2 Model Membrane Systems

In addition to studying the kinetics of amyloid formation, there is also a great deal of interest in their interaction with cellular and model membrane systems. Amyloid peptides have been shown to be cytotoxic and be disruptive to model membrane systems *(18, 21-26),* as well as be implicated in facilitating membrane fusion *(26)* and changing the overall curvature of the membrane itself. The effects on the two systems (peptide and membrane) that are of particular focus in this thesis are highlighted in Figure 1.3.

The direction of much membrane research in relation to their interaction with peptides, specifically amyloid peptides, is looking at the role of different lipid compositions on binding and interaction with the peptides. Electrostatic interactions are known to play a major role in peptide interaction, where a cationic peptide will preferentially bind and interact with anionic membranes *(19, 21).* In addition to specific lipid components, there is also research being performed on lipid raft systems, or

membranes that have two separate distinct phases being a liquid-ordered phase and a liquid-disordered phase coexisting *(27-29)*. Mimicing physiological membranes exactly in model systems proves very difficult, as there a number of different components comprising a cellular membrane, however these model membranes give a good approximation of what could be happening in the peptide's natural environment.

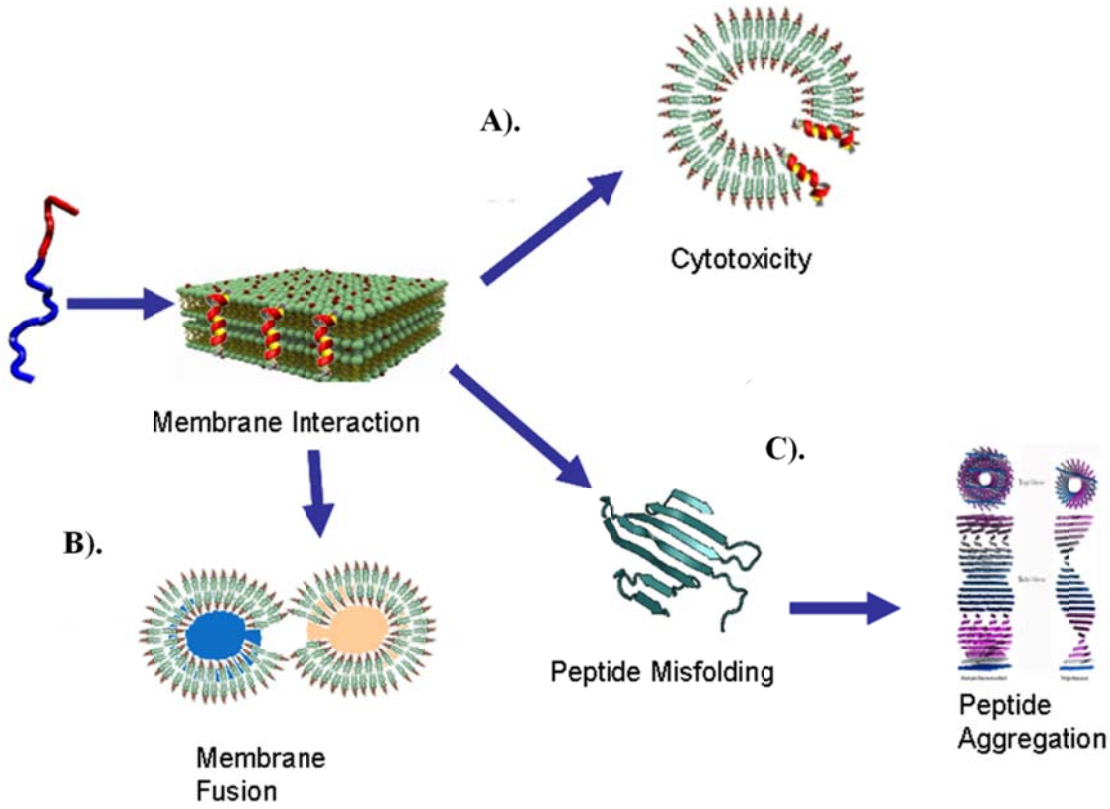

Figure 1.3 The interaction of amyloid peptides with membrane systems. These interactions can induce a number of changes on both the peptide and the membrane environment including (A) Membrane Disruption, (B) Membrane Fusion, and (C) Peptide aggregation.

These interactions, mostly on model membrane systems, are a primary focus of this research, in addition to studying the amyloid growth kinetics. The two particular peptides to be focused on are Islet Amyloid Polypeptide which is a peptide known to

enhance the effects of type II diabetes, and a fragment of Prostatic Acid Phosphatase, residues 248-286, which in its fiber form has been see to enhance the infectivity of HIV and other viruses.

1.3 Islet Amyloid Polypeptide and Type II Diabetes

Islet amyloid polypeptide (IAPP) or Amylin is a 37 residue peptide which is co-secreted with insulin, and stored in the secretory granules of the islets of Langerhans in the β-cells of the pancreas *(30, 31).* The primary physiological function of the amylin peptide is related to glucose regulation and appetite suppression both directly and indirectly by aiding in the control of gastric emptying *(32-34).* It is also an amyloidogenic peptide which undergoes misfolding from a monomeric random coil conformation, to an aggregated β-sheet amyloid fiber. These fibrous deposits are heavily found post-mortem in patients suffering from Type II Diabetes *(35-37).* It is because of these findings, that the aggregated fiber form was studied heavily in the past.

Type II Diabetes or Diabetes mellitus, is adult onset diabetes, a disease that effects approximately 20.8 million people in the United States as of 2005 *(38).* With the average age of the population increasing, and as a result of changing dietary patterns, the number of new cases of type II diabetes has significantly increased in recent years. Complications associated with type II diabetes include heart disease, stroke, high blood pressure, blindness and kidney diseases *(38).* With such a large number of associated complications and a large portion of the population suffering from the disease, the estimated medical cost was approximately $92 billion in 2002 *(38)* and would be greater

today. With the rising costs of treatment of type II diabetes and its complications, there is continually increasing attention being drawn to understanding the disease and with that, increased attention and study of amylin.

The effects of amylin on the progression of type II diabetes is in the membrane disruptive and cytotoxic effect the peptide has on the membranes of the β-cells. Amylin is stored in the β-cells of the pancreas at high concentrations (mM range) along with insulin at an approximate 1:4 ratio. Under normal circumstances, the two proteins are co-secreted with no negative effects on the cellular membrane, however in those patients with type II diabetes, the amylin being released disrupts the membranes of the β-cells, thus killing the cells. With the destruction of β-cells, insulin production is inhibited and the remaining cells must release more insulin to account for the loss, however this also releases additional amylin, and so the overall effect is a spiraling scenario where amylin destroys the insulin producing β-cells, causing remaining cells to release more insulin (and amylin) which in turn destroys more cells worsening and progressing type II diabetes.

Figure 1.4 The sequence of the Amylin peptide. The peptide is amidated and a disulfide bridge occurs between C2 and C7 under physiological conditions. The membrane binding region (residues 1-19) is highlighted in blue, and the primary amyloidogenic region (residues 20-29) is highlighted in red.

Initial studies of amylin focused on the fibers themselves and their formation, as >95% of those patients with type II diabetes were found to have large amyloid plaques deposited in the pancreas *(39)*. Through these early studies it was determined that the more amyloidogenic prone region of the peptide is residues 20-29 *(13-44)* shown in Figure 1.4. It was determined by Fourier transform infrared spectroscopy, that these fibers have an anti-parallel β-sheet structure *(45)*. While this region of amylin is the most prone to amyloid formation, it is not the only fragment susceptible to amyloid aggregation *(46-51)*. Studies looking at inhibitory effects of small molecules and peptide fragments were done in order to possibly prevent the peptide from undergoing aggregation to stop the formation of these amyloid fibers *(52-56)*.

It was then determined that the fibers themselves are in fact non-toxic and non-membrane disruptive, and that smaller intermediate species were described as being toxic to cellular membranes *(22)*. It was found that amylin species of approximately 25-6000 subunits were responsible for the toxicity to cells, and that the mature fibers displayed little if any cytotoxic effect *(22)*. This result was further supported by work with protofibrils, which showed pore-like disruption of model membrane systems *(23,57)* as well as other studies that confirmed the fact that the fully formed amyloid fibers were not targeting the β-cells and progressing type II diabetes, but that the smaller oligomeric aggregates of amylin were causative agent in β-cell death *(58-61)*. The focus of the field was then shifted from studying the fully formed fibers, to the monomeric and oligomeric forms of the peptide as well as the kinetic pathways of fiber formation.

Studies looking at specific fragments of the peptide were also being conducted, to determine which species would be most detrimental to membrane disruption and

cytotoxicity, as well as which residues were responsible for this. Initial studies one amylin using DOPC/DOPG model membrane systems, show interaction with the N-terminal of the peptide which seemed to form pre-amyloid conformations in contrast to the C-terminal which displayed little activity *(19)*. This had then prompted work to be done on specifically the N-terminal fragment of the peptide, residues 1-19 (Figure 1.4). Work on the N-terminal fragment showed substantial interaction with the membrane as a monomer, where the monomeric form of residues 20-29, the main fiber formation fragment, showed little interaction *(62)*. The pre-fibrillar states were determine by circular dichroism spectroscopy to be α-helical in structure *(21),* after which a number of studies confirmed the transition from random coil to membrane bound α-helical intermediate for both the full length peptide, and the N-terminal 1-19 fragment *(18, 20, 63).* In particular, studies with the membrane binding fragment of amylin, residues 1-19, concluded that this region of the peptide is capable of causing membrane disruption to POPG model membrane systems, where the primary region necessary for amyloid formation, residues 20-29, does not *(18).* What is particularly interesting about this is that it was shown that not only are membrane disruption and fiber formation a result of two separate regions in the amylin sequence, but that amyloid formation is not needed for the peptide to maintain its membrane disruptive ability *(18).*

While the formation of amyloid fibers is not needed to cause the disruption of model membrane systems, the peptide displays a bi-phasic disruption, where there is initial disruption to membrane systems without the formation of amyloid fibers, and there is then continued disruption which corresponds to amyloid fiber growth *(64)*. Therefore it would be advantageous to study both fiber growth of the peptide as well as its inherent

membrane disruptive ability. Determining what factors present in the body are able to inhibit both of these abilities of the amylin peptide under normal circumstances would be of critical importance, and seeing how these factors change with the onset of type II diabetes would greatly increase the understanding of the progression of the disease.

The physiological area this thesis focuses on is the secretory granule located in the β-cells of the Islets of Langerhans in the pancreas, where the amylin is stored prior to the granule being exocytosed and its contents released into the body. The amylin concentration within the granule *in vivo* is very high in the mM range. These concentrations *in vitro* are known to be highly prone to fiber formation and membrane disruption, so the other compounds within the granule must be preventing the amylin from utilizing these abilities. The three different factors located in the granule that were looked at individually were the low pH of the granule (~pH 6.0), the high concentration of zinc present (~14mM) *(65, 66)*, and the high concentration of insulin (~4x amylin concentration) *(67-69)*. By observing how each factor affects the amylin peptide individually, and monitoring them as a function of type II diabetes progression, one could identify the primary cause of amylin's misfolding and the initiation of its membrane disruptive ability.

In the secretory granule, the acidic conditions prove to be very effective and the inhibition of both the growth of amylin fibers *(47, 71)* and the peptide's membrane disruptive ability *(72, 73)*. The pH can play a very important role in how amyloid peptides fibrillize and interact with membrane systems. While a low pH will inhibit amylin fiber formation, it is able to initiate fiber growth for other amyloidogenic peptides such as amyloid-β *(74-78)*. Here it is determined that a single point mutation H18R can

inhibit the peptides ability to disrupt membrane systems by adopting a different binding orientation *(72, 73)*. The primary cause of this would be electrostatic interactions and charge-charge repulsions. With a lower pH which causes protonation of His-18 the charge distribution is the same as with the mutation, and is seen to also inhibit the disruption and change binding orientations *(71, 72)*.

In addition to the acidic environment of the secretory granule, the very high zinc concentration of ~14mM would also play a role in the fiber formation and membrane disruptive ability of the amylin peptide. Zinc is known to affect fiber growth and membrane interaction with other amyloid peptides in different ways. Specifically with amyloid β, zinc is known to enhance the kinetics, and initiating the growth of amyloid fibers *(78-81)*, yet as shown with the amylin peptide, the presence of zinc inhibits the formation of these fibers and slows their kinetic formation *(82)*. Other metals are also known to play roles in the enhancement or inhibition of amyloid fiber formation, where copper specifically has been shown to inhibit the kinetics of both amylin and amyloid-β *(78, 82-86)*. With the secretory granule containing the highest localized physiological concentration of zinc, its interaction with amylin and its ability to inhibit both fibrillization and membrane disruption would prove critical in future research relating the amylin peptide and the progression of type II diabetes.

Along with a very high concentration of zinc, the secretory granule also contains very high concentrations of insulin. The amylin and insulin are co-secreted during the exocytosis of the granule and therefore are both in high concentrations, with insulin at approximately 4x the concentration of amylin. The insulin in the granule is shown to complex with amylin *(87-89)* as well as inhibit the growth of amyloid fibers *(68, 69, 88-*

94). Because of this, it is also generally thought to inhibit the membrane disruptive ability of amylin *(68, 87, 91)*. Here it is shown that while the insulin can slightly inhibit the formation of amyloid fibers associated with amylin, the membrane disruptive pattern of amylin is biphasic, and the presence of insulin only suppresses the secondary disruptive phase associated with fiber growth *(64)*. The initial membrane disruptive characteristic of the amylin peptide is still present, prior to the formation of the amyloid fibers *(64)*.

These three specific conditions within the granule each play a role in the inhibition and suppression of fiber growth and membrane disruption associated with the amylin peptide. While there are a number of other factors present within the secretory granule, the three are the most pronounced with the highest concentrations, and would therefore serve a more prominent purpose. The conditions within the granule are able to prevent the amylin contained within, from fibrillizing and causing disruption during exocytosis, indicating that changes related to these conditions could lead to the fibrillization and membrane disruption by amylin, killing the insulin producing β-cells, and progressing type II diabetes.

1.4 Prostatic Acid Phosphatase and HIV Transmission

Auto-immune deficiency syndrome (AIDS) is a global pandemic caused by the transmission of the human immune-deficiency virus (HIV). AIDS currently affects approximately 0.6% of the entire world population *(95)* and in 2008 claimed between 1.7 and 2.4 million lives, many of which were children *(96)*. While AIDS and HIV transmission is a global pandemic, the virus itself is actually relatively weak *in vitro*, with

only ~0.1% of virus particles able to infect host cells *(97, 98)*. Many studies have determined that attachment to the membrane of the host cell is the limiting factor in cell-virus fusion and infection *(99-101)*. The typical life cycle of HIV infection is shown in Figure 1.5 where step 2 is presumed to be the limiting step, of virus attachment to the cellular membrane, prior to membrane fusion, transcription and replication of the virus. With the very low efficiency of HIV *in vitro*, it surprising that it is such a global pandemic *in vivo*.

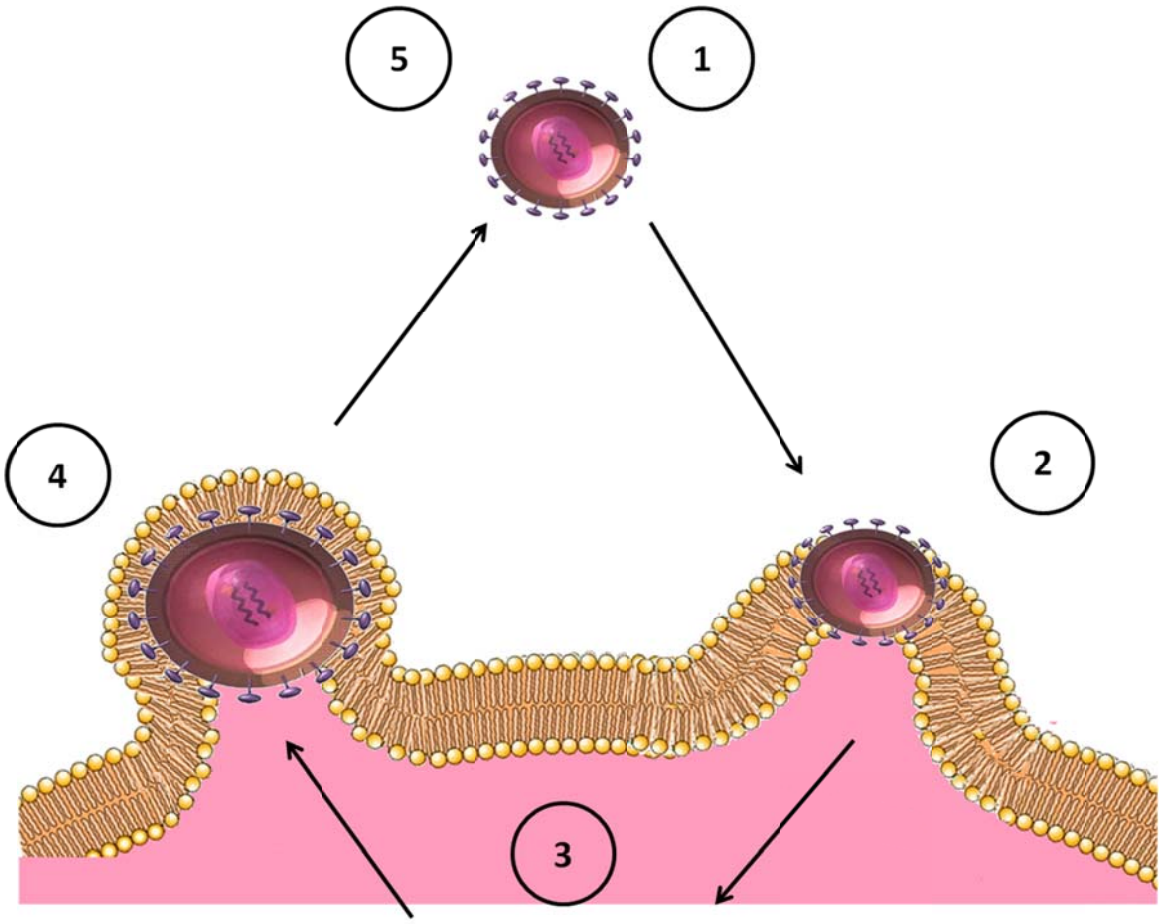

Figure 1.5 The life cycle of HIV infection. The mature virus (1) is attracted to and binds to the membrane of the host cell, and fusion occurs (2). Transcription and replication of the viral RNA occurs in the nucleus of the host cell (3) and newly formed virons bud from the host cell membrane (4) and are released to become a mature virus (5) capable of infection of other host cells.

It is very possible that there are certain cofactors present at the time of HIV infection that enable the virus particle to overcome these cell membrane attachment limitations, and cause the virus to be much more infectious. One of these cofactors was recently discovered by Munch et. al. as being present in human semen *(7)*. Semen was screened for small compounds which could be possible cofactors, as it is the main vector for transmission of HIV. A fragment of Prostatic Acid Phosphatase (PAP), residues 248-286, (shown in Figure 1.6) was found to be a very potent enhancer of HIV infectivity when in its aggregated amyloid fiber form *(7)*. These $PAP_{248-286}$ fibers, termed SEVI (semen-derived enhancer of viral infection), were seen to cause significant increase in HIV infectivity across a range of HIV strains *(7)*. It is unclear how the fragment is actually cleaved from the original PAP protein, however it is believed to be due to lysosyme. With such little known about the structure and function of this peptide fragment, characterizing its membrane interaction and fibril formation kinetics would be key to determining how this enhances HIV infection, and what measures can be taken to eliminate these effects.

Figure 1.6 The sequence of $PAP_{248-286}$, which aggregates to form SEVI amyloid fibers. The large positive charge of the peptide is indicated at K4, K6, K8, R10, K25, R26, K34, & K35.

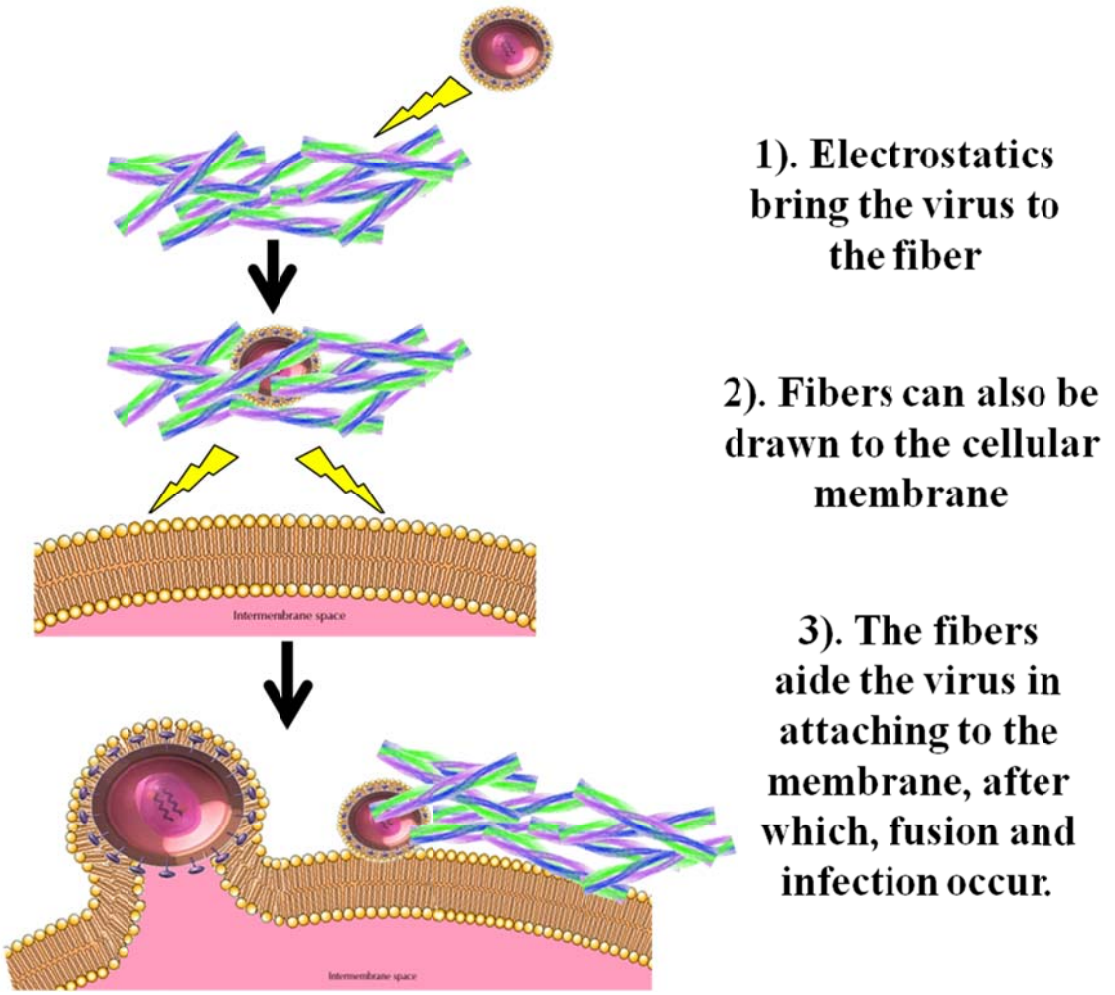

Figure 1.7 The proposed model of how the SEVI fibers enhance the infectivity of HIV and other viruses. Electrostatics play a dominant role in the aggregation of membranes as mediated by the SEVI fibers.

It is well established that only the fiber form of $PAP_{248-286}$ is responsible for increasing the infection of HIV as well as other viruses *(102, 103)*, while the monomeric form of the peptide shows little enhancing ability. Understanding what triggers the formation of these fibers and what factors present in human semen and in the body could inhibit the aggregation of $PAP_{248-286}$ would give light as to why these fibers form in vivo. With the formed fibers, their interaction with membranes of both the host cells and the

viral envelope of HIV has been proposed to be largely electrostatic. There are a number of positively charged residues along the entire $PAP_{248-286}$ sequence (Figure 1.6), and many of the binding areas on host cells and viral envelopes are anionic *(104),* indicating electrostatic attraction between the two. The proposed model for how the SEVI fibers interact with the two membranes and eliminate or reduce the electrostatic repulsion between the two anionic membranes is shown in Figure 1.7, where the cationic fibers are able to bind both viral envelope and host cellular membrane and allow the fusion of the virus to take place.

Here this thesis focuses on the membrane interactions of the $PAP_{248-286}$ monomeric peptide to characterize how pre-fibrillar forms of the peptide interact with the model membrane systems, as well as determining the growth kinetics of the fibrillar form. Amyloid growth kinetics are very sensitive to their surrounding environments and the presence of any additional molecules or surfaces for which to nucleate off of. By studying the impact of fiber inhibitors, as well as what compounds or surfaces are seen to initiate the growth of these SEVI fibers, more specific treatments to prevent further infection of HIV can be developed by inhibiting the ability of SEVI fibers to enhance the infectivity of HIV and cap the ever growing problem of the AIDS pandemic.

The $PAP_{248-286}$ peptide, like other amyloid peptides, is seen to interact extensively with model membrane systems. Unlike other amyloids such as amyloid β and IAPP, which adopt a very prominent α-helical structure upon membrane binding *(72, 105-107)* the $PAP_{248-286}$ remains largely unstructured with only small helices present *(108)*. Like other amyloid peptides, the $PAP_{248-286}$ peptide is also shown to be disruptive to model membrane systems *(26)*. Yet unlike other amyloidogenic peptides, the large positive

charge distribution on the PAP248-186 peptide causes a great deal of vesicle aggregation and is indicated to be involved in the fusion of model membranes *(26)*. This fusion enhancement and lipid aggregative ability could play a key role in a synergistic relationship between the gp41 fusion protein located on the membrane of the HIV viral envelope and could be a reason why the HIV enhancement in the presence of the SEVI fibers is possible.

With the SEVI fibers being the cause of the primary enhancement of HIV and other viruses *(102, 103)*, their inhibition would be critical to lessen their effect on the enhancement of HIV transmission. The polyphenolic compound epigallocatechin-3-gallate (EGCG) found in green tea extract, has proven a very effective inhibitor to amyloid aggregation. Studies with $PAP_{248-286}$ as well as amyloid-β and IAPP have shown that EGCG can both inhibit the formation of amyloid fibers when incubated with the monomeric peptide *(109-112)*, as well as having the ability to disaggregate the fibers themselves causing the formation of an off pathway oligomer which is non-disruptive to membrane systems *(113)*. Here it is shown that while initially thought to be a general binding to the amyloidogenic peptides that caused fiber inhibition, the EGCG is relatively residue specific, and that the lysine residues in $PAP_{248-286}$ play a great role in the binding of EGCG and the formation of amyloid fibers.

While the inhibition of SEVI fibers is a preventative treatment for HIV transmission enhancement, there is also the question of what possible factors initiate the growth of these SEVI fibers *in vivo*. The $PAP_{248-286}$ peptide has proven relatively stable, and requires somewhat harsh conditions to generate the SEVI amyloid fibers *in vitro*. High peptide concentration, elevated temperature and rigorous agitation are required for

the $PAP_{248-286}$ to fibrillize into amyloid fibers *(114)*. This is different than other amyloid peptides such as amyloid-β and IAPP which readily fibrillize *in vitro* with minimal concentration, little to no agitation and room temperature conditions. Here the bacterial curli amyloid protein fibers are studied in relation to $PAP_{248-286}$ in order to study and monitor the kinetics of fiber growth as well as the initiated fibers relative enhancement on HIV transmission.

The SEVI amyloid fibers and of their precursor peptide, $PAP_{248-286}$ are becoming increasingly studied. Their interaction with membrane systems and their potential initiation of membrane fusion would prove very helpful in determining exactly how the SEVI fibers are able to cause infection enhancement of HIV and other viruses. Also, by determining what is causing the $PAP_{248-286}$ to aggregate in vivo to generate the active SEVI fibers and what can be used to inhibit this fiber growth are sure to play a key role in the future directions of the study of this peptide.

1.5 Bibliography

1. Bunker J.P., Frazier H.S., and Mosteller F., (1994) Improving health: measuring effects of medical care. *Milbank Quarterly 72,* 225-58.

2. Hensley, K., Carney, J.M., Mattson, M.P., Aksenova, M., Harris, M., Wu J.F., Floyd, R.A., and Butterfield, D.A. (1994) A model for β-amyloid aggregation and neurotoxicity based on free radical generation by the peptide: relevance to Alzheimer disease. *Proceedings of the National Academy of Sciences. 91*, 3270-3274.

3. Mirzabekov, T.A., Lin, M.C., and Kagan, B.L. (1996) Pore formation by the cytotoxic islet amyloid peptide amylin. *Journal of Biological Chemistry 271*, 1988-1992.

4. Tabner, B.J., Turnbull, S., El-Agnaf, O., and Allsop, D. (2001) Production of reactive oxygen species from aggregating proteins implicated in Alzheimer‟s disease, Parkinson‟s disease and other neurodegenrative diseases. *Current Topics in Medical Chemistry 1*, 507-517.

5. Rubinsztein, D., and Carmichael, J. (2003) Huntington‟s disease: molecular basis of neurodegeneration. *Expert Reviews in Molecular Medicine 5*, 1-21.

6. Dobson, C.M. (2001) The structural basis of protein folding and its links with human disease. *Philisophical Transactions of the Royal Society B: Biological Sciences 356*, 133-145.

7. Munch, J., Rucker, E., Standker, L., Adermann, K., Goffinet, C., Schindler, M., Wildum, S., Chinnadurai, R., Rajan, D., Specht, A., Gimenez-Gallego, G., Sanchez, P.C., Fowler, D.M., Koulov, A., Kelly, J.W., Mothes, W., Grivel, J.C., Margolis, L., Keppler, O.T., Forssmann, W.G., and Kirchhoff, F. (2007) Semen-derived amyloid fibrils drastically enhance HIV infection. *Cell 131*, 1059-1071.

8. Soto, C., Castano, E.M., Frangione, B., and Inestrosa, N.C. (1995) The alpha-helical to beta-strand transition in the amino terminal fragment of the amyloid beta peptide modulates amyloid formation. *Journal of Biological Chemistry* 270, 3063–3067

9. Soto, C., and Castano, E.M. (1996) The conformation of Alzheimer's beta peptide determines the rate of amyloid formation and its resistance to proteolysis. *Biochemical Journal* 314, 701–707.

10. Kerth, A., Erbe, A., Dathe, M., and Blume, A., (2004) Infrared Reflection Absorption Spectroscopy of Amphipathic Model Peptides at the Air/Water Interface, *Biophysical Journal 86,* 3750-3658.

11. Zhao, H., Tuominen, E.K.J., and Kinmunen, P.K.J., (2004) Formation of Amyloid Fibers Triggered by Phosphatidylserine Containing Membranes, *Biochemistry 43,* 10302-10307.

12. Vieira, E.P., Hermel, H., and Mohwald, H., (2003) Change and stabilization of the amyloid-β(1-40) secondary structure by fluorocompounds. *Biochimica et Biophysica Acta 1645,* 6-14.

13. Eakin, C.M., Knight, J.D., Morgan, C.J., Gelfand, M.A., and Miranker, A.D. (2002) Formation of a copper specific binding site in non-native states of beta-2-microglobulin. *Biochemistry 41*, 10646–10656.

14. Talmard, C., Yona, R.L., and Faller, P. (2009) Mechanism of zinc (II) promoted amyloid formation: zinc (II) binding facilitates the transition from the partially alpha helical conformer to aggregates of amyloid beta protein(1-28). *Journal of Biological Inorganic Chemistry 14*, 449–455.

15. Yamin, G., Glaser, C.B., Uversky, V.N., and Fink, A.L., (2003) Certain metals trigger fibrillation of methionine-oxidized alpha synuclein. *Journal of Biological Chemistry 278*, 27630–27635.

16. Yamin, G., Munishkina, L. A., Karymov, M.A., Lyubchenko, Y.L., Uversky, V. N., and Fink, A.L., (2005) Forcing non-amyloidogenic beta synuclein to fibrillate. *Biochemistry 44*, 9096–9107.

17. Terzi, E. Holzemann, G., and Seelig, J., (1997) Interaction of Alzheimer β-Amyloid Peptide (1-40) with Lipid Membranes, *Biochemistry 36,* 14845-14852.

18. Brender, J.R., Lee, E.L., Cavitt, M.A., Gafni, A., Steel, D.G., and Ramamoorthy, A. (2008) Amyloid fiber formation and membrane disruption are separate processes localized in two distinct regions of IAPP, the type-2-diabetes-related peptide. *Journal of the American Chemical Society 130*, 6424-6429.

19. Knight, J.D., and Miranker, A.D., (2004) Phospholipid catalysis of diabetic amyloid assembly, *Journal of Molecular Biology 341,* 1175–1187.

20. Knight, J.D., Hebda, J.A., and Miranker, A.D., (2006) Conserved and cooperative assembly of membrane-bound alpha-helical states of islet amyloid polypeptide, *Biochemistry 45,* 9496–9508.

21. Jayasinghe, S.A., and Langen, R., (2005) Lipid membranes modulate the structure of islet amyloid polypeptide, *Biochemistry 44,* 12113–12119.

22. Janson, J., Ashley, R.H., Harrison, D., McIntyre, S., and Butler, P.C., (1999) The mechanism of islet amyloid polypeptide toxicity is membrane disruption by intermediate-sized toxic amyloid particles, *Diabetes 48,* 491–498.

23. Anguiano, M., Nowak, R.J., and Lansbury Jr., P.T., (2002) Protofibrillar islet amyloid polypeptide permeabilizes synthetic vesicles by a pore-like mechanism that may be relevant to type II diabetes, *Biochemistry 41,* 11338–11343.

24. Arispe, N., Pollard, H.B., and Rojas, E., (1993) Giant multilevel cation channels formed by Alzheimer disease amyloid beta-protein [AbP-(1–40)] in bilayer membranes, *Proceedings of the National Academy of Sciences 90,* 10573–10577.

25. Volles, M.J., Lee, S.J., Rochet, J.C., Shtilerman, M.D., Ding, T.T., Kessler, J.C., and Lansbury Jr., P.T., (2001) Vesicle permeabilization by protofibrillar a-synuclein: implications for the pathogenesis and treatment of Parkinson's disease, *Biochemistry 40,* 7812–7819.

26. Brender, J., Hartman, K., Gottler, L., Cavitt, M., Youngstrom, D., and Ramamoorthy, A., (2009) Helical Conformation of the SEVI Precursor Peptide $PAP_{248-286}$, a Dramatic Enhancer of HIV Infectivity, Promotes Lipid Aggregation and Fusion. *Biophysical Journal 97,* 2474-2483.

27. Stottrup, B.L., Veatch, S.L., and Keller, S.L., (2004) Nonequilibrium Behavior in Supported Lipid Membranes Containing Cholesterol. *Biophysical Journal 86,* 2942-2950.

28. Davis. J.H., Clair, J.J., and Juhasz, J., (2009) Phase Equilibria in DOPC/DPPC-d62/Cholesterol Mixtures, *Biophysical Journal 96,* 521-539.

29. Dietrich, C., Bagatolli, L.A., Volovyk, Z.N., Thompson, N.L., Levi, M., Jacobson, K., and Gratton, E., (2001) Lipid Rafts Reconstituted in Model Membranes, *Biophysical Journal 80,* 1417-1428.

30. Kanatsuka, A., Makino, H., Ohsawa, H., Tokuyama, Y., Yamaguchi, T., Yoshida, S., and Adachi, M. (1989) Secretion of islet amyloid polypeptide in response to glucose. *Federation of European Biochemical Societies Journal 259*, 199-201.

31. Khan, S.E., D'Alessio, D.A., Schwartz, M.W., Fujimoto, W.Y., Ensinck, J.W., Taborsky, G.J.J., and Porte, D.J.J. (1990) Evidence of cosecretion of islet amyloid polypeptide and insulin by beta-cells. *Diabetes 5*, 634-638.

32. Bailey, C.J. (1999) New pharmacological approaches to glycemic control. *Diabetes Review 7*, 94-113.

33. Cooper, G.J.S. (1994) Amylin compared with calcitonin-gene-related peptides-Structure, biology, and relevance to metabolic disease. *Endocrinology Review 15*, 163-201.

34. Reda, T.K., Geliebter, A., and Pi-Sunyer, F.X. (2002) Amylin, food intake, and obesity. *Obesity Research 10*, 1087-1091.

35. Ludwig, G., and Heitner, H. (1967) Zur Haufigkeit der Inselamyloidose des Pankreas beim Diabetes mellitus. *Zschr. Inn. Med. 22*, 814-818.

36. Westermark, P., Wilander, E. (1978) The influence of amyloid deposits on the islet volume in maturity onset diabetes mellitus. *Diabetologia 15*, 417-421.

37. Bell, E.T. (1959) Hyalinization of the islets of Langerhans in nondiabetic individuals. *American Journal of Pathology 35*, 801-805.

38. Centers for Disease Control and Prevention. National Diabetes Fact Sheet. United States. 2005. Available at http://www.cdc.gov/diabetes/pubs/pdf/ndfs_2005.pdf.

39. Westermark, P., Wersnstedt, C., Wilander, E., Hayden, D.W., O'Brien, T.D., and Johnson, K.H. (1987) *Proceedings of the National Academy of Sciences* 84, 3381–3385

40. Betsholtz, C., Svensson, V., Rorsman, F., Engstrom, U., Westermark, G. T., Wilander, E., Johnson, K., and Westermark, P. (1989) Islet amyloid polypeptide (IAPP): cDNA cloning and identification of an amyloidogenic region associated with the species-specific occurrence of age-related diabetes mellitus. *Experimental Cell Research 183*, 484-493.

41. Westermark, P., Engstrom, U., Johnson, K.H., Westermark, G.T., and Betsholtz, C. (1990) Islet amyloid polypeptide: Pinpointing amino acid residues linked to amyloid fibril formation. *Proceedings of the National Academy of Sciences 87*, 5036-5040.

42. Moriarty, D.F., and Raleigh, D.P. (1999) Effects of sequential proline substitutions on amyloid formation by human amylin20-29. *Biochemistry 38*, 1811-1818.

43. Tenidis, K., Waldner, M., Bernhagen, J., Fischle, W., Bergmann, M., Weber, M., Merkle, M-L., Voelter, W., Brunner, H., and Kapurniotu, A. (2000) Identification of a penta- and hexapeptide of islet amyloid polypeptide (IAPP) with amyloidogenic and cytotoxic Properties. *Journal of Molecular Biology 295*, 1055-1071.

44. Azriel, R., and Gazit, E. (2001) Analysis of the minimal amyloid-forming fragment of the islet amyloid polypeptide: An experimental support for the key role of the phenylalanine residue in amyloid formation. *Journal of Biological Chemistry 276*, 34156-34161.

45. Ashburn, T.T., Auger, M., and Lansbury, P.T., Jr. (1992) The structural basis of pancreatic amyloid formation: isotope-edited spectroscopy in the solid state. *Journal of the American Chemical Society 114*, 790-791.

46. Nilsson, M.R., and Raleigh, D.P. (1999) Analysis of amylin cleavage products provides new insights into the amyloidogenic region of human amylin. *Journal of Molecular Biology 294*, 1375-1385.

47. Jaikaran, E.T.A.S., Higham, C.E., Serpell, L.C., Zurdo, J., Gross, M., Clark, A., and Fraser, P.E. (2001) Identification of a novel human islet amyloid polypeptide β-sheet domain and factors influencing fibrillogenesis. *Journal of Molecular Biology 308*, 515-525.

48. Mazor, Y., Gilead, S., Benhar, I., and Gazit, E. (2002) Identification and characterization of a novel molecular-recognition and self-assembly domain within the islet amyloid polypeptide. *Journal of Molecular Biology 322*, 1013-1024.

49. Scrocchi, L.A., Ha, K., Chen, Y., Wu, L., Wang, F., and Fraser, P.E. (2003) Identification of minimal peptide sequences in the (8-20) domain of human islet amyloid polypeptide involved in fibrillogenesis. *Journal of Structural Biology 141*, 218-227.

50. Abedini, A., and Raleigh, D.P. (2006) Destabilization of Human IAPP Amyloid Fibrils by Proline Mutations Outside of the Putative Amyloidogenic Domain: Is There a Critical Amyloidogenic Domain in Human IAPP? *Journal of Molecular Biology 355*, 274-281.

51. Fox, A., Snollaerts, T., Casanova, C.E., Calciano, A., Nogaj, L. A., and Moffet, D.A. (2010) Selection for Nonamyloidogenic Mutants of Islet Amyloid Polypeptide (IAPP) Identifies an Extended Region for Amyloidogenicity. *Biochemistry 49*, 7783-7789.

52. Scrocchi, L.A., Chen, Y., Waschuk, S., Wang, F., Cheung, S., Darabie, A.A., McLaurin, J., and Fraser. P.E. (2002) Design of peptide-based inhibitors of human islet amyloid polypeptide fibrillogenesis. *Journal of Molecular Biology 318*, 697-706.

53. Kapurniotu, A., Schmauder, A., and Tenidis, K. (2002) Structure-based design and study of non-amyloidogenic, double N-methylated IAPP amyloid core sequences as inhibitors of IAPP amyloid formation and cytotoxicity. *Journal of Molecular Biology 315*, 339-350.

54. Tatarek-Nossol, M., Yan, L-M., Schmauder, A., Tenidis, K., Westermark, G., and Kapurniotu, A. (2005) Inhibition of hIAPP amyloid-fibril formation and apoptotic cell death by a designed hIAPP amyloid-core-containing hexapeptide. *Biological Chemistry 12*, 797-809.

55. Yan, L-M., Tatrek-Nossol, M., Velkova, A., Kazantzis, A., and Kapurniotu, A. (2006) Design of a mimic of nonamyloidogenic and bioactive human islet amyloid polypeptide (IAPP) as nanomolar affinity inhibitor of IAPP cytotoxic fibrillogenesis. *Proceedings of the National Academy of Sciences103*, 2046-2051.

56. Abedini, A., Meng, F., and Raleigh, D.P. (2007) A single-point mutation converts the highly amyloidogenic human islet amyloid polypeptide into a potent fibrillization inhibitor. *Journal of the American Chemical Society 129*, 11300-11301.

57. Balali-Mood, K., Ashley, R.H., Haub, T., and Bradshaw, J.P. (2005) Neutron diffraction reveals sequence-specific membrane insertion of prefibrillar islet amyloid polypeptide and inhibition by rifampicin. *Federation of European Biochemical Societies Letters 579*, 1143-1148.

58. Sparr, E., Engel, M.F.M., Sakharov, D.V., Sprong, M., Jacobs, J., Kruijff, B.D., Hoppener, J.W.M., and Killian, J.A. (2004) Islet amyloid polypeptide-induced membrane leakage involves uptake of lipids by forming amyloid fibers. *Federation of European Biochemical Societies Letters 577*, 117-120.

59. Konarkowska, B., Aitken, J.F., Kistler, J., Zhang, S., and Cooper, G.J.S. (2006) The aggregation potential of human amylin determines its cytotoxicity towards islet β-cells. *Federation of European Biochemical Societies Journal 273*, 3614-3624.

60. Ritzel, R.A., Meier, J. J., Lin, C-Y., Veldhuis, J.D., and Butler, P.C. (2007) Human islet amyloid polypeptide oligomers disrupt cell coupling, induce apoptosis, and impair insulin secretion in isolated human islets. *Diabetes 56*, 65-71.

61. Gurlo, T., Ryazantsey, S., Huang, C-J., Yeh, M.W., Reber, H.A., Hines, O.J., O‟Brien, T.D., Glabe, C.G., and Butler, P.C. (2010) Evidence for proteotoxicity in β cells in type II diabetes: Toxic islet amyloid polypeptide oligomers form intracellularly in the secretory pathway. *American Journal of Pathology 176*, 861-869.

62. Engel, M.F.M., Yigittop, H., Elgersma, R.C., Rijkers, D.T.S., Liskamp, R.M.J., Kruijff, B.D., Hoppener, J.W.M., and Killian, A. (2006) Islet amyloid polypeptide inserts into phospholipid monolayers as monomer. *Journal of Molecular Biology 356*, 783-789.

63. Lopes, D.H.J., Meister, A., Gohlke, A., Hauser, A., Blume, A., and Winter, R. (2007) Mechanism of islet amyloid polypeptide fibrillation at lipid interfaces studied by infrared reflection absorption spectroscopy. *Biophysical Journal 93*, 3132-3141.

64. Brender, J.R., Lee, E.L., Hartman, K., Wong, P.T., Ramamoorthy, A., Steel, D.G., Gafni, A., (2011) Biphasic Effects of Insulin on Islet Amyloid Polypeptide Membrane Disruption, *Biophysical Journal 100,* 685-692.

65. Foster, M.C., Leapman, R.D., Li, M.X., and Atwater, I. (1993) Elemental composition of secretory granules in pancreatic islets of Langerhans. *Biophysical Journal 64*, 525–532.

66. Taylor, C.G., (2005) Zinc, the pancreas, and diabetes: insights from rodent studies and future directions. *BioMetals 18*, 305–312

67. Wei, L., Jiang, P., Yau, Y.H., Summer, H., Shochat, S.G., Mu, Y., and Pervushin, K., (2009) Residual structure in islet amyloid polypeptide mediates its interactions with soluble insulin. *Biochemistry. 48,* 2368–2376.

68. Larson, J.L., and A.D. Miranker. (2004) The mechanism of insulin action on islet amyloid polypeptide fiber formation. *Journal of Molecular Biology 335,* 221–231.

69. Jaikaran, E.T., Nilsson, M.R., and Clark, A., (2004) Pancreatic β-cell granule peptides form heteromolecular complexes which inhibit islet amyloid polypeptide fibril formation. *Biochemical Journal 377,* 709–716.

70. Abedini, A., and Raleigh, D.P., (2005) The role of His-18 in amyloid formation by human islet amyloid polypeptide. *Biochemistry 44,* 16284–16291.

71. Brender, J.R., Hartman K., Reid, K.R., Kennedy, R.T., and Ramamoorthy A. (2008) A single mutation in the nonamyloidogenic region of islet amyloid polypeptide greatly reduces toxicity. *Biochemistry 47,* 12680–12688.

72. Nanga, R.P.R., Brender, J.R., Xu, J., Veglia, G., and Ramamoorthy, A., (2008) Structures of rat and human islet amyloid polypeptide IAPP(1-19) in micelles by NMR spectroscopy. *Biochemistry 47,* 12689–12697.

73. Fraser, P.E., Nguyen, J.T., Surewicz, W.K., and Kirschner, D.A. (1991) pH-dependent structural transitions of Alzheimer amyloid peptides. *Biophysical Journal 60,* 1190–1201

74. Lomakin, A., Chung, D., Benedek, G., Kirschner, D., and Teplow, D. (1996) On the nucleation and growth of amyloid beta protein fibrils: detection of nuclei and quantitation of rate constants. *Proceedings of the National Academy of Sciences 93*, 1125–1129

75. Whittingham, J.L., Scott, D.J., Chance, K., Wilson, A., Finch, J., Brange, J., and Guy Dodson, G. (2002) Insulin at pH 2: structural analysis of the conditions promoting insulin fibre formation. *Journal of Molecular Biology 318*, 479–490

76. Bucciantini, M., Giannoni, E., Chiti, F., Baroni, F., Formigli, L., Zurdo, J., Taddei, N., Ramponi, G., Dobson, C.M., and Stefani, M. (2002) Inherent toxicity of aggregates implies a common mechanism for protein misfolding diseases. *Nature 416*, 507–511

77. Chiti, F., Bucciantini, M., Capanni, C., Taddei, N., Dobson, C.M., and Stefani, M. (2001) Solution conditions can promote formation of either amyloid protofilaments or mature fibrils from the HypF N-terminal domain. *Protein Science 10*, 2541–2547

78. Atwood C.S., Moir R.D., Huang X., Scarpa R.C., Bacarra N.M., Romano D.M., Hartshorn M.A., Tanzi R.E. and Bush A.I. (1998) Dramatic aggregation of Alzheimer abeta by Cu(II) is induced by conditions representing physiological acidosis. *Journal of Biological Chemistry 273*, 12817–12826.

79. Deshpande A., Kawai H., Metherate R., Glabe C.G. and Busciglio J. (2009) A role for synaptic zinc in activity-dependent Abeta oligomer formation and accumulation at excitatory synapses. *Journal of Neuroscience 29*, 4004–4015.

80. Dong J., Shokes J.E., Scott R.A. and Lynn D.G. (2006) Modulating amyloid self-assembly and fibril morphology with Zn(II). *Journal of the American Chemical Society 128*, 3540–3542.

81. Miller Y., Ma B. and Nussinov R. (2010) Zinc ions promote Alzheimer Abeta aggregation via population shift of polymorphic states. *Proceedings of the National Academy of Science 107,* 9490–9495.

82. Brender, J.R., Hartman, K., Nanga, R.P., Popovych, N., Salud Bea, R., Vivekanandan, S., Marsh, E.N., and Ramamoorthy, A., (2010) Role of Zinc in Human Islet Amyloid Polypeptide Aggregation. *Journal of the American Chemical Society 132,* 8973-8983.

83. Ward, B., Walker, K., and Exley, C., (2008) Copper (II) inhibits the formation of amylin amyloid in vitro. *Journal of Inorganic Biochemistry 102*, 371-375

84. Miura, T., Suzuki, K., Kohata, N., and Takeuchi, H. (2000) Metal binding modes of Alzheimer's amyloid beta peptide in insoluble aggregates and soluble complexes. *Biochemistry 39*, 7024-7031.

85. Zou, J., Kajita, K., and Sugimoto, N. (2001) Cu^{2+} Inhibits the aggregation of amyloid beta peptide(1-42) in vitro. *Angewandte Chemie International Edition 40*, 2274-2277.

86. Jiao, Y., and Yang, P., (2007) Mechanism of copper (II) inhibiting Alzheimer's amyloid beta peptide from aggregation: a molecular dynamics investigation. *Journal of Physical Chemistry B 111*, 7646-7655.

87. Wei, L., Jiang P., Yau, Y.H., Summer, H., Shochat, S.G., Mu, Y.G., and Pervushin K. 2009. Residual structure in islet amyloid polypeptide mediates its interactions with soluble insulin. *Biochemistry 48,* 2368–2376.

88. Wiltzius, J.J., Sievers, S.A., Sawaya, M.R., and Eisenberg, D., (2009) Atomic structures of IAPP (amylin) fusions suggest a mechanism for fibrillation and the role of insulin in the process. *Protein Science 18*, 1521–1530.

89. Knight, J.D., Williamson J.A., and Miranker A.D. (2008) Interaction of membrane-bound islet amyloid polypeptide with soluble and crystalline insulin. *Protein Science 17,* 1850–1856.

90. Gilead, S., Wolfenson H., and Gazit E. (2006) Molecular mapping of the recognition interface between the islet amyloid polypeptide and insulin. *Angewandte Chemie International Edition 45,* 6476–6480.

91. Kudva, Y.C., Mueske C., Butler, P.C., and Eberhardt, N.L. (1998) A novel assay in vitro of human islet amyloid polypeptide amyloidogenesis and effects of insulin secretory vesicle peptides on amyloid formation. *Biochemical Journal 331,* 809–813.

92. Cui W, Ma J.W., Lei P, Wu W.H., Yu Y.P., Xiang Y, Tong A.J., Zhao Y.F., Li Y.M. (2009) Insulin is a kinetic but not a thermodynamic inhibitor of amylin aggregation. *Federation of European Biochemical Societies Journal 276,* 3365–3371.

93. Sellin, D., Yan L.M, Kapurniotu, A., and Winter R. (2010) Suppression of IAPP fibrillation at anionic lipid membranes via IAPP-derived amyloid inhibitors and insulin. *Biophysical Chemistry 150,* 73–79.

94. Westermark, P., Li Z.C., Westermark, A., Leckstrom, A., and Steiner D.F. (1996) Effects of β cell granule components on human islet amyloid polypeptide fibril formation. *Federation of European Biochemical Societies Letters 379,* 203–206.

95. Joint United Nations Programme on HIV/AIDS (UNAIDS). Report on the Global HIV/AIDS Epidemic 2008. Available at http://www.unaids.org/en/dataanalysis/epidemiology/2008reportontheglobalaidsepidemic/

96. Joint United Nations Programme on HIV/AIDS (UNAIDS). AIDS Epidemic Update. 2009. Available at

http://www.unaids.org/en/media/unaids/contentassets/dataimport/pub/report/2009/jc1700_epi_update_2009_en.pdf

97. Dimitrov, D.S., Willey, R.L., Sato, H., Chang, L.J., Blumenthal, R., and Martin, M. A. (1993) Quantitation of human immunodeficiency virus type 1 infection kinetics. *Journal of Virology 67*, 2182-2190.

98. Rusert, P., Fischer, M., Joos, B., Leemann, C., Kuster, H., Flepp, M., Bonhoeffer, S., Gunthard, H.F., and Trkola, A. (2004) Quantification of infectious HIV-1 plasma viral load using a boosted in vitro infection protocol. *Virology 326*, 113-129.

99. Perelson, A.S., Neumann, A.U., Markowitz, M., Leonard, J.M., and Ho, D.D. (1996) HIV-1 dynamic in vivo: virion clearance rate, infected cell life-span, and viral generation time. *Science 271*, 1582-1586.

100. Berg, H.C., and Purcell, E.M. (1977) Physics of chemoreception. *Biophysical Journal 20*, 193-219.

101. Eckert, D.M., and Kim, P.S. (2001) Mechanism of viral membrane fusion and its inhibition. *Annual Reviews in Biochemistry. 70*, 777-810.

102. Wurm, M., Schambach, A., Lindemann, D., Hanenberg, H., Standker, L., Forssmann, W.G., Blasczyk, R. and Horn, P. A. (2010). The influence of semen-derived enhancer of virus infection on the efficiency of retroviral gene transfer. *Journal of Gene Medicine 12*, 137-146.

103. Hong, S.H., Klein, E.A., Das Gupta, J., Hanke, K., Weight, C.J., Nguyen, C., Gaughan, C., Kim, K.A., Bannert, N., Kirchhoff, F., Munch, J. and Silverman, R.H. (2009). Fibrils of prostatic acid phosphatase fragments boost infections with XMRV (xenotropic murine leukemia virus-related virus), a human retrovirus associated with prostate cancer. *Journal of Virology 83*, 6995-7003.

104. Aloia, R.C., Tian, H.R., and Jensen, F.C., (1993) Lipid-composition and fluidity of the human-immunodeficiency-virus envelope and host-cell plasma-membranes. *Proceedings of the National Academy of Sciences 90,* 5181–5185.

105. Patil, S.M., Xu, S.H., Sheftic, S.R., and Alexandrescu, A. T. (2009) Dynamic alpha-Helix Structure of Micelle-bound Human Amylin, *Journal of Biological Chemistry 284*, 11982-11991.

106. Nanga, R.P.R., Brender, J.R., Vivekanandan, S., and Ramamoorthy, A., (2011) Structure and membrane orientation of IAPP in its natively amidated form at physiological pH in a membrane environment. *Biochimica et Biophysica Acta 1808,* 2337-2342.

107. Shao, H., Jao, S., Ma, K., and Zagorski, M.G., (1999) Solution structures of micelle bound amyloid beta (1-40) and beta (1-42) peptides of Alzheimer's disease. *Journal of Molecular Biology 285*, 755-773.

108. Nanga R.P.R, Brender J.R, Vivekanandan S, Popovych N, Ramamoorthy A. (2009) NMR Structure in a Membrane Environment Reveals Putative Amyloidogenic Regions of the SEVI Precursor Peptide PAP(248-286). *Journal of the American Chemical Society 131*, 17972-17979.

109. Hauber, I., Hohenberg, H., Holstermann, B., Hunstein, W. and Hauber, J. (2009). The main green tea polyphenol epigallocatechin-3-gallate counteracts semen-mediated enhancement of HIV infection. *Proceedings of the National Academy of Sciences 106*, 9033-9038.

110. Rezai-Zadeh, R., Shytle, D., Sun, N., Mori, T., Hou, H., Jeanniton, D., Ehrhart, J., Townsend, K., Zeng, J., Morgan, D., Hardy, J., Town, T., and Tan, J., (2005) Green tea epigallocatechin-3-gallate (EGCG) modulates amyloid precursor protein cleavage and reduces cerebral amyloidosis in alzheimer transgenic mice. *Journal of Neuroscience 25,* 8807-8814.

111. Ehrnhoefer, D.E., Bieschke, J., Boeddrich, A., Herbst, M., Masino, L., Lurz, R., Engemann, S., Pastore, A. and Wanker, E.E. (2008). EGCG redirects amyloidogenic polypeptides into unstructured, off-pathway oligomers. *Nature Structural and Molecular Biology 15*, 558-566.

112. Meng, F.L., Abedini, A., Plesner, A., Verchere, C.B. and Raleigh, D.P. (2010). The flavanol (-)-epigallocatechin 3-gallate inhibits amyloid formation by islet amyloid polypeptide, disaggregates amyloid fibrils, and protects cultured cells against IAPP-induced toxicity. *Biochemistry 49*, 8127-8133.

113. Porat, Y., Abramowitz, A. and Gazit, E. (2006). Inhibition of amyloid fibril formation by polyphenols: Structural similarity and aromatic interactions as a common inhibition mechanism. *Chemical Biology and Drug Design 67*, 27-37.

114. Ye Z.Q., French K.C., Popova L.A., Lednev I.K., Lopez M.M. and Makhatadze G.I. (2009) Mechanism of Fibril Formation by a 39-Residue Peptide (PAPf39) from Human Prostatic Acidic Phosphatase. *Biochemistry 48,* 11582-11591.

CHAPTER 2

A SINGLE MUTATION IN THE NON-AMYLOIDOGENIC REGION OF ISLET AMYLOID POLYPEPTIDE GREATLY REDUCES TOXICITY

2.1 Summary

Islet amyloid polypeptide (IAPP or amylin) is a 37-residue peptide secreted with insulin by β-cells in the islets of Langerhans. The aggregation of the peptide into either amyloid fibers or small soluble oligomers has been implicated in the death of β-cells during type II diabetes through disruption of the cellular membrane. The actual form of the peptide responsible for *β*-cell death has been a subject of controversy. Previous research has indicated that the N-terminal region of the peptide (residues 1-19) is primarily responsible for the membrane-disrupting effect of the hIAPP peptide and induces membrane disruption to a similar extent as the full-length peptide without forming amyloid fibers when bound to the membrane. The rat version of the peptide, which is both non-cytotoxic and non-amyloidogenic, differs from the human peptide by only one amino acid residue: Arg18 in the rat version while His18 in the human version. To elucidate the effect of this difference, we have measured in this study the effects of the rat and human versions of $IAPP_{1-19}$ on islet cells and model membranes. Fluorescence microscopy shows a rapid increase in intracellular calcium levels of islet cells after the

---

This chapter is a version of a published paper: Brender, J.R., Hartman, K., Reid, K.R., Kennedy, R.T., and Ramamoorthy, A., (2008) A Single Mutation in the Nonamyloidogenic Region of Islet Amyloid Polypeptide Greatly Reduces Toxicity. Biochemistry 47, 12680-12688.

addition of $hIAPP_{1-19}$, indicating disruption of the cellular membrane, while the rat version of the $IAPP_{1-19}$ peptide is significantly less effective. Circular dichroism experiments and dye leakage assays on model liposomes show that $rIAPP_{1-19}$ is deficient in binding to and disrupting lipid membranes at low but not at high peptide to lipid ratios, indicating that the ability of $rIAPP_{1-19}$ to form small aggregates necessary for membrane binding and disruption is significantly less than $hIAPP_{1-19}$. At pH 6.0, where H18 is likely to be protonated, $hIAPP_{1-19}$ resembles $rIAPP_{1-19}$ in its ability to cause membrane disruption. Differential scanning calorimetry suggests a different mode of binding to the membrane for $rIAPP_{1-19}$ compared to $hIAPP_{1-19}$. Human $IAPP_{1-19}$ has a minimal effect on the phase transition of lipid vesicles, suggesting a membrane orientation of the peptide in which the mobility of the acyl chains of the membrane is relatively unaffected. Rat $IAPP_{1-19}$, however, has a strong effect on the phase transition of lipid vesicles at low concentrations, suggesting that the peptide does not easily insert into the membrane after binding to the surface. Our results indicate that the modulation of the peptide orientation in the membrane by His18 plays a key role in the toxicity of non-amyloidogenic forms of hIAPP.

2.2 Introduction

It has been known for many years that insoluble, highly aggregated amyloid deposits of human islet amyloid polypeptide protein (hIAPP, also known as amylin) are found postmortem in the islets of Langerhans of pancreatic β-cells in the majority (>90%) of type II diabetic patients but not in non-diabetic patients of the same age cohort (*1*). The high tissue visibility of the amyloid deposits and their prevalence in diabetic patients has

led to the hypothesis that the formation of amyloid fibers plays a causative role in the development of the disease (*2, 3*).

The hypothesis that extracellular amyloid fibers directly cause *β*-cell apoptosis has been challenged by both *in vitro* and *in vivo* studies. Transgenic mice models have been particularly useful in this respect as rats do not spontaneously develop type II diabetes and have an IAPP variant that is both non-cytotoxic and non-amyloidogenic (Figure 2.1) (*4*). Transgenic mice expressing the human version of IAPP develop complications with metabolic characteristics similar to human type II diabetes (*5-8*). However, there is poor spatial and temporal overlap between amyloid formation and β-cell apoptosis in transgenic mice. Extracellular amyloid in homozygous transgenic mice is only detected after the phase of rapid *β*-cell death has passed, and the *β*-cells undergoing apoptosis are not adjacent to amyloid fibers (*9-11*). Furthermore, some transgenic mice models expressing hIAPP form extensive amyloid fiber deposits but do not develop type II diabetes (*12*). The lack of correlation between islet amyloid formation and the pathology of type II diabetes in transgenic mice mirrors findings in humans, in that islet amyloid is found in people without diabetes as well as not found in all people with diabetes (*13, 14*). Studies directly measuring the effect of IAPP upon *β*-cells have confirmed the relatively low toxicity of mature amyloid fibers of IAPP (*15-19*).

Unlike mature fibers, small hIAPP oligomers have been demonstrated to be cytotoxic to *β*-cells (*5, 15-18, 20, 21*). Soluble oligomers of IAPP, in common with other amyloidogenic proteins, have been implicated in the disruption of cellular homeostasis either by the formation of relatively nonselective ion channels or by direct fragmentation of the cellular membrane (*22, 23*). The kinetics of oligomer formation is complex and is

likely to involve multiple pathways *(24-26)*. Inhibition studies have suggested that the toxic oligomers are a distinct species of amyloid proteins and not simply direct intermediates of mature fibers. Inhibitors have been found that suppress the formation of toxic oligomers but not the formation of amyloid fibers *(27)*. Conversely, other inhibitors have been shown to have the opposite effect, suppressing the formation of amyloid fibers but not the formation of toxic oligomers *(18, 27)*. The ability of some inhibitors to suppress the formation of small oligomers independently of their effect on the formation of amyloid fibers suggests the toxic oligomers are at least partly off the kinetic pathway for the formation of amyloid fibers. Although amyloidogenic proteins can disrupt membranes through the formation of toxic oligomers, new evidence suggests the formation of toxic oligomers may not be unique to amyloidogenic proteins. An antibody specific for the soluble oligomeric form of amyloidogenic proteins also recognizes several non-amyloidogenic pore-forming proteins *(28)*. More directly, the N-terminal fragment of human IAPP (residues 1-19) has been found to disrupt synthetic vesicles to nearly the same extent as full-length IAPP but does not form amyloid fibers while bound to the membrane *(25)*. Significantly, the sequences of human IAPP and rat IAPP are identical in this region of the protein except for residue 18, which is His in the human version and Arg in the rat version of the peptide (Figure 2.1). In a companion paper of this issue, high-resolution structures of $hIAPP_{1-19}$ and $rIAPP_{1-19}$ in DPC micelles were solved by solution NMR. Although the structures are largely similar, $rIAPP_{1-19}$ is more disordered at the N-terminus than the $hIAPP_{1-19}$ peptide. More significantly, $hIAPP_{1-19}$ is shielded from the paramagnetic quencher Mn^{2+} while $rIAPP_{1-19}$ is exposed. The

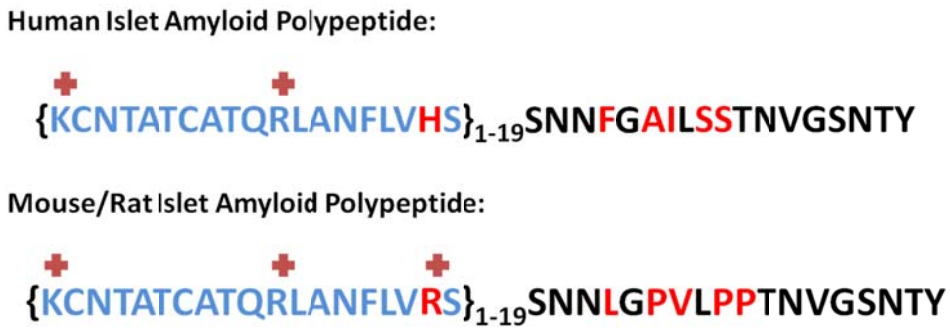

Figure 2.1 Amino acid sequences of rat and human IAPP. The 1-19 fragment that is used in this study is shown in blue, and the differences between the two sequences are shown in red. Positive charged residues are indicated above sequences. A disulfide bond exists between residues 2 and 8. The C-termini are amidated like the naturally occurring peptide.

difference in the accessibility of Mn^{2+} to the two peptides when bound to DPC micelles suggests $rIAPP_{1-19}$ adopts a different orientation in the membrane than $hIAPP_{1-19}$. This effect is likely due to the difference in charge at residue 18, as $hIAPP_{1-19}$ becomes significantly more solvent exposed at pH 6.0 where the histidine residue is likely to be ionized. To see the impact of this difference on the toxicity of the two peptides, we have performed *in vivo* and *in vitro* assays of the ability of the two peptides to permeabilize the membranes of both β-cell islets and model membranes. We report here that the $rIAPP_{1-19}$ peptide is significantly impaired in its ability to disrupt phospholipid membranes compared to the corresponding $hIAPP_{1-19}$ peptide, highlighting the role of this key residue in controlling the toxicity of the peptide.

2.3 Experimental Procedures

2.3.1 Materials

POPG (1-palmitoyl-2-oleoyl-*sn*-glycero-3-phospho-*rac*-(1-glycerol)), DMPG (1,2-dimyristoyl-*sn*-glycero-3-phospho-*rac*-(1-glycerol)), and DMPC (1,2-dimyristoyl*sn*-

glycero-3-phosphocholine) phospholipids were obtained from Avanti (Alabaster, AL); DMSO (dimethyl sulfoxide), carboxyfluorescein, and HFIP (1,1,1,3,3,3-hexafluoro-2-propanol) were obtained from Sigma-Aldrich; $hIAPP_{1-19}$ and $rIAPP_{1-19}$ with amidated C-termini (>95% purity) were purchased from Genscript. Before use, lyophilized $rIAPP_{1-19}$ and $hIAPP_{1-19}$ were dissolved in HFIP at a concentration of 10 mg/mL for 1 hr to break up any preformed aggregates present in the solution. Aliquots of the peptide stock solution were flash-frozen in liquid nitrogen and then lyophilized again for more than 16 hr at less than 1 mTorr vacuum to completely remove HFIP. All experiments were conducted at room temperature (approximately 23 °C). POPG vesicles for the circular dichroism and dye leakage experiments were prepared as previously described (*25*).

2.3.1 Islet Isolation Protocol

Pancreatic islets were obtained from 20 to 30 g male CD-1 mice as previously described (*29*). Briefly, mice were sacrificed by cervical dislocation, and collagenase type XI was injected into the pancreas through the main pancreatic duct. The pancreas was removed and incubated in 5 mL of a collagenase solution at 37 °C. Islets that were used for experiments were 100-200 μm in diameter, had an intact islet membrane, and were oblong to spherical in shape. Islets were placed in tissue culture dishes and incubated in RPMI 1640 containing 10% fetal bovine serum, 100 units/mL penicillin, and 100 μg/mL streptomycin at 37 °C, 5% CO_2, pH 7.4. Islets were used 1-6 days following isolation.

2.3.3 Intracellular Ca^{2+} Measurements

Calcium flux measurements were performed on islets after a 40 min incubation with 2 μM fluorescent calcium-sensitive dye, fura-2. Afterward, individual islets were loaded into an open cell chamber on a microfluidic chip. Islet media and stimulants were perfused over the islet at a rate of 0.6 μL/min. The chip was placed atop the stage of a Nikon Diaphot 300 microscope. The fura-2 was alternately excited using a filter wheel with 340 and 380 nm light from a xenon arc lamp. The fluorescence emission from both excitation wavelengths was collected through a 510 (10 nm bandpass filter. Images of the islet were collected at 1 Hz, and the intensity over islet area was integrated using Metamorph software. Intracellular calcium concentration was calculated by determining the ratio of the emission at 340 and 380 nm excitation after calibration of the system.

2.3.4 Circular Dichroism Spectroscopy

Lyophilized peptide was dissolved in sodium phosphate buffer (10 mM, pH 7.3), briefly vortexed and sonicated (approximately 15 s), and transferred to a 0.1 cm cuvette. After the initial spectrum of the peptide in solution was taken, POPG vesicles from a 40 mg/mL stock solution were titrated into the cuvette. Spectra were measured at 1 nm intervals from 185 to 260 nm at a scanning speed of 50 nm/min and a bandwidth of 5 nm. Each spectrum reported is the average of four scans after subtraction of the baseline spectrum of buffer and vesicles without peptide.

2.3.5 Membrane Disruption Assay

For the dye leakage experiments, carboxyfluorescein containing POPG vesicles was prepared by rehydrating the dried lipid film in 50 mM sodium phosphate buffer (pH 7.5) containing 40 mM carboxyfluorescein, adjusted to pH 7.5 by the addition of sodium hydroxide. Non-encapsulated carboxyfluorescein was removed from the vesicles through size exclusion chromatography using a PD-10 column (Amersham Pharmacia Biotech, Uppsala, Sweden). Vesicle solutions were used immediately, and a fresh vesicle solution was used for each experiment. Fluorescence readings were taken at an excitation wavelength of 493 nm and an emission wavelength of 518 nm. A baseline reading was taken on the solutions prior to the addition of the peptide. After injection, the fluorescence intensity was recorded after 100 s of interaction. The fluorescence signal given by the addition of peptide was then normalized by the addition of Triton X detergent, causing all vesicles present to release any remaining dye to obtain the total possible fluorescent signal.

2.3.6 Differential Scanning Calorimetry

Multilamellar vesicles of DMPC and DMPG (70% DMPC, 30% DMPG) were prepared as described for the dye leakage experiments. Sodium phosphate buffer (10 mM) with 150 mM NaCl at pH 7.3 was used to hydrate the samples. The total molar concentration of lipid was kept constant (5.9 mM) for each sample while the molar peptide concentration was varied as indicated. Scans were run on a Calorimetry Sciences N-DSC II over a temperature range of 5-45 °C with a total of four heating and four cooling scans. The heating scans were run at 0.25 °C/min while the cooling scans were

run at 1.0 °C/ min, in between each of which there was a 10 min equilibration period. The buffer solution without the sample was used as the reference cell. The data were converted to molar heat capacity using the average molecular weight of the lipids, the lipid concentration, and a partial specific volume of 0.988 mL/g. Excess heat capacity was calculated by subtracting a baseline with buffer in both the reference and sample cells at the same scanning rate.

2.4 Results & Discussion

2.4.1 Membrane Disruption Induced by $hIAPP_{1-19}$ and $rIAPP_{1-19}$ in POPG Vesicles.

To test for differences in the extent of membrane disruption induced by $hIAPP_{1-19}$ and $rIAPP_{1-19}$ peptides, leakage of the dye carboxyfluorescein from large unilamellar POPG vesicles (Figure 2.2) was measured as a function of the concentration of POPG at three different concentrations of the peptide. Carboxyfluorescein in intact vesicles is at a high concentration (40 mM) and self-quenched. Disruption of the membrane of the vesicle by the peptide allows carboxyfluorescein to escape, eliminating the self-quenching effect and therefore increasing fluorescence of carboxyfluorescein. For each graph in Figure 2.2, the peptide-to-lipid-ratio was varied by the addition of empty POPG vesicles (vesicles not containing carboxyfluorescein) while the concentrations of peptide and carboxyfluorescein-containing vesicles were kept constant. Decreasing the peptide-to-lipid ratio in this manner has two effects. First, peptide binding and membrane disruption for empty vesicles not containing carboxyfluorescein are not detected. Binding of peptide to empty vesicles reduces the amount of peptide available to bind to

carboxyfluorescein containing vesicles. The membrane disruption induced by the peptide should accordingly decrease in a near-linear fashion as the amount of empty vesicles is increased (values to the right on the *x*-axis in Figure 2.2). Second, the amount of peptide bound to each vesicle is decreased as the total lipid concentration is increased. If the process of membrane disruption is nonlinearly dependent on the concentration of the peptide bound to the membrane, the amount of membrane disruption can also be expected to be nonlinearly dependent on the peptide-to-lipid ratio. This can occur if either the peptide oligomerizes to form peptide channels in the membrane or if membrane disruption occurs by a weakening of the membrane via a carpet-type mechanism as reported for antimicrobial peptides (*30-32*).

Human $IAPP_{1-19}$ strongly induced membrane disruption at all concentrations tested (Figure 2.2). Membrane disruption decreased as the peptide-to-lipid ratio is decreased, but the plots are relatively linear for peptide concentrations of 1 and 5 μM (Figure 2.2B, C). Only at the lowest peptide concentration of 250 nM is a nonlinear dependence of membrane disruption on the concentration of POPG apparent. At a 5 μM peptide concentration, $rIAPP_{1-19}$ is slightly more effective than $hIAPP_{1-19}$ at disrupting the membrane (Figure 2.2C). This effect is most likely due to the greater charge on the $rIAPP_{1-19}$ peptide at pH 7.3 (+4 vs. +3 for the $hIAPP_{1-19}$ assuming H18 is uncharged at pH 7.5) which facilitates partitioning into membranes containing anionic lipids. At a lower peptide concentration (1 μM, Figure 2.2B), $rIAPP_{1-19}$ shows a striking nonlinear dependence on the peptide-to lipid ratio. At high peptide-to-lipid molar ratios, the $rIAPP_{1-19}$ peptide is nearly as effective as the $hIAPP_{1-19}$ peptide. However, as the peptide-to-lipid ratio is decreased, the membrane-disrupting activity of $rIAPP_{1-19}$ is abruptly lost,

dropping off suddenly as a critical peptide-to-lipid ratio is surpassed (approximately 1:100). At the lowest peptide concentration tested in this study, $rIAPP_{1-19}$ induces significant membrane disruption only at the highest peptide-to lipid ratio (1:6) measured (Figure 2.2C).

The physiologically relevant peptide-to-lipid ratio is difficult to establish exactly, as IAPP is stored at high concentrations (0.8-4 mM) in secretory granules before being released into the bloodstream (*33*). After release from the secretory granule, the peptide is diluted in the bloodstream to quite low concentrations (*34*). While the equilibrium concentration of IAPP in the bloodstream is quite low, islet cells are briefly exposed to high concentrations of IAPP immediately upon the release of IAPP from the secretory granule. The amount of IAPP bound to the islet membrane and the consequent peptide-to-lipid ratio therefore depend on a variety of factors that are poorly understood at present, including the dynamics of the release of IAPP from the secretory granule, the reversibility of the membrane binding process, and the affinity for IAPP for the cellular membrane. It is also important to note that cell membranes, unlike model membranes, are highly heterogeneous, and it is probable that IAPP is concentrated in certain regions of the cell membrane, an effect seen previously for the related Aβ1-40 peptide (*35, 36*). In light of the uncertainty about the kinetics of the process of IAPP release from the secretory granule and also the binding of IAPP to the β-cell membrane, it is difficult to establish a narrow range of peptide-to-lipid ratios as being physiologically relevant. Nevertheless, low peptide-to-lipid ratios are more likely to be physiologically relevant than high peptide-to-lipid ratios as the equilibrium concentration of IAPP is low.

Human IAPP differs from $rIAPP_{1-19}$ only by the H18R substitution. At the slightly alkaline pH of the extracellular matrix (~7.3), H18 will be deprotonated while R18 will remain charged. This ionization state of H18 has previously been shown to have an effect on the fibrillization of full length hIAPP, with hIAPP fibrillizing faster at acidic pH where H18 is charged (*37, 38*). To test the effect of the ionization state of H18 on the membrane disruption, the vesicle disruption assay was repeated at pH 6.0 using 1 μM $hIAPP_{1-19}$ or $rIAPP_{1-19}$ (Figure 2.3). The ionization state at residue 18 appears to be critical for membrane disruption, as $hIAPP_{1-19}$ causes significantly less disruption at lower peptide-to-lipid ratios at pH 6.0 than at pH 7.3 (compare Figure 2.2B and Figure 2.3). The amount of disruption induced by $hIAPP_{1-19}$ at pH 6.0 is very similar to $rIAPP_{1-19}$; suggesting $hIAPP_{1-19}$ disrupts liposomes by a similar mechanism as $rIAPP_{1-19}$ at pH 6.0 but not at pH 7.3 where histidine is deprotonated.

The pH dependence of membrane disruption for $hIAPP_{1-19}$ is supported by the paramagnetic quenching experiments detailed in the companion paper (*39*). Human $IAPP_{1-19}$ in DPC micelles is strongly quenched by Mn^{2+} at pH 6.0 but not at pH 7.3. Rat $IAPP_{1-19}$, by contrast, is strongly quenched at pH 7.3. As the Mn^{2+} ion quenches the signals of residues near the membrane-solution interface, it is expected that a surface-associated peptide will be more strongly quenched than a peptide more deeply inserted into the membrane. The enhancement of paramagnetic quenching of $hIAPP_{1-19}$ at pH 6.0 indicates $hIAPP_{1-19}$ binds closer to the surface of the micelle when H18 is protonated, adopting a surface-associated binding mode similar to $rIAPP_{1-19}$.

2.4.2 Membrane Disruption Induced by $hIAPP_{1-19}$ and $rIAPP_{1-19}$ in Pancreatic Islets.

The results of the dye leakage assay indicate $hIAPP_{1-19}$ strongly disrupts phospholipid membranes; on the other hand, $rIAPP_{1-19}$ also disrupts phospholipid

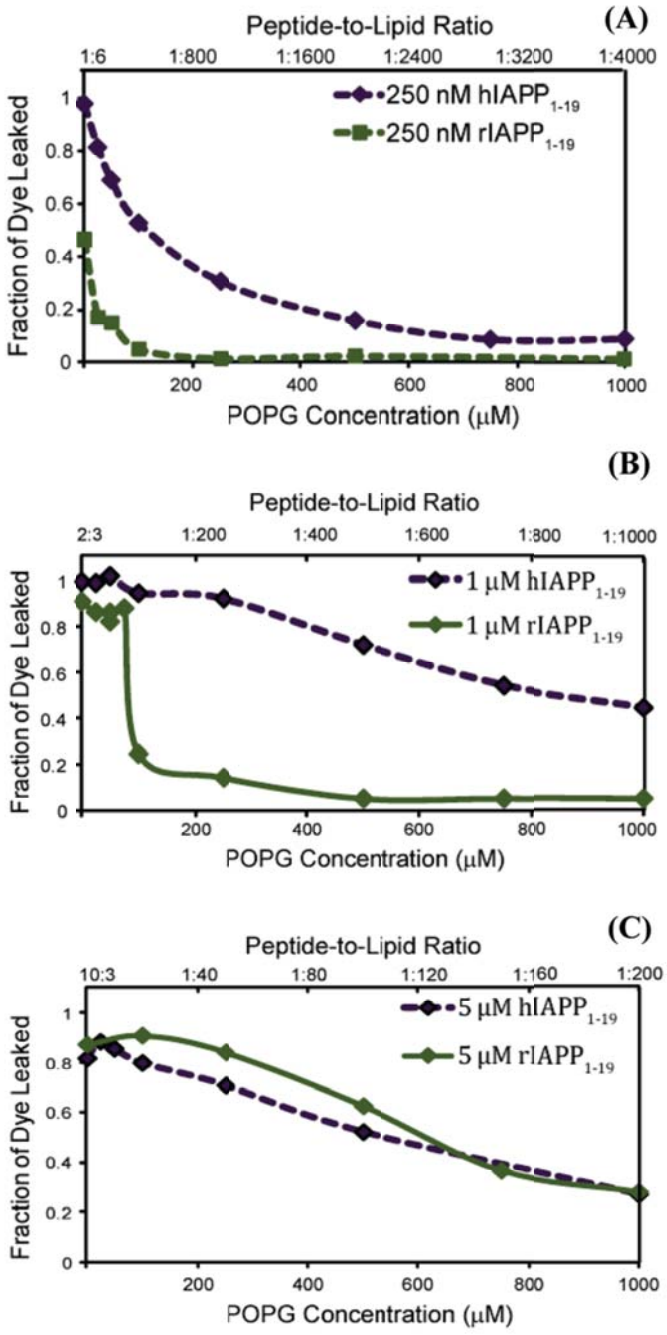

Figure 2.2 Liposome leakage induced by $hIAPP_{1-19}$ (blue diamonds) and the $rIAPP_{1-19}$ fragment (green diamonds) at pH 7.5. The peptide-to-lipid ratio was varied by adding 250 nM (A), 1 μM (B), and 5 μM (C) solutions of either $rIAPP_{1-19}$ or $hIAPP_{1-19}$ to POPG

liposomes containing carboxyfluorescein (1.5 μM) and enough empty POPG liposomes (not containing carboxyfluorescein) to create the indicated molar ratio of peptide to lipid. The fluorescence signal was recorded at 100 s after peptide injection and normalized to the total possible signal upon addition of detergent.

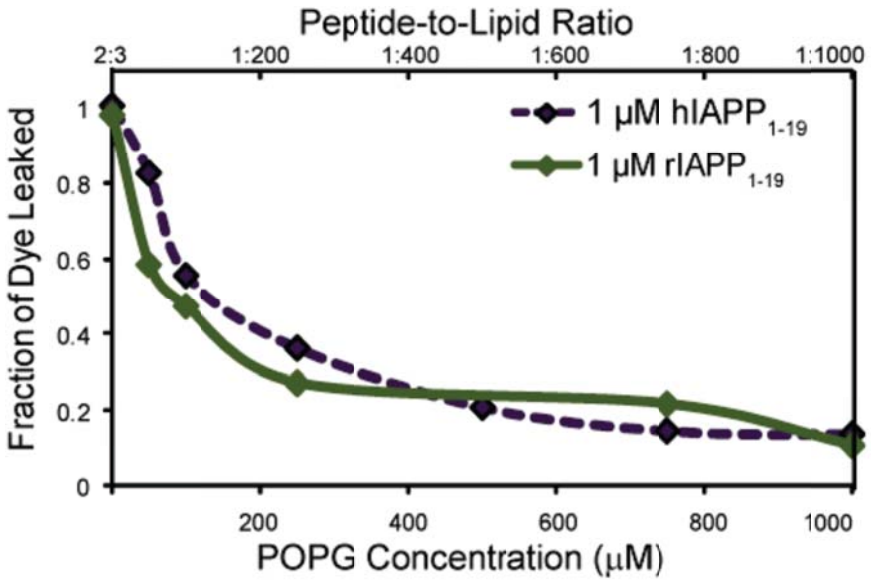

Figure 2.3 Liposome leakage induced by $hIAPP_{1-19}$ (blue diamonds) and the $rIAPP_{1-19}$ fragment (green diamonds) at pH 6.0. Except for the pH, the liposome leakage assay was performed as indicated for the pH 7.3 sample using 1 μM solutions of either $rIAPP_{1-19}$ or $hIAPP_{1-19}$.

membranes if the peptide-to-lipid ratio is high enough. These results are in agreement with our previous study which showed that the $hIAPP_{1-19}$ fragment, which is non-amyloidogenic if bound to a membrane, disrupted POPG vesicles to a similar extent as the strongly amyloidogenic full-length IAPP peptide (*25*). However, all of these assays were performed under conditions that maximized peptide binding (low ionic strength, high content of anionic lipids) and differ from the conditions found in the *in vivo* setting. A more accurate assessment of the damage induced by IAPP could be done by the use of cells loaded with a calcium sensitive dye to monitor changes in intracellular calcium

levels due to the membrane permeabilization induced by IAPP (*15, 40-43*). Full-length hIAPP is known to disrupt the calcium homeostasis of neuroblastoma (SH-SY5Y) cells in a conformation-dependent manner (*15*). Demuro et al. have shown that the addition of monomeric hIAPP and mature fibers of hIAPP had little effect on intercellular calcium levels but the addition of a prefibrillar oligomeric form of hIAPP caused the influx of calcium into the cell. The rise in intercellular calcium concentrations induced by prefibrillar oligomeric hIAPP was dependent on the concentration of hIAPP used, with a maximal response at 12 μg/mL and an EC50 of approximately 3.5 μg/mL (*15*). The membrane disruption induced by hIAPP was large enough to permit leakage of calcein dye from the cell, indicating that prefibrillar oligomeric hIAPP does not simply disrupt calcium homeostasis by the activation of endogenous calcium channels (*15*) as has been reported for the fibrillar form of hIAPP (*43*).

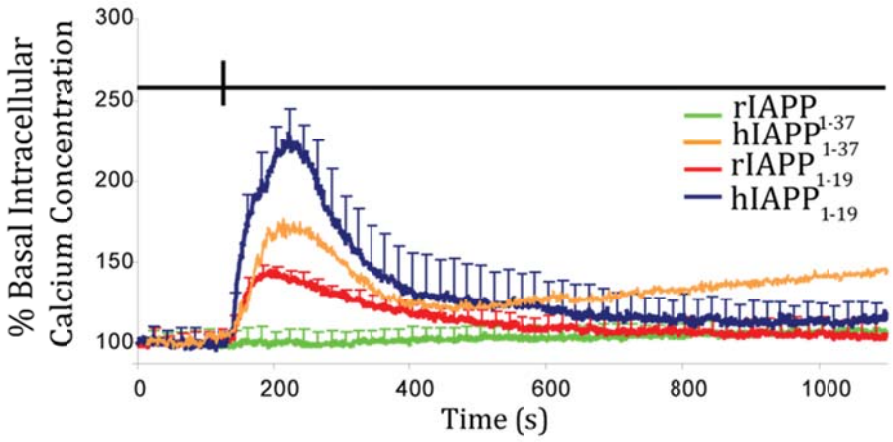

Figure 2.4 Membrane permeabilization in pancreatic islets induced by IAPP. Whole mouse pancreatic islets were loaded 45 min prior to the experiment with 2 μM calcium-sensitive dye fura-2 AM. At 140 s (indicated by a vertical line at the top) 12 μg/mL $hIAPP_{1-19}$, $rIAPP_{1-19}$, or rIAPP1-37 was perfused over the cells. The values given are the average of five islet samples; error bars indicate standard error of the mean.

To test the toxic effect of $hIAPP_{1-19}$ and $rIAPP_{1-19}$ peptides on pancreatic islets, we performed an analogous experiment by measuring the influx of calcium into single islets upon the addition of $hIAPP_{1-19}$ and $rIAPP_{1-19}$. Figure 2.4 shows the effect of $hIAPP_{1-19}$, $rIAPP_{1-19}$, and the full length rIAPP1-37 peptide on the intracellular calcium levels of pancreatic islets. Both $hIAPP_{1-19}$ and $rIAPP_{1-19}$ are toxic at relatively low concentrations, as measured by their ability to disrupt the cellular membrane and allow the influx of calcium into the cell. However, $hIAPP_{1-19}$ is significantly more effective than $rIAPP_{1-19}$ at disrupting the islet membrane as shown in Figure 2.4. The rise in intracellular calcium levels occurred immediately, without the presence of a lag phase that has been detected for the full-length peptide (*15*). Full-length rat IAPP prepared in the same manner does not induce the influx of intracellular calcium into the cell, in agreement with the low cytotoxicity of full-length rIAPP reported in previous studies (*9, 15, 16*).

2.4.3 Comparison of the Binding Affinity of $hIAPP_{1-19}$ and $rIAPP_{1-19}$ for POPG Vesicles

The differences in the membrane disruption induced by $hIAPP_{1-19}$ and $rIAPP_{1-19}$ suggest a difference may exist in the degree of cooperativity in binding to the membrane. Figure 2.5 shows the binding of $rIAPP_{1-19}$ and $hIAPP_{1-19}$ to POPG vesicles as approximated by the measurement of the conformational changes occurring upon binding to lipid membranes. This method is well established for the qualitative measurement of peptide membrane binding (*44*), although conformational changes occurring after membrane binding can complicate quantitative analysis. Like the full-length peptide, both $hIAPP_{1-19}$ and $rIAPP_{1-19}$ exist in a random coil conformation in solution and adopt an R-

helical conformation upon binding to the membrane (*33, 45*). However, noticeable differences can be seen in the binding curves of $hIAPP_{1-19}$ and $rIAPP_{1-19}$ titrated with increasing concentrations of POPG vesicles (Figure 2.5).

As shown in Figure 2.5, $rIAPP_{1-19}$ is nearly as effective in binding as $hIAPP_{1-19}$ at saturating concentrations of POPG but is somewhat less effective at lower concentrations. The binding of full-length human and rat IAPP is known to be a cooperative process with membrane binding proceeding much more efficiently after the formation of small aggregates of IAPP on the membrane (*33*). Full-length rat IAPP differs from full-length human IAPP in that the nucleation of small aggregates by rat IAPP is noticeably impaired as compared to that of human IAPP (*33*). The lower affinity of $rIAPP_{1-19}$ for the membrane at lower concentrations of POPG suggests the rat 1-19 fragment, like full-length rIAPP, is impaired in forming the small aggregates that enhance membrane binding.

2.7 Interaction of $hIAPP_{1-19}$ and $rIAPP_{1-19}$ with Membrane Determined by Differential Scanning Calorimetry

In the accompanying paper detailing the structures of $hIAPP_{1-19}$ and $rIAPP_{1-19}$ in dodecylphosphocholine (DPC) micelles, we show a significant difference in the accessibility of $hIAPP_{1-19}$ and $rIAPP_{1-19}$ to manganese ions (*39*). This indicates $hIAPP_{1-19}$ is located significantly deeper within the hydrophobic core of the micelle than $rIAPP_{1-19}$ and suggests a different mode for the binding to phospholipid bilayers. To test this model, the interaction of $hIAPP_{1-19}$ and $rIAPP_{1-19}$ peptides with membrane was characterized by differential scanning calorimetry (DSC). In general, the phase behavior of lipid membrane systems is highly affected by the presence of guest molecules such as peptides

(*46, 47*). In particular, the effect on the thermally induced gel to liquid-crystalline phase transition and the related thermodynamic variables (melting temperature (*T*m), enthalpy change (ΔH), and entropy change (ΔS)) depends on the nature of the interactions between the peptide and the membrane and on the topology of the peptide relative to the lipid bilayer (*48, 49*). A peptide randomly distributed on the surface of the bilayer disorders the surrounding lipids when the membrane is in the gel phase, lowering the ΔH and *T*m associated with the gel to liquid-crystalline phase transition. The disruption of the lipid-lipid interactions within the membrane also decreases the stability and rigidity of the membrane and therefore decreases the cooperativity of the phase transition. This results in a decreased sharpness of the peak relative to the pure lipid system. The pretransition, reflective of a change in the orientation of the head group of phospholipids, is affected as well. A peptide inserted in a transmembrane orientation has less effect on the physical properties of the membrane because the lipid-lipid interactions are disrupted to a much lower degree than with a surface-associated peptide (*49*). The aggregation of the peptide decreases the perturbation on the membrane by decreasing the surface area of the membrane in contact with the peptide (*50, 51*).

Figure 2.6 shows the effect of $hIAPP_{1-19}$ on mixed DMPC/DMPG vesicles (7/3 ratio). The DSC of pure DMPC/DMPG vesicles shows a single main transition at 24.5 °C indicative of the gel to liquid-crystalline phase transition and a smaller pretransition at 5.4 °C indicative of the rippled gel-to-gel phase transition. The addition of $hIAPP_{1-19}$ up to 2 mol % had a very little effect on the thermodynamics of the gel to liquid-crystalline phase transition. This indicates the lipid-lipid interactions stabilizing the membrane are largely intact and could suggest that the peptide binds in a transmembrane orientation in an

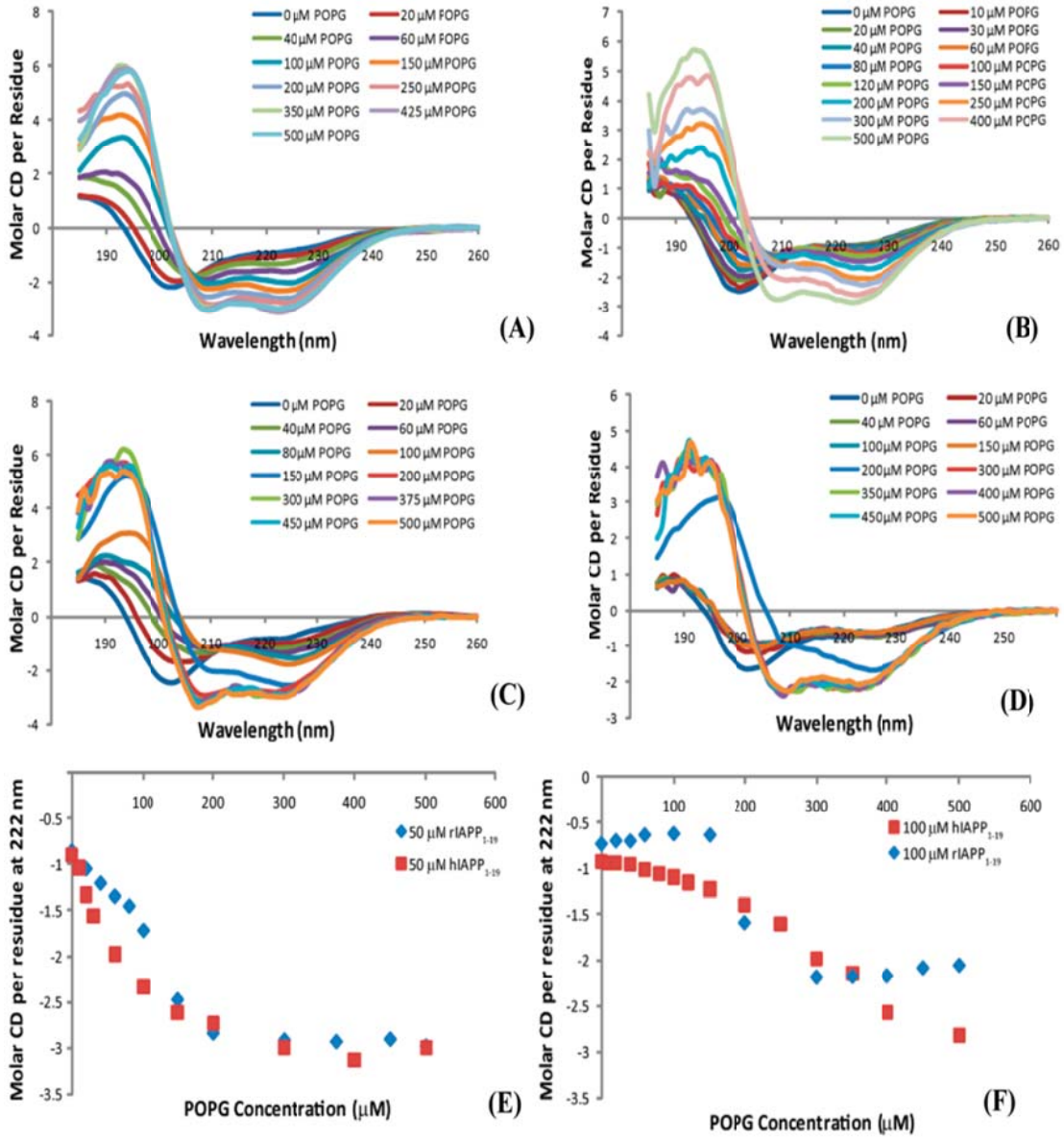

Figure 2.5 CD spectra of 50 μM hIAPP$_{1\text{-}19}$ (A), 100 μM hIAPP$_{1\text{-}19}$ (B), 50 μM rIAPP$_{1\text{-}19}$ (C), and 100 μM rIAPP$_{1\text{-}19}$ (D) at the indicated concentrations of POPG. Plots of the molar CD per residue at 222 nm for 50 μM hIAPP$_{1\text{-}19}$ and rIAPP$_{1\text{-}19}$ (E) and 100 μM hIAPP$_{1\text{-}19}$ and rIAPP$_{1\text{-}19}$ (F) with the indicated concentrations of POPG. All spectra were obtained in 10 mM sodium phosphate buffer, pH 7.3.

aggregated state, as previously inferred for the full-length human peptide (*33, 52, 53*). Self-association of the peptide reduces the number of lipid molecules in contact with the peptide and is therefore expected to decrease the influence of the peptide on the physical properties of the membrane.

Rat $IAPP_{1-19}$ has a much different effect on the membrane (Figure 7). At low concentrations of peptide (0.5-0.75 mol %) the peptide only slightly reduces the ΔH of the main phase transition, but the peptide has a large effect on the pretransition peak reflective of the rippled gel-to-gel phase transition, shifting it to higher temperatures and dramatically increasing the height of the peak for membranes containing 0.5 mol % $rIAPP_{1-19}$. An increase in the pretransition peak height is unusual as most substances tend to reduce the enthalpy change associated with the rippled gel-to-gel phase transition. The rippled gel phase is similar to the gel phase except for the existence of point defects in the

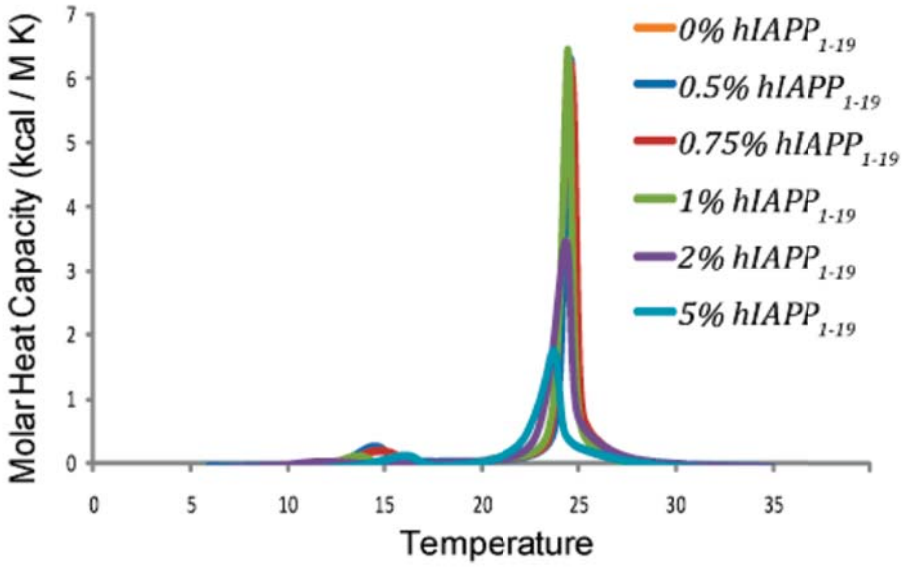

Figure 2.6 Differential scanning calorimetry of the pretransition and the main gel to liquid-crystalline phase transition of DMPC/DMPG (7/3) vesicles at the indicated molar

ratio of $hIAPP_{1-19}$ to lipid. Peptide and lipids were codissolved in a chloroform/ethanol solution, dried, and resuspended in sodium phosphate buffer, pH 7.3, with 150 mM NaCl.

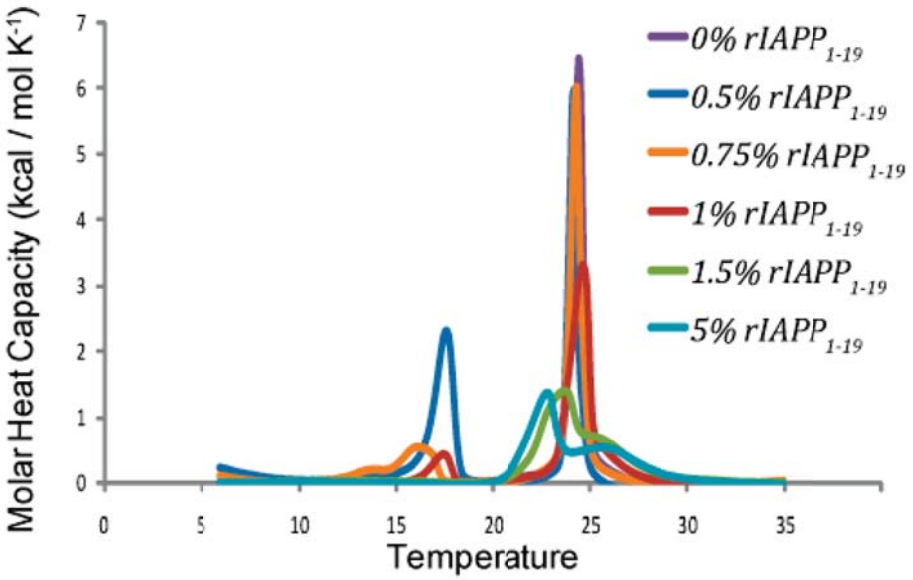

Figure 2.7 Differential scanning calorimetry of the pretransition and the main gel to liquid-crystalline phase transition of DMPC/DMPG (7/3) vesicles at the indicated molar ratio of $rIAPP_{1-19}$ to lipid. Peptide and lipids were codissolved in a chloroform/ethanol solution, dried, and resuspended in 10 mM sodium phosphate buffer, pH 7.3, with 150 mM NaCl.

bilayer caused by a small percentage of molecules in the fluid phase (*54*). The existence of these defects in turn leads to periodic ripples in the membrane surface. Most peptides disorder the gel phase therefore reducing the enthalpy change associated with the rippled gel-to-gel phase transition as defects are present in both phases. An increase in ΔH for the pretransition can be associated with a decrease in the ripple periodicity, which in turn is related to curvature changes in the membrane region and hydrophobic core of the bilayer induced by the peptide binding to the surface of the membrane (*54, 55*). The formation of ripples in a lipid bilayer has been detected with a surfactant that induces positive curvature in the membrane (*56*). Unlike $hIAPP_{1-19}$, the gel to liquid-crystalline phase transition of membranes containing $rIAPP_{1-19}$ is significantly different at higher

concentrations of peptide. At higher concentrations the gel to liquid-crystalline transition is greatly reduced in height and splits into two peaks, one peak with a phase transition at a lower temperature than the pure lipid peak and one peak at a higher temperature than the pure lipid peak. The splitting of a phase transition peak is usually indicative of lipid domain formation, with one peak corresponding to peptide-enriched domains of lipids and the other to peptide-poor domains of lipid (*57, 58*). The greater perturbation of the lipid bilayer by $rIAPP_{1-19}$ indicated by the DSC results suggests that, unlike $hIAPP_{1-19}$, $rIAPP_{1-19}$ may be bound to the surface of the bilayers and not in the active conformation necessary to form pores. This is consistent with the membrane orientation of IAPP peptides determined from our NMR studies (*39*).

2.5 Conclusions Regarding Membrane Disruptive Effects of $IAPP_{1-19}$

The $_{1-19}$ peptide fragment of human IAPP (or amylin) is of particular interest in amyloidogenic protein research as it disrupts model anionic membranes to a near-identical extent as the full-length IAPP peptide but is conformationally stable; once bound to the membrane in an active α-helical form, it does not proceed to form amyloid fibers (*25*). This feature is important for the study of the IAPP peptide, whose rapid and complex aggregation process leads to considerable difficulties in biophysical studies. One of the key arguments for the importance of IAPP amyloid fibers, rather than other oligomeric states of the peptide, in the death of *β*-cells during type II diabetes is the lack of toxicity of the non-amyloidogenic rat version of the peptide. In light of the nearly identical sequences of the rat and human versions of IAPP sequence in the 1-19 region of

the peptide, the membrane disrupting effect of $hIAPP_{1-19}$ is surprising. In this study, we confirmed that the membrane-disrupting activity previously reported for highly charged model membranes also exists for islet cells under physiological conditions. Our results suggest an important role for His18 in the early stages of aggregation and membrane binding. Histidine-18 has previously been implicated in the rate of assembly of amyloid fibers, with amyloid fiber formation proceeding much more slowly when His18 is protonated at a low pH (*38*). In fact, the R18H substitution in the $rIAPP_{1-37}$ is sufficient to turn the peptide from being non-amyloidogenic to slightly amyloidogenic, which is most likely due to the disruption of the stacking of the β-sheets forming the amyloid fiber by the protonated arginine residue (*59*). However, mature amyloid fibers show relatively little toxicity to *β*-cells, and a different mechanism is likely to operate during the earlier stages of aggregation where the toxicity of the peptide is highest and large aggregates are absent. Our results show, for the relatively non-amyloidogenic but toxic 1-19 fragments of the peptide, that the His18 residue also plays a key role in controlling the toxicity of the peptide by modulating the interactions of IAPP with the phospholipid membrane.

I would like to thank Professor Ari Gafni and his research group for their interest in this work and for generous access to their CD spectrometer. Jeffery Brender in help with the preparation of the manuscript, and Kendra Reid and the Kennedy group for the calcium influx measurements and islet extraction.

2.6 Bibliography

1. Clark, A., and Nilsson, M.R. (2004) Islet amyloid: a complication of islet dysfunction or an aetiological factor in type 2 diabetes? *Diabetologia 47*, 157–169.

2. Hoppener, J.W.M., and Lips, C.J.M. (2006) Role of islet amyloid in type 2 diabetes mellitus. *The International Journal of Biochemistry & Cell Biology 38*, 726–736.

3. Lorenzo, A., and Yankner, B.A. (1996) Amyloid fibril toxicity in Alzheimer's disease and diabetes, in *Neurobiology of Alzheimer's Disease*, pp 89-95.

4. Matveyenko, A.V., and Butler, P.C. (2006) Islet amyloid polypeptide (IAPP) transgenic rodents as models for type 2 diabetes. *Institute for Laboratory and Animal Research Journal 47*, 225–233.

5. Haataja, L., Gurlo, T., Huang, C.J., and Butler, P.C. (2008) Islet amyloid in type 2 diabetes, and the toxic oligomer hypothesis. *Endocrine Reviews 29*, 302–316.

6. Hoppener, J.W.M., Oosterwijk, C., Nieuwenhuis, M.G., Posthuma, G., Thijssen, J.H.H., Vroom, T.M., Ahren, B., and Lips, C.J.M. (1999) Extensive islet amyloid formation is induced by development of type II diabetes mellitus and contributes to itsprogression: pathogenesis of diabetes in a mouse model. *Diabetologia 42*, 427–434.

7. Soeller, W.C., Janson, J., Hart, S.E., Parker, J.C., Carty, M.D., Stevenson, R.W., Kreutter, D.K., and Butler, P.C. (1998) Islet amyloid-associated diabetes in obese A(vy)/a mice expressing human islet amyloid polypeptide. *Diabetes 47*, 743–750.

8. Matveyenko, A.V., and Butler, P.C. (2006) Beta-cell deficit due to increased apoptosis in the human islet amyloid polypeptide transgenic (HIP) rat recapitulates the metabolic defects present in type 2 diabetes. *Diabetes 55*, 2106–2114.

9. Huang, C. J., Haataja, L., Gurlo, T., Butler, A.E., Wu, X., Soeller, W.C., and Butler, P.C. (2007) Induction of endoplasmic reticulum stress-induced beta-cell apoptosis and accumulation of polyubiquitinated proteins by human islet amyloid polypeptide. *Am. J Physiol. Endocrinol. Metab. 293*, E1656–E1662.

10. Janson, J., Soeller, W.C., Roche, P.C., Nelson, R.T., Torchia, A. J., Kreutter, D. K., and Butler, P. C. (1996) Spontaneous diabetes mellitus in transgenic mice expressing human islet amyloid polypeptide. *Proceedings of the National Academy of Sciences. U.S.A. 93*, 7283–7288.

11. Butler, A.E., Janson, J., Soeller, W.C., and Butler, P.C. (2003) Increased beta-cell apoptosis prevents adaptive increase in beta-cell mass in mouse model of type 2 diabetes Evidence for role of islet amyloid formation rather than direct action of amyloid. *Diabetes 52*, 2304–2314.

12. Hull, R.L., Shen, Z.P., Watts, M.R., Kodama, K., Carr, D.B., Utzschneider, K. M., Zraika, S., Wang, F., and Kahn, S.E. (2005) Long-term treatment with rosiglitazone and metformin reduces the extent of, but does not prevent, islet amyloid deposition in mice expressing the gene for human islet amyloid polypeptide. *Diabetes 54*, 2235–2244.

13. Tasaka, Y., Nakaya, F., Matsumoto, H., Iwamoto, Y., and Omori, Y. (1995) Pancreatic amylin content in human diabetic subjects and its relation to diabetes. *Pancreas 11*, 303–308.

14. Bell, E.T. (1959) Hyalinization of the islets of Langerhans in non-diabetic individuals. *Am. J. Pathol. 35*, 801–805.

15. Demuro, A., Mina, E., Kayed, R., Milton, S.C., Parker, I., and Glabe, C.G. (2005) Calcium dysregulation and membrane disruption as a ubiquitous neurotoxic mechanism of soluble amyloid oligomers. *J. Biol. Chem. 280*, 17294–17300.

16. Janson, J., Ashley, R.H., Harrison, D., McIntyre, S., and Butler, P.C. (1999) The mechanism of islet amyloid polypeptide toxicity is membrane disruption by intermediate-sized toxic amyloid particles. *Diabetes 48*, 491–498.

17. Konarkowska, B., Aitken, J.F., Kistler, J., Zhang, S.P., and Cooper, G.J.S. (2006) The aggregation potential of human amylin determines its cytotoxicity towards islet beta-cells. *FEBS J. 273*, 3614–3624.

18. Meier, J.J., Kayed, R., Lin, C.Y., Gurlo, T., Haataja, L., Jayasinghe, S., Langen, R., Glabe, C.G., and Butler, P.C. (2006) Inhibition of human IAPP fibril formation does not prevent beta-cell death: evidence for distinct actions of oligomers and fibrils of human IAPP. *Am. J. Physiol. 291*, E1317-E1324.

19. Ritzel, R.A., and Butler, P.C. (2003) Replication increases beta-cell vulnerability to human islet amyloid polypeptide-induced apoptosis. *Diabetes 52*, 1701–1708.

20. Anguiano, M., Nowak, R.J., and Lansbury, P.T. (2002) Protofibrillar islet amyloid polypeptide permeabilizes synthetic vesicles by a pore-like mechanism that may be relevant to type II diabetes. *Biochemistry 41*, 11338–11343.

21. Lin, C.Y., Gurlo, T., Kayed, R., Butler, A.E., Haataja, L., Glabe, C.G., and Butler, P.C. (2007) Toxic human islet amyloid polypeptide (h-IAPP) oligomers are intracellular, and vaccination to induce anti-toxic oligomer antibodies does not prevent h-IAPP induced beta-cell apoptosis in h-IAPP transgenic mice. *Diabetes 56*, 1324–1332.

22. Quist, A., Doudevski, L., Lin, H., Azimova, R., Ng, D., Frangione, B., Kagan, B., Ghiso, J., and Lal, R. (2005) Amyloid ion channels: A common structural link for protein-misfolding disease. *Proceedings of the National Academy of Sciences U.S.A. 102*, 10427–10432.

23. (a) Porat, Y., Kolusheva, S., Jelinek, R., and Gazit, E. (2003) The human islet amyloid polypeptide forms transient membrane-active prefibrillar assemblies. *Biochemistry 42*, 10971–10977. (b) Brender, J.R., Durr, U.H.N., Heyl, D., Budarapu, M.B., and Ramamoorthy, A. (2007) Membrane fragmentation by human islet amyloid polypeptide detected by solid-state NMR spectroscopy of membrane nanotubes. *Biochimica et Biophysica Acta 1768*, 2026–2029.

24. Powers, E.T., and Powers, D.L. (2008) Mechanisms of protein fibril formation: Nucleated polymerization with competing off pathway aggregation. *Biophysical Journal 94*, 379–391.

25. Brender, J.R., Lee, E.L., Cavitt, M.A., Gafni, A., Steel, D.G., and Ramamoorthy, A. (2008) Amyloid fiber formation and membrane disruption are separate processes localized in two distinct regions of IAPP, the type-2-diabetes-related peptide. *Journal of the American Chemical Society 130*, 6424–6429.

26. Khemtemourian, L., Killian, J.A., Hoppener, J.W., and Engel, M.F. (2008) Recent insights in islet amyloid polypeptide induced membrane disruption and its role in beta-cell death in type 2 diabetes mellitus. *Experimental Diabetes Research* 421287.

27. Necula, M., Kayed, R., Milton, S., and Glabe, C.G. (2007) Small molecule inhibitors of aggregation indicate that amyloid beta oligomerization and fibrillization pathways are independent and distinct. *Journal of Biological Chemistry 282*, 10311–10324.

28. Yoshiike, Y., Kayed, R., Milton, S.C., Takashima, A., and Glabe, C.G. (2007) Pore-forming proteins share structural and functional homology with amyloid oligomers. *Neuromolecular Medicine 9*, 270-275.

29. Pralong, W.F., Bartley, C., and Wollheim, C.B. (1990) Single islet beta-cell stimulation by nutrients Relationship between pyridine-nucleotides, cytosolic Ca2+ and secretion. *European Molecular Biology Organization Journal 9*, 53–60.

30. Bechinger, B., and Lohner, K. (2006) Detergent-like actions of linear amphipathic cationic antimicrobial peptides. *Biochimica et Biophysica Acta1758*, 1529–1539.

31. Shai, Y. (1999) Mechanism of the binding, insertion and destabilization of phospholipid bilayer membranes by R-helical antimicrobial and cell non-selective membrane-lytic peptides. *Biochimica et Biophysica Acta1462*, 55–70.

32. Hoskin, D.W., and Ramamoorthy, A. (2008) Studies on anticancer activities of antimicrobial peptides. *Biochimica et Biophysica Acta1778*, 357–375.

33. Knight, J.D., Hebda, J.A., and Miranker, A.D. (2006) Conserved and cooperative assembly of membrane-bound R-helical states of islet amyloid polypeptide. *Biochemistry 45*, 9496–9508.

34. Vanhulst, K.L., Hackeng, W.H.L., Hoppener, J.W.M., Vanjaarsveld, B.C., Nieuwenhuis, M.G., Blankenstein, M.A., and Lips, C.J.M. (1994) An improved method for the determination of islet amyloid polypeptide levels in plasma. *Annals of Clinical Biochemistry 31*, 165–170.

35. Ariga, T., McDonald, M.P., and Yu, R.K. (2008) Role of ganglioside metabolism in the pathogenesis of Alzheimer's disease; a review. *Journal of Lipid Research 49*, 1157–1175.

36. Lee, S.J., Liyanage, U., Bickel, P.E., Xia, W.M., Lansbury, P.T., and Kosik, K.S. (1998) A detergent-insoluble membrane compartment contains A beta in vivo. *Nature Medicine 4*, 730–734.

37. Jaikaran, E., Higham, C.E., Serpell, L.C., Zurdo, J., Gross, M., Clark, A., and Fraser, P.E. (2001) Identification of a novel human islet amyloid polypeptide beta-sheet domain and factors influencing fibrillogenesis. *Journal of Molecular Biology 308*, 515–525.

38. Abedini, A., and Raleigh, D.P. (2005) The role of His-18 in amyloid formation by human islet amyloid polypeptide. *Biochemistry 44*, 16284–16291.

39. Nanga, R.P.R., Brender, J.R., Xu, J., Veglia, G., and Ramamoorthy, A. (2008) Structures of rat and human islet amyloid polypeptide IAPP1-19 in micelles by NMR spectroscopy. *Biochemistry 47*, 12689–12697.

40. Kawahara, M., Kuroda, Y., Arispe, N., and Rojas, E. (2000) Alzheimer's beta-amyloid, human islet amylin, and prion protein fragment evoke intracellular free calcium elevations by a common mechanism in a hypothalamic GnRH neuronal cell line. *Journal of Biological Chemistry. 275*, 14077–14083.

41. Mattson, M.P., and Goodman, Y. (1995) Different amyloidogenic peptides share a similar mechanism of neurotoxicity involving reactive oxygen species and calcium. *Brain Research 676*, 219-224.

42. Casas, S., Gomis, R., Gribble, F.M., Altirriba, J., Knuutila, S., and Novials, A. (2007) Impairment of the ubiquitin-proteasome pathway is a downstream endoplasmic reticulum stress response induced by extracellular human islet amyloid polypeptide and contributes to pancreatic beta-cell apoptosis. *Diabetes 56*, 2284–2294.

43. Casas, S., Novials, A., Reimann, F., Gomis, R., and Gribble, F.M. (2008) Calcium elevation in mouse pancreatic beta cells evoked by extracellular human islet amyloid polypeptide involves activation of the mechanosensitive ion channel TRPV4. *Diabetologia* 51, 2252-2262.

44. Ladokhin, A. S., and White, S. H. (1999) Folding of amphipathic alpha-helices on membranes: Energetics of helix formation by melittin. *Journal of Molecular Biology 285*, 1363–1369.

45. Jayasinghe, S. A., and Langen, R. (2005) Lipid membranes modulate the structure of islet amyloid polypeptide. *Biochemistry 44*, 12113–12119.

46. Pappalardo, G., Milardi, D., Magri, A., Attanasio, F., Impellizzeri, G., La Rosa, C., Grasso, D., and Rizzarelli, E. (2007) Environmental factors differently affect human and rat IAPP: Conformational preferences and membrane interactions of IAPP17-29 peptide derivatives. *Chemistry A European Journal. 13*, 10204–10215.

47. Grasso, D., Milardi, D., La Rosa, C., and Rizzarelli, E. (2001) DSC study of the interaction of the prion peptide PrP106-126 with artificial membranes. *New Journal of Chemistry. 25*, 1543–1548.

48. Henzler-Wildman, K.A., Martinez, G.V., Brown, M.F., and Ramamoorthy, A. (2004) Perturbation of the hydrophobic core of lipid bilayers by the human antimicrobial peptide LL-37. *Biochemistry 43*, 8459–8469.

49. McElhaney, R.N. (1986) Differential scanning calorimetric studies of lipid protein interactions in model membrane systems. *Biochimica et Biophysica Acta864*, 361–421.

50. Ivanova, V.P., Makarov, I.M., Schaffer, T.E., and Heimburg, T. (2003) Analyzing heat capacity profiles of peptide-containing membranes: cluster formation of gramicidin A. *Biophysical Journal. 84*, 2427–2439.

51. Ramamoorthy, A., Lee, D.K., Santos, J.S., and Henzler-Wildman, K.A. (2008) Nitrogen-14 solid-state NMR spectroscopy of aligned phospholipid bilayers to probe peptide-lipid interaction and oligomerization of membrane associated peptides. *Journal of the American Chemical Society 130*, 11023–11029.

52. Knight, J.D., and Miranker, A.D. (2004) Phospholipid catalysis of diabetic amyloid assembly. *Journal of Molecular Biology 341*, 1175–1187.

53. Mishra, R., Bulic, B., Sellin, D., Jha, S., Waldmann, H., and Winter, R. (2008) Small-molecule inhibitors of islet amyloid polypeptide fibril formation. *Angewandte Chemie International Edition 47*, 4679–4682.

54. Heimburg, T. (2000) A model for the lipid pretransition: Coupling of ripple formation with the chain-melting transition. *Biophysical Journal 78*, 1154–1165.

55. Sun, X.Q., and Gezelter, J.D. (2008) Dipolar ordering in the ripple phases of molecular-scale models of lipid membranes. *Journal of Physical Chemistry B 112*, 1968–1975.

56. Brasseur, R., Braun, N., El Kirat, K., Deleu, M., Mingeot-Leclercq, M.P., and Dufrene, Y.F. (2007) The biologically important surfactin lipopeptide induces nanoripples in supported lipid Bilayers. *Langmuir 23*, 9769–9772.

57. Epand, R.M. (2007) Detecting the presence of membrane domains using DSC. *Biophysical Chemistry. 126*, 197–200.

58. Epand, R.F., Schmitt, M.A., Gellman, S.H., and Epand, R.M. (2006) Role of membrane lipids in the mechanism of bacterial species selective toxicity by two alpha/beta-antimicrobial peptides. *Biochimica et Biophysica Acta1758*, 1343–1350.

59. Green, J., Goldsbury, C., Min, T., Sunderji, S., Frey, P., Kistler, J., Cooper, G., and Aebi, U. (2003) Full-length rat amylin forms fibrils following substitution of single residues from human amylin. *Journal of Molecular Biology 326*, 1147–1156.

CHAPTER 3

THE ROLE OF ZINC IN THE AGGREGATION OF HUMAN ISLET AMYLOID POLYPEPTIDE

3.1 Summary

Human Islet Amyloid Polypeptide (hIAPP) is a highly amyloidogenic protein found in islet cells of patients with type II diabetes. Because hIAPP is highly toxic to β-cells under certain conditions, it has been proposed that hIAPP is linked to the loss of β-cells and insulin secretion in type II diabetics. One of the interesting questions surrounding this peptide is how the toxic and aggregation prone hIAPP peptide can be maintained in a safe state at the high concentrations that are found in the secretory granule where it is stored. We show here zinc, which is found at millimolar concentrations in the secretory granule, significantly inhibits hIAPP amyloid fibrillogenesis at concentrations similar to those found in the extracellular environment. Zinc has a dual effect on hIAPP fibrillogenesis: it increases the lag-time for fiber formation and decreases the rate of addition of hIAPP to existing fibers at lower concentrations, while having the opposite effect at higher concentrations. Experiments at an acidic pH which partially neutralizes the change in charge upon zinc binding show inhibition is largely due to an electrostatic effect at His18. High-resolution structures of

This chapter is a version of a published paper Brender, J.R., Hartman, K., Nanga, R.P., Popovych, N., Salud Bea, R., Vivekanandan, S., Marsh, E.N., and Ramamoorthy, A., (2010) Role of Zinc in Human Islet Amyloid Polypeptide Aggregation. Journal of the American Chemical Society 132, 8973-8983.

hIAPP determined from NMR experiments confirm zinc binding to His18 and indicate zinc induces localized disruption of the secondary structure of IAPP in the vicinity of His18 of a putative helical intermediate of IAPP. The inhibition of the formation of aggregated and toxic forms of hIAPP by zinc provides a possible mechanism between the recent discovery of linkage between deleterious mutations in the SLC30A8 zinc transporter, which transports zinc into the secretory granule, and type II diabetes.

3.2 Introduction

Human Islet Amyloid Polypeptide (hIAPP) is a polypeptide hormone secreted from pancreatic *β*-cells in response to glucose or other chemical signals. Under normal conditions, hIAPP is involved in glycemic control *(1).* However, in type II diabetics, hIAPP aggregates in the pancreas to form dense, insoluble extracellular fibrillar deposits known as amyloid fibers. The amyloid deposits are composed of *β*-sheet aggregates with a characteristic structure similar to those found in Alzheimer's, Parkinson's, Huntington's, and a variety of other degenerative diseases *(2).* While hIAPP aggregates at nanomolar concentrations *in vitro*, forming both the amyloid fibers characteristic of type II diabetes and smaller oligomeric species that have been repeatedly linked to *β*-cell destruction *(3-7),* it is safely stored in the secretory granule at millimolar concentrations *(8).* The aggregation of hIAPP is highly sensitive to circumstances in which the experiment is run*;* both the kinetics and the morphology and yield of the final amyloid product of IAPP can be influenced by subtle variations in experimental conditions *(9, 10).* Given that hIAPP in isolation spontaneously aggregates at concentrations 2 to 3 orders of magnitude lower than those present in the secretory granule where it is stored, it

is reasonable to look for other factors that act as chaperones to stabilize hIAPP in a nontoxic form in normal individuals *(11, 12).* There is considerable evidence that the dysregulation of such amyloid chaperones acts as a trigger for the pathological aggregation of other amyloid proteins *(11, 12).* The dysregulation of metal ion homeostasis in particular has received attention due to the early discovery of a high prevalence of metal ions in amyloid deposits. High affinity metal binding sites have been identified in a high percentage of amyloid proteins including *β*2-microglubulin *(13, 14),* amyloid-beta (amyloid *β*) *(15-19),* α-synuclein *(20-22),* superoxide dismutase *(23),* ABri *(24),* NAC *(25),* and mammalian prion protein *(26).* In some cases, such as with Parkinson's disease, clinical and epidemiological evidence directly links an increased heavy metal intake in environmental contaminated areas to an abnormally high incidence of neurodegenerative disease *(27-29).* In other cases, a pathological amyloid aggregation appears to be caused by a deficient metal transport process as shown by the significant reduction in amyloid plaques found in mice deficient for the zinc transporter ZnT3 *(30).* The binding of metal ions can have profound effects on amyloid aggregation, frequently causing rapid precipitation, a dramatic increase in fibrillogenesis, changes in the toxicity of the amyloid aggregates, and alterations in the morphology of the final aggregate product. Even the transient millisecond exposure to zinc upon the synaptic pulsing of neurons can rapidly stimulate amyloid *β* aggregation *(19).* In contrast to other amyloid proteins for which high-affinity metal binding sites have been identified, the influence of metal binding on hIAPP has not been clearly established. There is evidence that copper can stimulate the production of H_2O_2 by hIAPP *(31),* possibly generating oxidative stress in a manner similar to Amyloid β *(32).* In addition to its possible role in generating *β*-cell

oxidative stress, copper (II) has also been found to mediate the membrane-interaction of a fragment (17-29) of hIAPP *(33).* Similar modifications of membrane interactions have been found with calcium and full-length hIAPP *(34).* While evidence exists for the interaction of Cu (II) with hIAPP, the ability of other metals to affect hIAPP has been almost entirely unexplored. Zinc is of particular interest as the zinc content of pancreatic *β*-cells is among the highest in the body and various clinical and epidemiological studies suggest zinc deficiency is a common symptom of type II diabetes *(35, 36).* The recent discovery between the genetic linkage between the SLC30A8 gene *(37-40),* which transports zinc into the secretory granule where insulin and hIAPP are stored *(41-43),* and type II diabetes suggests zinc could have an impact on hIAPP cytotoxicity toward *β*-cells.

3.3 Experimental Procedures

3.3.1 Peptide Synthesis.

Human-IAPP (sequence KCNTATCATQRLANFLVHSSNNFGAILSSTNVGSNTY) was synthesized with an amidated C-terminus and a disulfide bridge between residues 2 and 7 using *t*-Boc-protected amino acids on MBHA resin using a standard solid-phase synthesis protocol *(44).* The crude product was dissolved in 3.5 M GuHCl and purified on a reverse-phase HPLC on a Waters semi-preparative C18 column equilibrated in 0.1% trifluoroacetic acid and eluted with a linear gradient from 0% to 80% acetonitrile at a flow rate of 10 mL/min. After lyophilization, the semi-pure product was then dissolved in pure water to 2 mg/mL and oxidized with Thallium (III) trifluoroacetate according to the method of Page et al., *(45)* using a 2 h reaction time with stirring followed by additional

purification by reverse-phase HPLC. The purity of the final product (>95%) was checked by analytical HPLC and MALDI-MS.

3.3.2 Kinetic Studies Using Thioflavin Fluorescence.

The kinetics of hIAPP amyloid formation was measured using the increase in fluorescence intensity upon binding of the amyloid fiber to the amyloid specific dye Thioflavin T (ThT). Before the start of the experiment, hIAPP was first solubilized in hexafluoroisopropanol at a concentration of 250 μM to break up any pre-existing aggregates and subsequently lyophilized. To start the aggregation experiment, the lyophilized peptide was first dissolved in deionized water at 4 °C to a concentration of 250 μM, spun through a 0.22 μm filter, and then diluted to a concentration of either 5 or 10 μM with a buffer containing the appropriate amount of $ZnCl_2$ (100 mM Tris with 100 mM NaCl and 25 μM ThT for experiments at pH 7.5, 100 mM sodium acetate with 100 mM NaCl and 25 μM ThT for experiments at pH 5.5). The pH of each sample was individually adjusted to the correct value due to the acidity of $ZnCl_2$. All buffers were previously passed through a Chelex-100 column to remove trace amounts of endogenous zinc. Tris buffer was used due to its low affinity for zinc. Experiments were performed in sealed Corning 96 well clear bottom half area, nonbinding surface plates. Time traces were recorded with Biotek Synergy 2 plate reader using a 440 excitation filter and a 485 emission filter at a constant temperature of 25 °C without shaking. The time-dependence of ThT fluorescence was fitted to a sigmoidal growth model that has empirically been found to reproduce most of the features of amyloid aggregation: where I_0 and I_{max} are the initial and maximum fluorescence values, $t_{1/2}$ is the time required to reach half intensity,

and k is an apparent first-order rate constant for the addition of hIAPP to existing fibers *(46)*. The lag-time t_0, the time predicted by nucleation dependent polymerization theory before detectable amyloid formation occurs, is described by $t_0 = t_{1/2} - 2/k$.

$$I = \frac{I_{\max} - I_0}{1 + e^{(t - t_{1/2})/k}}$$

Equation 3.1 Kinetics of amyloid fiber formations follow a sigmoidal growth curve from which a Boltzman distribution equation can be used to determination of lag time and fiber growth rate obtained from ThT binding experiments.

3.3.3 Electron Microscopy.

Solutions of hIAPP were allowed to incubate for 2 days at pH 7.5 before loading in the presence of either 0, 100, or 1000 μM $ZnCl_2$. Samples were prepared identically to those used for ThT kinetic experiments except the concentration of hIAPP was 100 μM and ThT was not included in the sample. After incubation, 5 μL aliquots were loaded onto Formvar-coated copper grids (Ernest F. Fullam, Inc., Latham, NY) for 2 min, washed twice with 10 μL of deionized water, and then negatively stained for 90 s with 2% uranyl acetate. Samples were imaged with a Philips CM10 Transmission Electron Microscope at 6500× or 15 000× magnification.

3.3.4 NMR Sample Preparation.

Preformed aggregates of hIAPP were removed by dissolving the peptide in hexafluoroisopropanol (HFIP) and removing the solvent by lyophillization as described above. The lyophilized powder was then dissolved first in deuterated HFIP/trifluoroethanol (TFE) and then buffer so that the final solution was 1 mM hIAPP

in 22% HFIP, 8%TFE, 20 mM deuterated Tris at pH 7.5. The spectrum with zinc was obtained by adding zinc to a final concentration of 10 mM from a 100 mM stock solution.

3.3.5 NMR Data Collection and Processing.

All the NMR spectra of hIAPP were recorded at 30 °C using a 900 MHz Bruker Avance NMR spectrometer equipped with a triple-resonance z-gradient cryogenic probe optimized for 1H-detection. Backbone and sidechain assignments were done with the help of homonuclear experiments such as 2D 1H-1H TOCSY (Total Correlation Spectroscopy) and 2D 1H-1H NOESY (Nuclear Overhauser Enhancement Spectroscopy) recorded at 80 and 300 ms mixing time, respectively. Complex data points were acquired for quadrature detection in both frequency dimensions for the 2D experiments and all the spectra were zero-filled in both dimensions to yield matrices of 2048 × 2048 points. Proton chemical shifts were referenced to the methyl signal of 2,2-dimethyl-2-silapentane-5-sulfonate (Cambridge Isotope Laboratories) as an external reference at 0 ppm. All 2D spectra were processed using TopSpin 2.1 software and analyzed using SPARKY *(47).* Initial resonance assignments were carried out using a standard approach reported elsewhere *(48).*

3.3.6 Structure Calculations.

The final structure was calculated with the CYANA 2.1 program package using simulated annealing in combination with molecular dynamics in torsion angle space *(49).* Dihedral angle restraints were calculated directly from the NOE connectivities *(50).* During the first round of structure calculations, only unambiguous long-range NOE

constraints were used to generate a low-resolution fold for the structure. Assignments of the remaining ambiguous NOE cross-peaks were made in an iterative fashion by applying a structure-aided filtering strategy in repeated rounds of structure calculations *(51)*. After the complete assignment of resonances, a total of 100 conformers were calculated in 8000 annealing steps each and the best 10 low energy conformers were selected and visualized using MOLMOL *(52)*.

3.4 Results & Discussion

3.4.1 Zinc Reduces the Extent of hIAPP Amyloid Formation.

To determine if zinc can directly affect amyloidogenesis by hIAPP, we monitored the rate of fibril formation of solutions of 5 and 10 μM hIAPP in the presence of micromolar to millimolar concentrations of $ZnCl_2$ using the fluorescence of the dye Thioflavin T (Figure 3.1) as a marker. Thioflavin T's fluorescence increases markedly upon binding to the stacked β-sheets of amyloid fibers making it a useful specific marker of amyloid formation as other prefibrillar aggregates which lack the characteristic cross β-sheet superstructure of the amyloid fibers do not increase its fluorescence substantially. Zinc significantly affects the formation of IAPP amyloid fibers, as shown by the sharp reduction in Thioflavin T fluorescence when zinc is added to the incubation solution (Figure 3.2). Amyloid formation is strongly affected by zinc in the micromolar concentration range, with the final Thioflavin T fluorescence value at the end of the incubation period decreasing to an intensity of about half the zinc free value at 250 μM $ZnCl_2$ before apparent saturation is reached at approximately 750 μM $ZnCl_2$ (Figure 3.2).

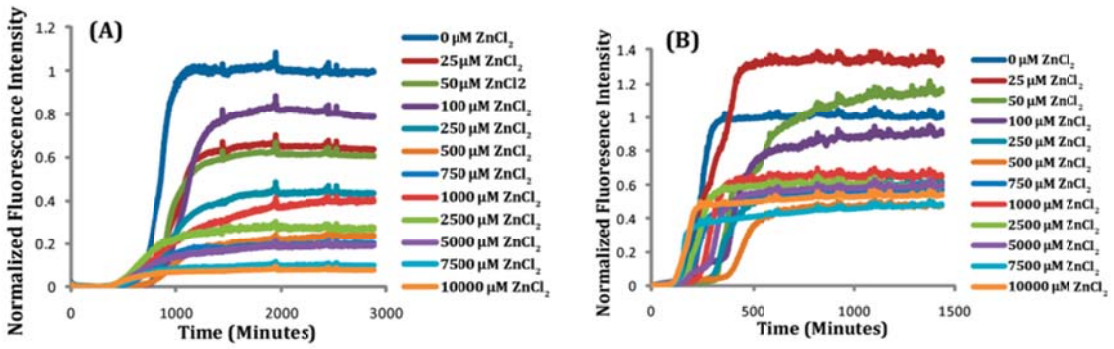

Figure 3.1 Zinc inhibits hIAPP amyloid fibril formation at pH 7.5. Amyloid formation by hIAPP as a function of zinc concentration as followed by the amyloid-specific dye Thioflavin T: (A) 5 μM and (B) 10 μM hIAPP with indicated concentrations of ZnCl2. Traces are averages for *n*) 9 (5 μM hIAPP) and *n*) 7 (10 μM hIAPP) runs. The kinetic analysis of these traces and the variation of the final THT fluorescence intensity as a function of zinc concentration (along with the associated error bars) are given in Figures 4 and 2, respectively.

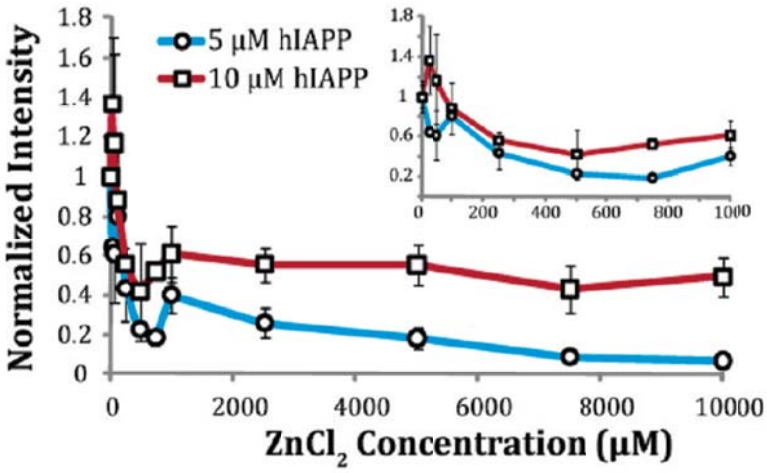

Figure 3.2 Zinc decreases the equilibrium concentration of hIAPP fibers at pH 7.5. Variation in the fluorescence intensity of the amyloid-bonding dye Thioflavin T as a function of ZnCl2 concentration after fibrillogenesis has completed as extracted from the experimental results presented in Figure 1. Values for 5 and 10 μM were determined after 2 and 1 day(s), respectively. The intensity values were normalized to hIAPP in the absence of zinc. Error bars indicate standard error of measurement (S.E.M) for *n*) 9 (5 μM hIAPP) and *n*) 7 (10 μM hIAPP). Inset shows the effect at lower ZnCl2 concentrations (0-1000 μM).

3.4.2 Zinc Reduces Amyloid Deposition but Does Not Significantly Alter the Final Fiber Morphology.

The results from the Thioflavin T fluorescence assay suggest the stability of the amyloid fibers is negatively affected by zinc. However, some inhibitors are known to interfere with the binding of Thioflavin T to amyloid fibers, leading to a false positive result for inhibition *(53, 54)*. Accordingly, we confirmed the results of the Thioflavin T assay by examining the ultrastructure of the amyloid fibers using electron microscopy. In the absence of zinc, 100 μM solutions of hIAPP massively aggregate to form the dense mats of the long branched fibers typical of amyloid proteins within 48 h (Figure 3.3A). The addition of either 100 μM or 1 mM $ZnCl_2$ during incubation causes a significant reduction in the amount of amyloid deposition on the grid (compare panels B and C to panel A in Figure 3.3), giving an independent confirmation of the results of the Thioflavin T assay. The morphology of amyloid fibers is frequently sensitive to the conditions at which they assemble *(18-19)*. Typically, amyloid fibers grown in the presence of an amyloid inhibitor are usually both thinner and shorter than those grown in its absence due to an enhancement of the fiber breakage rate and impairment of the association of the protofilament subunits that make up the amyloid fiber bundle *(55-59)*. Interestingly, while the total amount of fibers is greatly reduced by zinc, the overall morphology of the individual amyloid fibers remains similar within the limits of the resolution of our instrument. Fibril diameters of ~10 nm were observed consistently in all samples in agreement with previous reports *(9),* indicating zinc does not lead to a decrease in filament width (Figure 3.3D-F). Noticeably shorter or significantly thinner fibers were not seen, indicating Zn^{2+} does not significantly enhance breakage of the fiber or greatly impair the lateral attachment of protofilaments to mature amyloid fibers.

Similar results have been obtained with $CuCl_2$ *(31).* Furthermore, large amorphous nonfibrillar precipitates, which have frequently been observed with other metal-complexed amyloids *(19, 24, 60),* were not detected at either zinc concentration. The inability of the zinc to alter the final fiber morphology likely indicates that some of the IAPP fibers are relatively unaffected by zinc while another significant fraction remains soluble and not extensively aggregated.

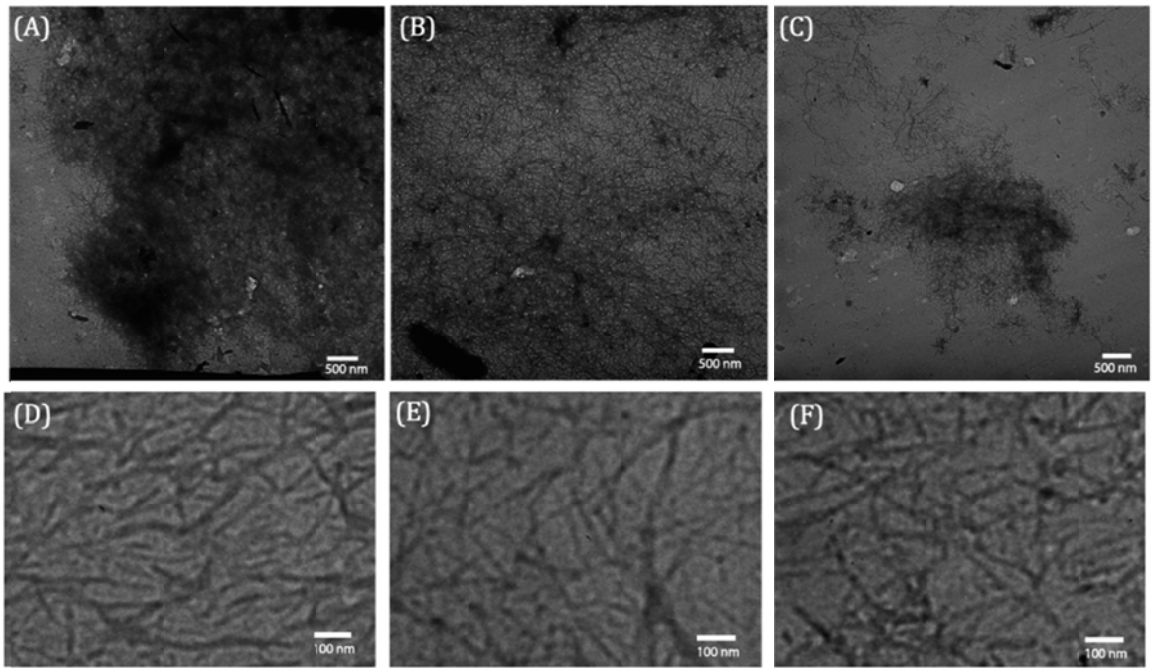

Figure 3.3 Zinc reduces the density of hIAPP fibrils while maintaining a similar fibril morphology. (Top) Electron micrographs showing the effect of zinc on total amyloid deposition and fiber morphology. Aliquots from a 100 μM hIAPP solution incubated with (A) 0 μM ZnCl2, (B) 100 μM ZnCl2, and (C) 1000 μM ZnCl2 were deposited on copper grids after an incubation period of 2 days and imaged at 6500× magnification. (Bottom) Electron micrographs of hIAPP incubated with (D) 0 μM ZnCl2, (E) 100 μM ZnCl2, and (F) 1000 μM ZnCl2 imaged at 15 000× magnification.

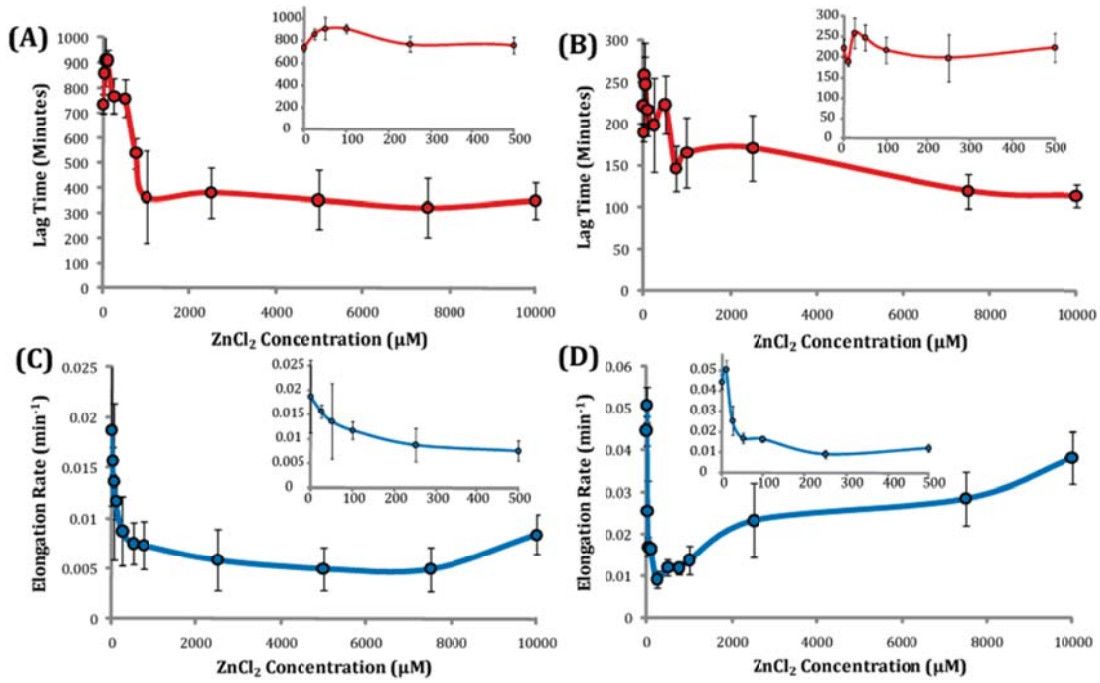

Figure 3.4. Zinc has a bimodal effect on hIAPP fibrillogenesis at pH 7.5. Analysis of the kinetics of hIAPP at pH 7.5 according to a sigmoidal growth model. A variation in the lag-time ($t1/2 - 2/k$) before detectable fiber formation as a function of ZnCl2 at (A) 5 μM and (B) 10 μM hIAPP. Variations in the apparent first-order elongation rate constant (k) at (C) 5 μM and (D) 10 μM hIAPP. Error bars indicate standard error of measurement (SEM) for n) 9 (5 μM hIAPP) and n) 7 (10 μM hIAPP). Insets show the effect from 0-500 μM ZnCl2.

3.4.3 Zinc Decreases the Rate of Amyloid Formation at Low Concentrations but Stimulates It at Higher Concentrations.

Amyloid fibers are typically formed in a multistep process that is highly dependent on the formation of energetically unfavorable nuclei. In the initial stages of aggregation before a sufficient population of nuclei are formed (the lag-phase), amyloid formation proceeds very slowly and only trace amounts of amyloid fibers are formed. Once a critical concentration of nuclei is reached, aggregation proceeds exponentially by the addition of protein to the ends of the existing fibers until virtually all of the protein is

converted to amyloid at equilibrium. Examination of the effect of an inhibitor on the kinetic profile is frequently helpful in distinguishing its mode of action. The length of the lag-time before detectable amounts of amyloid fibers are formed, for example, is an indication of the relative stability of early intermediates in the aggregation process. A compound that stabilizes this rare intermediate can be expected according to the nucleation polymerization model to reduce the lag-time, while one that destabilizes it can be expected to have the opposite effect unless it is excessively stabilized to form a stable intermediate. Similarly, the steepness of the polymerization reaction is a reflection of the rate of growth at fiber ends and secondary nucleation (creation of growth sites by fiber breakage or branching). It has been empirically found that amyloid kinetics frequently follow a sigmoidal growth model (Eq. 3.1) *(46)*. Analysis of the aggregation kinetics by this equation reveals a complex dependence of the aggregation rate on the zinc concentration with differing effects on the rate of nucleation and the rate of fibril growth. In particular, the nucleation rate is affected in a multimodal fashion as depicted in a plot of the lag-time before the onset of fiber growth (Figure 3.4). While low concentrations of zinc up to approximately 100 μM cause a modest increase in the lag-time of 5 μM hIAPP (Figure 3.4A inset), this effect is reversed as the zinc concentration is further increased with the lag-time decreasing nearly linearly before it plateaus at approximately half the zinc free value at 1000 μM $ZnCl_2$ (Figure 3.4A). A similar effect can be seen when hIAPP is incubated at 10 μM concentration, although the concentration range in which the lag-time is decreased is comparatively much less (Figure 3.4B). While zinc has a relatively modest effect on the nucleation rate at physiological concentrations, it has a stronger and relatively consistent effect on the fibril growth rate. Zinc has a strong

inhibitory effect on the fibril growth rate of 5 μM hIAPP at all concentrations decreasing it monotonically at all zinc concentrations except the two highest (Figure 3.4C). However, at 10 μM hIAPP, the multimodal effect of zinc becomes apparent for the elongation rate as well, decreasing the fiber growth rate sharply up to 250 μM (approximately 80% reduction) but then slowly increasing the rate at millimolar concentrations. Two competing mechanisms are apparently in simultaneous operation, one mechanism dominant at lower $ZnCl_2$ concentrations leading to an increase in the lag-phase and retardation of fibril growth and another dominant at higher $ZnCl_2$ concentrations leading to a both reduction in the lag phase and acceleration of fibrillation but a reduction in the amount of the total amount of amyloid present at equilibrium.

3.4.4 Inhibition of Fiber Formation Is Specific for Metals That Are Good Ligands for Histidine.

To determine if the effect of $ZnCl_2$ on the aggregation of IAPP is specific to Zn^{2+} or is mediated by a nonspecific process, fibril formation of 7.5 μM IAPP was monitored in the presence of 100 μM NH_4Cl, $CaCl_2$, $MgCl_2$, $ZnCl_2$, or $CuCl_2$. As shown in Figure 3.5, the strongly kosmotropic salt NH_4Cl had little effect on the aggregation of IAPP in comparison to $ZnCl_2$. The equilibrium THT fluorescence at 3000 min, lag-time, and elongation rate are similar to the control sample without NH_4Cl. Similarly, the chaotropic salts $CaCl_2$ and $MgCl_2$ also had little effect on the aggregation kinetics. This is significant because, although Ca^{2+} and Mg^{2+} are divalent cations like Zn^{2+}, they are poor ligands for imidazole which implies imidazole has a specific role in zinc influenced IAPP aggregation. On the other hand, $CuCl_2$, which has a strong affinity for the imidazole group and is known to specifically bind to IAPP, had an even stronger effect than $ZnCl_2$.

This is an indication that $ZnCl_2$ exerts its influence by specific binding to imidazole, rather than through a nonspecific change in solvent structure, at least at lower cation concentrations.

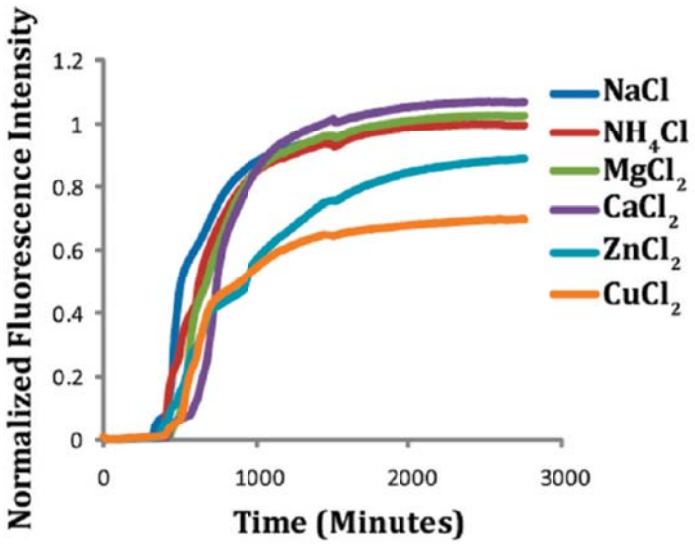

Figure 3.5 Inhibition of IAPP aggregation is specific for cations that bind imidazole. A total of 100 μM NaCl, NH4Cl, MgCl2, CaCl2, or ZnCl2 was added to 7.5 μM hIAPP in 100 mM Tris, 100 mM NaCl, pH 7.5 buffer and amyloid formation was followed by changes in the fluorescence of the amyloid specific dye Thioflavin T (25 μM). Samples were shaken at 60 Hz. Traces are averages for n = 8 experiments.

3.4.5 Fibrillogenesis Is Accelerated by Zinc at Acidic pH.

To partially isolate the electrostatic effect of zinc binding, we performed experiments at a lower pH. In contrast to the complex effects zinc has on the kinetic profile at pH 7.5, zinc has a much simpler effect at pH 5.5 when His-18 is already protonated and the change in charge upon zinc binding is dramatically reduced. At pH 5.5, zinc decreases the lag-time and increases the elongation rates in a monotonic and nearly linear fashion (Figure 3.6) in contrast to the more complex effects seen at pH 7.5.

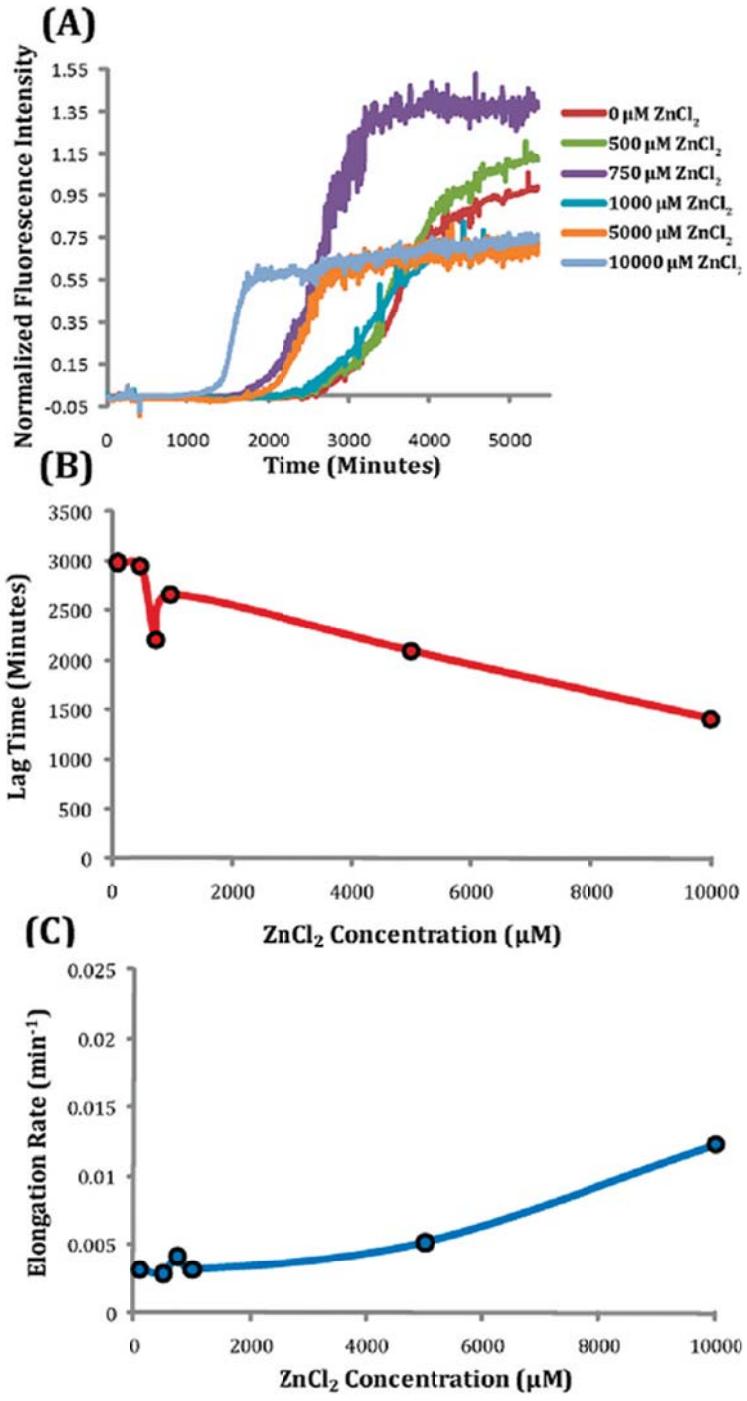

Figure 3.6 Zinc accelerates hIAPP amyloid fibril formation at pH 5.5. Kinetics of hIAPP amyloid formation at pH 5.5. (A) Amyloid formationby 10 μM hIAPP as a function of zinc concentration. (B) Decrease in the lag-time ($t1/2$ - $2/k$) before detectable fiber formation as a function of ZnCl2 concentration according to the sigmoidal growth model (eq 1). (C) Increase in the elongation rate as a function of ZnCl2 concentration according to the sigmoidal growth model.

These results suggest that, while the inhibitory effect of zinc is likely due to the unfavorable electrostatics of incorporating zinc into the amyloid fiber, an additional mechanism also exists that is not dominated by this effect and favors the creation of the amyloid fiber.

3.4.6 Zinc Binding Causes Localized Disruption of the Secondary Structure Near His-18.

To gain structural insight into this process, we solved the atomic-level resolution structure of hIAPP in an organic solvent solution (22% HFIP, 8%TFE) which strongly promotes the formation of α-helices in the presence and absence of a 10-fold excess of $ZnCl_2$ (Figure 3.7) using NMR experiments. This solvent mixture was used to both minimize the rapid aggregation of IAPP at neutral pH and to capture some features of the helical intermediate proposed as a critical step in the progression of the largely unstructured hIAPP monomer to amyloid fibers *(61, 62)*. Helix-formation is frequently thermodynamically linked to aggregation *(61, 62),* possibly because of the smaller conformational space that must be searched to bring two aggregation-prone regions together for peptides that are initially partially helical as opposed to completely unstructured *(8, 63, 64)*. In hIAPP, this relationship has been shown by the dramatic decrease in the length of the lag-phase by the addition of cosolvents which favor the formation of the helical conformation *(65-67),* the rapid onset of aggregation after the conformational transition to the helical state that occurs upon binding to phospholipid membranes *(5, 8, 67, 68),* and by the effect of mutations that are expected to alter the

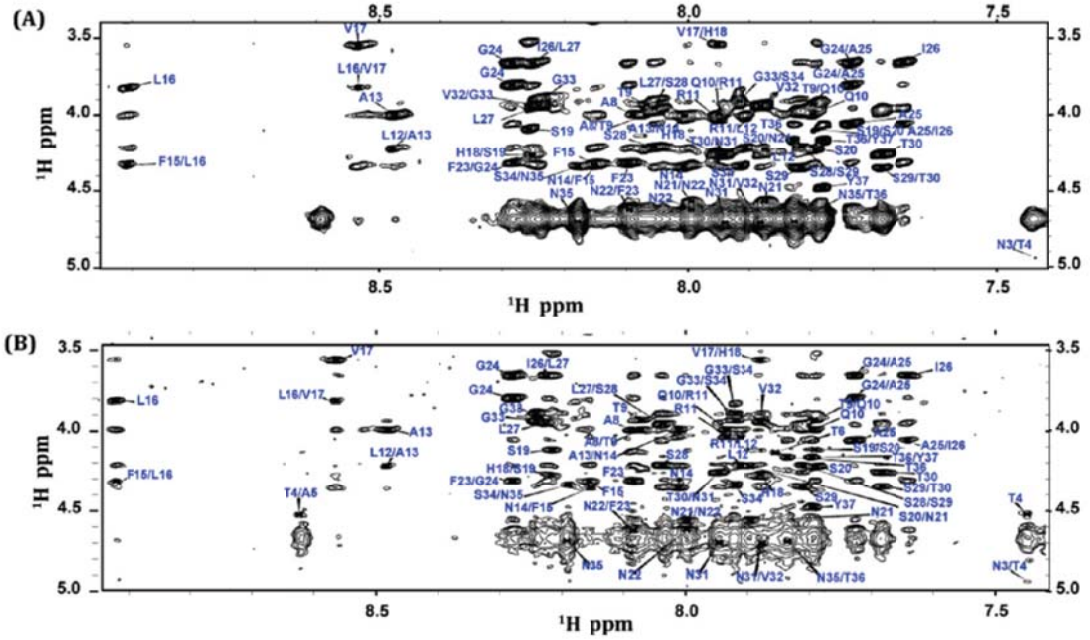

Figure 3.7 The fingerprint region of 2D 1H-1H NOESY spectra of hIAPP in the absence (A) and presence (B) of 10 mM ZnCl2 showing the connectivities among HR nuclei and resonance assignment.

intermolecular interfaces likely to be present in helical oligomers but not in the *β*-sheet conformation of the amyloid fiber *(69, 70).*

The structure of hIAPP in the absence of zinc is defined by a kinked helix from R11 to T30 (Figure 3.8, statistics are reported in Table 3.1). The kink is most likely stabilized by a clustering of hydrophobic residues on one side of the helix. The N- and C-terminal regions beyond these residues are disordered, consistent with previously determined structures of hIAPP *(71-73).* As expected, it strongly resembles the structure of hIAPP in 35% HFIP *(71).* Significantly, the structure is also a relatively close match to the crystal structure of the hIAPP dimmer fused to maltose-binding protein (MBP) as it preserves the helix-kink helix architecture that is the central motif in both structures *(69).* The similarity in this respect is likely significant, as previous studies have shown that the

helix-kink-helix motif detected here is very likely an early on-pathway intermediate to aggregation *(69)*. Mutations that destabilized the N-terminal helix or disrupted the packing interface between helices resulted in severely disrupted amyloid formation *(69, 70)*. Conformational changes in the NMR structure after zinc binding can therefore reasonably be interpreted as a conformational change in early intermediates in hIAPP aggregation.

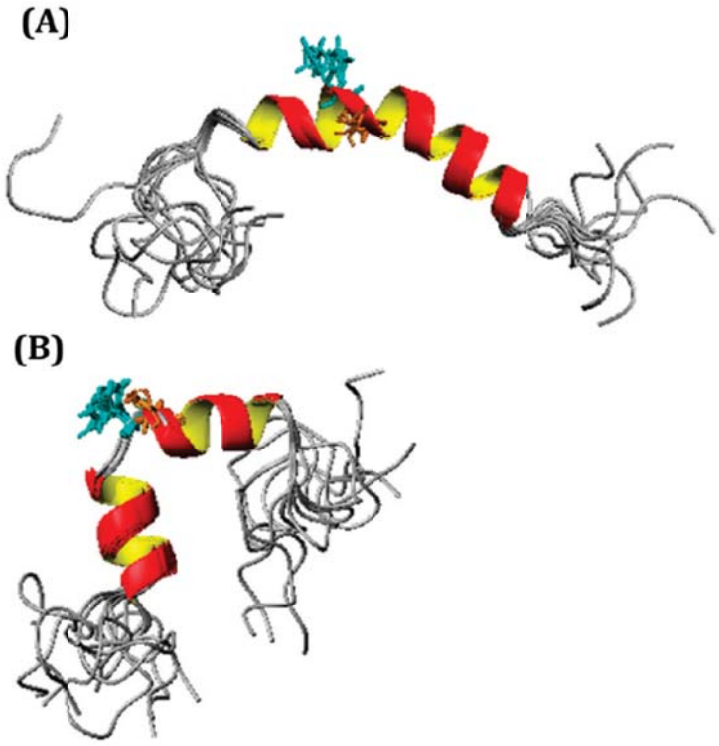

Figure 3.8 Zinc binding causes a local disruption of the secondary structure in the vicinity of His-18. High-resolution NMR structures of hIAPP in the absence (A) and presence of 10 mM ZnCl2 (B).

The structure of IAPP in the presence of zinc has similarities but important differences from the zinc-free structure (Figure 3.8). The structural differences are localized around His-18, and can be correlated with the chemical shift changes observed (a plot of the changes in HR and HN chemical shifts is provided in Figure 3.9). A

significant change in the chemical shift of the Hε and Hδ atoms on the imidazole side chain of His-18 by 0.208 and 0.106 ppm, respectively, was observed. These values are similar in magnitude to values previously reported for the change in chemical shift upon Zn^{2+} binding to the imidazoles of Amyloid β *(74)*. By contrast, the Asn-14 and Tyr-37 residues of hIAPP, which are infrequent but possible ligands for zinc *(75)*, did not show significant chemical shift differences when compared to the zinc free spectra.

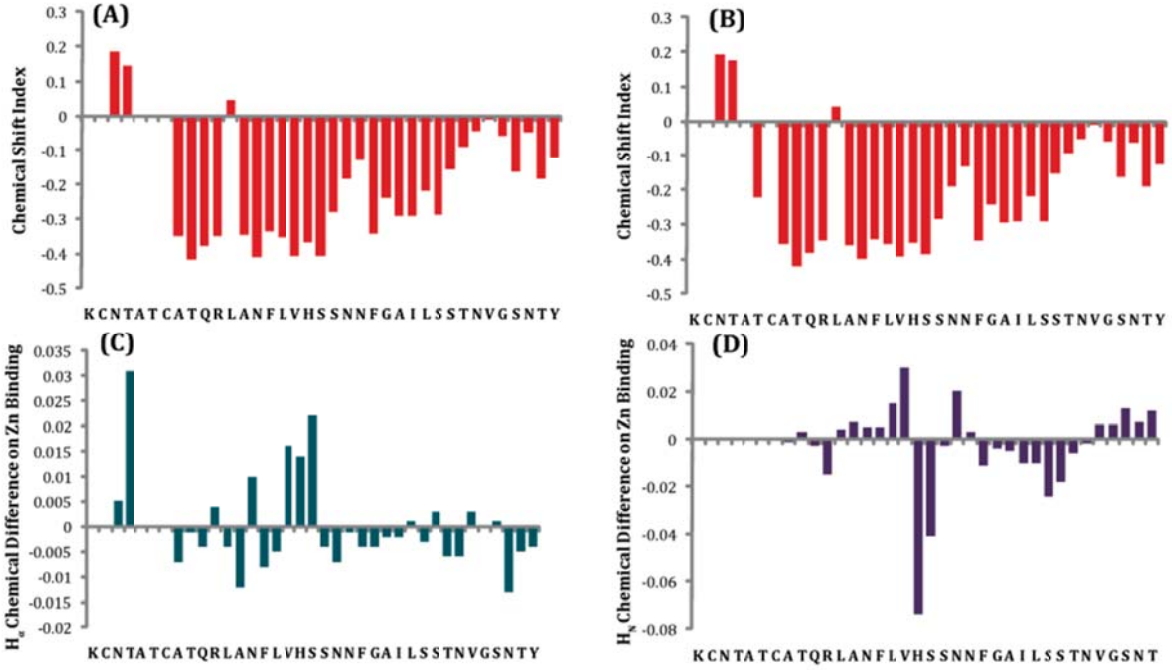

Figure 3.9 Alpha proton chemical shift indexes (CSI) for hIAPP (A) and hIAPP in the presence of 10 mM zinc (B). The CSI was calculated by subtracting the appropriate random coil shifts reported in the literature. A CSI e 0.1 is considered indicative of helical conformations. Changes in HR (C) and HN (D) chemical shifts upon binding to zinc.

3.4.7 Zinc Inhibits the Membrane Disruptive Ability of IAPP

Upon binding to the His-18 residue, zinc changes the overall charge distribution of the IAPP. It was shown previously that charge distribution of the membrane binding region (residues 1-19) of IAPP and protonation of the His-18 residue greatly effects the membrane disruptive ability *(3)*. The binding of zinc to this residue would give a similar effect. By placing a charge on the His-18 residue, the interaction of IAPP with model membrane systems would be changed, and most likely would be more surface associated as the now positive His-18 residue would have difficulty penetrating into the hydrophobic core of a lipid bilayer. Figure 3.10 displays the similarities in the initial membrane disruption as a result of a positive charge on the His-18 residue. By a single H18R substitution, membrane disruption of the membrane binding fragment is severely reduced, as is when the pH is lowered to 6.0, thereby protonating the His-18 residue. The addition of zinc to full length hIAPP gives a very similar trend in reducing the peptide's ability to cause membrane disruption indicating that the electrostatic interaction between the peptide and membrane systems plays a large role in the disruptive ability and any charge placed on or near His-18 would most likely cause reduction in membrane disruptive ability and the peptides ability to aggregate into amyloid fibers.

3.5 Conclusions Regarding the Interaction of Zinc with hIAPP

The most significant finding in this study is the inhibition of hIAPP aggregation by zinc at concentrations typical for the extracellular space where amyloidosis occurs (10-25 μM) *(76)*. At pH 7.5, zinc was found to adversely affect the kinetics of the aggregation reaction by increasing the length of the lag phase and decreasing the

cooperativity of the transition. An extracellular concentration of 25 μM $ZnCl_2$ leads to an approximate 25% increase in the length of the lag phase and a 50% reduction in the elongation rate (Figure 3.4B,D). While the reduction at 25 μM is significant, it is important to remember that the distribution of zinc is neither spatially homogeneous nor static in time. Zinc is concentrated near the plasma membrane which is both a catalyst for aggregation and the likely target for many of hIAPP's toxic effects. The temporal dynamics of zinc distribution, particularly the spike in zinc concentration that occurs upon the exocytosis of the insulin/hIAPP granule, may also contribute to a magnified effect of zinc on hIAPP aggregation. When the secretory granule is exocytosed, the fusion of the secretory granule with the beta cell plasma membrane releases the entire contents of the secretory

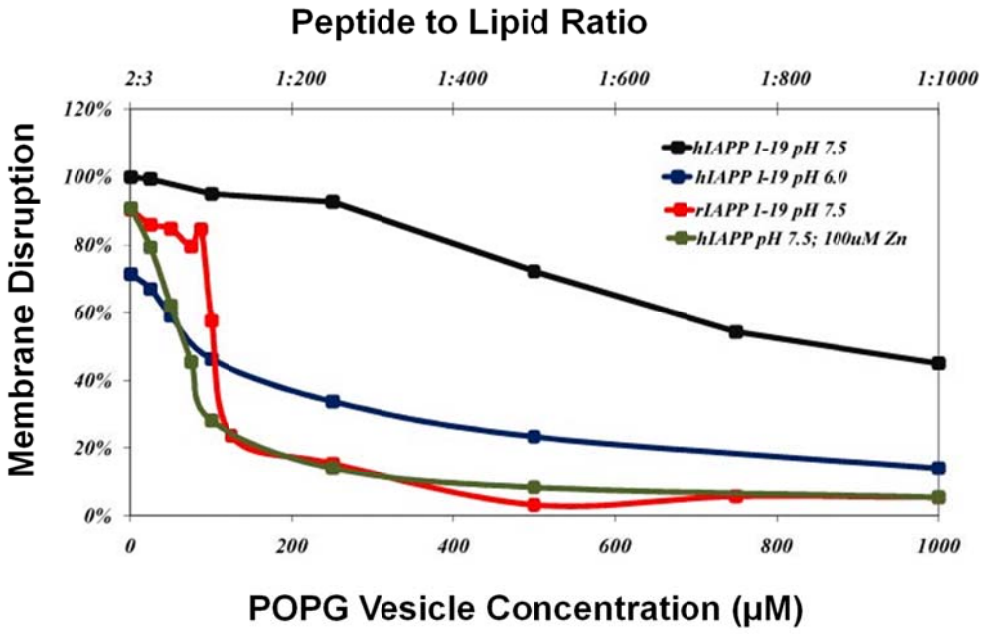

Figure 3.10. Membrane disruptive effect of hIAPP when inducing a positive charge on the His-18 residue. hIAPP1-19 at pH 7.5 (Black) induces disruption up to a 1:1000 peptide to lipid ratio. When His-18 displays a positive charge through protonation at pH 6.0 (Blue), substitution of His-18 to Arg-18 in the rat variant of the peptide (Red) or by incorporation of small amounts of Zinc to the full length peptide (Green), the disruptive ability of the peptide is greatly decreased.

granule into the extracellular space (see a cartoon depiction in Figure 3.11). Since the concentration of zinc within the granule is much higher than in the extracellular environment (mM vs. μM) *(35, 76),* emptying the granule therefore causes a brief spike in the zinc concentration near the site of exocytosis *(77).* This is important because the release of the granule contents does not occur simultaneously with the opening of the granule fusion pore*,* typically, 1-2 s elapse before the granule contents are fully released, but in some cases, the process takes minutes to complete *(78, 79).* The acidic pH of the granule, on the other hand, is neutralized immediately upon the opening of the fusion pore and the exposure of the granule contents to the extracellular matrix. During this time, hIAPP is both highly concentrated and at a pH very favorable for aggregation. It is also in close proximity to the plasma membrane which is both a target for attack and a dramatic facilitator of aggregation *(5, 68, 80).* The simultaneous release of zinc with hIAPP may allow hIAPP to safely diffuse away from the plasma membrane and be diluted in the bloodstream before it can aggregate on the cell surface.

In contrast to the micromolar inhibition of aggregation seen at neutral pH, zinc is not likely to directly contribute to the observed stability of hIAPP in the secretory granule. The acidic environment of the secretory granule considerably reduces the rate of aggregation (Figure 3.4 vs. Figure 3.6), similar to the results of previously reported groups *(55, 81).* We found that, contrary to its effects at neutral pH (7.5), zinc enhances rather than retards aggregation. However, it is unlikely that zinc contributes to pathological aggregation in the secretory granule in this manner, even at the zinc concentrations present in the secretory granule. First, the effect is diminished by the reduced affinity of the protonated His-18 residue for zinc. Moreover, aggregation in the

secretory granule is diminished to a much greater extent first by the acidic pH and further by the strong inhibitory action of insulin *(12, 55, 82-85).* The combined action of these two strong inhibiting effects is likely to suppress aggregation to a point beyond the lifetime of the secretory granule. It should be mentioned, however, that zinc may have a strong indirect effect on hIAPP fibrillogenesis by modulating the monomer to hexamer equilibrium of insulin *(41),* since the hexameric and monomeric forms of insulin likely display different affinities for hIAPP *(69, 84).*

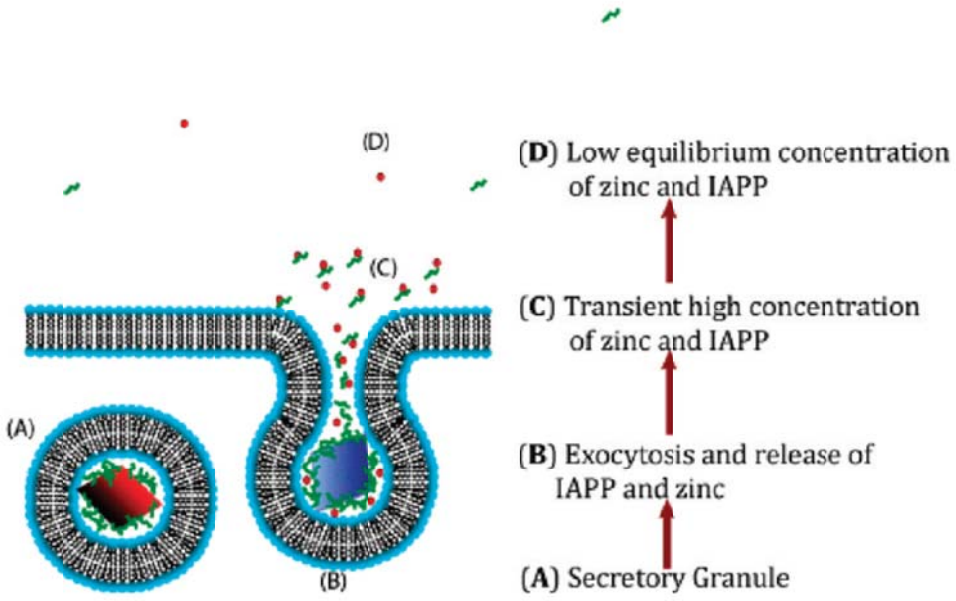

Figure 3.11 Cartoon schematic of how zinc may influence IAPP aggregation and toxicity. (A) In the secretory granule, IAPP is prevented from aggregation by the acidic environment and the inhibitory action of insulin. (B) Exocytosis of the secretory granule simultaneously releases IAPP and zinc into the extracellular space. (C) A high local concentration of IAPP near the plasma membrane is prevented from disrupting the _-cell by transient binding to zinc. (D) Zinc dissociates from IAPP at the low equilibrium concentrations found in the extracellular space, however, IAPP is now diluted past the critical concentration for aggregation.

While the action of zinc on hIAPP fibrillogenesis at pH 5.5 is probably not directly physiologically relevant, it is useful in illuminating the mechanism of zinc inhibition of fibrillogenesis. Zinc exhibits both inhibitory and catalytic effects on the aggregation rate at pH 7.5, with the inhibitory effect being dominant at lower concentrations (Figure 3.4). The propensity for a protein to form amyloid is determined by a variety of factors similar to those that influence protein folding including a favorable potential for hydrogen bonding, favorable hydrophobic interactions, and favorable electrostatics. From an exclusively electrostatic point of view, the binding of zinc should strongly disfavor the amyloid state, as His-18 is located in the hydrophobic interior of the fiber near a turn between strands 1 and 2 *(55, 86)*. Charged residues in amyloid fibers are intrinsically disfavored unless stabilized by salt bridges as the parallel stacking of the *β*-sheets brings the charges on each monomer unit close in space in the final structure *(87, 88)*. This is particularly true of charged residues in the low dielectric environment of the interior of the fiber. At pH 5.5, this effect is mitigated as His-18 already carries a positive charge. In contrast to pH 7.5, zinc enhances the rate of fibrillogenesis uniformly and nearly linearly with concentration at pH 5.5 indicating the inhibitory effect is indeed largely electrostatic in origin and related to destabilization of the amyloid fiber by the addition of a charge in an unfavorable position.

While the origin of zinc inhibition is relatively clear, the origin of its catalytic effect is less certain and cannot be concretely established from the data from this study. The pathway to amyloid formation is complex and involves a variety of on and off-pathway intermediates. Stabilization of any on-pathway intermediate would be expected to reduce the length of the lag phase and may also increase the fiber elongation rate

through either direct addition of the intermediate to the fiber or interconversion to a plaque-competent species. Alternatively, zinc may enhance both aspects of the fibrillogenesis rate by breaking existing amyloid fibers into smaller fragments, which then act as new sites for fiber growth *(89).* However, we did not see significant fragmentation of the amyloid fibers by electron microscopy, only a reduced amount of amyloid deposition was observed (Figure 3.3). It therefore seems more likely that stabilization of on-pathway intermediates, rather than increased secondary nucleation, is responsible for the partial compensation of zinc inhibition at high zinc concentrations.

While the exact binding constant of zinc to hIAPP was not determined in this study, zinc's effects are clearly noticeable in the micromolar concentration range. Since this apparent binding constant is too high for hIAPP to be attached to only a single histidine *(90),* another residue is likely to act as a second ligand which must be either a non-histidine residue or another histidine on an adjacent molecule. The NMR structure places Ser-19 in close proximity to the side chain of His-18, opening the possibility that the zinc ion is chelated by the side chains of both His-18 and Ser-19. While the hydroxyl group of serine is a hard ligand and is less than ideal for zinc binding in comparison to histidine, the favorable entropy change caused by the chelating effect may overcome the less favorable enthalpy contribution to binding. The backbone oxygen of Ser-19, another possible but enthalpically unfavorable ligand, is exposed in the zinc bound structure of IAPP and may be a possible binding site. Another possibility is that zinc bridges multiple molecules of IAPP. There is some precedence for this type of bridging interaction as zinc catalyzes the formation of hexamers of insulin, which shares some sequence homology with hIAPP. Each insulin hexamer is held together by two zinc molecules, which each

bind three insulin monomers by coordination to three histidines *(91)*. A similar structure may be present in the hIAPP-Zn molecule, although the exact structure of the putative hIAPP-Zn oligomers (if they exist) remains to be determined.

This study was supported by research funds from NIH (DK078885 to A.R.) and Michigan Diabetes Research Training Center at the University of Michigan. I would like to thank thank Professor Robert Kennedy of the University of Michigan for discussion on the role of zinc in β-cell function, and the 900 MHz NMR facility at the Michigan State University. Jeffery Brender helped in the preparation of the manuscript, Roberto de la Salud Bea synthesized the peptide used in the study, Nataliya Popovych obtained the electron microscopy images, and Ravi Nanga and Subramanian Vivekanandan preformedand analyzed the NMR experiments and structure calculations.

3.6 Bibliography

1. Scherbaum, W.A. (1998) The role of amylin in the physiology of glycemic control. *Experimental and Clinical Endocrinology & Diabetes 106*, 97–102.

2. Harrison, R.S., Sharpe, P.C., Singh, Y., and Fairlie, D.P. (2007) Amyloid peptides and proteins in review. *Reviews of Physiology, Biochemistry and Pharmacology 159*, 1–77.

3. Brender, J.R., Hartman, K., Reid, K.R., Kennedy, R.T., and Ramamoorthy, A. (2008) A single mutation in the non-amyloidogenic region of islet amyloid polypeptide greatly reduces toxicity. *Biochemistry 47*, 12680–12688.

4. Brender, J.R., Lee, E.L., Cavitt, M.A., Gafni, A., Steel, D.G., and Ramamoorthy, A. (2008) Amyloid fiber formation and membrane disruption are separate processes localized in two distinct regions of IAPP, the type-2-diabetes related peptide. *Journal of the American Chemical Society 130*, 6424–6429.

5. Knight, J.D. and Miranker, A.D. (2004) Pospholipid catalysis of diabetic amyloid assembly. *Journal of Molecular Biology 341*, 1175–1187.

6. Quist, A., Doudevski, L., Lin, H., Azimova, R., Ng, D., Frangione,B., Kagan, B., Ghiso, J., and Lal, R. (2005) Amyloid ion channels: A common structural link for protein-misfolding disease. *Proceedings of the National Academy of Sciences 102*, 10427–10432.

7. Mirzabekov, T.A., Lin, M.C., and Kagan, B.L. (1996) Pore formation by the cytotoxic islet amyloid peptide amylin. *Journal of Biological Chemistry 271*, 1988–1992.

8. Knight, J.D., Hebda, J.A., and Miranker, A.D. (2006) Conserved and cooperative assembly of membrane-bound α-helical states of islet amyloid polypeptide. *Biochemistry 45*, 9496–9508.

9. Goldsbury, C.S., Cooper, G.J., Goldie, K.N., Muller, S.A., Saafi, E.L., Gruijters, W.T., Misur, M.P., Engel,A., Aebi, U., and Kistler, J. (1997) Polymorphic fibrillar assembly of human amylin. *Journal of Structural Biology 119*, 17–27.

10. Radovan, D., Smirnovas, V., and Winter, R. (2008) Effect of pressure on islet amyloid polypeptide aggregation: revealing the polymorphic nature of the fibrillization process. *Biochemistry 47*, 6352–6360.

11. Alexandrescu, A.T. (2005) Amyloid accomplices and enforcers. *Protein Science 14*, 1–12.

12. Larson, J.L., and Miranker, A.D. (2004) The mechanism of insulin action on islet amyloid polypeptide fiber formation. *Journal of Molecular Biology 335*, 221–231.

13. Calabrese, M.F., Eakin, C.M., Wang, J.M., Miranker, A.D. (2008) A regulatable switch mediates self-association in an immunoglobulin fold. *Nature Structural & Molecular Biology 15*, 965–971.

14. Eakin, C.M., Knight, J.D., Morgan, C.J., Gelfand, M.A., and Miranker, A.D. (2002) Formation of a copper specific binding site in non-native states of β-2-microglobulin. *Biochemistry 41*, 10646–10656.

15. Talmard, C., Yona, R.L., and Faller, P. (2009) Mechanism of zinc(II)-promoted amyloid formation: zinc(II) binding facilitates the transition from the partially α-helical conformer to aggregates of amyloid β-protein(1-28). *Journal of Biological Inorganic Chemistry 14*, 449–455.

16. Talmard, C., Bouzan, A., and Faller, P. (2007) Zinc binding to amyloid-β: isothermal titration calorimetry and Zn competition experiments with Zn sensors. *Biochemistry 46*, 13658–13666.

17. Talmard, C., Guilloreau, L., Coppel, Y., Mazarguil, H., and Faller, P. (2007) Amyloid-Beta peptide forms monomeric complexes with Cu^{2+} and Zn^{2+} prior to aggregation. *ChemBioChem 8*, 163–165.

18. Huang, X.D., Atwood, C.S., Moir, R.D., Hartshorn, M.A., Tanzi, R.E., and Bush, A.I. (2004) Trace metal contamination initiates the apparent auto-aggregation, amyloidosis, and oligomerization of Alzheimer's Amyloid β peptides. *Journal of Biological Inorganic Chemistry 9*, 954–960.

19. Noy, D., Solomonov, I., Sinkevich, O., Arad, T., Kjaer, K., and Sagi, I. (2008) Zinc-amyloid-β interactions on a millisecond time scale stabilize non-fibrillar Alzheimer related species. *Journal of the American Chemical Society 130*, 1376–1383.

20. Uversky, V.N., Li, J., and Fink, A.L. (2001) Metal-triggered structural transformations, aggregation, and fibrillzation of human α-Synuclein: A possible molecular link between Parkinson's Desease and heavy metal exposure. *Journal of Biological Chemistry 276*, 44284–96.

21. Yamin, G., Glaser, C.B., Uversky, V.N., and Fink, A.L. (2003) Certain metals trigger fibrillation of methionine oxidized α-Synuclein. *Journal of Biological Chemistry 278*, 27630–27635.

22. Yamin, G., Munishkina, L.A., Karymov, M.A., Lyubchenko, Y.L., Uversky, V.N., and Fink, A.L. (2005) Forcing nonamyloidogenic β-synuclein to fibrillate. *Biochemistry 44*, 9096–9107.

23. Potter, S.Z., Zhu, H., Shaw, B.F., Rodriguez, J.A., Doucette, P.A., Sohn, S.H., Durazo, A., Faull, K.F., Gralla, E.B., Nersissian, A.M., and Valentine, J.S. (2007) Binding of a single zinc ion to one subunit of copper-zinc superoxide dismutase apoprotein substantially influences the structure and stability of the entire homodimeric protein *Journal of the American Chemical Society 129*, 4575–4583.

24. Khan, A., Ashcroft, A.E., Korchazhkina, O.V., and Exley, C. (2004) Metal mediated formation of fibrillar ABri amyloid. *Journal of Inorganic Biochemistry 98*, 2006–2010.

25. Khan, A., Ashcroft, A.E., Higenell, V., Korchazhkina, O.V., and Exley, C. (2005) Metals accelerate the formation and direct the structure of amyloid fibrils of NAC. *Journal of Inorganic Biochemistry 99*, 1920–1927.

26. Jobling, M.F., Huang, X.D., Stewart, L.R., Barnham, K.J., Curtain, C., Volitakis, I., Perugini, M., White, A.R., Cherny, R.A., Masters, C.L., Barrow, C.J., Collins, S.J., Bush, A.I., and Cappai, R. (2001) Copper and zinc binding modulates the aggregation and neurotoxic properties of the prion peptide PrP106-126. *Biochemistry 40*, 8073–8084.

27. Gorell, J.M., Johnson, C.C., Rybicki, B.A., Peterson, E.L., Kortsha, G.X., Brown, G.G., and Richardson, R.J. (1999) Occupational exposure to manganese, copper, lead, iron, mercury and zinc and the risk of Parkinson's Disease. *NeuroToxicology 20*, 239–247.

28. Gorell, J.M., Johnson, C.C., Rybicki, B.A., Peterson, E L., Kortsha, G.X., Brown, G.G., and Richardson, R.J. (1997) Occupational exposures to metals as risk factors for Parkinson's disease. *Neurology 48*, 650–658.

29. Rybicki, B.A., Johnson, C.C., Uman, J., and Gorell, J.M. (1993) Parkinson's disease mortality and the industrial use of heavy metals in Michigan. *Movement Disorders 8*, 87–92.

30. Lee, J.Y., Cole, T.B., Palmiter, R.D., Suh, S.W., and Koh, J.Y. (2002) Contribution by synaptic zinc to the gender-disparate plaque formation in human Swedish mutant APP transgenic mice. *Proceedings of the National Academy of Sciences 99*, 7705–7710.

31. Masad, A., Hayes, L., Tabner, B.J., Turnbull, S., Cooper, L.J., Fullwood, N.J., German, M.J., Kametani, F., El-Agnaf, O.M., and Allsop, D. (2007) Copper mediated formation of hydrogen peroxide from the amylin peptide: A novel mechanism for degeneration of islet cells in type-2 diabetes mellitus? *Federation of European Biochemical Societies Letters 581*, 3489–3493.

32. Schubert, D., Behl, C., Lesley, R., Brack, A., Dargusch, R., Sagara, Y., and Kimura, H. (1995) Amyloid peptides are toxic via a common oxidative mechanism. *Proceedings of the National Academy of Sciences 92*, 1989–1993.

33. Pappalardo, G., Milardi, D., Magri, A., Attanasio, F., Impellizzeri, G., La Rosa, C., Grasso, D., and Rizzarelli, E. (2007) Environmental factors differently affect human and rat IAPP: Conformational preferences and membrane interactions of IAPP17-29 peptide derivatives. *Chemistry A European Journal 13*, 10204–10215.

34. Sciacca, M.F.M., Pappalardo, M., Milardi, D., Grasso, D.M., and La Rosa, C. (2008) Calcium activated membrane interaction of the islet amyloid polypeptide: Implications in the pathogenesis of type II diabetes mellitus. *Archives of Biochemistry and Biophysics 477*, 291–298.

35. Foster, M.C., Leapman, R.D., Li, M.X., and Atwater, I. (1993) Elemental composition of secretory granules in pancreatic islets of Langerhans. *Biophysical Journal 64*, 525–532.

36. Taylor, C.G. (2005) Zinc, the pancreas, and diabetes: insights from rodent studies and future directions. *BioMetals 18*, 305–312.

37. Sladek, R., Rocheleau, G., Rung, J., Dina, C., Shen, L., Serre, D., Boutin, P., Vincent, D., Belisle, A., Hadjadj, S., Balkau, B., Heude, B., Charpentier, G., Hudson, T.J., Montpetit, A., Pshezhetsky, A.V., Prentki, M., Posner, B.I., Balding, D.J., Meyre, D., Polychronakos, C., and Froguel, P., (2007) A genome-wide association study identifies novel risk loci for type 2 diabetes. *Nature 445*, 881–885.

38. Zeggini, E., Weedon, M.N., Lindgren, C.M., Frayling, T.M., Elliot, K.S., Lango, H., Timpson, N.J., Perry, J.R.B., Rayner, N.W., Freathy, R.M., Barrett, J.C., Shields, B., Morris, A.P., Ellard, S., Groves, C.J., Harries, L.W., Marchini, J.L., Owen, K.R., Knight, B., Cardon, L. R., Walker, M., Hitman, G.A., Morris, A.D., Doney, A.S.F., McCarthy, M.I., and Hattersley, A.T., (2007) Replication of genome-wide association signals in UK samples reveal risk loci for type 2 diabetes. *Science 316*, 1336–1341.

39. Kirchhoff, K., Machicao, F., Haupt, A., Schafer, S. A., Tschritter, O., Staiger, H., Stefan, N., Haring, H.U., and Fritsche, A. (2008) Polymorphisms in the TCF7L2, CDKAL1, and SLC30A8 genes are associated with impaired proinsulin conversion. *Diabetologia 51*, 597–601.

40. Staiger, H., Machicao, F., Stefan, N., Tschritter, O., Thamer, C., Kantartzis, K., Schafer, S. A., Kirchhoff, K., Fritsche, A., and Haring, H.U. (2007) Novel meta-analysis-derived Type 2 Diabetes risk loci do not determine prediabetic phenotypes. *PLoS One 2*, e832.

41. Lemaire, K., Ravier, M. A., Schraenen, A., Creemers, J.W.M., Van De Plas, R., Granvik, M., Van Lommel, L., Waelkens, E., Chimienti, F., Rutter, G.A., Gilon, P., in't Veld, P.A., and Schuit, F. C. (2009) Insulin crystallization depends on zinc transporter ZnT8 expression, but is not required for normal glucose homeostasis in mice. *Proceedings of the National Academy of Sciences 106*, 14872–14877.

42. Salazar, G., Falcon-Perez, J.M., Harrison, R., and Faundez, V. (2009) SLC30A3 (ZnT3) Oligomerization by dityrosine bonds regulates its subcellular localization and metal transport capacity. *PLoS One 4*, e5896.

43. Ruchat, S.M., Elks, C.E., Loos, R.J.F., Vohl, M.C., Weisnagel, S.J., Rankinen, T., Bouchard, C., and Perusse, L. (2009) Association between insulin secretion, insulin sensitivity and type 2 diabetes susceptibility variants identified in genome-wide association studies. *Acta Diabetologica 46*, 217–226.

44. Schnolzer, M., Alewood, P., Jones, A., Alewood, D., and Kent, S.B.H. (2007) In Situ neutralization in Boc-chemistry solid phase peptide synthesis rapid, high yield assemply of difficult sequences. *International Journal of Peptide Research. 13*, 31–44.

45. Page, K., Hood, C.A., Patel, H., Fuentes, G., Menakuru, M., and Park, J.H. (2007) Fast Fmoc synthesis of hAmylin1-37 with pseudoproline assisted on-resin disulfide formation. *Journal of Peptide Science 13*, 833–838.

46. Naiki, H., Higuchi, K., Nakakuki, K., and Takeda, T. (1991) Kinetic analysis of amyloid fibril polymerization in vitro. *Laboratory Investigations 65*, 104–110.

47. Goddard, T.D., and Kneller, D.G. *SPARKY 3,* University of California: San Francisco, 1999.

48. Wuthrich, K. *NMR of Proteins and Nucleic Acids,* John Wiley and Sons: New York., 1986.

49. Guntert, P., Mumenthaler, C., and Wuthrich, K. (1997) Torsion angle dynamics for NMR structure calculation with the new program DYANA. *Journal of Molecular Biology 273*, 283–298.

50. Cornilescu, G., Delaglio, F., and Bax, A. (1999) Protein backbone angle restraints from searching a database for chemical shift and swquense homology. *Journal of Biomolecular NMR 13*, 289– 302.

51. Herrmann, T., Guntert, P., and Wuthrich, K. (2002) Protein NMR structure determinations and automated NOE assignment using software CANDID and the torsion angle dynamics algorithy DYANA. *Journal of Molecular Biology 319*, 209– 227.

52. Koradi, R., Billeter, M., and Wuthrich, K. (1996) MOLMOL: A program for display and analysis of macromolecular structures. *Journal of Molecular Graphics 14*, 51–55.

53. Groenning, M., Norrman, M., Flink, J.M., van de Weert, M.,Bukrinsky, J.T., Schluckebier, G., and Frokjaer, S. (2007) Binding mode of Thioflavin T in insulin amyloid fibrils. *Journal of Structural Biology 159*, 483–497.

54. Hudson, S.A., Ecroyd, H., Kee, T.W., and Carver, J.A. (2009) The thioflavin T fluorescence assay for amyloid fibril detection can be biased by the presence of exogenous compounds. *Federation of European Biochemical Societies Journal 276*, 5960–5972.

55. Abedini, A., and Raleigh, D.P. (2005) The role of His-18 in amyloid formation by human islet amyloid polypeptide. *Biochemistry 44*, 16284–16291.

56. Porat, Y., Mazor, Y., Efrat, S., and Gazit, E. (2004) Inhibition of islet amyloid polypeptide fibril formation: a potential role for heteroaromatic interactions. *Biochemistry 43*, 14454–14462.

57. Janciauskiene, S., Eriksson, S., Carlemalm, E., and Ahren, B. (1997) β cell granule peptides affect human islet amyloid polypeptide (IAPP) fibril formation in vitro. *Biochemical and Biophysical Research Communications 236*, 580–585.

58. Tatarek-Nossol, M., Yan, L.M., Schmauder, A., Tenidis, K., Westermark, G., and Kapurniotu, A. (2005) Inhibition of hIAPP Amyloid-fibril formation and apoptotic ceal death by a designed amyloid core containing hexapeptide. *Chemical Biology 12*, 797–809.

59. Cao, P., Meng, F., Abedini, A., and Raleigh, D.P. (2010) The ability of rodent islet amyloid polypeptide to inhibit amyloid formation by human islet amyloid polypeptide has important implications for the mechanism of amyloid formation and the design of inhibitors. *Biochemistry 49*, 872–881.

60. Olofsson, A., Lindhagen-Persson, M., Vestling, M., Sauer-Eriksson, A.E., and Ohman, A. (2009) Quenched hydrogen/deuterium exchange NMR characterization of amyloid-β peptide aggregates formed in the presence of Cu^{2+} or Zn^{2+} *Federation of European Biochemical Societies Journal 276*, 4051–4060.

61. Abedini, A., and Raleigh, D.P. (2009) A critical assessment of the role of helical intermediates in amyloid formation by natively unfolded proteins and polypeptides. *Protein Engineering Design and Selection 22*, 453–459.

62. Abedini, A., and Raleigh, D.P. (2009) A role for helical intermediates in amyloid formation by natively unfolded polypeptides? *Physical Biology 6*, 15005.

63. Hall, D., Hirota, N., and Dobson, C. M. (2005) A toy model for predicting the rate of amyloid formation from unfolded protein. *Journal of Molecular Biology 351*, 195–205.

64. Nanga, R.P., Brender, J.R., Vivekanandan, S., Popovych, N., and Ramamoorthy, A. (2009) NMR structure in a membrane environment reveals putative amyloidogenic regions of the SEVI precursor peptide $PAP_{248-286}$. *Journal of the American Chemical Society 131*, 17972–17979.

65. Higham, C.E., Jaikaran, E., Fraser, P.E., Gross, M., and Clark, A. (2000) Preparation of synthetic human islet amyloid polypeptide (IAPP) in a stable conformation to enable study of conversion to amyloid-like fibrils. *Federation of European Biochemical Societies Letters 470*, 55–60.

66. Williamson, J.A., Loria, J.P., and Miranker, A.D. (2009) Helix stabilization precedes aqueous and bilayer-catalyzed fiber formation in islet amyloid polypeptide. *Journal of Molecular Biology 393*, 383–396.

67. Saraogi, I., Hebda, J.A., Becerril, J., Estroff, L.A., Miranker, A.D., and Hamilton, A. D. (2010) Synthetic α-helix mimetics as agonists and antagonists of islet amyloid polypeptide aggregation. *Angewandte Chemie International Edition 49*, 736–739.

68. Jayasinghe, S.A., and Langen, R. (2005) Lipid membranes modulate the structure of islet amyloid polypeptide. *Biochemistry 44*, 12113–12119.

69. Wiltzius, J.J., Sievers, S.A., Sawaya, M.R., and Eisenberg, D. (2009) Atomic structures of IAPP (amylin) fusions suggest a mechanism for fibrillation and the role of insulin in the process. *Protein Science 18*, 1521–1530.

70. Koo, B.W., Hebda, J.A., and Miranker, A.D. (2008) Amide inequivalence in the fibrillar assembly of islet amyloid polypeptide. *Protein Engineering Design and Selection. 21*, 147–154.

71. Cort, J.R., Liu, Z., Lee, G.M., Huggins, K.N., Janes, S., Prickett, K., and Andersen, N.H. (2009) Solution state structures of human pancreatic amylin and pramlintide. *Protein Engineering Design and Selection. 22*, 497–513.

72. Patil, S. M., Xu, S., Sheftic, S.R., and Alexandrescu, A.T. (2009) Dynamic α-helix structure of micelle-bound human amylin. *Journal of Biological Chemistry 284*, 11982–11991.

73. Nanga, R.P., Brender, J.R., Xu, J., Hartman, K., Subramanian, V., and Ramamoorthy, A. (2009) Three-dimensional structure and orientation of rat islet amyloid polypeptide protein in a membrane environment by solution NMR spectroscopy. *Journal of the American Chemical Society 131*, 8252–8261.

74. Gaggelli, E., Janicka-Klos, A., Jankowska, E., Kozlowski, H., Migliorini, C., Molteni, E., Valensin, D., Valensin, G., and Wieczerzak, E. (2008) NMR studies of the Zn^{2+} interactions with rat and human β-amyloid(1-28) peptides in water-micelle environment. *Journal of Physical Chemistry B 112*, 100–109.

75. Alberts, I.L., Nadassy, K., and Wodak, S.J. (1998) Analysis of zinc binding sites in protein crystal structures. *Protein Science 7*, 1700–1716.

76. Aspinwall, C.A., Brooks, S.A., Kennedy, R.T., and Lakey, J.R.T. (1997) Effects of intravesicular H^+ and Zn^{2+} on insulin secretion in pancreatic beta cells. *Journal of Biological Chemistry 272*, 31308–31314.

77. Qian, W. J., Gee, K. R., and Kennedy, R. T. (2003) Imaging of Zn^{2+} release from pancreatic β-cells at the level of single exocytotic events. *Analytical Chemistry 75*, 3468–3475.

78. Barg, S., Olofsson, C. S., Schriever-Abeln, J., Wendt, A., Gebre- Medhin, S., Renstrom, E., and Rorsman, P. (2002) Delay between fusion pore opening and peptide release from large dense-core vesicles in neuroendocrine cells. *Neuron 33*, 287–299.

79. Michael, D.J., Ritzel, R.A., Haataja, L., and Chow, R.H. (2006) Pancreatic β-cells secrete insulin in fast and slow release forms. *Diabetes 55*, 600–607.

80. Jha, S., Sellin, D., Seidel, R., and Winter, R. (2009) Amyloidogenic propensities and conformational properties of ProIAPP and IAPP in the presence of lipid bilayer membranes. *Journal of Molecular Biology 389*, 907–920.

81. Mishra, R., Geyer, M., and Winter, R. (2009) NMR spectroscopic investigation of early events in IAPP amyloid fibril formation. *ChemBioChem 10*, 1769–1772.

82. Gilead, S., Wolfenson, H., and Gazit, E. (2006) Molecular mapping of the recognition interface between the islet amyloid polypeptide and insulin. *Angewandte Chemie International Edition 45*, 6476–6480.

83. Knight, J.D., Williamson, J.A., and Miranker, A.D. (2008) Interaction of membrane-bound islet amyloid polypeptide with soluble and crystalline insulin. *Protein Science 17*, 1850–1856.

84. Jaikaran, E., Nilsson, M.R., and Clark, A. (2004) Pancreatic beta-cell granule peptides form heteromolecular complexes which inhibit islet amyloid polypeptide fibril formation. *Biochemical Journal 377*, 709– 716.

85. Wei, L., Jiang, P., Yau, Y.H., Summer, H,, Shochat, S.G., Mu, Y., and Pervushin, K. (2009) Residual structure in islet amyloid polypeptide mediates its interactions with soluble insulin. *Biochemistry 48*, 2368–2376.

86. Luca, S., Yau, W.M., Leapman, R., and Tycko, R. (2007) Peptide conformation and supramolecular organization in amylin fibrils: constraints from solid-state NMR. *Biochemistry 46*, 13505–13522.

87. Richardson, J.S., and Richardson, D.C. (2002) Natural β-sheet proteins use negative design to avoid edge-to-edge aggregation. *Proceedings of the National Academy of Sciences. 99*, 2754–2759.

88. Reumers, J., Maurer-Stroh, S., Schymkowitz, J., and Rousseau, F. (2009) Protein sequences encode safeguards against aggregation. *Human Mutation 30*, 431–437.

89. Knowles, T.P., Waudby, C.A., Devlin, G.L., Cohen, S.I., Aguzzi, A., Vendruscolo, M., Terentjev, E.M., Welland, M.E., and Dobson, C.M. (2009) An analytical solution to the kinetics of breakable filament assembly. *Science 326*, 1533–1537.

90. Aruga, R. (1983) Thermodynamics of complex formation of 1-methlimidazole with cobalt(II), nickel(II), copper(II), and zinc(II) cations in aqueous solution. *Transition Met. Chem. 8*, 56–58.

91. Baker, E.N., Blundell, T.L., Cutfield, J.F., Dodson, E.J., Dodson, G.G., Hodgkin, D.M., Hubbard, R.E., Isaacs, N.W., Reynolds, C.D., Sakabe, K., Sakabe, N., and Vijayan, N.M., (1988) The structure of 2Zn pig insulin crystals at 1.5A resolution. *Philos. Trans. R. Soc. London 319*, 369–456.

CHAPTER 4

BIPHASIC EFFECTS OF INSULIN ON ISLET AMYLOID POLYPEPTIDE MEMBRANE DISRUPTION

4.1 - Summary

Type II diabetes, in its late stages, is often associated with the formation of extracellular islet amyloid deposits composed of islet amyloid polypeptide (IAPP or amylin). IAPP is stored before secretion at millimolar concentrations within secretory granules inside the β-cells. Of interest, at these same concentrations *in vitro*, IAPP rapidly aggregates and forms fibrils, yet within secretory granules of healthy individuals, IAPP does not fibrillize. Insulin is also stored within the secretory granules before secretion, and has been shown *in vitro* to inhibit IAPP fibril formation. Because of insulin's inhibitory effect on IAPP fibrillization, it has been suggested that insulin may also inhibit IAPP-mediated permeabilization of the β-cell plasma membrane *in vivo*. We show that although insulin is effective at preventing fiber-dependent membrane disruption, it is not effective at stopping the initial phase of membrane disruption before fibrillogenesis. These results suggest that insulin has a more complicated role in inhibiting IAPP fibrillogenesis, and that other factors, such as the low pH of the secretory granule and high zinc concentrations, may also play a role.

This chapter is a version of a published paper: Brender, J.R., Lee, E.L., Hartman, K., Wong, P.T., Ramamoorthy, A., Steel, D.G., and Gafni, A., (2011) Biphasic Effects of Insulin on Islet Amyloid Polypeptide Membrane Disruption. Biophysical Journal 100, 685-692.

4.2 Introduction

Although the exact cause of β-cell death in Type II diabetes is unknown, there is strong evidence that human islet amyloid polypeptide (IAPP) plays an important role *(1–3).* It is well known through *in vitro*, tissue culture, and transgenic animal studies, as well as postmortem clinical examinations, that large β-sheet aggregates of IAPP, known as islet amyloid, are often associated with the development of Type II diabetes *(1–3)*. Similar extracellular proteinaceous deposits composed of large aggregates of proteins in a characteristic cross β-sheet conformation are being found in a growing number of pathologies, including Alzheimer's, Huntington's, and Parkinson's disease among many others *(4)*. An aggregated (but not necessarily fibrillar) form of the peptides and proteins implicated in these amyloid-associated diseases has been found to disrupt the integrity of cellular membranes to various degrees by allowing the uncontrolled influx of ions (in particular calcium) into the cell and subjecting the cell to membrane-associated stress *(5,6)*.

The relevant factors that trigger IAPP aggregation and pancreatic β-cell membrane disruption in some individuals but not others are elusive, as the pathology of IAPP aggregation occurs most often with the wild-type peptide and is not associated with mutations of the IAPP sequence, except for the rare S20G polymorphism *(7–10)*. Because wild-type IAPP is both aggressively amyloidogenic and toxic at low concentrations (<1 mM) when it is added exogenously, yet is stored in the secretory granule of β-cells at concentrations orders of magnitude higher (0.8–4 mM) without apparent dysfunction in non-diabetic individuals, it is unknown how IAPP is regulated to prevent both its aggregation and its inherent cytotoxicity. In fact, considering the high toxicity of IAPP *in*

vitro, it may be more relevant to question what stops IAPP from permeabilizing β-cells in healthy individuals, rather than what triggers IAPP-induced toxicity to β-cells in diabetics.

Insulin, which is co-packaged and co-secreted with IAPP within the secretory granule, has emerged as a possible regulator of IAPP fibrillogenesis. Insulin forms heterocomplexes with IAPP *(11–13)*. Several studies have reported that these heterocomplexes can inhibit IAPP amyloid formation *(12–20)*, although there is also evidence for either little change or a slight increase in the rate of fibril formation at lower ratios of IAPP to insulin *(21)*. Because insulin suppresses IAPP amyloid fiber formation and is found in great excess over IAPP in the secretory granule, it is frequently assumed that insulin also inhibits the inherent toxicity of IAPP *(11,14,17)*. However, studies on other amyloid inhibitors have shown that these two actions are not necessarily linked. For instance, compounds that bind to the end-stage of aggregation and consist mostly of amyloid fibrils are frequently unsuccessful in reducing the toxicity of amyloidogenic proteins, most likely due to the low toxicity of the end-stage amyloid fibers *(22)*. A prime example of this effect is the anti-amyloid-$\beta_{1\text{-}11}$ antibody, which was shown to inhibit amyloid-$\beta_{1–42}$ fibrillization yet failed to prevent amyloid-$\beta_{1–42}$ toxicity *(23)*. Other compounds have been shown to actually increase the toxicity of amyloid proteins by inhibiting the formation of the relatively inert amyloid fibrils while increasing the amount of peptide in the small oligomeric, more toxic form. An example of this effect is clusterin (apolipoprotein J), a protein found in Alzheimer's disease plaques that inhibits Amyloid $\beta_{1–42}$ from forming amyloid yet increases the cytotoxicity of the Amyloid $\beta_{1–42}$ peptide *(24–26)*. Conversely, other inhibitors have been shown to block the toxicity of these

peptides without affecting or increasing amyloid formation. In this study, we show that insulin does not suppress the ability of IAPP to cause model membrane disruption, an effect that is believed to be one of the prime indicators of IAPP toxicity, in a simple manner. Instead, insulin appears to eliminate only later fiber-dependent membrane disruption, without affecting earlier events in the membrane permeabilization process.

4.3 Experimental Procedures

4.3.1 IAPP and insulin preparation

IAPP was purchased from Anaspec (San Jose, CA). Recombinant human insulin expressed in yeast was purchased from Sigma-Aldrich (St. Louis, MO). The IAPP peptide used in this study was amidated at the C-terminus like the natural peptide. Preformed aggregates in both peptide preparations were disaggregated by first dissolving the peptide in a 75% acetonitrile/water solution at a concentration of 1 mg/mL. The peptides were then lyophilized and the lyophilized powder was redissolved in hexafluoroisopropanol (HFIP) at a concentration of 2–4 mg/mL. The HFIP was removed by lyophilization overnight at high vacuum *(27)*. After lyophilization was completed, the peptide was first dissolved in pure water to a concentration of 25 μM in siliconized Eppendorf tubes and then diluted with 2_ buffer to create the final working solution (final buffer composition: 10 mM sodium phosphate, pH 7.4, 100 mM NaCl) (28).

4.3.2 Liposome preparation

1-Palmitoyl-2-oleoyl-sn-glycero-3-[phospho-rac-(1-glycerol)] (POPG) and 1-Palmitoyl-2-oleoyl-sn-glycero-3-phosphocholine (POPC) dissolved in chloroform were purchased from Avanti (Alabaster, AL). To make liposomes, chloroform lipid stocks were dried with a stream of nitrogen and then placed under vacuum overnight to remove residual solvent. The lipid films were then rehydrated for 1–2 h with 10 mM NaPi buffer at pH 7.4 containing 100 mM NaCl. The rehydrated lipids were vortexed and then subjected to eight freeze-thaw cycles. The resulting multilamellar vesicles were extruded 21 times through two 100 nm polycarbonate Nucleopore membrane filters (Whatman) to create unilamellar vesicles. To prepare liposomes with dye encapsulated inside, we created vesicles as above except that the buffer also contained 50 mM 5(6)-carboxyfluorescein. Free dye was separated from the dye-encapsulated lipid vesicles by running the sample through a 10 mL Sephadex G-50 gel filtration column (Sigma-Aldrich). Lipid concentrations were determined using the Stewart method (29). Liposomes with encapsulated dye were mixed with liposomes without dye in a 1:20 ratio to create the final stock solution.

4.3.3 Membrane Disruption experiments with direct addition of IAPP/insulin samples

IAPP (10 μM concentration) was directly mixed with 200 μM POPG/POPC liposomes (1:1 molar ratio) in 50 mM sodium phosphate buffer pH 7.4, 100 mM NaCl. The fluorescence was then recorded using a Biotek Synergy 2 plate reader equipped with 494 nm excitation filter with a 2 nm band-pass, and a 512 nm emission filter with a 2 nm band-pass for 400 min at 25°C under 17 Hz linear shaking. The fluorescence signal

recorded was normalized against the value at 100% permeabilization by adding Triton-X detergent to 0.2% v/v after 400 min, which effectively permeabilized any remaining intact dye-encapsulated large unilamellar vesicles (LUVs). Dye leakage was plotted according to the following equation:

$$Dye\ Leakage = \frac{F_{sample}(t) - F_{baseline}}{F_{detergent} - F_{baseline}}$$

4.3.4 Membrane Disruption experiments with preincubation of IAPP/insulin

IAPP or IAPP/insulin was preincubated for the indicated length of time at a 25 mM concentration in siliconized Eppendorf tubes at 25°C without shaking, and then diluted and added to a concentrated POPG vesicle stock solution to initiate membrane permeabilization. The final concentrations for the assay were 1 μM IAPP, 200 μM POPG, and 0, 1, or 10 μM insulin.

4.3.5 Thioflavin T Fiber Formation assay

Peptides were initially solubilized with deionized water. Buffer and Thioflavin T (ThT) were then added to make the final concentrations 5 μM ThT, 25 μM IAPP, and 25 or 250 μM insulin in 100 mM NaCl, 10 mM NaPi, pH 7.4 buffer. The aggregation reaction was performed without shaking in sealed Corning 96-well, clear-bottom, half-area, nonbinding surface plates at a constant temperature of 25°C. The fluorescence from the ThT reporter dye was recorded by a Biotek Synergy 2 plate reader using a 440 excitation filter equipped with a 30 nm band-pass, and a 485 emission filter with a 20 nm band-pass.

4.4 Results & Discussion

4.4.1 IAPP Membrane Disruption is Biphasic with the Second Phase Associated with Fiber Formation

One of the primary mechanisms of IAPP-induced toxicity is believed to be disruption of the cellular membrane *(5, 6, 30–36)*, which leads to dysregulation of calcium homeostasis, mitochondrial overload, and eventually apoptosis. We used a dye leakage assay to measure the ability of IAPP to permeabilize model membranes. A self-quenching dye, (6)-carboxyfluorescein, was entrapped at high concentrations in POPC/POPG vesicles (1:1 molar ratio, 200 mM lipid concentration) and incubated with either IAPP alone or IAPP with varying concentrations of insulin. Disruption of the integrity of the membrane surface releases the vesicle contents into solution, where dilution of the self-quenching dye results in a large increase in fluorescence. A time-trace of dye leakage induced by 10 μM IAPP is shown in Figure 4.1. In the absence of insulin, membrane permeabilization by IAPP occurs in two distinct stages. Typically, membrane-disrupting agents (e.g., antimicrobial peptides) cause rapid, near-exponential increases in fluorescence as transient pores form on the membrane *(37, 38)*. The final normalized fluorescence value as t/N may not approach one, as would be expected for total disruption of all vesicles (graded leakage). This phenomenon has been observed for antimicrobial peptides and reported for IAPP *(36)*, and is believed to result from a relaxation process that relieves mechanical stress on the membrane, resulting in mass imbalance on the outer leaflet of the membrane caused by the binding of the peptide *(39)*. Several mechanisms have been proposed for the relaxation process, including translocation of the peptide across the membrane *(40, 41)*, which may occur through the

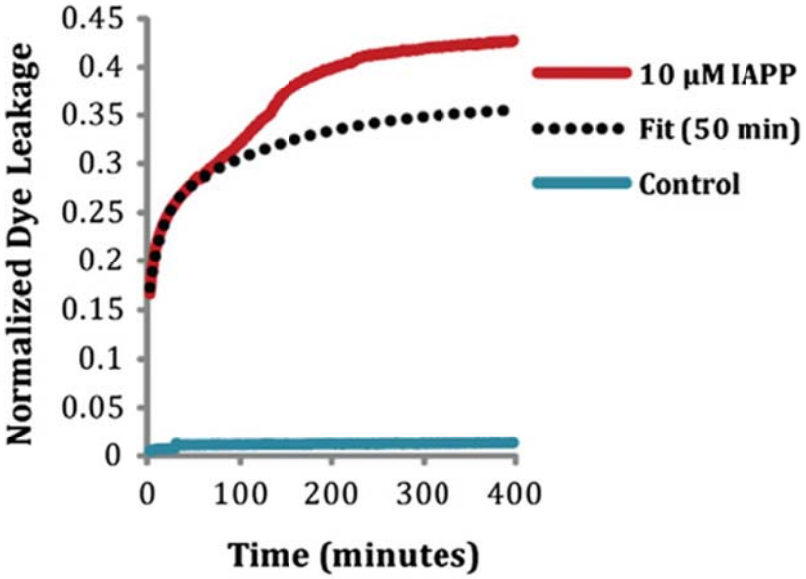

Figure 4.1 Mean (n = 5) kinetic trace of membrane disruption of 10 μM IAPP added to 200 μM POPG/POPC vesicles (1:1 molar ratio). The initial phase (t = 0–50 min) of membrane disruption was fit to a double exponential curve: Vesicles were stable over the time course of the experiment in the absence of IAPP, as shown by the negligible dye leakage that occurred in control liposomes

formation of toroidal pores *(42)* or by the removal of IAPP-lipid adducts from the membrane *(31,34,43,44)*.

The early stage of membrane disruption by IAPP (t = 0 to ~50 min) indeed displays the double exponential kinetics that is typical of antimicrobial peptides (Figure 4.1, dashed line) and readily apparent on this timescale, with the initial rise in fluorescence followed by the gradual decrease in the rate-of-efflux from the vesicle. However, a second phase is also apparent after ~50 min in which the fluorescence begins to rise once again, as shown in Figure 4.1. This second phase has been linked to damage to the membrane through the growth of amyloid fibers on the membrane, because the kinetic profile of the second phase of dye leakage is consistent with the kinetic profile of

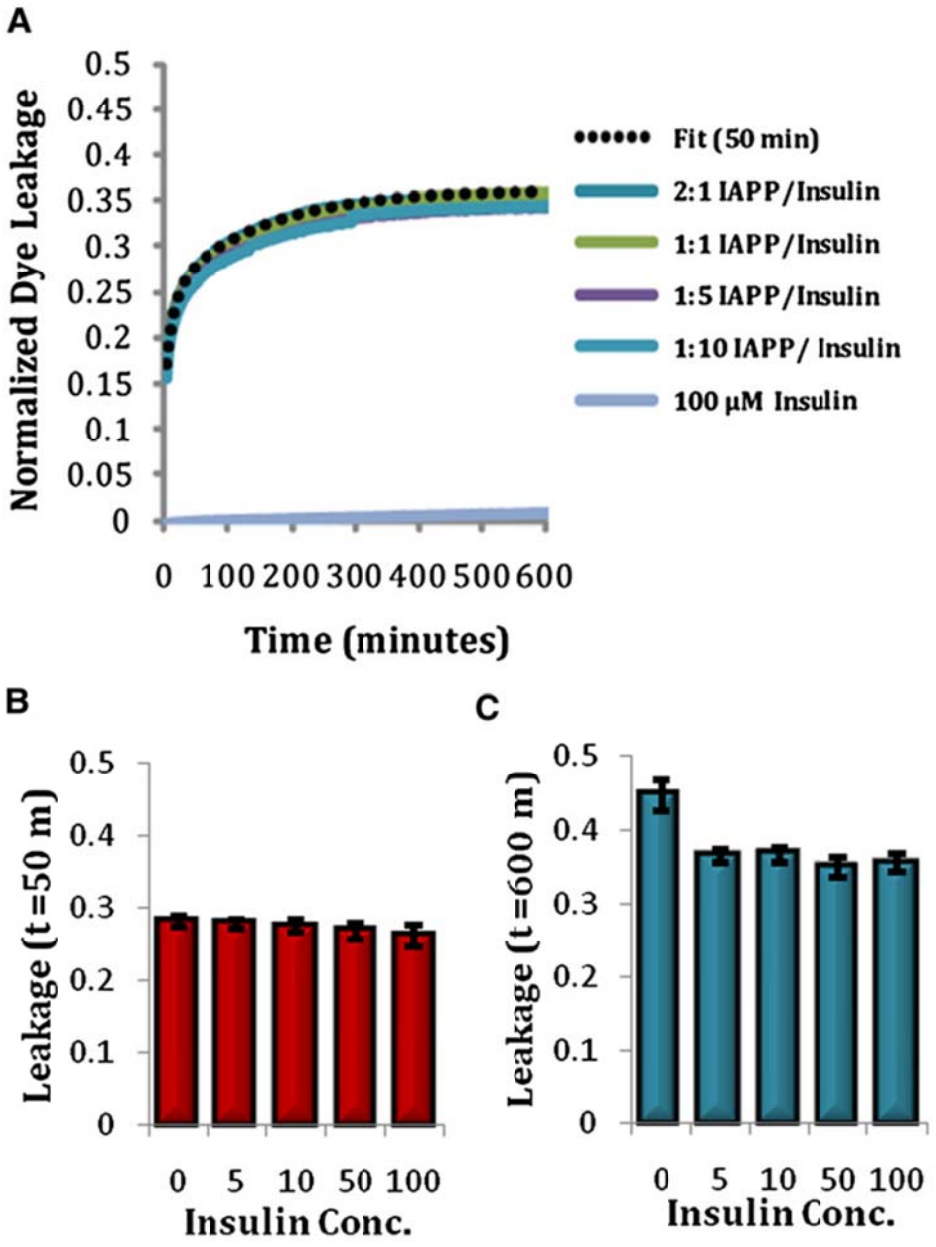

Figure 4.2 (A) Mean (n = 5) kinetic traces of membrane disruption by IAPP/insulin mixtures. The double exponential fit to the initial (t = 0–50 min) phase of membrane disruption by IAPP alone is shown for comparison (dashed line, ðdashed line; dye leakage ¼ 0:16662þ 0:11203 _ ð1 _ e_t=143:3Þ þ 0:08171 _ ð1 _ e_t=12:82ÞÞ. Insulin by itself did cause membrane disruption at any concentration over the course of the experiment (data for 5, 10, and 50 µM insulin not shown). (B) Membrane disruption caused by IAPP/insulin mixtures at t ¼ 50 min. Error bars indicate mean 5 SE (n = 5). (C) Membrane disruption caused by IAPP/insulin mixtures at t = 600 min. Error bars indicate mean 5 SE (n = 5).

amyloid formation (see Figure 4.3), as previously shown for IAPP *(31)*. The fitted curve is the same for both Figures 4.1 and 4.2.

4.4.2 Insulin Blocks IAPP Fibril-Dependent Membrane Disruption but Not Initial Membrane Permeabilization

If fibril formation correlates with the later phase of membrane disruption, molecules that block fibril formation should also inhibit or block membrane permeabilization. Because insulin has been shown to block fibril formation in both aqueous and membrane environments *(14–19)*, it is likely that it will also block fibril-dependent membrane damage. Figure 4.3 shows that even substoichiometric amounts of insulin (2:1 IAPP/insulin molar ratio) block the second phase of membrane disruption. The total amount of membrane disruption in the presence of insulin is similar to that expected based on a model of the first phase alone (Figure 4.3 B), a strong indication that suppression of IAPP amyloid formation by insulin also eliminates damage to the membrane associated with the amyloid formation process. This is in agreement with previous results that showed a decrease in the total membrane leakage by IAPP in 7:3 POPC/POPS liposomes after 1000 min in the presence of insulin *(31)*.

Of interest, although the second phase of membrane disruption is blocked, the initial rise in fluorescence is almost entirely unaffected by insulin (insulin by itself only negligibly affects the stability of the dye-loaded vesicles). For this lipid composition, insulin apparently does not block association of IAPP with the membrane, in agreement with previous attenuated total reflectance Fourier transform infrared (ATR-FTIR) results that showed a reduced, but still substantial, attachment of IAPP in 7:3 POPC/POPS

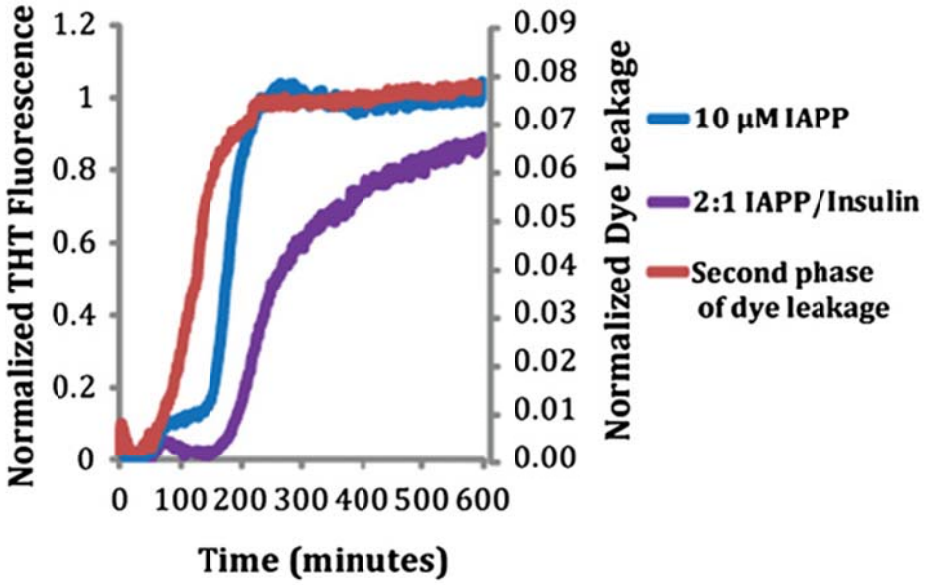

Figure 4.3 Amyloid fiber formation in relation to the second phase of membrane disruption. Amyloid fiber formation by 10 mM IAPP and 10 mM IAPP/5 mM insulin as tracked by ThT fluorescence is plotted on the left axis, and the second phase of membrane disruption is plotted on the right axis. The second phase of membrane disruption was defined as the difference between the observed fluorescence values and those predicted by a double exponential fit of the first 50 min (see Figure 4.1). Higher concentrations of insulin led to high background signals of THT fluorescence, possibly due to nonspecific binding of THT to non-amyloid forms of insulin.

liposomes in the presence of insulin *(19)*. In addition, once it is bound to the membrane, IAPP apparently is still able to affect membrane disruption.

4.4.3 Insulin Slows Time-Dependent Decrease of IAPP to Cause Membrane Disruption Associated with the Formation of Amyloid Fibrils in Solution

The varying ability of different oligomeric forms of amyloid proteins to cause membrane disruption has been the subject of intensive research. Although the exact toxicity of particular oligomeric species has been the subject of much controversy,

mature amyloid fibrils that are fully preformed in solution before addition to the membrane have been found almost universally to be less damaging to the membrane than oligomeric forms of the same peptides. For this reason, some investigators have hypothesized that the formation of amyloid fibrils serves as a protective mechanism against the toxic effects of smaller oligomeric species *(45)*. Because the amyloid form of the peptide is less effective at disrupting membranes than the freshly dissolved peptide, the ability of IAPP to permeabilize membranes declines with incubation time in solution before addition to the membrane as the percentage of preformed amyloid in the sample increases. We monitored this effect by adding IAPP (with or without insulin) to fresh lipid preparations at each time point to measure how membrane disruption changed with the growth of amyloid fibrils (Figure 4.4). IAPP's ability to permeabilize liposomes in the absence of insulin declined rapidly after 5 h of preincubation in solution before it was added to the liposomes, which roughly corresponds with the start of exponential fibril growth in solution measured by ThT fluorescence at ~15 h (Figure 4.4 B). This result is in agreement with numerous reports that have shown mature IAPP amyloid fibrils to be non-disruptive to membranes and non-toxic to cells, in contrast to earlier forms of the peptide.

In contrast to the rapid decrease in permeabilization activity with preincubation time in the absence of insulin, the ability of the IAPP/insulin mixture to permeabilize liposomes declined only a little over the course of the experiment. The membrane disruptive activity of 1:1 IAPP/ insulin did not fully disappear until after ~50 h, when it started to slowly polymerize (Figure 4.4 B). At a higher concentration of 250 μM (10x the equimolar concentration to IAPP), insulin completely prevented the time-dependent

decrease in permeabilization over the course of the experiment. Insulin by itself did not cause membrane disruption over the course of the experiment.

4.5 Conclusions Regarding Insulin's Effects on IAPP Membrane Disruption

Although insulin has been demonstrated to be an *in vitro* inhibitor of IAPP fibrillization, its effects on IAPP membrane disruption and toxicity are less understood. To test the impact of insulin on IAPP toxicity, we observed the ability of insulin to inhibit IAPP fibril formation, as well as IAPP's ability to disrupt model membranes under buffer conditions that approximate the pH and ionic strength found after secretion. We found that in POPC/POPG vesicles, 1), insulin does not inhibit the rapid permeabilization that occurs immediately after addition of IAPP to membranes; 2), insulin blocks the later rise in membrane permeabilization that is associated with fiber formation; 3), insulin only inhibits amyloid fibrillization; 4), the ability of IAPP to permeabilize membranes decreases rapidly with the time the peptide is incubated in solution in the absence of membranes; and 5), insulin arrests the time-dependent decrease in permeabilization activity, and actually maintains IAPP in such a state that it is able to permeabilize liposomes for a far longer period of time.

Membrane disruption is believed to be one of the primary causes of cell death caused by amyloidogenic proteins *(30, 35, 46).* Although there is very strong evidence that hIAPP has a deleterious effect on cell membranes, the molecular mechanisms by which this occurs are not understood. Studies so far have been conflicting: some have provided evidence for the *in vitro* formation of discrete ion-channel-like pores, whereas others have provided evidence for the total disruption of the bilayer through membrane

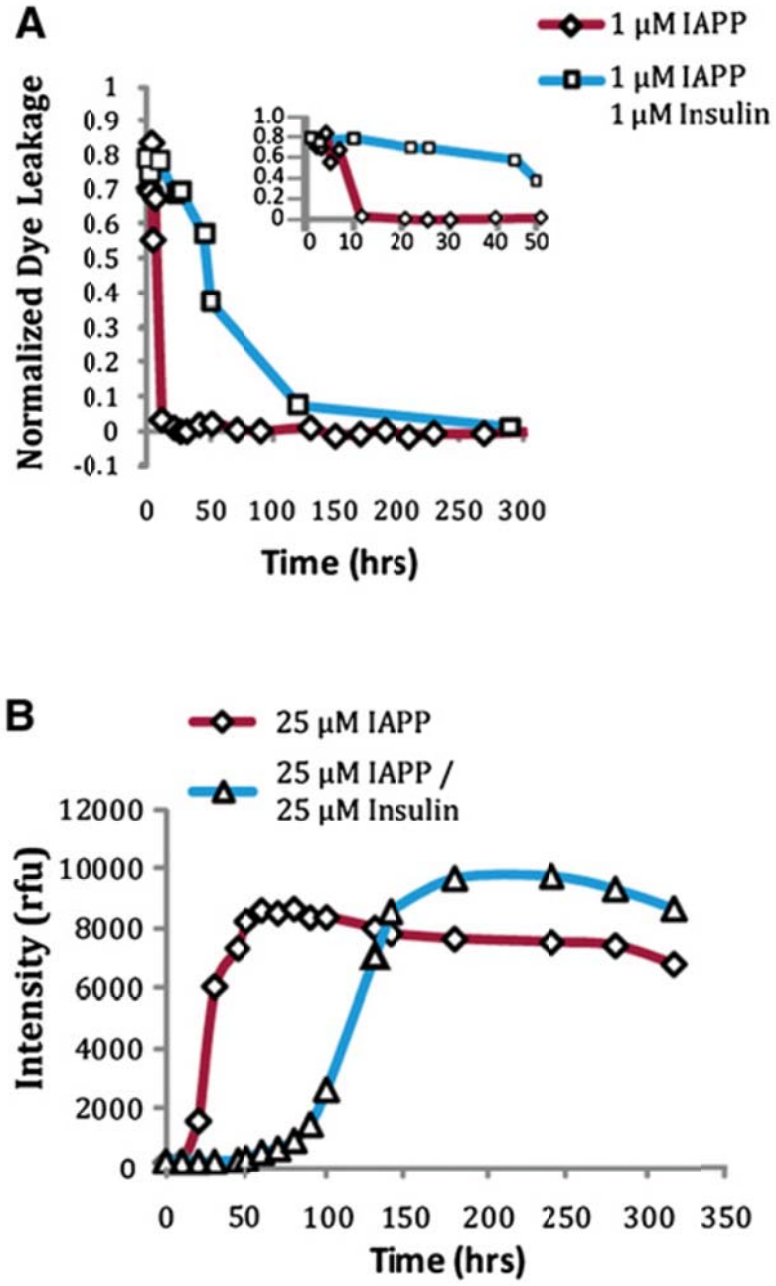

Figure 4.4 (A) Time course of membrane disruption by IAPP preincubated with insulin. First, 25 mM IAPP were incubated in solution with 0, 25, or 250 mM insulin in the absence of lipids for the indicated time points. A 1:25 dilution (1 mM IAPP and 0, 1, or 10 mM insulin) was then added to 200 mM POPG vesicles and the dye leakage that was induced after 100 s was recorded. (B) Amyloid fiber formation by 25 mM IAPP incubated with 0, 25, or 250 mM insulin in the absence of lipids as shown by ThT fluorescence.

fragmentation. Strong evidence for non-specific membrane disruption through fibril growth at the membrane comes from Engel et al. *(31),* who showed that the time course of calcein leakage from vesicles was strongly correlated with amyloid fibril formation, and that the kinetics of dye-leakage could be strongly altered by seeding amyloid formation, implying a direct link between fibril formation and membrane disruption. Furthermore, electron micrographs of giant unilamellar vesicles in the presence of IAPP showed the vesicles to be severely distorted *(31),* indicating that membrane permeabilization occurs non-specifically by mechanical fragmentation of the membrane, as has been observed in other studies *(34, 43, 44)*. On the other hand, channel-like structures have also been observed in membranes by atomic force microscopy, and discrete electrical conductances suggestive of channels have been recorded that could be reversibly blocked by zinc and other ligands *(33, 47, 48)*. In addition, a fragment of IAPP comprising the putative membrane active domain caused a rapid rise in intracellular calcium when added to islet cells, but did not form amyloid fibrils when bound to the membrane *(6, 49, 50)*. It is difficult to account for these findings with the membrane-damage-through-fibril-growth model alone, suggesting a role for non-fibril-dependent membrane damage in the early stages of membrane disruption. Indeed, early membrane permeabilization events were observed in the study by Engel et al. *(31)*, albeit with a smaller degree of disruption compared with our findings (~10% vs. ~30%). This difference is most probably due to the higher anionic content of the vesicles used here (50% vs. 30%), and their use of calcein (MW 622.6) versus carboxyfluorescein (MW 376.3), which permits leakage through smaller pores. It is likely that both channel-like and non-specific permeabilization occurs when IAPP is added to membranes, with the

amount of each being dependent on other factors such as the IAPP concentration and lipid environment, as has been proposed for the related Amyloid β peptide *(51)*. In particular, the ratio of disruption in the early to late-phase disruption has been shown to depend on the ratio of charged to zwitterionic lipids in binary POPC/POPS mixtures, with the fiber-dependent late-phase disruption dominating at the low charged to zwitterionic ratios typical of cells *(31, 35)*. Channel-like activity has also been shown to be diminished in the presence of cholesterol *(3, 5)*. On the other hand, in more complex raft-like lipid mixtures, complete disruption of the membrane occurred immediately upon addition of IAPP, even in the absence of anionic lipids and despite a much slower fibrillization rate in comparison with mixed POPC/POPS membranes *(52)*.

Insulin was found to inhibit only the later fibril-dependent process, in agreement with a study by Larson and Miranker *(14)* that showed that insulin strongly inhibits the elongation step of monomer addition to existing fibrils at substoichiometric concentrations. This inhibition of the elongation process can be expected to strongly affect membrane disruption through mechanical stress caused by fiber growth at the membrane. On the other hand, the lack of effect on the initial membrane permeabilization activity is consistent with ATR-FTIR studies showing that insulin does not completely suppress the binding of IAPP to 7:3 POPC/POPS liposomes *(19)*. The initial rise in membrane permeabilization could be linked to formation of channel-type structures; however, definite identification is inconclusive and outside the scope of this study. Among amyloid peptides, IAPP is somewhat unusual in that the highest amount of membrane disruption is detected immediately after solubilization and then decreases monotonically (Figure 4.4) *(53, 54)*. This is in contrast to most other amyloid proteins, in

which membrane disruption first increases with time, as toxic membrane-binding oligomers form in solution, and then decreases as the protofibrillar species are converted into relatively inert mature amyloid fibrils *(55–64)*. The transient nature of the protofibrillar species limits the amount of time the β-cell is exposed to the highly toxic IAPP species, because IAPP either diffuses away from the secretion point, where it rapidly disassociates below non-aggregating concentrations, or is sequestered in less toxic amyloid fibrils *(36, 65–67)*. In the act of blocking IAPP fibril formation, insulin actually prolonged the lifetime of membrane-damaging IAPP species long past its normal span in the absence of insulin (Figure 4.4). In the absence of insulin, IAPP formed fibrils in solution, and the ability of IAPP to cause membrane disruption was rapidly reduced after 5 h (Figure 4.4). However, in the presence of an equimolar amount of insulin, the ability of IAPP to induce membrane disruption was maintained for far longer and only decreased slowly after ~50 h (Figure 4.4). It is notoriously difficult to extrapolate from results on model systems to the *in vivo* situation, especially for a system as complex as IAPP/insulin/membrane. Taking these difficulties into consideration, it is worthwhile to consider what other factors besides insulin may be responsible for maintaining IAPP in a non-toxic state in normal individuals in the secretory granule and immediately after secretion. The anionic content of the membrane, which is known to change in type II diabetics *(68)*, is likely to be an important factor *(69)*. The changes in membrane cholesterol and free fatty acid levels that occur in the development of type II diabetes have been shown to have a complex effect on Amyloid β toxicity *(70)*. Preliminary results suggest that a similar effect may exist for IAPP as well *(33, 52, 71)*. Of significance, hIAPP transgenic mice only develop symptoms of diabetes when fed a high-

fat diet *(72)*, indicating a possible role of lipid metabolism in the etiology of IAPP in type II diabetes. An additional important factor may be the acidic pH of the vesicle. Acidic pH is known to strongly inhibit the fibrillogenesis of the IAPP peptide *(73, 74)*, and an acidic pH has been shown to significantly reduce the amount of membrane disruption by fragments of the IAPP peptide by altering the position of IAPP fragment within the membrane, causing it to occupy a more surface-associated topology than it would at neutral pH *(6, 50)*. Other contents of the β-cell secretory granule, such as zinc, which has been shown to reversibly blockade IAPP channels, may suppress the remaining disruptive activity that is unaffected by insulin *(48)*. Further work is needed, particularly in live cell systems, to clarify these matters.

This work was supported by National Institutes of Health grants R21DK074714 (to A.G.) and DK078885 to A.R., and American Diabetes Association grant 7-06-RA-48 (to A.G.). Jeffery Brender helped in preparation of the manuscript. Edgar Lee preformed the disruption experiments using preincubated mixtures of IAPP and insulin.

4.6 Bibliography

1. Hoppener, J., Ahren, B., and Lips, C.M. (2000) Islet amyloid and type 2 diabetes mellitus. *New England Journal of Medicine 343*, 411–419.

2. Kahn, S., Andrikopoulos, S., and Verchere, C.B. (1999) Islet amyloid: a long-recognized but underappreciated pathological feature of type 2 diabetes. *Diabetes 48,* 241–253.

3. Hull, R.L., Westermark, G.T., Westermark, P., and Kahn, S.E. (2004) Islet amyloid: a critical entity in the pathogenesis of type 2 diabetes. *Journal of Clinical Endocrinology and Metabolism 89,* 3629–3643.

4. Harrison, R.S., Sharpe, P.C., Singh, Y., and Fairlie D. P. (2007) Amyloid peptides and proteins in review. *Reviews of Physiology, Biochemistry and Pharmacology 159,* 1–77.

5. Demuro, A., Mina E., Kayed, R., Milton, S.C., Parker, I., and Glabe C.G. (2005) Calcium dysregulation and membrane disruption as a ubiquitous neurotoxic mechanism of soluble amyloid oligomers. *Journal of Biological Chemistry 280,* 17294–17300.

6. Brender, J. R., Hartman K., Reid, K. R., Kennedy, R. T., and Ramamoorthy A. (2008) A single mutation in the nonamyloidogenic region of islet amyloid polypeptide greatly reduces toxicity. Biochemistry. *47,* 12680–12688.

7. Esapa, C., Moffitt J.H., Novials, A., McNamara, C.M., Levy, L.C., Laakso, M., Gomis, R., and Clark A. (2005) Islet amyloid polypeptide gene promoter polymorphisms are not associated with type 2 diabetes or with the severity of islet amyloidosis. *Biochimica et Biophysica Acta* 1740:74–78.

8. Pildal, J., Lajer M., Hansen, S.K., Almind, K., Ambye, L., Borch-Johnsen, K., Carstensen, B., Hansen, T., and Pedersen O. (2003) Studies of variability in the islet amyloid polypeptide gene in relation to type 2 diabetes. *Diabetes Medicine 20,* 491–494.

9. Novials, A., Rojas I., Franco, C., Casamitjana, R., Usac, E.F., and Gomis R. (2001) A novel mutation in islet amyloid polypeptide (IAPP) gene promoter is associated with type II diabetes mellitus. *Diabetologia 44,* 1064–1065.

10. Sakagashira, S., Hiddinga H.J., Tateishi, K., Sanke, T., Hanabusa, T., Nanjo, K., and Eberhardt N.L. (2000) Compared to wild-type human amylin, S20G mutant amylin exhibits increased cytotoxicity in transfected COS-1 cells and increased amyloidogenicity in vitro. *Diabetes. 49,* A401–A401.

11. Wei, L., Jiang P., Yau, Y.H., Summer, H., Shochat, S.G., Mu, Y.G., and Pervushin K. 2009. Residual structure in islet amyloid polypeptide mediates its interactions with soluble insulin. *Biochemistry 48,* 2368–2376.

12. Wiltzius, J.J., Sievers, S.A., Sawaya, M.R., and Eisenberg, D., (2009) Atomic structures of IAPP (amylin) fusions suggest a mechanism for fibrillation and the role of insulin in the process. *Protein Science 18*, 1521–1530.

13. Knight, J.D., Williamson J.A., and Miranker A.D. (2008) Interaction of membrane-bound islet amyloid polypeptide with soluble and crystalline insulin. *Protein Science 17,* 1850–1856.

14. Larson, J. L., and Miranker A. D. (2004) The mechanism of insulin action on islet amyloid polypeptide fiber formation. *Journal of Molecular Biology 335,* 221–231.

15. Gilead, S., Wolfenson H., and Gazit E. (2006) Molecular mapping of the recognition interface between the islet amyloid polypeptide and insulin. *Angewandte Chemie International Edition 45,* 6476–6480.

16. Kudva, Y.C., Mueske C., Butler, P.C., and Eberhardt, N.L. (1998) A novel assay in vitro of human islet amyloid polypeptide amyloidogenesis and effects of insulin secretory vesicle peptides on amyloid formation. *Biochemical Journal 331,* 809–813.

17. Jaikaran, E.T., Nilsson M.R., and Clark A. (2004) Pancreatic β-cell granule peptides form heteromolecular complexes which inhibit islet amyloid polypeptide fibril formation. *Biochemical Journal 377,* 709–716.

18. Cui W, Ma J.W., Lei P, Wu W.H., Yu Y.P., Xiang Y, Tong A.J., Zhao Y.F., Li Y.M. (2009) Insulin is a kinetic but not a thermodynamic inhibitor of amylin aggregation. *Federation of European Biochemical Societies Journal 276,* 3365–3371.

19. Sellin, D., Yan L.M, Kapurniotu, A., and Winter R. (2010) Suppression of IAPP fibrillation at anionic lipid membranes via IAPP-derived amyloid inhibitors and insulin. *Biophysical Chemistry 150,* 73–79.

20. Westermark, P., Li Z.C., Westermark, A., Leckstrom, A., and Steiner D.F. (1996) Effects of β cell granule components on human islet amyloid polypeptide fibril formation. *Federation of European Biochemical Societies Letters 379,* 203–206.

21. Janciauskiene, S., Eriksson S., Carlemalm, E., and Ahren B. (1997) β cell granule peptides affect human islet amyloid polypeptide (IAPP) fibril formation in vitro. *Biochemical and Biophysical Research Communications 236,* 580–585.

22. Shoval, H., Weiner, L., Gazit, E., Levy, M., Pinchuk, I., and Lichtenberg, D. (2008) Polyphenol-induced dissociation of various amyloid fibrils results in a methionine-independent formation of ROS. *Biochimica et Biophysica Acta 1784,* 1570–1577.

23. Mamikonyan, G., Necula, M., Mkrtichyn, M., Ghochikyn, A., Petroshina, I., Movsesyan, N., Mina, E., Kiyatkin, A., Glabe, C.G., Cribbs, D.H., Agadjanyan, M.G. (2007) Anti-Amyloid β 1-11 antibody binds to different b-amyloid species, inhibits fibril formation, and disaggregates preformed fibrils but not the most toxic oligomers. *Journal of Biological Chemistry 282,* 22376–22386.

24. Lambert, M.P., Barlow, A.K., Chromy, B.A., Edwards, C., Freed, R., Liosatos, M., Morgan, T.E., Rozovsky, I., Trommer, B., Viola, K.L., Wals, P., Zhang, C., Finch, C.E., Krafft, G.A., Klein, W.L. (1998) Diffusible, nonfibrillar ligands derived from Amyloid β1-42 are potent central nervous system neurotoxins. *Proceedings of the National Academy of Sciences 95,* 6448–6453.

25. Oda T, Wals P, Osterburg H, Johnson S, Pasinetti G, Morgan T, Rozovsky I, Stine W, Snyder S, and Holzman T. (1995) Clusterin (apoJ) alters the aggregation of amyloid b-peptide (A b 1-42) and forms slowly sedimenting Amyloid β complexes that cause oxidative stress. *Experimental Neurology 136,* 22–31.

26. Klein, W.L., Krafft, G.A., and Finch, C.E. (2001) Targeting small Ab oligomers: the solution to an Alzheimer's disease conundrum? *Trends in Neuroscience 24,* 219–224.

27. Capone, R., Quiroz F.G., Prangkio, P., Saluja, I., Sauer, A.M., Bautista, M.R., Turner, R.S., Yang, J., and Mayer, M., (2008) Amyloid-β induced ion flux in artificial lipid bilayers and neuronal cells. *Neurotoxicity Research 15*, 608–650.

28. Higham, C.E., Jaikaran, E.T., Fraser, P.E., Gross, M., and Clark, A., (2000) Preparation of synthetic human islet amyloid polypeptide (IAPP) in a stable conformation to enable study of conversion to amyloid-like fibrils. *Federation of European Biochemical Society Letters 470,* 55–60.

29. Stewart, J.C. (1980) Colorimetric determination of phospholipids with ammonium ferrothiocyanate. *Analytical Biochemistry 104,* 10–14.

30. Engel, M.F. (2009) Membrane permeabilization by islet amyloid polypeptide. *Chemistry and Physics of Lipids 160,* 1–10.

31. Engel, M.F., Khemtemourian, L., Kleijer, C.C., Meeldijk, H.J.D., Jacobs, J., Verkleij, A.J., Kruijff, B., Killian, J.A., and Hoppener, J.W., (2008) Membrane damage by human islet amyloid polypeptide through fibril growth at the membrane. *Proceedings of the National Academy of Sciences 105,* 6033–6038.

32. Kayed, R., Sokolov, Y., Edmonds, B., McIntire, T.M., Milton, S.C., Hall, J.E., and Glabe, C.G., (2004) Permeabilization of lipid bilayers is a common conformation-dependent activity of soluble amyloid oligomers in protein misfolding diseases. *Journal of Biological Chemistry 279,* 46363–46366.

33. Mirzabekov, T.A., Lin, M.C., and Kagan, B.L., (1996) Pore formation by the cytotoxic islet amyloid peptide amylin. *Journal of Biological Chemistry 271,* 1988–1992.

34. Sparr, E., Engel, M.F., Sakharov, D.V., Sprong, M., Jacobs, J., de Kruijff, B., Hoppener, J.W., and Killian, J.A., (2004) Islet amyloid polypeptide-induced membrane leakage involves uptake of lipids by forming amyloid fibers. *Federation of European Biochemical Society Letters 577,* 117–120.

35. Hebda, J.A., and Miranker, A.D., (2009) The interplay of catalysis and toxicity by amyloid intermediates on lipid bilayers: insights from type II diabetes. *Annual Reviews of Biophysics 38,* 125–152.

36. Knight, J.D., Hebda, J.A., and Miranker, A.D., (2006) Conserved and cooperative assembly of membrane-bound a-helical states of islet amyloid polypeptide. *Biochemistry 45,* 9496–9508.

37. Rex, S., and Schwarz, G., (1998) Quantitative studies on the melittininduced leakage mechanism of lipid vesicles. *Biochemistry 37,* 2336–2345.

38. Schwarz, G., and Robert, C.H., (1992) Kinetics of pore-mediated release of marker molecules from liposomes or cells. *Biophysical Chemistry*. *42,* 291–296.

39. Almeida, P.F., and Pokorny, A., (2009) Mechanisms of antimicrobial, cytolytic, and cell-penetrating peptides: from kinetics to thermodynamics. *Biochemistry 48,* 8083–8093.

40. Gregory, S.M., Pokorny, A., and Almeida, P.F.F., (2009) Magainin 2 revisited: a test of the quantitative model for the all-or-none permeabilization of phospholipid vesicles. *Biophysical Journal 96,* 116–131.

41. Gregory, S.M., Cavenaugh, A., Journigan, V., Pokorny, A., and Almeida, P.F., (2008) A quantitative model for the all-or-none permeabilization of phospholipid vesicles by the antimicrobial peptide cecropin A. *Biophysical Journal 94,* 1667–1680.

42. Smith, P.E., Brender, J.R., and Ramamoorthy, A., (2009) Induction of negative curvature as a mechanism of cell toxicity by amyloidogenic peptides: the case of islet amyloid polypeptide. *Journal of the American Chemical Society 131,* 4470–4478.

43. Brender, J.R., Durr, U.H.N., Heyl, D., Budarapu, M.B., and Ramamoorthy, A., (2007) Membrane fragmentation by an amyloidogenic fragment of human islet amyloid polypeptide detected by solid-state NMR spectroscopy of membrane nanotubes. *Biochimica et Biophysica Acta 1768,* 2026–2029.

44. Domanov, Y.A., and Kinnunen, P.K.J., (2008) Islet amyloid polypeptide forms rigid lipid-protein amyloid fibrils on supported phospholipid bilayers. *Journal of Molecular Biology 376,* 42–54.

45. Treusch, S., Cyr, D.M., and Lindquist, S., (2009) Amyloid deposits: protection against toxic protein species? *Cell Cycle 8,* 1668–1674.

46. Khemtemourian, L., Killian, J.A., Hoppener, J.W.M., and Engel, M.F., (2008) Recent insights in islet amyloid polypeptide-induced membrane disruption and its role in b-cell death in type 2 diabetes mellitus. *Experimental Diabetes Research*, 421287.

47. Quist, A., Doudevski, I., Lin, H., Azimova, R., Ng, D., Frangione, B., Kagan, B., Ghiso, J., and Lal, R., 2005. Amyloid ion channels: a common structural link for protein-misfolding disease. *Proceedings of the National Academy of Sciences 102* 10427–10432.

48. Hirakura, Y., Yiu, W.W., Yamamoto, A., and Kagan, B.L., (2000) Amyloid peptide channels: blockade by zinc and inhibition by Congo red (amyloid channel block). *Amyloid 7,* 194–199.

49. Brender, J.R., Lee, E.L., Cavitt, M.A., Gafni, A., Steel, D.G., and Ramamoorthy, A., (2008) Amyloid fiber formation and membrane disruption are separate processes localized in two distinct regions of IAPP, the type-2-diabetes-related peptide. *Journal of the American Chemical Society 130,* 6424–6429.

50. Nanga, R.P.R., Brender, J.R., Xu, J., Veglia, G., and Ramamoorthy, A., (2008) Structures of rat and human islet amyloid polypeptide IAPP(1-19) in micelles by NMR spectroscopy. *Biochemistry. 47,* 12689–12697.

51. Schauerte, J.A., Wong, P.T., Wisser, K.C., Ding, H., Steel, D.G., and Gafni, A., (2010) Simultaneous single molecule fluorescence and conductivity studies reveal distinct classes of Amyloid β species on lipid bilayers. *Biochemistry 49,* 3031–3039.

52. Weise, K., Radovan, D., Gohlke, A., Opitz, N., and Winter, R., (2010) Interaction of hIAPP with model raft membranes and pancreatic β-cells: cytotoxicity of hIAPP oligomers. *ChemBioChem 11,* 1280–1290.

53. Anguiano, M., Nowak, R.J., and Lansbury, Jr. P.T., (2002) Protofibrillar islet amyloid polypeptide permeabilizes synthetic vesicles by a porelike mechanism that may be relevant to type II diabetes. *Biochemistry 41,* 11338–11343.

54. Porat, Y., Kolusheva, S., Jelinek, R., and Gazit, E., (2003) The human islet amyloid polypeptide forms transient membrane-active prefibrillar assemblies. *Biochemistry 42,* 10971–10977.

55. Smith, D.P., Tew, D.J., Hill, A.F., Bottomley, S.P., Masters, C.L., Barnham, K.J., and Cappai, R., (2008) Formation of a high affinity lipid-binding intermediate during the early aggregation phase of α-synuclein. *Biochemistry*. *47,* 1425–1434.

56. El-Agnaf, O.M.A., Nagala, S., Patel, B.P., and Austen, B.M., (2001) Non-fibrillar oligomeric species of the amyloid ABri peptide, implicated in familial British dementia, are more potent at inducing apoptotic cell death than protofibrils or mature fibrils. *Journal of Molecular Biology 310,* 157–168.

57. Shankar, G.M., Li, S.M., Mehta, T.H., Munoz, A.G., Shepardson, N.E., Smith, I., Brett, F.M., Farrell, M.A., Rowan, M.J., Lemere, C.A., Regan, C.M., Walsh, D.M., Sabatini, B.L., and Selkoe, D.J., (2008) Amyloid-β protein dimers isolated directly from Alzheimer's brains impair synaptic plasticity and memory. *Nature Medicine 14,* 837–842.

58. Townsend, M., Shankar, G.M., Mehta, T., Walsh, D.M., and Selkoe, D.J., (2006) Effects of secreted oligomers of amyloid b-protein on hippocampal synaptic plasticity: a potent role for trimers. *Journal of Physiology 572,* 477–492.

59. Cleary, J.P., Walsh, D.M., Hofmeister, J.J., Shankar, G.M., Kuskowski, M.A., Selkoe, D.J., and Ashe, K.H., (2005) Natural oligomers of the amyloid-b protein specifically disrupt cognitive function. *Nature Neuroscience 8,* 79–84.

60. Bitan, G., Lomakin, A., and Teplow, D.B., (2001) Amyloid β-protein oligomerization: prenucleation interactions revealed by photo-induced cross-linking of unmodified proteins. *Journal of Biological Chemistry 276,* 35176–35184.

61. Gong, Y., Chang, L., Viola, K.L., Lacor, P.N., Lambert, M.P., Finch, C.E., Krafft, G.A., and Klein, W.L., (2003) Alzheimer's disease affected brain: presence of oligomeric Amyloid β ligands (ADDLs) suggests a molecular basis for reversible memory loss. *Proceedings of the National Academy of Sciences 100,* 10417–10422.

62. Huang, T.H.J., Yang D.S., Plaskos, N.P., Go, S., Yip, C.M., Fraser, P.E., and Chakrabartty, A., (2000) Structural studies of soluble oligomers of the Alzheimer b-amyloid peptide. *Journal of Molecular Biology 297,* 73–87.

63. Lesne, S., Koh, M.T., Kotilinek, L., Kayed, R., Glabe, C.G., Yang, A., Gallagher, M., and Ashe, K.H., (2006) A specific amyloid-β protein assembly in the brain impairs memory. *Nature 440,* 352–357.

64. Hepler, RW., Grimm, K.M., Nahas, D.D., Breese, R., Dodson, E.C., Action, P., Keller, P.M., Yeager, M., Wang, H., Shughrue, P., Kinney, G., and Joyce, J.G., 2006. Solution state characterization of amyloid b-derived diffusible ligands. *Biochemistry*. *45,* 15157–15167.

65. Soong, R., Brender, J.R., Macdonald, P.M., and Ramamoorthy, A., (2009) Association of highly compact type II diabetes related islet amyloid polypeptide intermediate species at physiological temperature revealed by diffusion NMR spectroscopy. *Journal of the American Chemical Society 131,* 7079–7085.

66. Engel, M.F.M., Yigittop, H., Elgersma, R.C., Rijkers, D.T.S., Liskamp, R.M.J., de Kruijff, B., Hoppener, J.W.M., and Killian, J.A., (2006) Islet amyloid polypeptide inserts into phospholipid monolayers as monomer. *Journal of Molecular Biology 356,* 783–789.

67. Vaiana, S.M., Ghirlando, R., Yau, W.M., Eaton, W.A., and Hofrichter, J., (2008) Sedimentation studies on human amylin fail to detect low-molecular-weight oligomers. *Biophysical Journal 94,* L45–L47.

68. Rustenbeck, I., Matthies, A., and Lenzen, S., (1994) Lipid composition of glucose-stimulated pancreatic islets and insulin-secreting tumor cells. *Lipids 29,* 685–692.

69. Knight, J.D., and Miranker, A.D., (2004) Phospholipid catalysis of diabetic amyloid assembly. *Journal of Molecular Biology 341,* 1175–1187.

70. Schengrund, C.L. (2010) Lipid rafts: keys to neurodegeneration. *Brain Research Bulletin 82,* 7–17.

71. Cho, W.J., Trikha, S., and Jeremic, A.M., (2009) Cholesterol regulates assembly of human islet amyloid polypeptide on model membranes. *Journal of Molecular Biology 393,* 765–775.

72. Matveyenko, A.V., Gurlo, T., Daval, M., Butler, A.E., and Butler, P.C., (2009) Successful versus failed adaptation to high-fat diet-induced insulin resistance: the role of IAPP-induced b-cell endoplasmic reticulum stress. *Diabetes 58,* 906–916.

73. Abedini, A., and Raleigh, D.P., (2005) The role of His-18 in amyloid formation by human islet amyloid polypeptide. *Biochemistry 44,* 16284–16291.

74. Jaikaran, E.T., Higham, C.E., Serpell, L.C., Zurdo, J., Gross, M., Clark, A., and Fraser, P.E., (2001) Identification of a novel human islet amyloid polypeptide β-

sheet domain and factors influencing fibrillogenesis. *Journal of Molecular Biology 308,* 515–525.

CHAPTER 5

HELICAL CONFORMATION OF THE SEVI PRECURSOR PEPTIDE $PAP_{248-286}$, A DRAMATIC ENHANCER OF HIV INFECTIVITY, PROMOTES LIPID AGGREGATION AND FUSION

5.1 Summary

In previous *in vivo* studies, amyloid fibers formed from a peptide ubiquitous in human seminal fluid (semen-derived enhancer of viral infection (SEVI)) were found to dramatically enhance the infectivity of HIV (3–5 orders of magnitude by some measures). To complement those studies, we performed *in vitro* assays of $PAP_{248-286}$, the most active precursor to SEVI, and other polycationic polymers to investigate the physical mechanisms by which the $PAP_{248-286}$ promotes the interaction with lipid bilayers. At acidic (but not at neutral) pH, freshly dissolved $PAP_{248-286}$ catalyzes the formation of large lipid flocculates in a variety of membrane compositions, which may be linked to the promotion of convective transport in the vaginal environment rather than transport by a random Brownian motion. Furthermore, $PAP_{248-286}$ is itself fusiogenic and weakens the integrity of the membrane in such a way that may promote fusion by the HIV gp41 protein. An α-helical conformation of $PAP_{248-286}$, lying parallel to the membrane surface, is implicated in promoting bridging interactions between membranes by the screening of

This chapter is a version of a published paper: Brender, J.R., Hartman, K., Gottler, L.M., Cavitt, M.E., Youngstrom, D.W., and Ramamoorthy, A., (2009) Helical Conformation of the SEVI Precursor Peptide PAP248-286, a Dramatic Enhancer of HIV Infectivity, Promotes Lipid Aggregation and Fusion. Biophysical Journal 97, 2474-2483

the electrostatic repulsion that occurs when two membranes are brought into close contact. This suggests that nonspecific binding of monomeric or small oligomeric forms of SEVI in a helical conformation to lipid membranes may be an additional mechanism by which SEVI enhances the infectivity of HIV.

5.2 Introduction

A puzzling discrepancy in AIDS research is the low *in vitro* activity of the virus compared to the explosive growth of the AIDS pandemic. It is estimated that AIDS has killed 25 million people since it was first recognized in 1981, making it one of the most destructive epidemics in human history. Yet HIV is a surprisingly weak pathogen *in vitro*, with only a small percentage (0.1–.001%) of the virus particles able to replicate *in vitro (1,2)*. Given the high rate of mutation of HIV, it might seem reasonable to conclude that large numbers of structurally defective virus particles are produced, and only a small percentage of virus particles that are able to complete the steps of the virus life cycle are generated. Recent studies have shown that most virus particles are functional and, given the right opportunity, will infect their target cells *(3)*. However, in contrast to the *in vivo* situation, *in vitro* conditions are such that most virus particles are never given the correct opportunity to attach and fuse with the target cell before the virus particle is degraded.

What is this critical difference between the *in vivo* and *in vitro* situations? HIV has an incredible ability to evolve quickly due to the high error rate of the viral reverse transcriptase. Given HIV's ability to mutate rapidly, it also seems natural for the virus to exploit any available factors in the host environment that could be advantageous for infection. Because seminal fluid is ubiquitous during the sexual transmission of HIV, it is

a likely source for cofactors that either inhibit or enhance the infectivity of HIV *(4–6)*. Despite the presence of seminal fluid in the vast majority of HIV infections, surprisingly little is known about the effects of semen on HIV infectivity *(7–9)*. Although seminal fluid has been shown to enhance the binding of HIV virions to epithelial cells *(9)*, an active component in enhancing the infectivity of HIV has only recently been identified. Fragments of prostatic acid phosphatase (PAP), a highly abundant protein found in human semen, act as a very dramatic enhancer of HIV infectivity. Fragments of PAP, named semen-derived enhancer of viral infection (SEVI; Figure. 5.1), were shown to

Figure 5.1 Sequences of $PAP_{248-286}$ and IAPP. (Top row) Sequence of $PAP_{248-286}$. (Bottom row) Sequence of the control myloidogenic peptide human IAPP. The C-terminus is amidated and a disulfide bond exists between Cys2 and Cys7.

strongly promote HIV virus-cell attachment and fusion in multiple viral and host cell genotypes at physiological concentrations *(4)*. Most surprisingly, and most importantly, the SEVI peptide was found to drastically reduce the number of virus particles needed to establish infection under the low viral load conditions resembling sexual transmission. A truly remarkable enhancement of 4–5 orders of magnitude occurred when limiting amounts of virus were used. By comparison, most known endogenous enhancers had a much more modest 2–3-fold effect on the degree of HIV infectivity. In contrast to the large (and unrealistic) viral loads needed to infect cells *in vitro*, only 1–3 virus particles were necessary to establish a persistent infection in dendritic cells in the presence of SEVI *(4)*. Notably, these assays detected spreading HIV-1 infection, implying that the

detected virions were replication competent. The mechanism by which SEVI enhances this remarkable enhancement of HIV infection is largely unknown.

SEVI apparently has little effect on the transcription of viral RNA, as the reverse transcriptase inhibitor Efavirenz blocks viral gene expression in the presence of SEVI *(4)*. However, SEVI drastically enhances viral binding and entry into cells, enhancing HIV-1 viral fusion and subsequent gene expression ~10-fold *(4)*. Furthermore, some degree of aggregation of the peptide is necessary for activity, since freshly prepared, monomeric solutions of SEVI are ineffective at promoting viral infectivity, and the enhancement of HIV infectivity increases with time as SEVI is incubated in solution. It has been established that SEVI is an amyloidogenic peptide, and that amyloid fibers of the peptide are more effective than the monomeric peptide in promoting HIV cell binding and membrane fusion *(4)*. This is in agreement with previous studies that showed a more modest enhancement of infectivity of enveloped viruses by other amyloidogenic proteins, such as the Aβ peptide *(10)*. However, the form of SEVI responsible was not clearly identified, as the rise in infectivity induced by SEVI preceded the formation of amyloid fibers *(4)*.

Naturally occurring SEVI (the most active form of which is $PAP_{248-286}$) has a very large effect on the infectivity of HIV. The physical mechanism by which it enhances the infectivity of HIV virus is not understood, but it has been hypothesized that amyloid fibers of SEVI physically capture entering virus particles and promote their interaction with the target cell membrane without bypassing the requirement for the appropriate cell receptor *(4)*. The form of SEVI that is most active in this respect has not been identified and the available data are somewhat inconclusive in regard to the requirement for

amyloid formation for enhancement of HIV infection. $PAP_{248-286}$ isolated in the monomeric form by size exclusion chromatography is ineffective at promoting HIV infection, and centrifugation of $PAP_{248-286}$ has shown that activity resides in the high-molecular-weight pellet rather than in the low molecular- weight supernatant *(4)*. However, time-dependent assays have shown that the infection-promoting activity of $PAP_{248-286}$ begins to increase well before amyloid formation occurs, as measured by β-sheet formation by circular dichroism (CD), Thioflavin T binding, or Congo red staining *(4)*. In addition, the enhancement of infection shows up immediately when seminal fluid is spiked with freshly dissolved $PAP_{248-286}$ at pH 8.8, and within 30 min at pH 4.2 *(4)*. Munch et al. *(4)* noted that the polycationic polymer Polybrene also promoted HIV infection (to a lesser degree than SEVI), a phenomenon that has also been noted for other retroviruses *(11–14)*. The time-dependent results therefore suggest that an aggregated, but non-amyloid, form of $PAP_{248-286}$ can be as effective or even more effective than the fibrillar form of $PAP_{248-286}$ *(4)*. These experiments were performed on *in vivo* systems, whose complexity complicates attempts to determine the physical basis for the interaction of SEVI with membranes. The use of simpler model membranes allows the dissection of physicochemical effects caused by the peptide, such as increased fusiogenic activity and charge neutralization of the cellular membrane, from the effects on more complex properties such as cell viability and motility. The preliminary *in vitro* results shown here suggest that, under acidic conditions, freshly dissolved non-fibrillar $PAP_{248-286}$ appears to act similarly to other polycationic polymers, such as polybrene and polylysine, that act as general promoters of viral fusion *(11–17)*.

5.3 Experimental Procedures

5.3.1 Materials

The $PAP_{248-286}$ peptide was synthesized by Biomatik (Toronto, ON). Lipids (POPG (1- palmitoyl-2-oleoyl-*sn*-glycero-3-phospho-*rac*-(1-glycerol)), POPC (1-palmitoyl-2-oleoyl-*sn*glycero- 3-phosphocholine), POPS (1-palmitoyl-2-Oleoyl-*sn*-Glycero-3-[Phospho-L-Serine]), POPE (1-palmitoyl-2-oleoyl-*sn*-glycero-3-phosphoethanolamine), sphingomyelin (porcine brain), and cholesterol were acquired from Avanti (Alabaster, AL). HFIP (hexafluoroisopropanol) DMSO (dimethyl sulfoxide), TFA (trifluoroacetic acid), and carboxyfluorescein were obtained from Sigma-Aldrich. Polybrene (Hexadimethrine bromide) and polylysine (mol. wt. 1000-4000) were purchased from Sigma.

5.3.2 Sample Preparation

SEVI refers to the fibrillar form of a series of peptides derived from PAP that form amyloid fibers in solution and increase the infectivity of HIV. A variety of peptides within the 247-286 sequence of PAP are active, with a stringent requirement for the LIMY sequence (residues 283-286) at the C-terminus. We have chosen $PAP_{248-286}$ for this study as it is the most effective form of SEVI at enhancing HIV infectivity (sequence shown in Figure 5.1). Because preformed aggregates of the peptide can act as nuclei for further peptide aggregation and lead to inconsistent results, it is essential that the peptide be completely dissolved initially in a solvent that strongly disfavors further aggregation. Initial attempts to solubilize the peptide at a concentration of 1 mg/ml by hexafluorisopropanol (HFIP), a solvent commonly used for this purpose for other

amyloid proteins, failed. However, the peptide was soluble in a 1:1 solution of trifluoroacetic acid and HFIP at a concentration of 5 mg/ml and this method was used for the initial solubilization of the peptide in subsequent experiments. TFA and HFIP were removed from the sample by a stepwise procedure. The TFA/HFIP solvent mixture was first evaporated by a nitrogen stream and the subsequent peptide film was re-dissolved in pure HFIP at a concentration of 5 mg/mL. HFIP was then removed by lyophilization overnight (approximately 12 hours) at a 1 mTorr vacuum. The lyophilized peptide was then re-dissolved in either DMSO for dye leakage studies or buffer (50 mM sodium phosphate with 150 mM NaCl) at a concentration of 100 μM and used immediately. Human-IAPP was prepared identically to $PAP_{248-286}$ and used immediately. Polylysine and polybrene, which do not aggregate and are highly soluble in water, were directly prepared in buffer. Four types of model membranes were used in this study. The first, 7:3 POPC/POPG, is a simple model membrane commonly used to simulate a mixed anionic/zwitterionic membrane system. POPG vesicles were used in the dye leakage assays. A vesicle composition of 39.2% POPC, 18.5% POPE, 11.5% POPS, 7.7% Sphingomyelin and 23% Cholesterol was used to model the membrane of a typical host cell. *(18)* A typical viral cell membrane composition was modeled using 22% POPC, 17.3% POPE, 10% POPS, 17.3% Sphingomyelin and 33.3% Cholesterol *(18)*. Vesicles of 100 nm diameter for liposome aggregation and dye leakage studies were prepared by extrusion as previously described *(19)*. Small unilamellar vesicles (SUVs) were prepared by bath sonication of a 1 mg/ml solution of lipids for two periods of 10 minutes each.

5.3.3 Liposome Aggregation

The ability of human-IAPP, polybrene, polylysine, and $PAP_{248-286}$ to aggregate lipid vesicles was measured by the increase in turbidity at 350 nm immediately after the addition of a freshly prepared $PAP_{248-286}$ on a microplate recorder using clear polystyrene plates.

5.3.4 Membrane Disruption Assay

For the dye leakage experiments, carboxyfluorescein-containing POPG vesicles were prepared by rehydrating the dried lipid film in 50 mM sodium phosphate buffer (pH 7.5) containing 40 mM carboxyfluorescein, adjusted to pH 7.5 by the addition of sodium hydroxide. Non-encapsulated carboxyfluorescein was removed from the vesicles through size exclusion chromatography using a PD-10 column (Amersham Pharmacia Biotech, Uppsala, Sweden). Vesicle solutions were used immediately, and a fresh vesicle solution was used for each experiment. Fluorescence readings were taken at an excitation wavelength of 493 nm and an emission wavelength of 518 nm using 2 nm excitation and emission slit widths. A baseline reading was taken on the solutions prior to the addition of the peptide. After injection, the fluorescence intensity was recorded after 100 s of interaction. The fluorescence signal given by the addition of peptide was then normalized by the addition of Triton X detergent, causing all vesicles present to release any remaining dye to obtain the total possible fluorescent signal.

5.3.5 Differential Scanning Calorimetry

Peptide stock solutions in methanol (4 mg/ml) were prepared from lyophilized peptide treated as described above. The stock solution was then added to the lipid (either DiPOPE or 7:3 DMPC/DMPG) in choloroform and the solution first dried under a stream of nitrogen and then further dried under high vacuum for several hours to remove residual solvent. Buffer (10 mM Tris/HCl, 100 mM NaCl, 1 mM EDTA, 0.002 % w/v NaN3, pH 7.4 for the DiPOPE sample and 10 mM Sodium Phosphate, 150 mM NaCl, pH 7.3 for the DMPC/DMPG sample) was added to the film to produce 4 mg/ml solutions. The DMPC/DMPG samples were subjected to 5 freeze/thaw cycles before use. Changes in Cp was recorded from 10- 60°C with a heating rate of 1°C/min for the DiPOPE samples and 5-60°C with a heating rate of 0.5°C/min for the DMPC/DMPG samples.

5.3.6 Circular dichroism spectroscopy

CD samples were prepared by dissolving lyophilized peptide to a concentration of 14 μM in sodium phosphate buffer (10 mM with 150 mM NaF, pH 7.3) and briefly vortexing and sonicating (approximately 15 seconds) before transferring to a 0.1 cm cuvette. After the initial spectrum of $PAP_{248-286}$ in the absence of lipids was taken, POPE/POPG vesicles from a 40 mg/ml stock solution were titrated into the cuvette. Spectra were measured at 1 nm intervals from 185 nm to 260 nm at a scanning speed of 50 nm/min and a bandwidth of 1 nm. Each spectrum reported is the average of ten scans after subtraction of the baseline spectrum (buffer and vesicles without peptide).

5.3.7 Membrane Fusion Assay

Membrane fusion was followed by a lipid mixing assay based on the decrease in fluorescent resonance energy transfer (FRET) when labeled liposomes containing both a donor and acceptor pair fuse with unlabelled liposomes. Fusion of the labeled liposomes with unlabeled liposomes increases the average distance between the donor and acceptor lipids and therefore decreases the FRET efficiency. Small unilamellar vesicles (SUVs) containing 68% POPC, 30% POPG, and 1% NBD-PE and 1% Rhodamine-PE were prepared by sonication and mixed with a 20x fold excess of unlabelled SUVs. FRET was detected from the rhodamine emission peak at 590 nm using excitation of NBD at 440 nm. Samples were run on polystyrene microplates on a Synergy 2 microplate reader using deep blocking filters with an excitation bandwidth of 30 nm and emission bandwidth of 35 nm.

5.4 Results & Discussion

5.4.1 Freshly dissolved $PAP_{248-286}$ promotes the aggregation of lipid vesicles

SEVI peptides have been proposed to increase the infectivity of HIV by increasing the attachment of virus particles to the cell membrane through charge neutralization. To compare the efficiency of $PAP_{248-286}$ with that of other cationic polymers, we performed turbidity assays for the aggregation of lipid vesicles induced by $PAP_{248-286}$, polybrene, and the amyloidogenic peptide human islet amyloid polypeptide (IAPP) (Figure 5.2). The assays were performed at two different lipid concentrations to test the effects of the peptide/lipid ratio on vesicle aggregation. At pH 7.3, none of the compounds induced substantial vesicle aggregation at lipid concentrations of 200 mM or

1000 mM. Polybrene, a highly charged cationic polymer commonly used to increase the efficiency of gene transfection, caused the most aggregation of the compounds tested (Figure 5.2 A). Freshly dissolved human-IAPP, an amyloidogenic peptide with a charge of +3 at pH 7.3, caused slightly less aggregation. Significantly, freshly dissolved $PAP_{248-286}$ did not induce any aggregation at this pH, in agreement with the finding that freshly dissolved $PAP_{248-286}$ does not increase HIV infectivity and presumably does not increase the attachment of virus particles to the cell membrane.

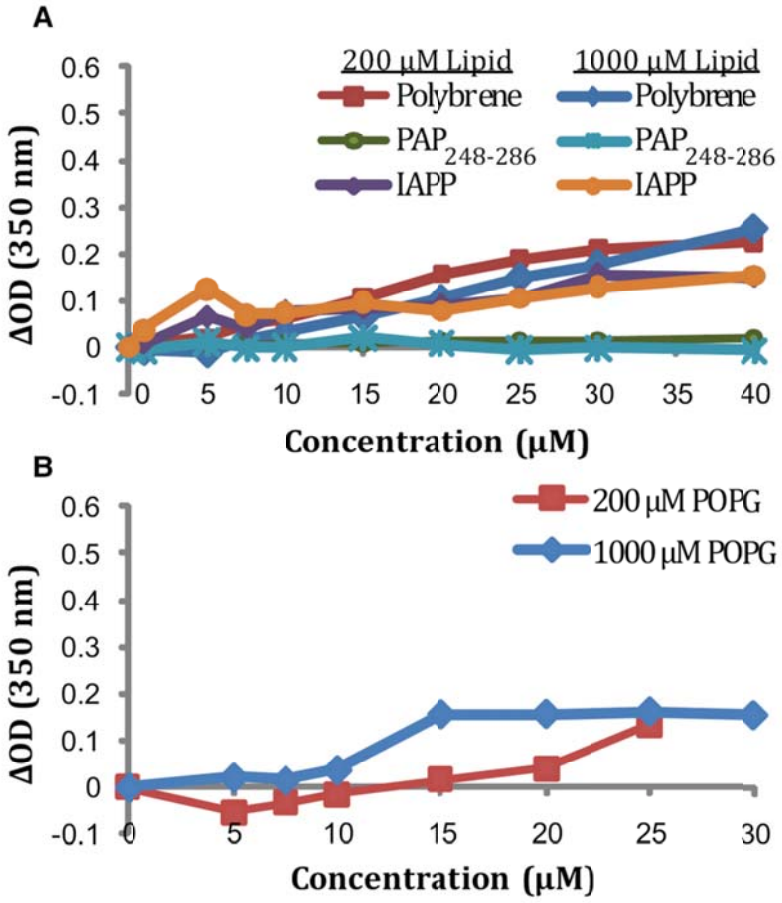

Figure 5.2 Lipid aggregation of liposomes detected by changes in turbidity at pH 7.3 (A) in the presence of POPC/POPG (7:3 ratio) vesicles and (B) POPG vesicles. Reported values are the changes in the absorbance at 350 nm relative to the control immediately after addition of the peptide or polymer and vigorous mixing. Two different lipid concentrations (200 µM and 1000 µM) were used as indicated.

The ability of SEVI to increase HIV infectivity has been linked to its cationic nature, since mutants in which the charged residues in $PAP_{248-286}$ are mutated to alanine form amyloid fibers but are not able to increase HIV infection rates *(20)*. To check the influence of electrostatics on $PAP_{248-286}$ binding, we used an alternate lipid composition of 100% POPG (Figure 5.2 B). The amount of lipid aggregation in this model membrane increased but was still less than has been reported for other amyloidogenic peptides *(21)*.

The vaginal environment is typically acidic (near pH 4), and polycation-induced membrane aggregation and membrane fusion increase substantially near this pH as the pH approaches the pKa of the phosphatidylglycerol or phosphatidylserine headgroup *(22–24)*. In addition, $PAP_{248-286}$ also has two Histadine residues that are likely to be charged at pH 4 but not at pH 7.3, resulting in a higher electrostatic interaction with the membrane at pH 4. In contrast to the neutral pH condition, $PAP_{248-286}$ caused appreciable lipid aggregation at acidic pH in 7:3 POPC/POPG liposomes (Figure 5.3 A). Furthermore, the lipid aggregates produced are considerably larger than those produced at neutral pH and could be visibly detected sedimenting to the bottom of the cuvette, even under the influence of shaking or stirring (Figure 5.3, D and E). Of interest, the decrease in pH had the opposite effect on human-IAPP, which caused more lipid aggregation than $PAP_{248-286}$ at neutral pH but did not cause any detectible lipid aggregation at pH 4, despite having an additional charged residue in Histidine. Similar results were obtained with membranes resembling the viral envelope (Figure 5.3 B) and host cell (Figure 5.3 C), albeit with a lesser degree of aggregation, most likely due to the decreased amount of anionic lipids or increased cholesterol content in these membranes.

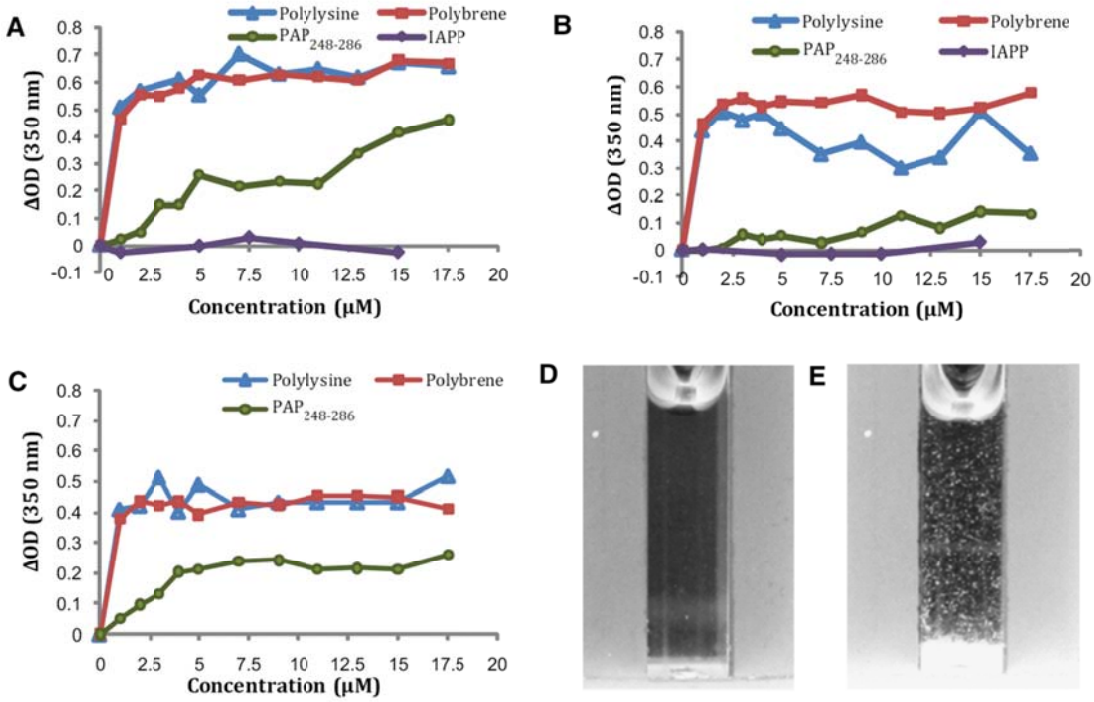

Figure 5.3 Lipid aggregation of liposomes of varying composition detected by changes in turbidity at pH 4: (A) 7:3 POPC/POPG, (B) viral membrane composition, and (C) host cell membrane composition. Reported values are the changes in the absorbance at 350 nm relative to the control immediately after addition of the peptide or polymer and vigorous mixing. (D) A photograph of the sample containing 100 nm 7:3 POPC/POPG liposomes at 500 mM concentration before the addition of 17.5 mM PAP248-286. (E) A photograph of the same sample 10 min after the addition of 17.5 mM PAP248-286.

5.4.2 Freshly dissolved $PAP_{248-286}$ promotes the mixing of lipid molecules between membranes in a manner suggestive of membrane fusion

In addition to promoting the binding of liposomes to each other, $PAP_{248-286}$ promotes the interchange of the membranes of both vesicles, measured by a fluorescence probe dilution assay. Small unilamellar vesicles (SUVs) doubly labeled with rhodamine and NBD-labeled glycerophosphocholine probes (1% each) were mixed with unlabeled vesicles in the presence of the indicated concentrations of peptide. Fusion of the labeled vesicles with the unlabeled ones results in an increased average distance between probes

and a decreased fluorescence resonance energy transfer (FRET) efficiency. Polylysine, polybrene, and $PAP_{248-286}$ all promoted the fusion of POPC/POPG SUVs in the absence of calcium (Figure 5.4). In contrast to vesicle aggregation, lipid mixing induced by low concentrations (<10 μM) of $PAP_{248-286}$ appears to be nearly as effective at neutral pH as at acidic pH. At higher concentrations (>12.5 μM) $PAP_{248-286}$ becomes as effective as polylysine at promoting the fusion of SUVs.

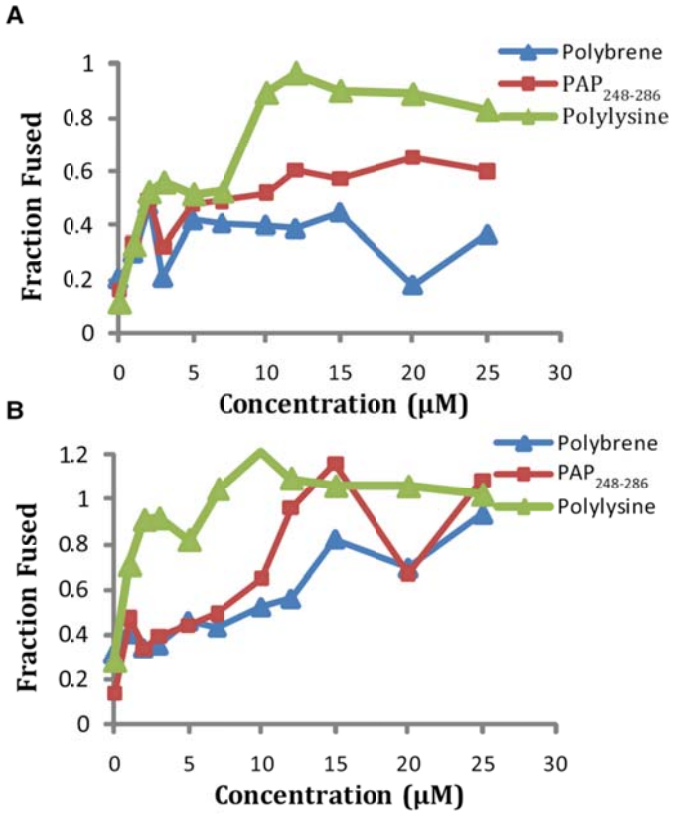

Figure 5.4 Membrane fusion induced at (A) pH 7.3 and (B) pH 4 by PAP248-286 in 7:3 POPC/POPG vesicles as measured by a FRET-based lipid mixing assay. Samples were normalized to 100% lipid mixing using the FRET efficiency in the presence of 1% Triton-X.

5.4.3 $PAP_{248-286}$ induces negative curvature in the membrane

The process of vesicle fusion is marked by the formation of a highly curved intermediate that is energetically unfavorable *(25)*. Peptides that interact with the membrane in such a way as to reduce the physical stress imposed on the membrane by the formation of this highly curved intermediate can be expected to enhance fusion *(26, 27)*. The stabilization of membrane curvature by $PAP_{248-286}$ can be conveniently followed by recording the shift in the phase transition temperature from the flat liquid crystalline (L_α) phase to the highly curved inverted hexagonal phase (H_{II}) in which the lipid molecules are arranged cylindrically with the polar headgroups facing inward *(26–30)*. Peptides that either stabilize negative (convex) membrane curvature or increase the bending elasticity of the membrane will favor the formation of the H_{II} phase, and will accordingly decrease the associated phase transition temperature (T_H) *(31–34)*. DiPoPE has a T_H of 47.8°C under these conditions in the absence of $PAP_{248-286}$. The incorporation of $PAP_{248-286}$ into DiPoPE multilamellar vesicles reduced T_H (Figure 5.5), indicating $PAP_{248-286}$ facilitates the formation of the highly curved H_{II} phase. The reduction of T_H with the incorporation of $PAP_{248-286}$ occurs as a two-step (or multiple-step) process. The incorporation of a very small percentage (0.00625 mol %) of $PAP_{248-286}$ into the DiPoPE vesicles led to a 0.9°C decrease in T_H, whereas larger percentages (0.25 and 0.4%) were required for further decreases in T_H. The reason for the multistage nature of the decrease in T_H is unclear at present.

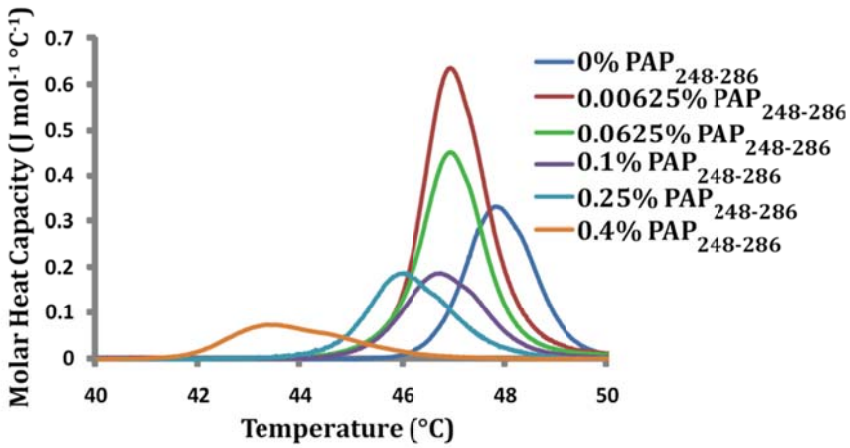

Figure 5.5 PAP248-286 promotes the formation of the negatively curved inverted hexagonal (HII) phase. DSC heating scans of DiPoPE multilamellar vesicless containing the listed molar %s of PAP248-286.

5.4.4 Freshly dissolved $PAP_{248-286}$ induces membrane disruption

Many amyloid peptides are disruptive to membranes, and damage to the integrity of the cellular membrane is believed to be one of the main causes of amyloid-related pathologies. To see whether the $PAP_{248-286}$ peptide also possesses this prominent feature of amyloid peptides, we performed dye leakage experiments on POPG vesicles as a function of peptide concentration. Carboxyfluorescein is self-quenched if it is incorporated into the vesicle at high (40 mM) concentrations. Disruption of the integrity of the membrane of the vesicle by the peptide allows carboxyfluorescein to escape, reducing the effective concentration and eliminating the self-quenching effect, which can be normalized by total disruption of the vesicles by Triton-X. Figure 5.6 shows the increase in fluorescence after the addition of $PAP_{248-286}$ to 100 μM POPG vesicles. The leakage of the dye carboxyfluorescein from large unilamellar vesicles upon the addition of $PAP_{248-286}$ indicates that $PAP_{248-286}$ induces significant membrane disruption if it binds to the membrane. $PAP_{248-286}$ did not induce significant disruption until a certain critical

concentration (~500 nM) was reached. Membrane disruption in POPG vesicles increases sigmoidally beyond this critical concentration, reaching saturation at ~1.5 mM or a peptide/lipid molar ratio of 1.5%. However, in vesicles that more closely resemble the composition of either the viral lipid envelope (Figure 5.6 C) or the host cell (Figure 5.6 B), disruption of the membrane is much less prominent. Although $PAP_{248-286}$ is very effective at permeabilizing POPG vesicles at nanomolar concentrations, even high peptide concentrations (50 μM) are insufficient for membrane disruption when the percentage of anionic lipids is lowered to levels that are typical of human cells.

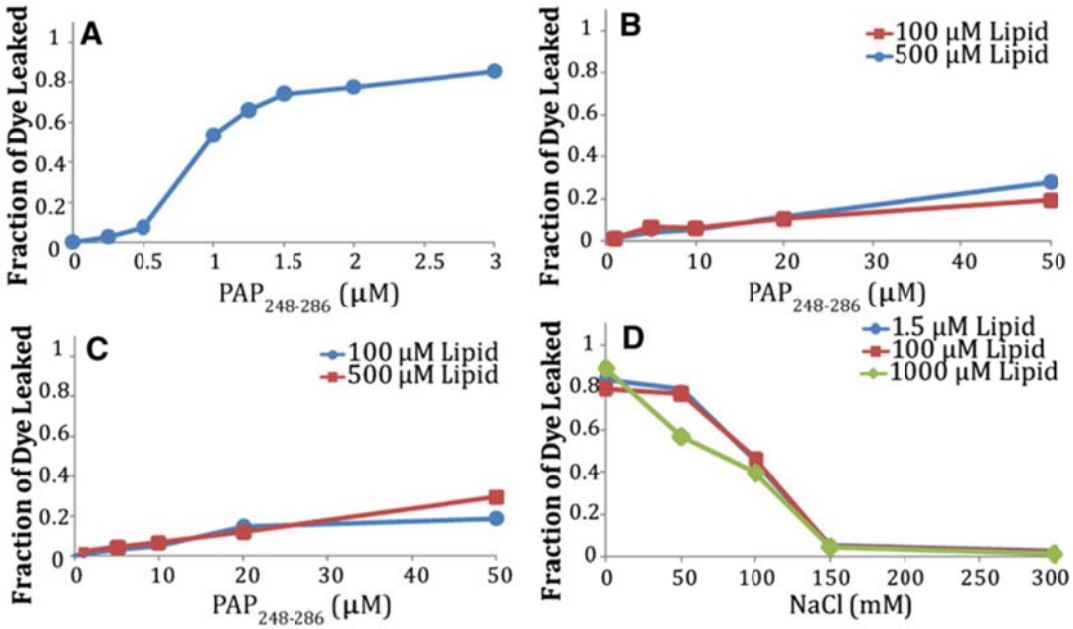

Figure 5.6 Membrane disruption caused by PAP248-286 as measured by a dye leakage assay. Dye leakage assay as a function of PAP248-286 concentration for 100 mM POPG vesicles (A), host-type vesicles by PAP248-286 (B), and viral-type vesicles (C). (D) Dye leakage of the indicated concentrations of POPG vesicles by 1 mMPAP248-286 as a function of NaCl concentration.

The ability of $PAP_{248-286}$ to effectively disrupt POPG vesicles, but not vesicles with a lower anionic lipid content, suggests that electrostatic interactions form a large share of the free energy of membrane binding *(35,36)*. To further investigate this possibility in model membrane systems, we recorded dye leakage from 7:3 POPG/POPC vesicles as a function of increasing salt concentration (Figure 5.6 D). At the 150 mM NaCl concentration used in previous experiments, the membrane disruption induced by $PAP_{248-286}$ is negligible for this lipid system. However, when the NaCl concentration is lowered to 100 mM NaCl, there is significant membrane permeabilization, and the vesicles are almost entirely disrupted at 50 mM NaCl. This result, along with the polar and cationic nature of the peptide and the known correspondence between basic residues and the ability of $PAP_{248-286}$ to enhance HIV activity, suggests that the binding of $PAP_{248-286}$ to the membrane is primarily electrostatic in nature. However, the binding may be modulated by other factors, such as the degree of cholesterol incorporation into the membrane and the phospholipid type *(37)*.

5.4.5 $PAP_{248-286}$ interacts weakly with the surface of lipid bilayers

The phase transition between the gel and liquid crystalline phases of lipids can be strongly perturbed by the binding of peptides to the membrane depending on the binding mode *(38, 39)*. The degree of perturbation is strongly dependent on the mode of binding. An amphiphilic peptide that partly penetrates into the interior of the membrane will interfere with lipid-lipid interactions within the membrane and therefore decrease the cooperativity of the phase transition, resulting in a decrease in the sharpness of the phase transition. Peptide binding at the water/membrane interface also disorders the

surrounding lipids because the acyl chains of the lipid molecules must reorganize to fill the void created beneath the peptide in the hydrophobic core of the membrane, resulting in a decrease in the ΔH and phase transition temperature (T_m) associated with the transition. On the other hand, a peptide that is bound only to the surface of the membrane and does not penetrate into the interior of the membrane, or is bound in a transmembrane orientation will not have a significant effect on the phase transition because the lipid-lipid interactions are disrupted to a much lower degree compared to a surface-associated peptide *(40)*.

Figure 5.7 A shows the effect of $PAP_{248-286}$ on the phase transition of mixed 7:3 DMPC/DMPG vesicles as determined by differential scanning calorimetry (DSC). The DSC thermogram of pure 7:3 DMPC/DMPG vesicles shows a single main transition at 24.5°C indicative of the main gel-to-liquid crystalline phase transition, and a smaller pretransition at 5.4°C indicative of the gel-to-rippled gel phase transition *(41)*. The addition of $PAP_{248-286}$ up to 2 mol % did not have a significant effect on the thermodynamics of the gel-to-liquid crystalline phase transition, except for a slight widening of the transition and a small shift of the transition to lower temperatures when the $PAP_{248-286}$ concentration exceeded 1 mol %. A similar effect was previously reported for low-molecular-weight polylysine. The absence of a significant effect suggests that the peptide is either peripherally bound to the surface of the membrane or is deeply inserted into the membrane in a transmembrane orientation, which would require less reorganization of the lipids to accommodate the peptide than a surface-bound orientation would. Although both types of binding would give rise to DSC thermograms similar to Figure 5.7 A, a deep insertion into the membrane seems unlikely considering the high

positive charge on the peptide and the lack of a hydrophobic or even amphipathic region in the peptide. Significantly, the main transition peak is nearly symmetrical at all concentrations of $PAP_{248-286}$, indicating that $PAP_{248-286}$ does not induce domain formation in the membrane or phase separation of the sample, as has been observed for some rigid polycationic compounds and high-molecular-weight polylysines at higher mole percentages.

5.4.6 $PAP_{248-286}$ binds to membranes in a partial a-helical conformation

In addition to the random coil and amyloid β-sheet conformations found in solution, amyloid proteins frequently bind to membranes in α-helical conformations *(42–44)*. The α-helical conformation represents an intermediate state before β-sheet aggregation and, perhaps paradoxically at first glance, is believed to catalyze the transition from the random coil conformation to the amyloid state *(45)*. The α-helical conformation has been implicated as being responsible for the membrane-perturbing effects of many amyloid proteins. To see whether $PAP_{248-286}$ binds to lipid membranes in an α-helical conformation, we obtained CD spectra of $PAP_{248-286}$ incubated with 7:3 POPC/POPG liposomes (Figure 5.7 B). The CD spectra show that freshly dissolved $PAP_{248-286}$ exists primarily in a random coil conformation, in agreement with previous findings. The addition of liposomes induces a conformational change in the peptide to a partial helical structure (Figure 5.7 B). Analysis of the spectra shown in Figure 5.7 B by the CONTINLL program suggests a helical content of ~30% *(46)*; however, it is likely

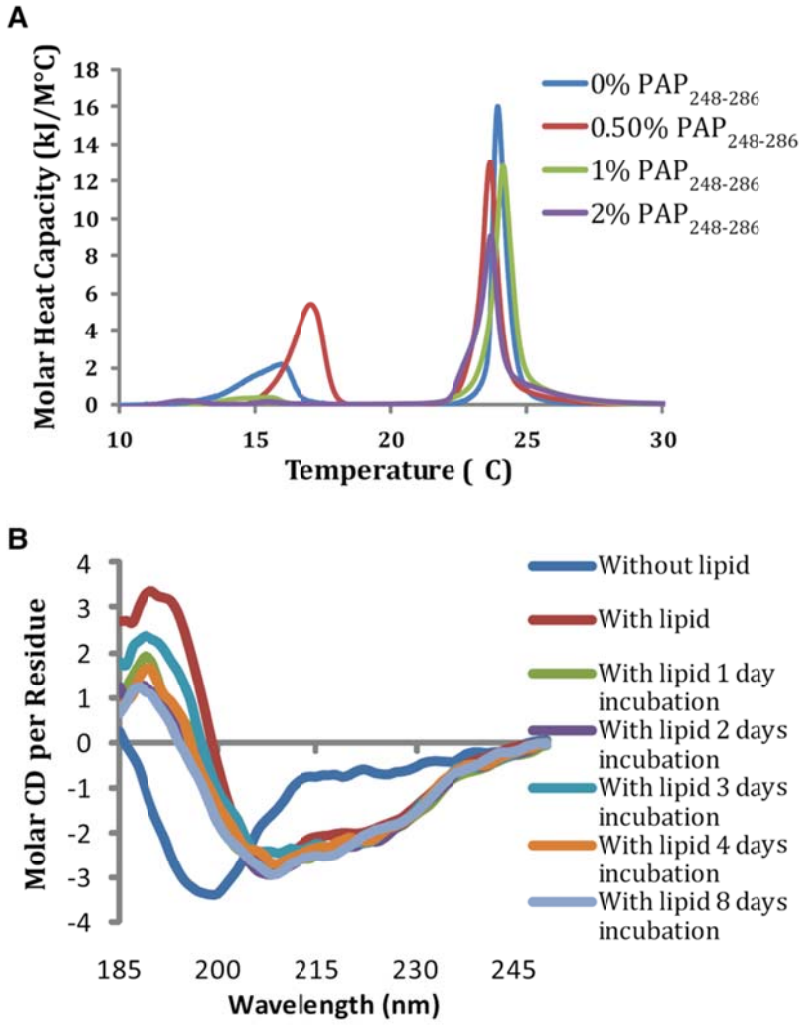

Figure 5.7 Surface interaction with membrane systems induces α-helix formation of $PAP_{248-286}$. (A) Differential scanning calorimetry of the pretransition and the main gel-to-liquid crystalline phase transition of 7:3 DMPC:DMPG vesicles at the indicated PAP248-286/lipid molar ratios. (B) CD spectra of 7 mM PAP248-286 in 10 mM sodium phosphate buffer with 150 mM NaF at pH 7.3 as a function of incubation time after the addition of 1 mM 7:3 POPC/POPG vesicles.

that this number underestimates the true helical content of the sample, as the signal from the peptide is apparently diminished at higher lipid concentrations where aggregation of the lipid vesicles is visible to the naked eye (see Figure 5.3 E). An artificially low apparent concentration of $PAP_{248-286}$ tends to reduce the apparent conformational change upon lipid binding, because the simulated spectra constructed by the CONTINLL program compensates for the missing peptide signal by adding a random coil component of opposite sign. A comparison of $PAP_{248-286}$ with the crystal structure of the full PAP protein predicts two α-helices (residues 3–12 and residues 16–27) for $PAP_{248-286}$ separated by a flexible region containing the two glycines at positions 13 and 14 *(47)*. Although $PAP_{248-286}$ is likely to adopt a different structure when bound to the membrane, the crystal structure of the full PAP protein does give an indication of the putative helical regions of membrane-bound $PAP_{248-286}$.

5.4.7 $PAP_{248-286}$ causes the formation of large lipid flocculates at acidic, but not neutral, pH

Freshly dissolved $PAP_{248-286}$ has a clear tendency to induce the aggregation of liposomes at acidic pH, but not at neutral pH, as indicated by the increase in optical density due to the higher scattering caused by larger aggregated liposomes. At neutral pH, none of the compounds tested, including the polycations polybrene and the amyloid peptides $PAP_{248-286}$ and human-IAPP, caused significant liposome aggregation. In fact, at neutral pH, $PAP_{248-286}$ had the least effect on liposome aggregation of all the compounds tested. At an acidic pH mirroring the vaginal environment before fertilization, the situation was quite different: $PAP_{248-286}$ and the polycationic polymer compounds caused significant aggregation at micromolar concentrations in partially anionic 7:3

POPC/POPG, host-type, and also in viral-type membranes to a somewhat smaller degree. Significantly, freshly dissolved human-IAPP, a strongly amyloidogenic peptide with a relatively high positive charge, did not strongly affect lipid aggregation. Furthermore, the lipid aggregates formed in this process were very large and rapidly fell out of solution and sedimented to the bottom.

The ability of $PAP_{248-286}$ to induce the formation of large lipid flocculates at acidic pH has interesting consequences if this result is confirmed *in vivo*. First, the presence of lipid aggregates confirms that $PAP_{248-286}$ interacts with model membranes, and, more importantly, has the ability to interact with two membranes simultaneously. Bridging interactions between the viral and host cell membranes induced by monomeric or small oligomeric species of $PAP_{248-286}$ can enhance infection by enhancing viral binding to the cell. Second, the formation of large lipid aggregates may alter the mechanism of the initial approach of the virus to the cell surface. Detailed mechanistic studies have shown that the entry of retroviruses is ultimately limited by the diffusion of the virus to the target cell surface *(48, 49)*. Given enough time, all retrovirus particles will reach the appropriate receptor necessary to trigger fusion of the retrovirus with the target cell through Brownian motion. However, retroviruses are unstable in solution and have short half-lives (estimated to be on the order of ~6 h for free virons of HIV) that limit the available window of opportunity for infection *(50)*. Brownian motion of the relatively small viral particle is inherently random and slow, and thus most virons are unable to reach the target cell surface before being destroyed. If viral particles aggregate together, the inefficient diffusion limited capture process may be bypassed in favor of much more rapid sedimentation of the virus to the cell surface by convective processes *(17)*. This

process has been shown to be effective in promoting retrovirus infection *in vitro*, where directed mass transfer of the virus to plated cells significantly enhances infection rates *(11, 17, 51–53)*. The effect of virus aggregation in the *in vivo* situation, where cell densities are much higher and target cells are in a three-dimensional matrix, is much less certain; however, the influence of $PAP_{248-286}$/SEVI on virus aggregation and convective transport warrants further investigation *(54, 55)*.

5.4.8 $PAP_{248-286}$ is fusiogenic and alters the physical properties of the membrane in a way that may favor fusion by gp41

In contrast to the formation of lipid flocculates, which can only be detected at acidic pH, $PAP_{248-286}$ causes lipid mixing at both neutral and acidic pH in the absence of calcium. Lipid mixing is one of the prerequisites for proper fusion of two membranes. In this instance, $PAP_{248-286}$ is more effective than polybrene but less effective than polylysine at both of the pH values tested. In addition to the direct promotion of fusion by $PAP_{248-286}$, binding of $PAP_{248-286}$ to the cell membrane changes the physical properties of the membrane in a way that may make it more susceptible to fusion by the gp41 protein of HIV. Specifically, $PAP_{248-286}$ induces negative curvature in the membrane and disrupts lipid-lipid contacts, thus reducing the force needed by the HIV gp41 protein to rupture the membrane and promote fusion *(56)*. Lastly, we have shown that $PAP_{248-286}$ can affect the membrane strongly enough to disrupt membrane integrity to allow the passage of small molecules (Figure 5.6). This is an indication of a general weakening of the membrane structure induced by $PAP_{248-286}$. There is also an indication that such additions of additives that alter membrane structure may have such an effect on viral fusion. Pretreatment of cultured cells with phosphatidylserine, a fusion-promoting lipid, results

in a relatively large increase (2- to 20-fold) in enveloped virus infection rates that is cumulative with the charge-shielding effect of polybrene *(57)*. This effect has been linked to facilitation of the viral fusion process, because it occurs without a concomitant increase in viral binding to cells or virus receptor levels *(57)*.

5.4.9 Role of a helical conformation of $PAP_{248-286}$ in lipid-bridging interactions

The CD spectra of $PAP_{248-286}$ bound to POPC/POPG vesicles suggest that $PAP_{248-286}$ binds initially to the membrane in a partial helical conformation, and that it can be stabilized at low concentration in this conformation for extended periods of time. This finding puts $PAP_{248-286}$ in the class of amyloid proteins that are essentially unstructured in solution but adopt a-helical conformations when initially bound to membranes *(58, 59)*. As helical conformations are also common early intermediates in the fibrillogenesis of amyloidogenic peptides, the binding of $PAP_{248-286}$ to the cellular membrane may be important for catalyzing the formation of SEVI from monomeric $PAP_{248-286}$. *(45, 60)* Although at first glance it might seem paradoxical that the stabilization of helical states of $PAP_{248-286}$ would promote the formation of an entirely different fold, the self-association of helical stretches in $PAP_{248-286}$ can catalyze the amyloid formation by increasing the effective concentration of unfolded and aggregation-prone sequences within $PAP_{248-286}$ through the reduction of translational and rotational diffusion. This templating effect is partially responsible for the acceleration of fibrillogenesis of many amyloidogenic proteins by lipid membranes, helix-promoting solvents, and molecular crowding agents. Although the partially helical structure detected here was found to be stable only when bound to membranes, it may also represent a transient conformation of the peptide in

solution. The CD spectra of $PAP_{248-286}$ in solution suggest a structure that is almost entirely in a random coil conformation; however, NMR studies have shown that other amyloidogenic peptides that appear unstructured by CD and FTIR transiently adopt helical structure *(61, 62)*.

A partially helical conformation of $PAP_{248-286}$ may also explain the fusiogenic activity of the peptide. In this a-helical conformation, the $PAP_{248-286}$ peptide can be expected to bind parallel to the surface of the bilayer, since a transmembrane orientation of the peptide is unlikely due to the difficulty in this orientation of simultaneously shielding all of the positively charged residues that radiate from the helix in all directions (see Figure 5.8). A surface-associated helical conformation of $PAP_{248-286}$ has several features that make it an attractive model to explain the bilayer fusion induced by the monomeric form of the peptide. First, electrostatic binding of the peptide to the surface is likely to partially dehydrate the lipid headgroup, removing a steric barrier to fusion in a manner similar to that caused by the binding of polyethyleneglycol *(63)*.

The removal of water from the lipid headgroup also has the effect of reducing the effective headgroup size of the lipid relative to the acyl chain. To compensate for this mismatch in relative sizes between the two regions of the lipid molecule, the membrane can curve outward, which is an obligate step for fusion that is strongly energetically unfavorable in the absence of $PAP_{248-286}$. Second, some of the lysine residues in this model face into the membrane, where they would interact with the lipid headgroups of the membrane, whereas other lysine residues face in the opposite direction into the

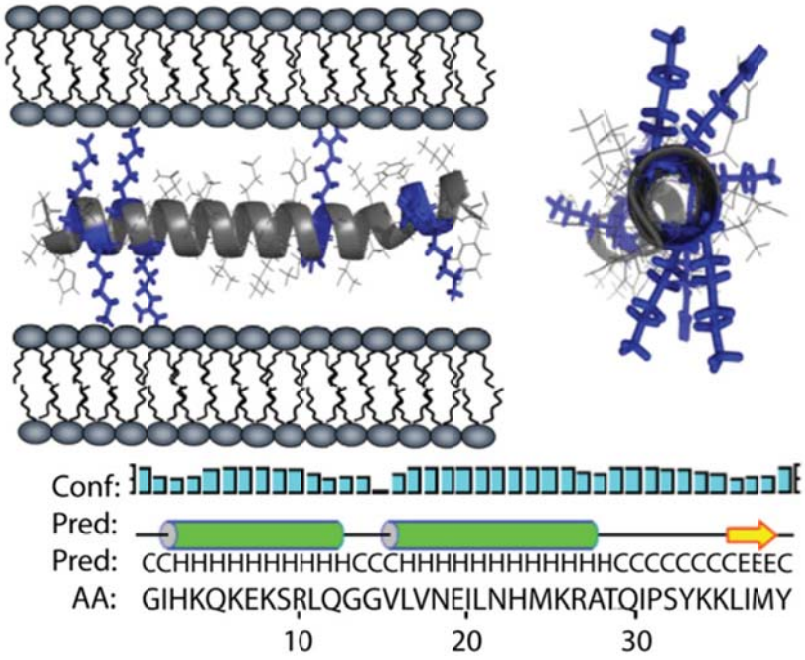

Figure 5.8 Two views of the proposed a-helical form of PAP248-286 showing the radial distribution of positively charged residues and the possible interaction with the membrane. The secondary structure of PAP248-286 within full-length PAP. The letter ‘‘C’’ represents a residue in the random coil conformation, ‘‘H’’ is a residue in a helical conformation, and ‘‘E’’ is a residue in the b-sheet conformation.

aqueous phase. In this position, they are optimally positioned to diminish the long-range Coulombic repulsion that occurs when two bilayers of like sign are brought into contact. Furthermore, as the two bilayers approach each other during the initial stages of fusion; it is likely that the lysine chains of $PAP_{248-286}$ reach into the second bilayer to serve as an anchor linking the two bilayers together. Since the structure of the amyloid form of $PAP_{248-286}$ is not known, it is difficult to make predictions about the possible membrane interactions of the amyloid form of $PAP_{248-286}$ as they are likely to be highly dependent on the supramolecular organization of the peptide. Notably, other amyloid proteins, which share the same gross cross-β sheet structure as the amyloid form of $PAP_{248-286}$, are

less effective at promoting HIV infectivity *(4)*. The determination of the high-resolution structure of the amyloid form of $PAP_{248-286}$ will likely be very informative in illuminating the nature of these differences.

5.6 Conclusions Regarding the Membrane Interactions of $PAP_{248-286}$

Freshly prepared $PAP_{248-286}$ that is initially in the random coil conformation interacts strongly with lipid membranes, adopting a partial helical conformation that appears to promote bridging interactions between membranes and their eventual fusion by screening unfavorable electrostatic interactions. In this state, $PAP_{248-286}$ induces alterations in a variety of model membranes that appear to weaken lipid-lipid interactions and promote curved lipid phases that would be conducive to fusion. These alterations in membrane structure are not specific for the amyloid form of $PAP_{248-286}$ and are similar to changes in membrane structure produced by other disordered, polycationic polymers that also promote retroviral infection. The relative importance of the partially helical conformation for SEVI enhancement of HIV infection warrants further investigation. Given the very high degree of enhancement of HIV infectivity induced by SEVI, and its ubiquity in seminal fluid, such research is likely to have a high impact on investigations regarding HIV transmission and prevention.

This study was supported by research funds from the National Institutes of Health (to A.R.).Jeffery Brender helped in the preparation of the manuscript. Lindsy Gottler preformed the aggregation experiments involving POPC/POPG. Marchello Cavitt prefomed the DSC experiments of DiPOPE. Dan Youngstrom helped in performing the aggregation experiments.

5.7 Bibliography

1. Dimitrov, D.S., Willey, R.L., Sato, H., Chang, L.J., Blumenthal, R., Martin, M.A., (1993) Quantitation of human-immunodeficiency-virus type-1 infection kinetics. *Journal of Virology 67,* 2182–2190.

2. Rusert, P., M. Fischer, M., B. Joos, B., C. Leemann, C., H. Kuster, H., Flepp, M., Bonhoeffer, S., Gunthard, H.F., Trkola, A., (2004) Quantification of nfectious HIV-1 plasma viral load using a boosted *in vitro* infection protocol. *Virology 326,* 113–129.

3. Thomas, J.A., Ott, D.E., and Gorelick, R.J., (2007) Efficiency of human immunodeficiency virus type 1 postentry infection processes: evidence against disproportionate numbers of defective virions. *Journal of Virology 81,* 4367–4370.

4. Munch, J., Rucker, E., Standker, L., Adermann, K., Goffinet, C., ., Schindler, M., Wildum, S., Chinnadurai, R., Rajan, D., Specht, A., Gimenez-Gallego, G., Sanchez, P.C., Fowler, D.M., Koulov, A., Kelly, J.W., Mothes, W., Grivel, J.C., Margolis, L., Keppler, O.T., Forssmann, W.G., Kirchhoff, F., (2007) Semen-derived amyloid fibrils drastically enhance HIV infection. *Cell 131,* 1059–1071.

5. Munch, J., Standker, L., Adermann, K., Schuz, A., Schindler, M., Chinnadurai, R., Pohlmann, S., Chaipan, C., Beit, T., Peters, T., Meyer, B., Wilhelm, D., Lu, H., Jing, W., Jiang, S., Forssmann, W.G., Kirchhoff, F., (2007) Discovery and optimization of a natural HIV-1 entry inhibitor targeting the gp41 fusion peptide. *Cell 129,* 263–275.

6. Sabatte, J., Ceballos, A., Raiden, S., Vermeulen, M., Nahmod, K., Magini, J., Salamone, G., Salomon, H., Amigorena, S., Geffner, J., (2007) Human seminal plasma abrogates the capture and transmission of human immunodeficiency virus type 1 to cd4(þ) t cells mediated by DC-Sign. *Journal of Virology 81,* 13723–13734.

7. Miller, C.J., and Shattock, R.J., (2003) Target cells in vaginal HIV transmission. *Microbes and Infection 5,* 59–67.

8. Sharkey, D. J., Macpherson, A.M., Tremellen, K.P., and Robertson, S.A., (2007) Seminal plasma differentially regulates inflammatory cytokine gene expression in human cervical and vaginal epithelial cells. *Molecular Human Reproduction 13,* 491–501.

9. Maher, D., Wu, X.Y., Schacker, Horbul, J., and Southern, P., (2005) HIV binding, penetration, and primary infection in human cervicovaginal tissue. *Proceedings of the National Academy of Science 102,* 11504–11509.

10. Wojtowicz, W.M., Farzan, M., Joyal, J.L., Carter, K., Babcock, G.J., Israel, D.I., Sodroski, J., Mirzabekov, T., (2002) Stimulation of enveloped virus infection by b-amyloid fibrils. *Journal of Biological Chemistry 277,* 35019–35024.

11. Landazuri, N., and Le Doux. J.M., (2004) Complexation of retroviruses with charged polymers enhances gene transfer by increasing the rate that viruses are delivered to cells. *Journal of Gene Medicine*. 6, 1304–1319.

12. Davis, H.E., Morgan, J.R., and Yarmush, M.L., (2002) Polybrene increases retrovirus gene transfer efficiency by enhancing receptor-independent virus adsorption on target cell membranes. *Biophysical Chemistry* 97, 159–172.

13. Abe, A., Miyanohara, A., and Friedmann, T., (1998) Polybrene increases the efficiency of gene transfer by lipofection. *Gene Therapy* 5, 708–711.

14. Arcasoy, S.M., Latoche, J.D., Gondor, M., Pitt, B.R., and Pilewski, J.M., (1997) Polycations increase the efficiency of adenovirus-mediated gene transfer to epithelial and endothelial cells *in vitro*. *Gene Therapy* 4, 32–38.

15. Aubin, R.J., Weinfeld, M., and Paterson, M.C., (1988) Factors influencing efficiency and reproducibility of polybrene-assisted gene-transfer. *Stomatic Cell and Molecular Genetics 14,* 155–167.

16. Bajaj, B., Lei, P., and Andreadis, S.T., (2001) High efficiencies of gene transfer with immobilized recombinant retrovirus: Kinetics and optimization. *Biotechnology Progress 17,* 587–596.

17. Davis, H.E., Rosinski, M., Morgan, J.R., and Yarmush, M.L., (2004) Charged polymers modulate retrovirus transduction via membrane charge neutralization and virus aggregation. *Biophysical Journal* 86, 1234–1242.

18. Aloia, R.C., Tian, H.R., and Jensen. F.C., (1993) Lipid-composition and fluidity of the human-immunodeficiency-virus envelope and host-cell plasma-membranes. *Proceedings of the National Academy of Science 90,* 5181–5185.

19. Brender, J.R., Lee, E.L., Cavitt, M.A., Gafni, A., Steel, D.G., Ramamoorthy, A., (2008) Amyloid fiber formation and membrane disruption are separate processes localized in two distinct regions of IAPP, the type-2-diabetes- related peptide. *Journal of the Americal Chemical Society 130,* 6424–6429.

20. Roan, N.R., Munch, J., Arhel, N., Mothes, W., Neidleman, J., Kobayashi, A., Smith-McCune, K., Kirchhoff, F., Greene, W.C., (2009) The cationic properties of sevi underlie its ability to enhance human immunodeficiency virus infection. *Journal of Virology 83,* 73–80.

21. Kurganov, B., Doh, M., and Arispe, N., (2004) Aggregation of liposomes induced by the toxic peptides Alzheimer's a b s, human amylin and prion (106–126): facilitation by membrane-bound GM1 ganglioside. *Peptides 25,* 217–232.

22. Tevi-Benissan, C., Belec, L., Levy, M., Schneider-Fauveau, V., Si Mohamed, A., Hallouin, M.C., Matta, M., Gresenquet, G., (1997) *In vivo* semen-associated pH neutralization of cervicovaginal secretions. *Clinical and Diagnostic Laboratory Immunology 4,* 367–374.

23. Lakhdarghazal, F., Tichadou, J.L., and Tocanne, J.F., (1983) Effect of pH and mono-valent cations on the ionization state of phosphatidylglycerol in monolayers—an experimental (surface-potential) and theoretical (Gouy-Chapman) approach. *European Journal of Biochemistry 134,* 531–537.

24. Walter, A., Steer, C.J., and Blumenthal, R., (1986) Polylysine induces pH-dependent fusion of acidic phospholipid vesicles: a model for polycation-induced fusion. *Biochimica et Biophysica Acta 861,* 319–330.

25. Chernomordik, L. (1996) Non-bilayer lipids and biological fusion intermediates. *Chemistry and Physics of Lipids 81,* 203–213.

26. Epand, R.M., and Epand. R.F., (1994) Relationship between the infectivity of influenza-virus and the ability of its fusion peptide to perturb bilayers. Biochem. Biophys. Res. Commun. 202:1420–1425.

27. Siegel, D.P., and Epand, R.M., (2000) Effect of influenza hemagglutinin fusion peptide on lamellar/inverted phase transitions in dipalmitoleoylphosphatidylethanolamine: Implications for membrane fusion mechanisms. *Biochimica et Biophysica Acta 1468,* 87–98.

28. Hallock, K.J., Lee, D.K., and Ramamoorthy, A., (2003) MSI-78, an analogue of the magainin antimicrobial peptides, disrupts lipid bilayer structure via positive curvature strain. *Biophysical Journal 84,* 3052–3060.

29. Wildman, K.A.H., Lee, D.K., and Ramamoorthy, A., (2003) Mechanism of lipid bilayer disruption by the human antimicrobial peptide, LL-37. *Biochemistry 42,* 6545–6558.

30. Epand, R.F., Martin, I., Ruysschaert, J.M., and Epand, R.M., (1994) Membrane orientation of the SIV fusion peptide determines its effect on bilayer stability and ability to promote membrane-fusion. *Biochemical and Biophysical Research Communications 205,* 1938–1943.

31. Epand, R.M. (1998) Lipid polymorphism and protein-lipid interactions. *Biochimica et Biophysica Acta 1376,* 353–368.

32. Israelachvili, J.N., Marcelja, S., and Horn, R.G., (1980) Physical principles of membrane organization. *Quarterly Reviews of Biophysics 13,* 121–200.

33. Cullis, P.R., and Dekruijff, B., (1979) Lipid polymorphism and the functional roles of lipids in biological-membranes. *Biochimica et Biophysica Acta 559,* 399–420.

34. Gruner, S.M. (1989) Stability of lyotropic phases with curved interfaces. *Journal of Physical Chemistry 93,* 7562–7570.

35. Bechinger, B., and Lohner, K., (2006) Detergent-like actions of linear amphipathic cationic antimicrobial peptides. *Biochimica et Biophysica Acta 1758,* 1529–1539.

36. Ramamoorthy, A. (2009) Beyond NMR spectra of antimicrobial peptides: dynamical images at atomic resolution and functional insights. *Solid State Nuclear Magnetic Resonance. 35,* 201–207.

37. Bechinger, B. (1999) The structure, dynamics and orientation of antimicrobial peptides in membranes by multidimensional solid-state NMR spectroscopy. *Biochimica et Biophysica Acta 1462,* 157–183.

38. Pappalardo, G., Milardi, D., Magri, A., Attanasio, F., Impellizzeri, G., La Rosa, C., Grasso, D., Rizzarelli, E., (2007) Environmental factors differently affect human and rat IAPP: conformational preferences and membrane interactions of IAPP17–29 peptide derivatives. *Chemistry A European Journal 13,* 10204–10215.

39. Grasso, D., Milardi, D., La Rosa, C., and Rizzarelli E., (2001) Dsc study of the interaction of the prion peptide Prp106–126 with artificial membranes. *New Journal of Chemistry* 25:1543–1548.

40. McElhaney, R.N. (1986) Differential scanning calorimetric studies of lipid protein interactions in model membrane systems. *Biochimica et Biophysica Acta 864,* 361–421.

41. Bayerl, T.M., Kochy, T., and Bruckner, S., (1990) On the modulation of a high-enthalpy pretransition in binary-mixtures of DMPC and DMPG by polar headgroup interaction. *Biophysical Journal 57,* 675–680.

42. Knight, J.D., Hebda, J.A., and Miranker, A.D., (2006) Conserved and cooperative assembly of membrane-bound a-helical states of islet amyloid polypeptide. *Biochemistry 45,* 9496–9508.

43. Jo, E.J., McLaurin, J., Yip, C.M., St George-Hyslop, P., and Fraser, P.E., 2000. a-Synuclein membrane interactions and lipid specificity. *Journal of Biological Chemistry 275,* 34328–34334.

44. Terzi, E., Holzemann, G., and Seelig, J., (1997) Interaction of Alzheimer β-amyloid peptide(1–40) with lipid membranes. *Biochemistry 36,* 14845–14852.

45. Kirkitadze, M.D., Condron, M.M., and Teplow, D.B., (2001) Identification and characterization of key kinetic intermediates in amyloid b-protein fibrillogenesis. *Journal of Molecular Biology 312,* 1103–1119.

46. Greenfield, N.J. (2006) Using circular dichroism spectra to estimate protein secondary structure. *Nature Protocols 1,* 2876–2890.

47. Jakob, C.G., Lewinski, K., Kuciel, R., Ostrowski, W., and Lebioda, L., 2000. Crystal structure of human prostatic acid phosphatase. *Prostate 42,* 211–218.

48. Tempaku, A. (2005) Random Brownian motion regulates the quantity of human immunodeficiency virus type-1 (HIV-1) attachment and infection to target cell. *Journal of Health Science 51,* 237–241.

49. Chuck, A.S., Clarke, M.F., and Palsson, B.O., (1996) Retroviral infection is limited by Brownian motion. Hum. *Gene Therapy 7,* 1527–1534.

50. Perelson, A.S., Neumann, A.U., Markowitz, M., Leonard, J.M., and Ho, D.D., (1996) HIV-1 dynamics *in vivo*: virion clearance rate, infected cell life-span, and viral generation time. *Science 271,* 1582–1586.

51. Landazuri, N., Gupta, M., and Le Doux. J.M., (2006) Rapid concentration and purification of retrovirus by flocculation with polybrene. *Journal of Biotechnolology 125,* 529–539.

52. Landazuri, N., Krishna, D., Gupta, M., and Le Doux, J.M., 2007. Retrovirus-polymer complexes: study of the factors affecting the dose response of transduction. *Biotechnology Progress 23,* 480–487.

53. Le Doux, J.M., Landazuri, N., Yarmush, M.L., and Morgan, J.R., 2001. Complexation of retrovirus with cationic and anionic polymers increases the efficiency of gene transfer. Hum. *Gene Therapy 12,* 1611–1621.

54. Sturman, L.S., Ricard, C.S., and Holmes, K.V., (1990) Conformational change of the coronavirus peplomer glycoprotein at pH 8.0 and 37_C correlates with virus aggregation and virus-induced cell fusion. *Journal of Virology 64,* 3042–3050.

55. Hirst, G.K., and Pons, M.W., (1973) Mechanism of influenza recombination. 2. Virus aggregation and its effect on plaque formation by so-called noninfective virus. *Virology 56,* 620–631.

56. Harada, S., Yusa, K., Monde, K., Akaike, T., and Maeda, Y., (2005) Influence of membrane fluidity on human immunodeficiency virus type 1 entry. *Biochemical and Biophysical Research Communications* 329, 480–486.

57. Coil, D.A., and Miller, A.D., (2005) Enhancement of enveloped virus entry by phosphatidylserine. *Journal of Virology 79,* 11496–11500.

58. Jayasinghe, S.A., and Langen, R.., (2005) Lipid membranes modulate the structure of islet amyloid polypeptide. *Biochemistry 44,* 12113–12119.

59. Abedini, A., and Raleigh, D.P., (2009) A role for helical intermediates in amyloid formation by natively unfolded polypeptides? *Physical Biology 6,* 15005.

60. Knight, J.D., and Miranker, A.D., (2004) Phospholipid catalysis of diabetic amyloid assembly. *Journal of Molecular Biology* 341, 1175–1187.

61. Williamson, J.A., and Miranker, A.D (2007) Direct detection of transient a-helical states in islet amyloid polypeptide. *Protein Science 16,* 110–117.

62. Yonemoto, I.T., Kroon, G.J., Dyson, H.J., Balch, W.E., and Kelly, J.W., (2008) Amylin proprotein processing generates progressively more amyloidogenic peptides that initially sample the helical state. *Biochemistry 47,* 9900–9910.

63. Cevc, G., and Richardsen, H., (1999) Lipid vesicles and membrane fusion. *Advances in Drug Delivery Reviews*. *38,* 207–232.

CHAPTER 6

SITE SPECIFIC INTERACTION WITH THE SEVI PRECURSOR $PAP_{248-286}$ BY GREEN TEA EXTRACT COMPOUND EPIGALLOCATECHIN-3-GALLATE

6.1 Summary

Recently, a 39 amino acid peptide fragment from prostatic acid phosphatase has been isolated from seminal fluid that can enhance infectivity of the HIV virus by up to four to five orders of magnitude. PAP(248-286) is effective in enhancing HIV infectivity only when it is aggregated into amyloid fibers termed SEVI. The polyphenol EGCG (epigallocatechin-3-gallate) has been shown to disrupt both SEVI formation and HIV promotion by SEVI, but the mechanism by which it accomplishes this task is unknown. Here we show by NMR spectroscopy that EGCG interacts specifically with the side-chains of monomeric PAP(248-286) in two regions (K251-R257 and N269-I277) of primarily charged residues, particularly lysine. This finding is contrary to previous studies on the interaction of EGCG with other amyloidogenic proteins, which showed the nonspecific interaction of EGCG with exposed backbone sites of unfolded amyloidogenic proteins. This interaction is specific to EGCG as the related gallocatechin (GC) molecule, which shows greatly decreased anti-amyloid activity, exhibits minimal interaction with

---

This chapter is a version of a paper in publishing: Popovych, N., Brender, J.R., Soong, R., Vivekanandan, S., Basrur, V., Hartman, K., Macdonald, P.M., and Ramamoorthy, A., (2012) Site Specific Interaction of EGCG with the SEVI Precursor PAP(248-286). Journal of Physical Chemistry B (In Press).

monomeric PAP(248-286). The EGCG binding was shown to occur in two steps, with the initial formation of a weakly bound complex followed by a pH dependent formation of a tightly bound complex. Experiments in which the lysine residues of PAP(248-286) have been chemically modified suggest the tightly bound complex is created by Schiff-base formation with lysine residues. The results of this study should be useful for the development of small molecule inhibitors of SEVI and other amyloid proteins.

6.2 Introduction

The HIV virus responsible for AIDS is the source of a global pandemic with over 33 million people worldwide currently infected with the virus. The scope of the AIDS pandemic sparks the question: why is HIV so prevalent in the population and transmitted so readily *in vivo*, while the virus itself has a very poor infection rate *in vitro*? One possibility is the presence of *in vivo* cofactors that facilitate entry of the virus, causing infection to occur at a higher rate *(1)*. Recently, a cofactor has been found in human seminal fluid that could prove to be a key component in HIV transmission *(2)*. A peptide fragment of prostatic acid phosphatase ($PAP_{248-286}$) *(1)* was discovered to increase the infection rate of HIV *(2-6)* and other enveloped viruses *(6, 7)* by several orders of magnitude when aggregated into amyloid fibrils termed SEVI.

The degree to which $PAP_{248-286}$ promotes HIV infection is dependent on the conformation and aggregation state of the peptide, with the monomeric peptide being ineffective at promoting HIV infection *(2, 8)*. Since $PAP_{248-286}$ is only effective in enhancing HIV infection in the aggregated SEVI form, molecules that suppress fibrillization of $PAP_{248-286}$ into the active amyloid form can decrease the effective

infectiousness of HIV. Given the potentially high impact SEVI amyloid formation may have on the sexual transmission of HIV, a low cost SEVI inhibitor incorporated into an antiretroviral microbicide may have a substantial effect on HIV transmission rates *(5, 9-10).*

A polyphenolic compound found in green tea (epigallocatechin-3-gallate or EGCG) inhibits the formation of SEVI fibers, disaggregates existing SEVI fibers, and blocks the SEVI mediated attachment of HIV virion to target cells and SEVI promotion of HIV infectivity *(9).* EGCG has also been able to show inhibition of amyloid formation for a number of different amyloids including amyloid-β and IAPP *(11-13)*. Polyphenolic compounds like EGCG, are among the most effective anti-aggregative agents discovered to date, effectively inhibiting aggregation of a broad-spectrum of amyloidogenic proteins *(14).* The exact mechanism by which polyphenols disrupt amyloid formation is unclear, but they appear to act at multiple points along the aggregation pathway to inhibit the elongation of existing fibers and to disrupt the formation of nuclei for further amyloid formation *(12, 15-17).* EGCG has been proposed to bind to backbone sites exposed in the disordered conformation of the monomeric species of many amyloid proteins, redirecting the aggregation pathway to amorphous aggregates that are non-toxic and do not share many of the common features of amyloid-based structures *(12, 16).* The general mechanism by which polyphenolic compounds block amyloid formation is of considerable importance, as amyloid formation is a common feature of many degenerative diseases including Alzheimer's, type II diabetes, Parkinson's, Creutzfield-Jacob's, Huntington's and others *(18).* Small molecules that disrupt aggregated forms of these proteins could have considerable clinical application, making a determination of the

mechanism by which polyphenols disrupt aggregated conformations essential for structure-activity assays. EGCG itself has been shown to both block amyloid formation and abrogate amyloid-associated toxicity for many of these proteins *(12,13, 16, 19-20).*

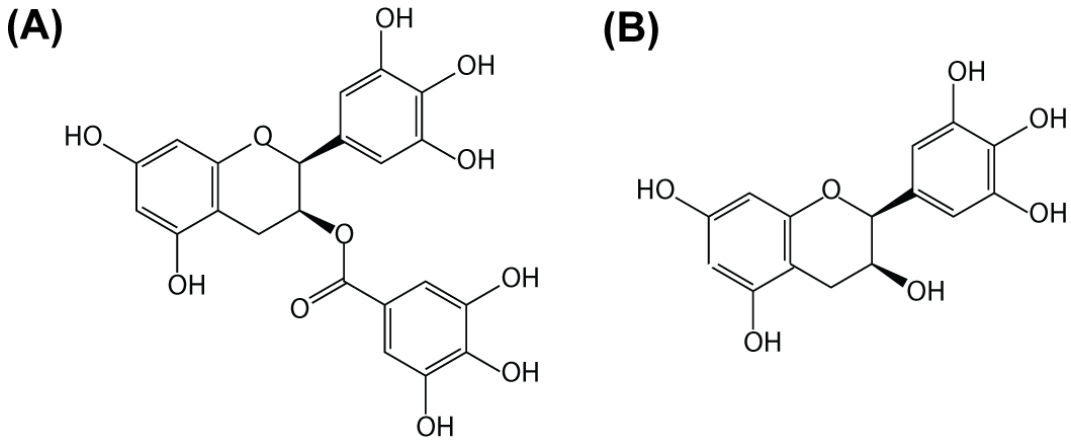

Figure 6.1 Chemical structures of Epigallochatechin Gallate (EGCG) (A) and the related compound Gallochatechin (GC) (B), polyphenolic antioxidants found in green tea.

To determine the mechanism by which EGCG disrupts SEVI amyloid formation from its precursor $PAP_{248-286}$, we analyzed binding of EGCG and the related catechin GC (chemical structures shown in Figure 6.1) to monomeric and small oligomeric forms of $PAP_{248-286}$ by fluorescence assays, NMR and other biophysical methods. We show that, contrary to the proposed general mechanism, EGCG interacts specifically with the side-chains of $PAP_{248-286}$.

6.3 Experimental Procedures

6.3.1 Sample preparation

$PAP_{248-286}$ obtained from Biomatik (Toronto, Ontario) was first disaggregated using a TFA (trifluoroacetic acid)/HFIP (hexafluoroisopropanol) mixture and lyophilized

as previously described *(21)* for all experiments. EGCG ((-)-epigallocatechin-3-gallate) and GC ((-)-gallocatechin) were purchased from Sigma. Stock solutions of EGCG and GC (50 mM and 30 mM respectively) were prepared in water and used immediately.

6.3.2 Thioflavin T fluorescence Fiber Formation Assay

The kinetics of $PAP_{248-286}$ amyloid formation in the absence of EGCG or GC was measured by monitoring the increase in fluorescence intensity upon binding of the amyloid fiber to the amyloid specific dye Thioflavin T (ThT). Before the start of the experiment, $PAP_{248-286}$ was solubilized in buffers containing 50 mM potassium phosphate and 25 μM ThT at two different pH values (pH 7.3 and 6.0) to achieve a final peptide concentration of 439 μM (2 mg/mL). All buffers were filtered and degassed before usage. Experiments were performed in sealed Corning 96 well clear bottom half area, nonbinding surface plates. Time traces were recorded with Biotek Synergy 2 plate reader using a 440 nm excitation filter and a 485 nm emission filter at a constant temperature of 37 °C with shaking.

6.3.4 Transmission Electron Microscopy (TEM)

For inhibition experiments using monomeric $PAP_{248-286}$ solutions at pH 6.0 or 7.3 as a starting point, $PAP_{248-286}$ and EGCG or GC were coincubated for 7 days at 37 °C with orbital agitation of the sample at 1500 rpm, using a $PAP_{248-286}$ concentration of 439 μM and a 1:5 molar ratio of EGCG or GC. After incubation, 10 μL aliquots were loaded onto Formvar-coated copper grids (Ernest F. Fullam, Inc., Latham, NY) for 2 min., washed twice with 10 μL of deionized water, and then negatively stained for 90 s with

2% uranyl acetate. Samples were imaged with Philips CM10 Transmission Electron Microscope at 8400x, 11000x, and 15000x magnification.

For disaggregation experiments, 439 μM $PAP_{248-286}$ was incubated alone for 4 days at 37 °C at pH 6 or 7.3 as described above. After 4 days (pH 7.3) or 8 days (pH 6.1), EGCG or GC was added to the sample in a 1:5 molar ratio and coincubated with the resulting SEVI amyloid fibers for 4 hours. The resulting solution was then stained and imaged as described above. A comparison to control grids in the absence of EGCG or GC confirmed the presence of amyloid fibers.

6.3.5 NMR spectroscopy

NMR samples were prepared by dissolving 0.5 mg of lyophilized unlabeled peptide in 50 mM phosphate buffer at either pH 6.0 or 7.3 containing 10% D_2O. The peptide concentration was determined from the absorbance at 276 nm and was in the range of 0.3-0.4 mM for each sample.

NMR spectra were recorded at 42 °C (315 K) on a 900 MHz Bruker Avance NMR spectrometer equipped with a triple-resonance z-gradient cryogenic probe optimized for ^{1}H-detection. All spectra were processed using TopSpin 2.1 software (from Bruker) and analyzed using SPARKY *(22)*. Binding experiments were performed by titration of the sample from a concentrated EGCG or GC stock solution to a 1:1 molar ratio. Backbone and side-chain assignments were performed using 2D ^{1}H−^{1}H TOCSY (total correlation spectroscopy) and 2D ^{1}H−^{1}H NOESY (nuclear Overhauser enhancement spectroscopy) recorded at two different mixing times 70 or 80 and 300 ms, respectively. Complex data points were acquired for quadrature detection in both

frequency dimensions for 2D experiments and all the spectra were zero-filled in both dimensions to yield matrices of 2048 × 2048 points.

6.3.6 Blocking ε-NH_2 of Lysine in $PAP_{248-286}$ using acetic anhydride

$PAP_{248-286}$ peptide was first dissolved in 50 mM borate buffer (pH 8.0) and then an equimolar amount of acetic anhydride was added to the solution of peptide *(22)*. The sample was then mixed with EGCG in a 1:5 molar ratio and preincubated at room temperature for 2-3 hours before experiments.

6.4 Results & Discussion

6.4.1 EGCG but not GC inhibits SEVI formation at neutral and acidic pH

Hauber et al. showed that an excess of EGCG inhibits SEVI amyloid formation from $PAP_{248-286}$ and slowly disaggregates existing SEVI fibers *(9)*. These experiments were performed at pH 7.3, however, a likely microbicide containing an anti-SEVI inhibitor would have to be effective in the vaginal environment where the pH is significantly acidic, with a pH closer to 6 than 7.3 *(24)*. $PAP_{248-286}$ has two histidine residues that are likely to have pKas in this range, which may in turn effect fiber formation and/or EGCG binding. It has previously been shown that a strongly acidic environment (20% acetic acid) maintains the peptide in a monomeric state but the effect of a moderately acidic environment on SEVI fiber formation and EGCG binding is not known *(25)*. We therefore first looked to see if EGCG would be effective at inhibiting the peptide $PAP_{248-286}$ aggregation in an acidic environment (pH 6) as it is in a neutral environment (pH 7.3).

In the absence of EGCG, $PAP_{248-286}$ fibrillizes within 53-62 hours at pH 7.3 to form a dense network of amyloid fibers (Figure 6.2B). Incubation with EGCG at a 1:5 $PAP_{248-286}$ to EGCG molar ratio is sufficient to eliminate fiber formation at pH 7.3 (Figure 6.2B). EGCG also disaggregated existing SEVI fibrils within 5 hours (Figure 6.3). The timescale of disaggregation was faster than that observed by Hauber et al ($t_{½}$ of 12 hours in ref. 9 compared to a $t_{½}$ of <5 hours). The origin of this difference is uncertain, but may reflect different fiber morphologies between the samples due to the different agitation conditions employed.

$PAP_{248-286}$ aggregated more slowly at pH 6 than at pH 7.3 (Figure 6.2A), although faster than in 20% acetic acid *(25),* most likely due to the greater electrostatic repulsion between peptides at pH 6 due to the additional charge on the two histidine residues. In the absence of EGCG, $PAP_{248-286}$ formed amyloid fibers at pH 6 with an overall morphology similar to those formed at pH 7.3 (Figure 6.2C). Rapid disaggregation of preformed SEVI amyloid fibers by the addition of EGCG also occurred at pH 6 (Figure 6.3C). In summary, EGCG inhibited aggregation of $PAP_{248-286}$ and disaggregated existing SEVI fibers at both pH 6 and 7.3. By contrast, the addition of the related catechin GC in a 1:5 $PAP_{248-286}$ to GC molar ratio did not disaggregate existing SEVI amyloid fibers (Figure 6.3B), in agreement with a previous report showing the absence of amyloid degradation when GC was incubated with SEVI and the lack of an inhibitory action on viral infectivity in the presence of GC *(9)*.

6.4.2 EGCG binds near the 251-257 and 269-277 regions of monomeric $PAP_{248-286}$

To investigate possible binding of EGCG to the monomeric form of $PAP_{248-286}$ and to identify target sites on the $PAP_{248-286}$ molecule, we carried out binding studies using NMR experiments. It has previously been reported that EGCG binds randomly to exposed sites on the backbone of α-synuclein, which was conjectured to be a mode of binding for most amyloid proteins (12).

The addition of EGCG at 1:1 molar ratio at pH 6 caused significant broadening of resonances and substantial chemical shift perturbations for many of the residues in the 2D ^{1}H-^{1}H TOCSY spectrum of $PAP_{248-286}$ (Figure 6.4B). This finding confirms that EGCG can bind to $PAP_{248-286}$ in the monomeric state and that the interaction involves considerable involvement of the side chain atoms of $PAP_{248-286}$. The distribution of changes is not uniform and shows larger effects for particular amino acid types and regions of the peptide. Residues near the central region of the peptide, such as N269, H270, M271, K272, R273 and I277, displayed a considerable shift of the ^{1}H resonances after binding EGCG. The N-terminal region, particularly K251, Q252, K253, K255, is similarly affected. The hydrophobic center of the peptide, proposed to be a spot of amyloid initiation (26, 27), was relatively unaffected. The distribution of amino acid type is similarly non-uniform, with positively charged residues (lysines, arginine, and histidine) along with methionine showing the strongest interaction.

By contrast, GC, which is not an effective SEVI inhibitor (9), did not show substantial changes in the ^{1}H-^{1}H TOCSY spectrum (Figure 6.4C). In contrast to the substantial changes seen in the ^{1}H-^{1}H TOCSY spectrum of EGCG/ $PAP_{248-286}$, the side-

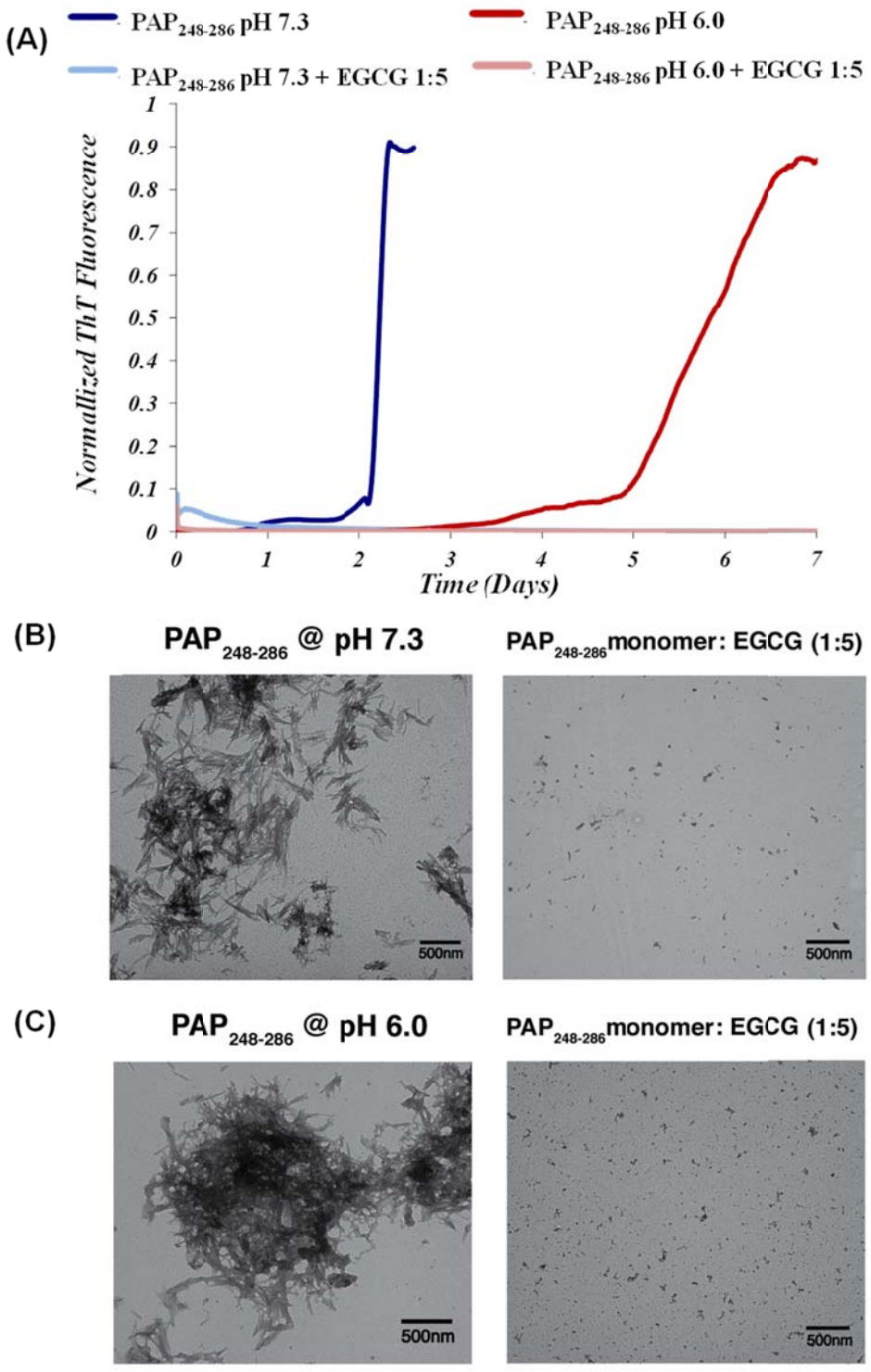

Figure 6.2 EGCG inhibits SEVI formation from $PAP_{248-286}$ **(A)** Thioflavin T fluorescence indicating Amyloid fiber formation. SEVI fiber formation is inhibited at pH 6.0 and eliminated in the presence of EGCG at both pH 7.3 and pH 6.0**(B)** TEM image of $PAP_{248-286}$ incubated alone for 4 days (left) and coincubated for 4 days with EGCG at a 1:5 molar ratio (right) at pH 7.3. **(C)** As above but for 7 days incubation at pH 6.

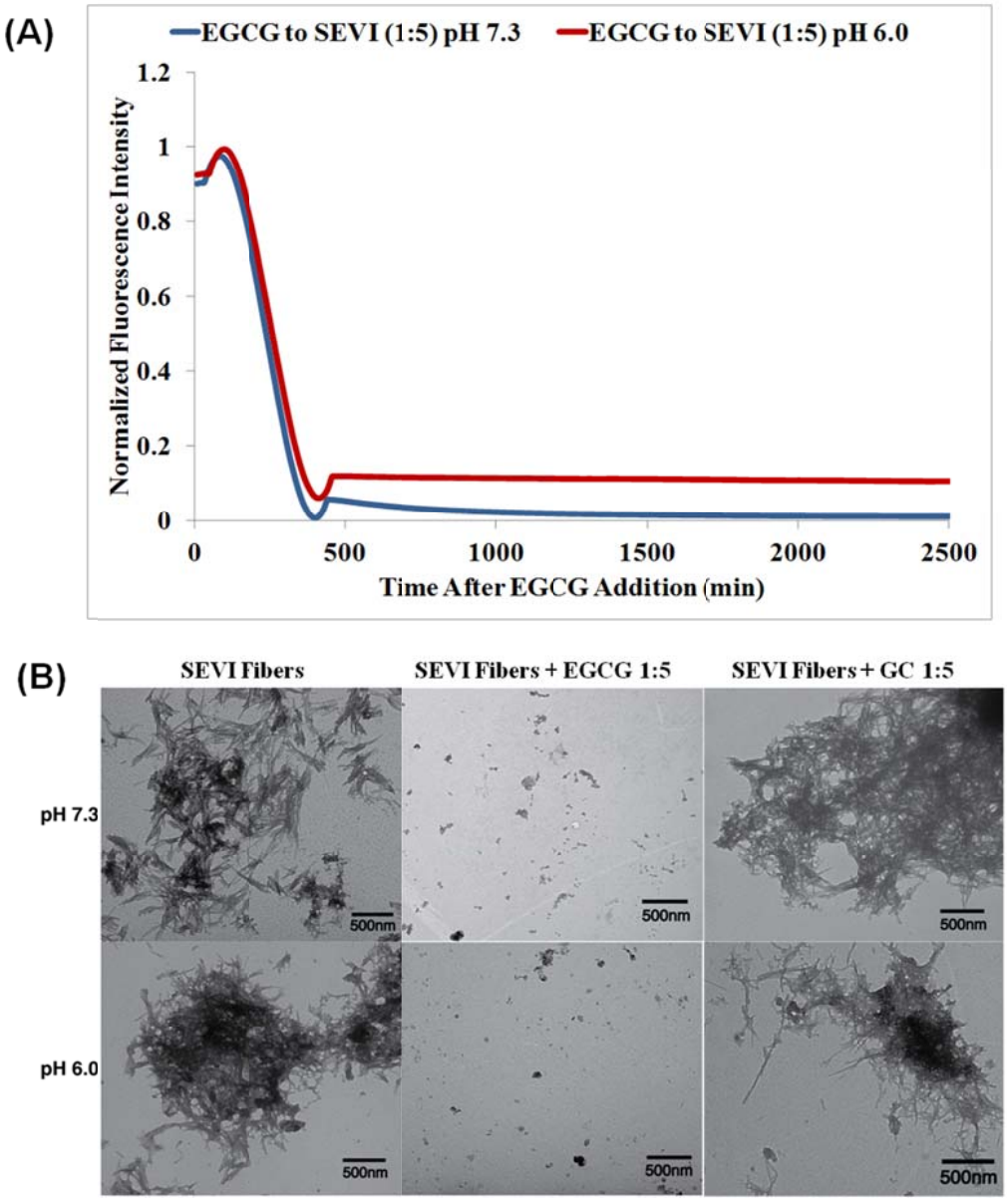

Figure 6.3 EGCG disaggregates existing fibers while the related catechin GC has a diminished effect. (A) Thioflavin T fluorescence of SEVI fibers after addition of EGCG at pH 7.3 and pH 6.0 showing decreasing amyloid presence (B) TEM images of existing SEVI amyloid fibers (left), SEVI amyloid fibers coincubated with EGCG for 5 hours (1:5 molar ratio)(center), and coincubated with GC for 5 hours (1:5 molar ratio)(right).

chain resonances of $PAP_{248-286}$ are almost unaltered by the addition of GC, indicating that GC does not have a significant interaction with the side-chains of $PAP_{248-286}$.

Initial attempts at obtaining a 2D $^{1}H-^{1}H$ TOCSY spectrum of a 1:1 EGCG/$PAP_{248-286}$ complex at pH 7.3 resulted in the rapid formation of a white precipitate followed by the formation of a brown solid. EGCG alone has a high propensity to oxidize at pH 7.3 and forms a brownish solution in the absence of $PAP_{248-286}$. This is likely the result of auto-oxidation and aggregation of EGCG, which increases with the basicity of the solution between pH 4-8 (28).

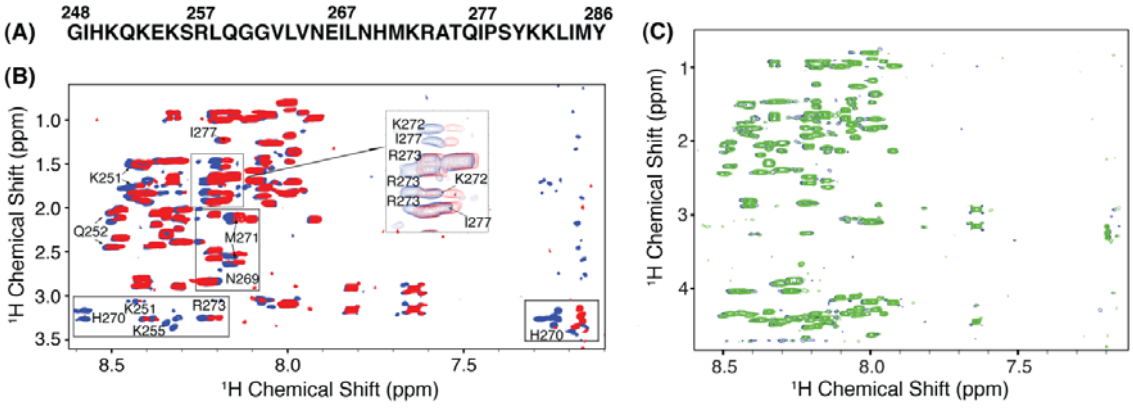

Figure 6.4 EGCG interacts with specific residues of $PAP_{248-286;}$ GC minimally interacts with $PAP_{248-286}$ (A) Amino acid sequence of $PAP_{248-286}$ peptide. (B) Overlaid 2D $^{1}H-^{1}H$ TOCSY spectra of $PAP_{248-286}$ alone (blue) and EGCG bound to peptide (red). (C) Overlaid 2D $^{1}H-^{1}H$ TOCSY spectra of GC bound to $PAP_{248-286}$ (green) and $PAP_{248-286}$ alone (blue).

6.4.3 Lysine residues are critical for the interaction of $PAP_{248-286}$ and EGCG

2D ^{1}H-^{1}H TOCSY and NOESY solution NMR experiments revealed the effect of EGCG on $PAP_{248-286}$ is not random but is instead heavily concentrated on the six lysines present. To examine the role of lysine in EGCG binding in more detail, we acetylated the lysine sites of $PAP_{248-286}$ by reaction with excess acetic anhydride. In the absence of

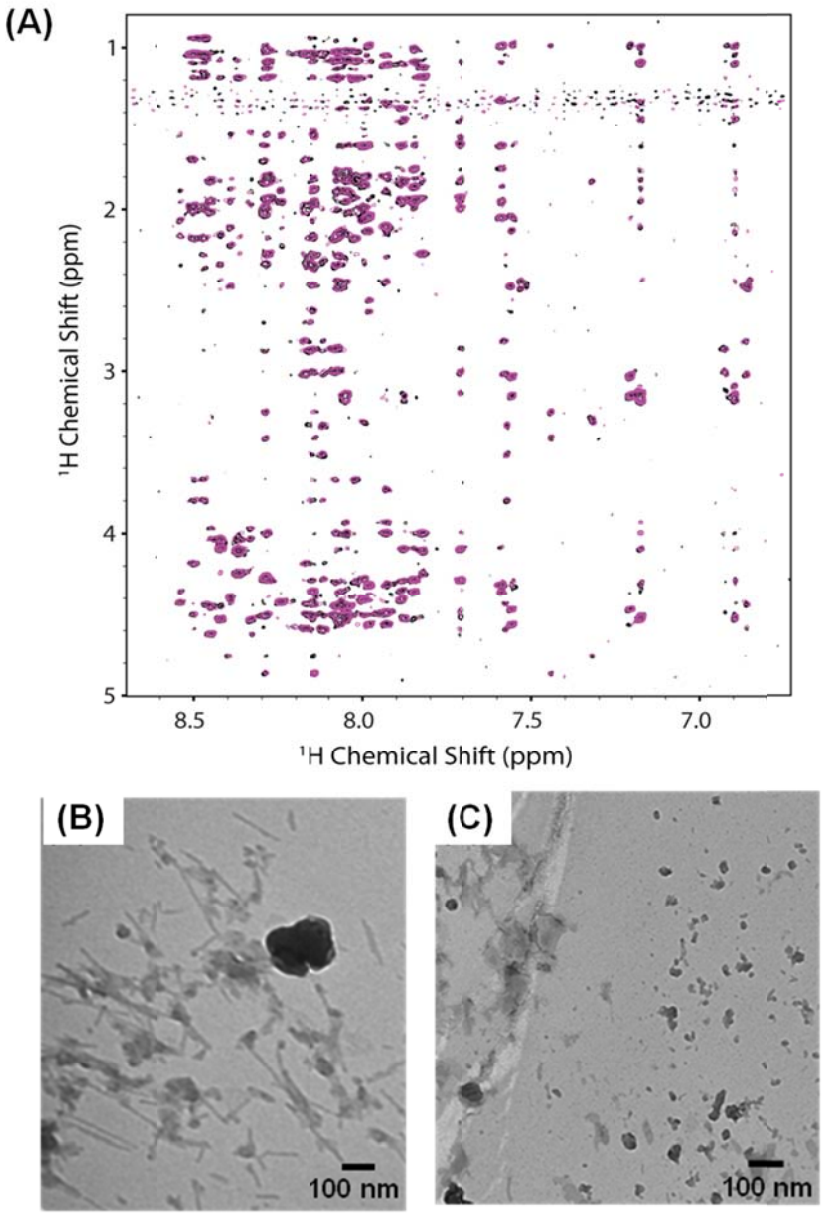

Figure 6.5 Lysine residues are critical EGCG binding and inhibition of amyloid formation. (A) Overlaid 2D ^{1}H–^{1}H NOESY spectra of EGCG incubated with $PAP_{248-286}$ bound to 400 mM SDS (magenta) and $PAP_{248-286}$ in 400 mM SDS alone (black). The absence of any significant shifts suggests residues essential for binding are occluded when $PAP_{248-286}$ is bound to SDS. (B) TEM images of lysine blocked $PAP_{248-286}$ after one week incubation at pH 8. (C) TEM of lysine blocked $PAP_{246-286}$ after week incubation at pH 8 with 5 molar equivalents of EGCG

EGCG, lysine-blocked $PAP_{248-286}$ formed a sparse network of thin short fibers (Figure 6.5B) after incubating for one week at pH 8. In the presence of 5 molar equivalents of EGCG, a similar network of thin short fibers can be seen in the lysine-blocked $PAP_{248-286}$ sample (Figure 6.5C). From these results, it is apparent that acetylation of the lysine of $PAP_{248-286}$ largely blocks the inhibiting effect of EGCG on $PAP_{248-286}$ amyloid formation.

The absence of perturbations in the NMR spectra of $PAP_{248-286}$ upon the addition of EGCG after it has been bound to SDS provided additional evidence for the importance of lysines in the interaction of $PAP_{248-286}$ with EGCG. In SDS micelles, $PAP_{248-286}$ adopts a disordered structure on the surface of the micelle *(27)*. While most of the backbone sites are exposed to solvent and available for binding in SDS, the lysine side-chains are buried within the micelle and shielded from interaction with EGCG *(27)*. No changes in either the side-chain or amide backbone resonances were apparent in the ^{1}H-^{1}H TOCSY spectrum of $PAP_{248-286}$ in 400 mM SDS at pH 6 upon the addition of EGCG (Figure 6.5A). The absence of significant changes in the ^{1}H-^{1}H TOCSY spectrum when the lysine sidechains are blocked is a strong indication that lysine residues are indeed essential for the formation of a tightly bound complex between $PAP_{248-286}$ and EGCG.

6.5 Conclusions Regarding the Binding of Green Tea Extract at $PAP_{248-286}$

Besides $PAP_{248-286}$, EGCG both inhibits amyloid fiber formation and destabilizes existing amyloid fibers formed from a variety of other amyloid proteins including α-synuclein, $A\beta_{1-42}$ and $A\beta_{1-40}$, IAPP, transthyretin, human and yeast prions, lysozyme, κ-casein and tau *(13, 19, 27-30)*. The molecular mechanism by which this is accomplished is not yet clear. Initially, it was proposed that EGCG diverts the normal aggregation

pathway of amyloidogenic proteins into the formation of spherical unstructured aggregates, which form a non-toxic, off-pathway state that does not progress further to the amyloid form *(12, 16, 30)*. On a molecular level, EGCG has been proposed to bind to the exposed backbone of the unfolded regions of proteins, presumably blocking the association of these aggregation prone regions *(12)*.

The evidence for this mechanism primarily comes from studies of α-synuclein and $A\beta_{1-42}$ *(12)*. NBT staining showed a strong, SDS stable, association of EGCG with both of these peptides and with denatured BSA but not with control proteins that were natively folded *(12)*. Further, NMR studies of α-synuclein showed changes in the HSQC spectrum induced by EGCG were concentrated in the flexible C-terminus of the peptide, and not in the more ordered N-terminus *(12)*. The changes were not concentrated on a particular type of residue, suggesting non-specific binding to peptide backbone rather than specific binding to the elements of the side-chains *(12)*.

Based on the apparent generality of amyloid inhibition by EGCG, the formation of off-pathway aggregates by non-specific binding of EGCG to exposed backbone sites was proposed as a generic mechanism for amyloid inhibition by EGCG *(12)*. However, more recent data suggests this mechanism is not entirely general. The crystal structure of EGCG bound to the tetrameric form of transthyretin reveals EGCG binds at specific sites in transthyretin, interacting with the folded transthyretin tetramer by a combination of specific hydrophobic and hydrophilic contacts with side-chains and interactions with exposed amide backbones *(31)*. EGCG has also been shown to interact with the helical native structure of the human prion protein and with nonflexible regions of κ-casein *(28)*, suggesting unfolded conformations are not a strict necessity for EGCG binding, in

agreement with reports of EGCG binding to multiple natively folded non-amyloidogenic proteins *(32)*.

In striking contrast to the apparently random distribution of residues affected by EGCG in α-synuclein and $A\beta_{1-42}$ *(12),* EGCG primarily interacts with $PAP_{248-286}$ through the side-chains of a specific set of residues. Chemical shift perturbations are concentrated at two clusters of residues, the first near the N-terminus and the second closer to the center of the peptide (Figure 6.4B). Pronounced changes in particular were detected for the side-chains of lysines, suggesting a specific interaction of EGCG with this residue. The changes in chemical shift of the initial $PAP_{248-286}$/ECGC at pH 6 are reflective of a relatively weak interaction with EGCG, with exchange occurring on a fast timescale, similar to what has been observed for the initial complexes of EGCG with the amyloidogenic proteins α-synuclein and MSP2 *(12, 27)*. It should be noted, however, that the formation of a covalent EGCG-$PAP_{248-286}$ complex is apparently not an absolute prerequisite for efficient inhibition of amyloid formation, as amyloid formation was inhibited by EGCG at acidic pH where formation of the covalent complex is disfavored and occurs slowly, in contrast to the relatively rapid disaggregation of amyloid fibrils observed by TEM. The eventual formation of a covalent complex is apparently also not sufficient to inhibit amyloid fiber formation, as the related compound GC does not have a strong inhibitory effect on amyloid formation even though it does slowly form a covalent or a non-covalent tightly bound complex (albeit less efficiently than EGCG). Instead, the stronger chemical shift perturbations found in the NMR spectra of the EGCG-$PAP_{248-286}$ complex reflect the greater ability of EGCG to inhibit amyloid formation compared to GC.

Our results show that EGCG inhibits SEVI fibril formation at both neutral and acidic pH in good agreement with biophysical, biochemical and genetic data for other amyloidogenic proteins. However, the binding mechanism of EGCG to $PAP_{248-286}$ deviates substantially from the proposed general model for polyphenols binding to amyloid proteins. Instead of driving the formation of large amorphous off-pathway aggregates, EGCG binds to $PAP_{248-286}$ in the monomeric form, disaggregating fibrils completely to small EGCG/ $PAP_{248-286}$ complexes. In addition, binding appears to be driven by interactions with the side-chains of $PAP_{248-286}$ with EGCG, rather than interactions with exposed backbone sites as previously proposed. These differences may be due to the unusually high charge and low overall hydrophobicity of the $PAP_{248-286}$ protein when compared to most other amyloid proteins.

This study was supported by research funds from NIH (DK078885 to A. R.). Jeffery Brender helped in preparation of the manuscript, Nataliya Popovych preformed the NMR studies and helped with acquiring TEM images.

6.7 Bibliography

1. Doncel, G.F., Joseph, T. and Thurman, A.R. (2010). Role of semen in HIV-1 transmission: Inhibitor or facilitator? *American Journal of Reproductive Immunology 65,* 292-301.

2. Munch, J., Rucker, E., Standker, L., Adermann, K., Goffinet, C., Schindler, M., Wildum, S., Chinnadurai, R., Rajan, D., Specht, A., Gimenez-Gallego, G., Sanchez, P.C., Fowler, D.M., Koulov, A., Kelly, J.W., Mothes, W., Grivel, J.C., Margolis, L., Keppler, O.T., Forssmann, W.G. and Kirchhoff, F. (2007). Semen-derived amyloid fibrils drastically enhance HIV infection. *Cell 131,* 1059-71.

3. Roan, N.R., Munch, J., Arhel, N., Mothes, W., Neidleman, J., Kobayashi, A., Smith-McCune, K., Kirchhoff, F. and Greene, W.C. (2009). The cationic properties of SEVI underlie its ability to enhance human immunodeficiency virus infection. *Journal of Virology 83,* 73-80.

4. Kim, K.A., Yolamanova, M., Zirafi, O., Roan, N.R., Staendker, L., Forssmann, W.G., Burgener, A., Dejucq-Rainsford, N., Hahn, B.H., Shaw, G.M., Greene, W.C., Kirchhoff, F. and Munch, J. (2010). Semen-mediated enhancement of HIV infection is donor-dependent and correlates with the levels of SEVI. *Retrovirology 7*, 55-67.

5. Roan, N.R., Sowinski, S., Munch, J., Kirchhoff, F. and Greene, W.C. (2010). Aminoquinoline surfen inhibits the action of SEVI (semen-derived enhancer of viral infection). *Journal of Biological Chemistry 285,* 1861-1869.

6. Wurm, M., Schambach, A., Lindemann, D., Hanenberg, H., Standker, L., Forssmann, W.G., Blasczyk, R. and Horn, P.A. (2010). The influence of semen-derived enhancer of virus infection on the efficiency of retroviral gene transfer. *Journal of Gene Medicine 12*, 137-146.

7. Hong, S.H., Klein, E.A., Das Gupta, J., Hanke, K., Weight, C.J., Nguyen, C., Gaughan, C., Kim, K.A., Bannert, N., Kirchhoff, F., Munch, J. and Silverman, R.H. (2009). Fibrils of prostatic acid phosphatase fragments boost infections with XMRV (xenotropic murine leukemia virus-related virus), a human retrovirus associated with prostate cancer. *Journal of Virology 83*, 6995-7003.

8. Brender, J.R., Hartman, K., Gottler, L.M., Cavitt, M.E., Youngstrom, D.W. and Ramamoorthy, A. (2009). Helical conformation of the SEVI precursor peptide PAP(248-286), a dramatic enhancer of HIV infectivity, promotes lipid aggregation and fusion. *Biophysical Journal 97*, 2474-2483.

9. Hauber, I., Hohenberg, H., Holstermann, B., Hunstein, W. and Hauber, J. (2009). The main green tea polyphenol epigallocatechin-3-gallate counteracts semen-mediated enhancement of HIV infection. *Proceedings of the National Academy of Sciences 106*, 9033-9038.

10. Olsen, J.S., Brown, C., Capule, C.C., Rubinshtein, M., Doran, T.M., Srivastava, R.K., Feng, C., Nilsson, B.L., Yang, J. and Dewhurst, S. (2010). Amyloid-binding small molecules efficiently block SEVI (semen-derived enhancer of virus infection)- and semen-mediated enhancement of HIV-1 infection. *Journal of Biological Chemistry* 285, 35488-96.

11. Rezai-Zadeh, R., Shytle, D., Sun, N., Mori, T., Hou, H., Jeanniton, D., Ehrhart, J., Townsend, K., Zeng, J., Morgan, D., Hardy, J., Town, T., and Tan, J., (2005) Green tea epigallocatechin-3-gallate (EGCG) modulates amyloid precursor protein cleavage and reduces cerebral amyloidosis in alzheimer transgenic mice. *Journal of Neuroscience 25,* 8807-8814.

12. Ehrnhoefer, D.E., Bieschke, J., Boeddrich, A., Herbst, M., Masino, L., Lurz, R., Engemann, S., Pastore, A. and Wanker, E.E. (2008). EGCG redirects amyloidogenic polypeptides into unstructured, off-pathway oligomers. *Nature Structural and Molecular Biology 15*, 558-566.

13. Meng, F.L., Abedini, A., Plesner, A., Verchere, C.B. and Raleigh, D.P. (2010). The flavanol (-)-epigallocatechin 3-gallate inhibits amyloid formation by islet amyloid polypeptide, disaggregates amyloid fibrils, and protects cultured cells against IAPP-induced toxicity. *Biochemistry 49*, 8127-8133.

14. Porat, Y., Abramowitz, A. and Gazit, E. (2006). Inhibition of amyloid fibril formation by polyphenols: Structural similarity and aromatic interactions as a common inhibition mechanism. *Chemical Biology and Drug Design 67*, 27-37.

15. Ladiwala, A.R.A., Lin, J.C., Bale, S.S., Marcelino-Cruz, A.M., Bhattacharya, M., Dordick, J.S. and Tessier, P.M. (2010). Resveratrol selectively remodels soluble oligomers and fibrils of amyloid Aβ into off-pathway conformers. *Journal of Biological Chemistry 285*, 24228-24237.

16. Bieschke, J., Russ, J., Friedrich, R.P., Ehrnhoefer, D.E., Wobst, H., Neugebauer, K. and Wanker, E.E. (2010). EGCG remodels mature alpha-synuclein and amyloid-beta fibrils and reduces cellular toxicity. *Proceedings of the National Academy of Sciences 107*, 7710-7715.

17. Ladiwala, A.R., Dordick, J.S. and Tessier, P.M. (2010). Aromatic small molecules remodel toxic soluble oligomers of amyloid β through three independent pathways. *Journal of Biological Chemistry 286*, 3209-3218.

18. Stefani, M. (2010). Biochemical and biophysical features of both oligomer/fibril and cell membrane in amyloid cytotoxicity. *Federation of European Biochemical Societies Journal 277*, 4602-4613.

19. Ferreira, N., Cardoso, I., Domingues, M.R., Vitorino, R., Bastos, M., Bai, G.Y., Saraiva, M.J. and Almeida, M.R. (2009). Binding of epigallocatechin-3-gallate to transthyretin modulates its amyloidogenicity. *Federation of European Biochemical Societies Letters 583*, 3569-3576.

20. Mandel, S.A., Amit, T., Weinreb, O., Reznichenko, L. and Youdim, M.B.H. (2008). Simultaneous manipulation of multiple brain targets by green tea catechins: A potential neuroprotective strategy for alzheimer and parkinson diseases. *CNS Neurosciences and Therapeutics 14*, 352-365.

21. Paz, M.A., Fluckiger, R., Boak, A., Kagan, H.M. and Gallop, P.M. (1991). Specific detection of quinoproteins by redox-cycling staining. *Journal of Biological Chemistry 266*, 689-692.

22. Hudson, S.A., Ecroyd, H., Kee, T.W. and Carver, J.A. (2009). The thioflavin t fluorescence assay for amyloid fibril detection can be biased by the presence of exogenous compounds. *Federation of European Biochemical Societies Journal 276*, 5960-5972.

23. Goddard, T.D. and Kneller, D.G. (1999). Sparky 3, university of california, san francisco.

24. Cao, D., Zhang, Y.J., Zhang, H.H., Zhong, L.W. and Qian, X.H. (2009). Systematic characterization of the covalent interactions between (-)-epigallocatechin gallate and peptides under physiological conditions by mass spectrometry. *Rapid Communications in Mass Spectrometry 23*, 1147-1157.

25. TeviBenissan, C., Belec, L., Levy, M., SchneiderFauveau, V., Mohamed, A.S., Hallouin, M.C., Matta, M. and Gresenguet, G. (1997). In vivo semen-associated pH neutralization of cervicovaginal secretions. *Clinical and Diagnostic Laboratory Immunology 4*, 367-374.

26. Ye, Z.Q., French, K.C., Popova, L.A., Lednev, I.K., Lopez, M.M. and Makhatadze, G.I. (2009). Mechanism of fibril formation by a 39-residue peptide (papf39) from human prostatic acidic phosphatase. *Biochemistry 48*, 11582-11591.

27. Eisenberg, D., Sievers, S.A., Karanicolas, J., Chang, H.W., Zhao, A., Jiang, L., Zirafi, O., Stevens, J.T., Munch, J. and Baker, D. (2011). Structure-based design of non-natural amino-acid inhibitors of amyloid fibril formation. *Nature 475*, 96-U117.

28. Nanga, R.P.R., Brender, J.R., Vivekanandan, S., Popovych, N. and Ramamoorthy, A. (2009). NMR structure in a membrane environment reveals putative amyloidogenic regions of the SEVI precursor peptide PAP(248-286). *Journal of the American Chemical Society 131*, 17972-17979.

29. Zhu, Q.Y., Zhang, A.Q., Tsang, D., Huang, Y. and Chen, Z.Y. (1997). Stability of green tea catechins. *Journal of Agricultural and Food Chemistry 45*, 4624-4628.

30. Chandrashekaran, I.R., Adda, C.G., MacRaild, C.A., Anders, R.F. and Norton, R.S. (2010). Inhibition by flavonoids of amyloid-like fibril formation by plasmodium falciparum merozoite surface protein 2. *Biochemistry 49*, 5899-5908.

31. Hudson, S.A., Ecroyd, H., Dehle, F.C., Musgrave, I.F. and Carver, J.A. (2009). (-)-epigallocatechin-3-gallate (EGCG) maintains kappa-casein in its pre-fibrillar state without redirecting its aggregation pathway. *Journal of Molecular Biology 392*, 689-700.

32. Roberts, B.E., Duennwald, M.L., Wang, H., Chung, C., Lopreiato, N. P., Sweeny, E.A., Knight, M.N. and Shorter, J. (2009). A synergistic small-molecule combination directly eradicates diverse prion strain structures. *Nature Chemical Biology 5*, 936-946.

33. He, J., Xing, Y.F., Huang, B., Zhang, Y.Z. and Zeng, C.M. (2009). Tea catechins induce the conversion of preformed lysozyme amyloid fibrils to amorphous aggregates. *Journal of Agricultural and Food Chemistry 57*, 11391-11396.

34. Miyata, M., Sato, T., Kugimiya, M., Sho, M., Nakamura, T., Ikemizu, S., Chirifu, M., Mizuguchi, M., Nabeshima, Y., Suwa, Y., Morioka, H., Arimori, T., Suico, M.A., Shuto, T., Sako, Y., Momohara, M., Koga, T., Morino-Koga, S., Yamagata, Y. and Kai, H. (2010). The crystal structure of the green tea polyphenol (-)-epigallocatechin gallate-transthyretin complex reveals a novel binding site distinct from the thyroxine binding site. *Biochemistry* I, 6104-6114.

35. Maiti, T.K., Ghosh, K.S. and Dasgupta, S. (2006). Interaction of (-)-epigallocatechin-3-gallate with human serum albumin: Fluorescence, fourier transform infrared, circular dichroism, and docking studies. *Proteins 64*, 355-362.

CHAPTER 7

BATERIAL CURLI PROTEIN PROMOTES THE IN VITRO CONVERSION OF $PAP_{248-286}$ INTO THE SEVI AMYLOID FORM

7.1 Summary

Fragments of prostatic acid phophatase in human semen drastically enhance HIV infection rates by increasing virus adhesion to target cells. $PAP_{248-286}$ only enhances HIV infection in the form of amyloid aggregates termed SEVI, however monomeric $PAP_{248-286}$ aggregates very slowly in isolation. It has therefore been suggested that SEVI fiber formation *in vivo* may be promoted by exogenous factors. We show here that a bacterially-produced extracellular amyloid (curli or Csg) acts as a catalytic agent for SEVI formation from $PAP_{248-286}$ at low concentrations *in vitro*, producing fibers that retain the ability to enhance HIV infection. Kinetic analysis of the cross-seeding effect shows an unusual pattern. Cross-seeding $PAP_{248-286}$ with curli only moderately affects the nucleation rate while significantly enhancing the growth of fibers from existing nuclei. This pattern is in contrast to most previous observations of cross-seeding, which show cross-seeding partially bypasses the nucleation step but has little affect on fiber elongation. Seeding other amyloidogenic proteins (IAPP and Amyloid β_{1-40}) with Curli

---

This chapter is a version of a manuscript in preparation for publishing: Hartman, K., Brender, J.R., Monde, K., Ono, A., Evans, M.L., Popovych, N., Chapman, M.R., and Ramamoorthy, A., (2012) Bacterial Curli Protein Promotes the Conversion of PAP(248-286) into the SEVI Amyloid: Cross-Seeding of Dissimilar Amyloid Sequences

shows varied results, with curli cross-seeding causing a strong inhibition of IAPP elongation but a decrease and lag-time and a complicated concentration dependent effect on Amyloid $\beta_{1\text{-}40}$ fibrillogenesis kinetics. Combined, these results suggest that the interaction of amyloidogenic proteins with preformed fibers of a different type can take a variety of forms and is not limited to epitaxial nucleation between proteins of similar sequence. The ability of curli fibers to interact with proteins of dissimilar sequences suggests cross-seeding may be a more general phenomenon than previously proposed

7.2 Introduction

The HIV virus responsible for AIDS is the source of a global pandemic with over 33 million people worldwide currently infected with the virus. The scope of AIDS pandemic sparks the question: why is HIV so prevalent in the population and transmitted so readily in vivo, while the virus itself has a very poor infection rate in vitro? One possibility is the presence of in vivo cofactors that facilitate entry of the virus, causing infection to occur at a higher rate. Recently, a cofactor has been found in human seminal fluid that could prove to be a key component in HIV transmission *(1)*. An peptide fragment of prostatic acid phosphatase ($PAP_{248\text{-}286}$) was discovered to increase the infection rate of HIV *(1)* and other retroviruses *(2, 3)* by several orders of magnitude when fibrillized into amyloid fibrils termed SEVI.

Since $PAP_{248\text{-}286}$ only enhances HIV infection when in the aggregated SEVI amyloid form, molecules that initiate fibrillization of $PAP_{248\text{-}286}$ can indirectly increase HIV infectivity. While amyloid formation is typically energetically favorable, the actual rate of formation can be very slow. Specifically, amyloid formation is a nucleation-

dependent process in which a slow rate-limiting nucleation step is followed by the faster process of extension of the fiber from the nuclei. $PAP_{248-286}$ is subject to significant proteolytic degradation in seminal plasma unless it is in the SEVI amyloid form *(4).* The total production of SEVI is therefore ultimately controlled by the rate of amyloidosis due to the proteolytic degradation of unfibrillized $PAP_{248-286.}$ $PAP_{248-286}$ is very slow to fibrillize in the absence of shaking in vitro *(5),* which suggests SEVI production will be very limited *in vivo*. Nevertheless, the SEVI amyloid form is found in semen at concentrations of up to 35 μg/mL *(1, 6)* This finding suggests an additional cofactor may be present that accelerates SEVI formation from $PAP_{248-286}$ before the $PAP_{248-286}$ monomer is degraded by the cell's proteolytic machinery.

One set of likely cofactors are other cellular proteins, since the factors that drive self-association of amyloidogenic proteins also tend to favor promiscuous binding to a variety of other proteins *(7, 8).* In particular, amyloidogenic proteins frequently have the ability to cross-polymerize, that is amyloid fibers from one protein can catalyze the formation of amyloid fibers from another amyloidogenic protein. Cross-seeding amyloid fibrillogenesis in this manner can dramatically enhance the kinetics of amyloid formation by providing preformed nuclei for further aggregation. Furthermore, the final amyloid fiber can in some cases takes on some of the characteristics of fibers from the initial seeding amyloid protein *(9-11).*

Amyloid nucleation is often considered a highly specific process dependent on a high degree of similarity in both peptide sequence and fiber morphology between the seed and the protein being nucleated. This conclusion has largely been motivated by research on prion amyloid fibers, where the inability of highly homologous prions to

cross-seed amyloid formation presents an inter-species barrier to prion transmission *(12, 13)*. However, this view has recently been challenged by the observation of efficient cross-polymerization between several non-prion amyloid species *(14-18)*. Seeds formed from amyloid fibers of some non-homologous proteins can either reduce or eliminate the lag-time of amyloid formation of another protein *(14-19)*, although the phenomenon is not universal and even single point mutations have been shown to disrupt cross-seeding in some cases *(18, 20-22)*.

The amyloids produced by many bacteria and fungi are of particular interest in considering possible cross-seeding reactions with $PAP_{248-286}$ because of the high incidence of microbial infection in the vagina and the frequent coexistence with bacterial and fungal infection with HIV infection *(23)*. In particular, *E. coli* and related bacteria produce a highly amyloidogenic protein, CsgA, that polymerizes into curli fibers that are involved in cell-to-cell and cell-to-surface interactions *(24, 25)*. Curli and curli-like amyloid fibers are ubiquitous in mammalian hosts *(26)*, in fact, the innate immune response invoked by almost all amyloids has been proposed to have evolved as a response to curli amyloid formation by *E. coli (27)*. Some functional amyloids such as curli have evolved to undergo fibrillization efficiently at the correct time and cellular location, an evolutionary strategy believed to minimize the formation of toxic oligomeric intermediates *(28)*. Interestingly, curli from different bacterial species can cross-seed each other to form mixed biofilms *(29)*, suggesting curli may have evolved an ability to cross-seed other amyloids to assist in biofilm formation *(30)*. Since curli amyloid fibers may be colocalized with $PAP_{248-286}$ at the initial site of HIV infection, we tested the effect of preformed curli amyloid fibrils on the kinetics of SEVI fiber formation. We found

Curli does significantly enhance the rate of SEVI fibrillization, although through an unusual mechanism for a cross-seeding interaction.

7.3 Experimental Procedures

7.3.1 Peptide preparation

$PAP_{248-286}$ was obtained from Biomatik Corporation. To prepare monomeric $PAP_{248-286}$, lyophilized $PAP_{248-286}$ was first quickly dissolved in 20% acetic acid to a final concentration of 1 mg/ml to remove preformed aggregates. The aggregate free solution was then lyophilized overnight. A 3 mg/ml stock solution was made from the lyophilized peptide in the assay buffer (10mM phosphate buffer, pH 7.3 containing 150mM NaCl).

Human IAPP was obtained from Genscript. Monomeric IAPP was prepared by first dissolving in hexafluoroisopropanol to a concentration of 1 mg/ml then lyophilizing overnight. Amyloid β_{1-40} was prepared in a similar way using 2% ammonium hydroxide instead of hexafluoroisopropanol. The lyophilized pellet of both peptides was dissolved directly in the assay buffer.

7.3.2 CsgA and CsgB preparation

Curli A and B were expressed *(28)* and purified *(29)* as previously described. Curli B is the truncated version missing the Briefly, Curli A and B were overexpressed as His-tag fusion proteins in LSR12 bacteria. Following centrifugation for 15 min at 10,000 x g, the bacterial pellet was incubated in 8M guanidine hydrochloride (pH 7.2) for 24 hours with stirring. After incubation, the cells were sonicated and centrifuged again for

15 min at 10,000 x g. The resulting supernatant was then passed over a HIS-Select™ HF nickel-nitrilotriacetic acid column, washing first with 12.5 mM imidazole to remove non-specifically bound proteins and then with 125 mM imidazole to elute Curli A or Curli B. To prepare amyloid fibers of Curli A and B, the Curli containing fractions from the HIS-Select™ column allowed to fibrillize overnight. Protein concentration was measured by the BCA assay prior to fibrillization. The resulting fibers were then centrifuged (15 min at 10,000 x g) and washed with water to remove the imidazole salt. This procedure was repeated four times and the pellet then lyophilized. The lyophilized pellets were then reconstituted in the assay buffer and sonicated with a probe sonicator (Sonic Dismembrator Model 100, Fischer Scientific) for approximately 1 minute prior to being loaded onto the plate. Amyloid fibers of Amyloid $\beta_{1\text{-}40}$ were prepared by aggregation for 2 days at 37 °C as detailed below. Amyloid $\beta_{1\text{-}40\ \text{fibers were sonicated}}$ for 1 minute before loading onto the plate for the seeding experiments.

7.3.3 Thioflavin T Fibril Formation Assays

Aggregation assays for $PAP_{248\text{-}286}$ were performed in 10mM phosphate buffer, pH 7.3 containing 150 mM NaCl. A total volume of 40μL was placed in each well of a 96 well half area plate with a clear bottom, with 2 mg/mL $PAP_{248\text{-}286}$, 25 μM Thioflavin T, and either 0, 1, 2.5, or 5 mol % preformed fibers of Curli A or B. Aggregation assays for IAPP and Amyloid $\beta_{1\text{-}40}$ were performed similarly except different concentrations of peptide (2.5 μM of IAPP and 5 μM Amyloid $\beta_{1\text{-}40}$) and CsgA and CsgB were used and the temperature for IAPP aggregation was set to 25 °C. A single 1 mm glass bead was placed in each well to increase the aggregation rate and promote sample reproducibility

(30). The loaded plate was sealed, and placed on a BioTek Synergy 2 plate reader set at 37° C ($PAP_{248-286}$ and Amyloid β_{1-40}) or 25° C (IAPP) with a constant linear shaking speed of 17 Hz. Absorbance was monitored at 350 nm and THT fluorescence measurements were taken with an emission filter at 440 nm with a bandwidth of 30 nm and an excitation filter at 485 nm with a bandwidth of 20 nm. Data points were collected every 10 minutes, with continual shaking occurring between data points. All experiments were performed with samples in triplicate. The kinetic curves were fitted to a sigmoidal growth model that has empirically been found to reproduce most of the features of amyloid aggregation:

$$I = \frac{I_{max} - I_0}{1 + e^{(t - t_{1/2})/k}}$$

where I_0 and I_{max} are the initial and maximum fluorescence values, $t_{1/2}$ is the time required to reach half intensity, and k is an apparent first order time constant for the addition of $PAP_{248-286}$ to existing fibers *(31)*. The lag-time t_0 before detectable aggregation occurs is described by $t_0 = t_{1/2} - 2\tau$.

7.3.4 Transmission Electron Microscopy

Samples of 6uL of $PAP_{248-286}$ solutions after the aggregation experiment were applied to 200 mesh carbon coated copper electron microscopy grids and allowed to stand for 2 minutes. The grids were then washed with water 20 times to remove salts, after which 6 μL of a 2% uranyl acetate solution was added and allowed to set for 1 minute before being removed. Fiber images were taken on a Phillips X-100 Transmission Electron Microscope.

7.3.5 Cell preparation for infectivity assays

A CEM-GFP cell line that expresses a green fluorescent protein (GFP) driven by the HIV-1 LTR promoter was obtained through the AIDS Research and Reference Reagent Program, Division of AIDS, NIAID, NIH from Dr. Jacques Corbeil and maintained in RPMI1640 (Invitrogen) media supplemented with 10% heat-inactivated fetal bovine serum (HyClone) (RPMI-10) and containing 500 μg/ml geneticin (Invitrogen) *(32)*.

7.3.6 Infectivity assays

Infectivity assays were performed as previously described *(33)*. A viral stock solution was prepared by transfection of HeLa cells with HIV-1_{NL4-3}. Supernatants of transfected cells were collected 2 days post-transfection, and viruses in the supernatant solution were pelleted by ultracentrifugation and resuspended in RPMI-10 media. These virus stocks (20,000 cpm RT activity) were combined with stock solutions of SEVI amyloid fibers (50 μg/ml from a stock solution of 440 μM $PAP_{248-286}$ incubated under aseptic conditions for 7 days at 37 °C under vigorous agitation (1300 rpm)) and used to inoculate 2 x 10^5 of CEM-GFP for 2 hours at 37 ºC. Cells were then washed and incubated in RPMI-10 at 37 ºC. Inoculations were perfomed in triplicate. To block the second round of infection, the CD4 blocking antibody Leu3a (0.25 μg/ml) (BD Biosciences) and the reverse transcriptase inhibitor AZT (1 μM) (Sigma) were added to the medium 12 hours post-infection. Two days post-infection, cells were fixed in 4% paraformaldehyde in PBS and analyzed using a FACSCanto flow cytometer and the FlowJo software ver. 8.7.1. Rates of infection were determined directly from the

percentage of GFP positive cells after subtraction of the baseline activity obtained in the absence of HIV-1_{NL4-3}. Comparisons between samples were made using a one-tailed unpaired Student t-test.

7.4 Results & Discussion

7.4.1 Seeding with Curli fibers greatly increases the rate of SEVI formation from $PAP_{248-286}$

To test the *in vitro* activity of curli on the kinetics of SEVI amyloid formation from $PAP_{248-286}$, we measured the kinetics of amyloid formation and aggregation of 440 μM $PAP_{248-286}$ solutions in the presence of curli nuclei *(30).* The curli amyloid fiber is actually a composite of several proteins *(25),* with CsgA serving as the main structural scaffold and CsgB nucleating amyloid formation from CsgA (sequences given in Figure 7.1) *(36).*

$PAP_{248-286}$ aggregated slowly in the absence of preformed nuclei of any type under the conditions tested, as shown by both turbidity measurements (a nonspecific indicator of general aggregation, Figure. 7.2B and 7.2D) and ThT fluorescence (a measurement specific for amyloid, Figs. 7.2A and 7.2C). The lag time of formation (~60 hrs) is considerably longerthan that previously described (~18 hrs) *(1, 5)*, at an identical concentration. We further explored these discrepancies in polymerization lag times and found that the type of shaking in each experiment differs. $PAP_{248-286}$ fibrillized more slowly under the linear shaking used in our studies (Figure 7.2) than orbital shaking at the same speed (data not shown). Turbidity increased before ThT fluorescence, suggesting

the formation of non-amyloid prefibrillar aggregates occurs before amyloid formation (Figure 7.2). Non-fibrillar aggregates of $PAP_{248-286}$ have been shown to have a similar effect on HIV infectivity as SEVI amyloid fibers *(1)*.

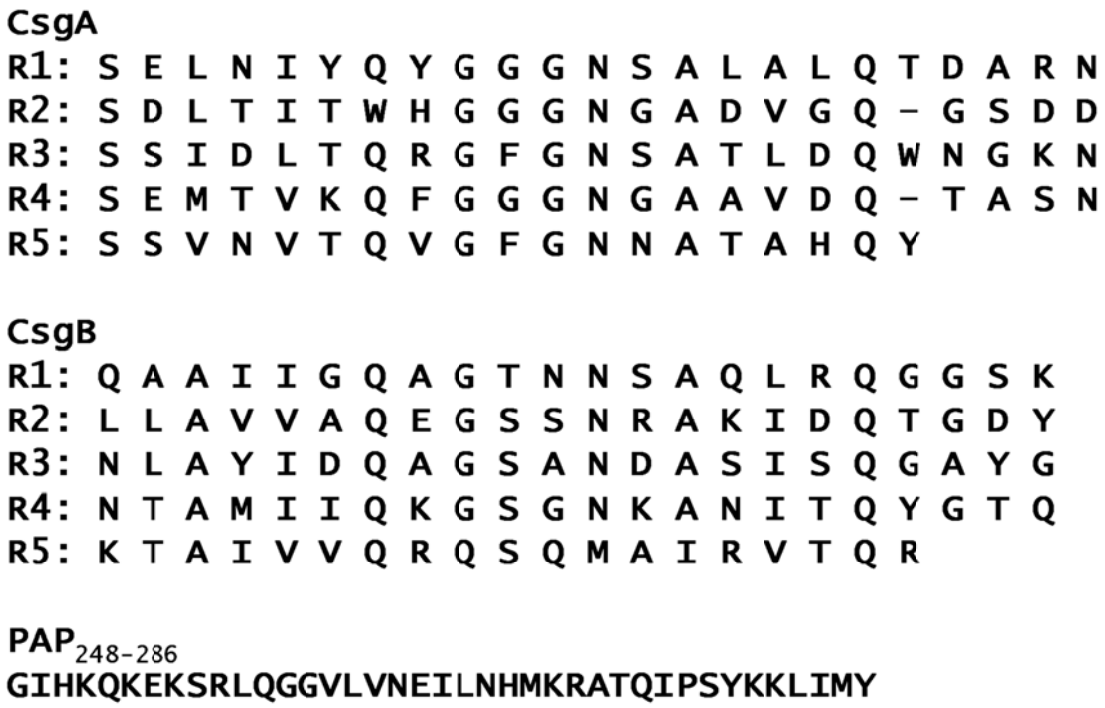

Figure 7.1 Amino acid sequences of CsgA, CsgB, and $PAP_{248-286}$. CsgA and B consist of five homologous subunits (R1-R5) that are believed to correspond to five β-sheets in the amyloid fiber.

The addition of preformed CsgA seed had a dramatic impact on the kinetics of SEVI amyloid formation. One mole % CsgA was sufficient to cause a six-fold increase in the elongation time constant, which is reflective of the rate of addition of $PAP_{248-286}$ to existing fibers (Figure 7.3B). CsgA seeds also decreased the lag-time for aggregation (Figure 7.3C), however, the effect is not as dramatic as that observed for the elongation rate and the lag-time is not decreased for the final amyloid product (Figure 7.3A). This is

an unexpected result, as the addition of seeds usually results in the reduction or elimination of the lag-time with little corresponding change in the rate of addition to pre-existing fibers *(14).* CsgB has qualitatively similar effects as CsgA on the kinetics of SEVI amyloid formation, however the magnitude of the effect is relatively less in comparison to CsgA (Figures 7.2 and 7.3).

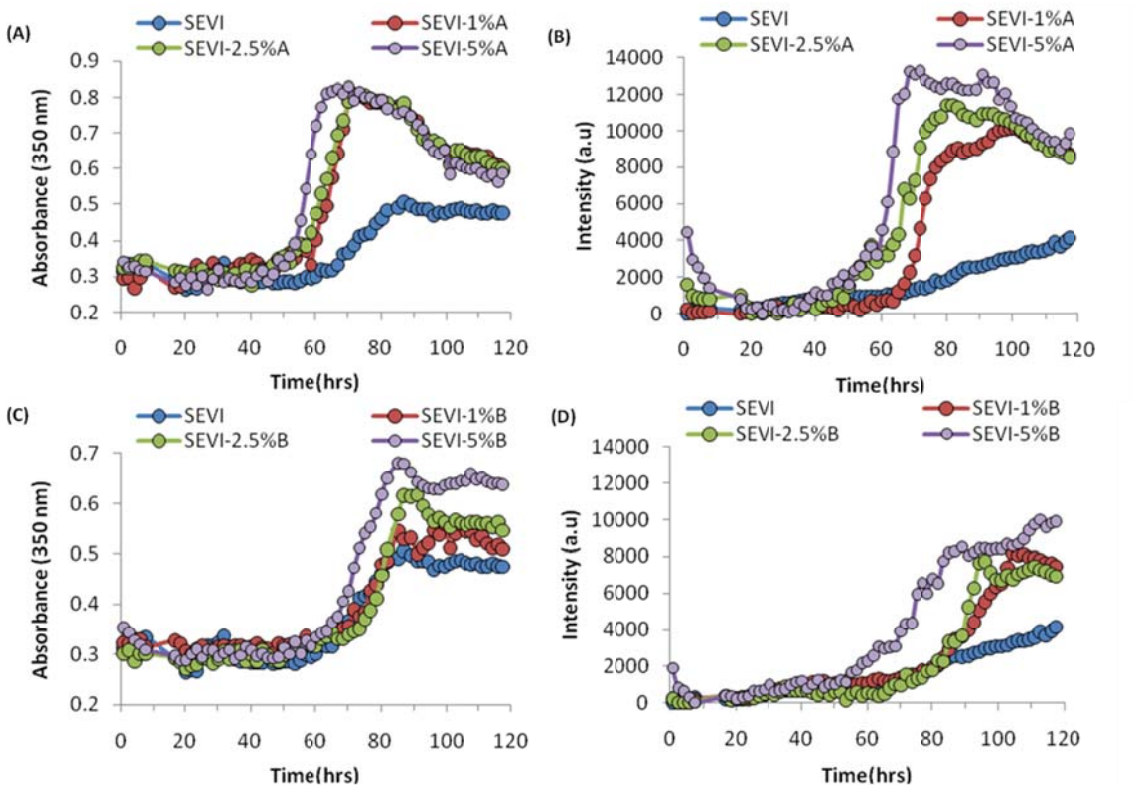

Figure 7.2. Kinetics of SEVI amyloid fiber formation in the presence of preformed fibers of CsgA and CsgB. Left: Turbidity measurements at 350 nm (A) $PAP_{248-286}$ + CsgA, (C) $PAP_{248-286}$ + CsgB. Right: ThT fluorescence measurements (B) $PAP_{248-286}$ + CsgA, (D) $PAP_{248-286}$ + Csg B. Curves are averages for 3 measurements.

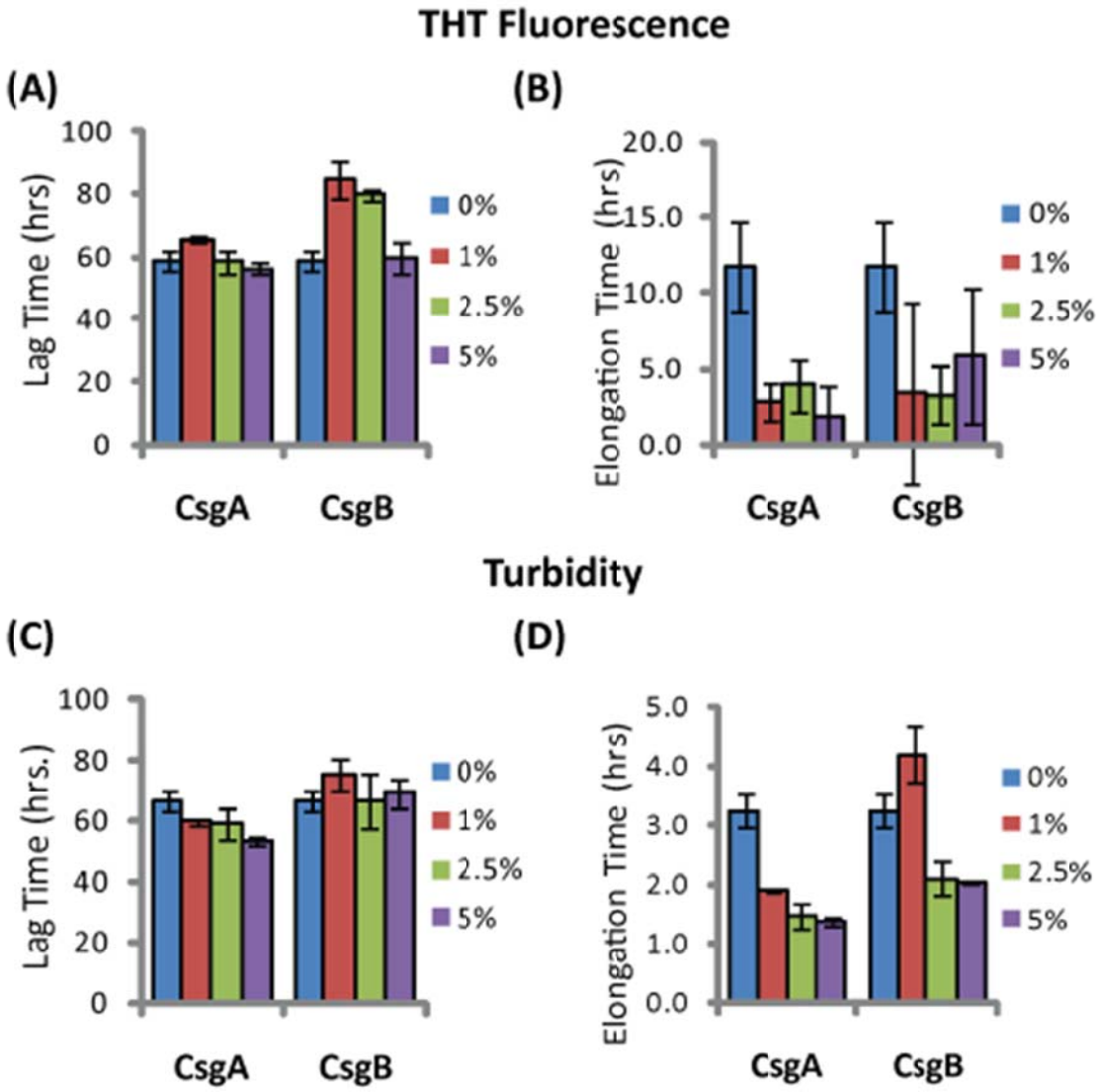

Figure 7.3. Elongation of SEVI amyloid fibers is significantly enhanced by preformed fibers of CsgA and CsgB lag time is less affected. Impact of preformed curli A and B fibers on the lag time (A and C) and elongation time (B and D) of SEVI formation. (A and B): Kinetic constants as determined by ThT fluorescence. (C and D): Kinetic constants as determined by turbidity measurements. Error bars represent S.E.M.

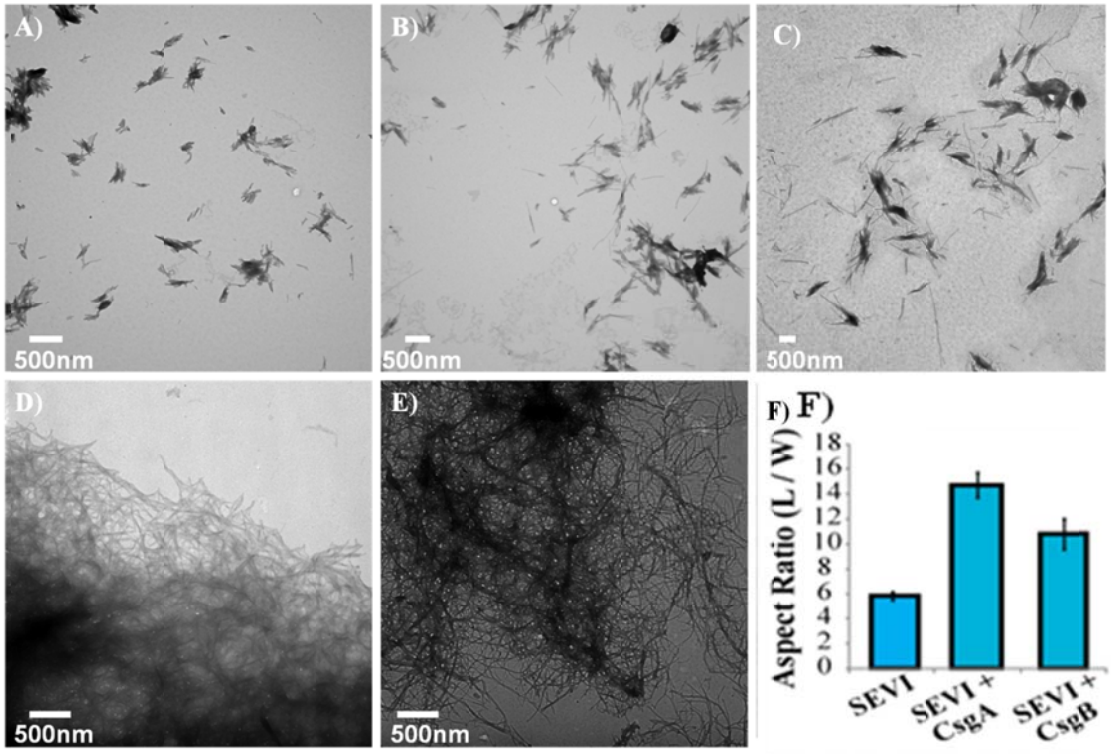

Figure 7.4. Curli nucleation produces longer SEVI fibers. Top**:** TEM images of SEVI fibers formed in the absence of Curli (A) and in the presence of 5 mol% CsgA (B) and CsgB (C) fibers. Bottom: TEM images of CsgA (D) and CsgB (E) fibers. (F) Aspect ratios of individual fibers grown with and without Curli nucleation. Fibers were grown at a concentration of 440μM $PAP_{248-286}$ at 37ºC under 1400 rpm orbital shaking for 7 days.

The difference in elongation rates for Csg initiated $PAP_{248-286}$ fiber formation is reflected in the morphology of individual fibers. Fibers samples initiated by curli and those grown in their absence are morphologically similar, except for a large difference in the aspect ratios (Figure 7.4A-C.). Standard SEVI fibers have an aspect ratio of approximately 5.8, while those grown with CsgA and CsgB are much longer, with aspect ratios of approximately 14.7 and 10.8 respectively (Figure 7.4F). This finding is in agreement with the greatly enhanced fiber elongation rate found in the presence of either of the curli fibers. The very short and broken fibers of all $PAP_{248-286}$ samples are different than typical amyloid fibers, such as the CsgA and CsgB fibers formed under quiescent conditions

(Figure 7.4D and E.), most likely because the high degree of agitation required for SEVI fiber formation fragments nascent amyloid fibers.

7.4.2 SEVI amyloid fibers obtained from Curli nucleation retain the ability to enhance HIV infection

We next confirmed that Curli nucleated SEVI fiber samples retain a similar ability to promote HIV infection as SEVI fibers generated *de novo*. The activity of the Csg derived SEVI fibrils was tested using an infectivity assay based on the expression of GFP in the host cell that is driven by an HIV linked promoter *(32)*. In the absence of SEVI, flow cytometry showed a low percentage of GFP-positive cells, in agreement with the low virulence of HIV under the conditions employed. The addition of SEVI fibrils generated *de novo* caused an approximately 8-fold increase in the infectivity rate (Figure 7.5), roughly matching results of other studies of SEVI under conditions of high viral load *(37-39)*. The much larger degree of enhancement shown in some studies (>100,000 times) is only apparent at very high viral dilution *(1)*. Neither the $PAP_{248-286}$ monomer nor equivalent amounts of CsgA or CsgB alone had an effect on HIV infection rates (Figure 7.5A). On the other hand, CsgA and CsgB nucleated fibers enhanced HIV infection roughly to the same extent as *de novo* generated SEVI fibers (13 and 16 times respectively, Figure 7.5). From these results, it can be seen that the SEVI fiber samples, regardless of how they were nucleated, show a comparable ability to enhance the rate of HIV infection.

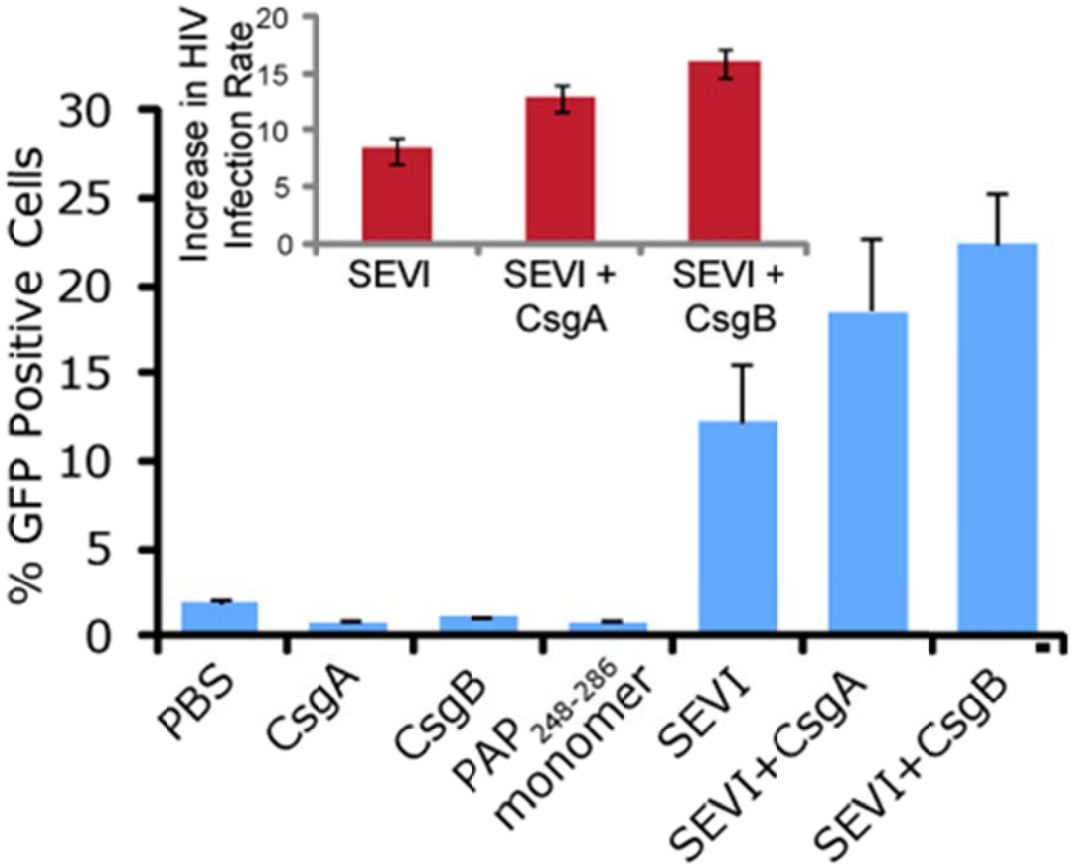

Figure 7.5 Curli nucleated SEVI fibers enhance HIV infectivity to a similar degree as SEVI generated *de novo*. CEM-GFP cells were infected with HIV-1_{NL4-3} (20,000 cpm RT activity) supplemented either with 50 μg/ml of the proteins indicated or PBS (polybuffered saline). SEVI samples were fibrillized for 7 days prior to infection. Measurements were performed in triplicate, error bars indicate S.E.M. *P* values were determined using a one-tailed unpaired Student t-test against the control sample.

7.4.3 Cross-seeding with Curli at low concentrations affects the amyloidogenesis of other proteins besides $PAP_{248-286}$

The ability of curli to seed SEVI formation in the absence of any obvious sequence similarity suggests curli may seed other amyloid proteins as well. To test this possibility, we performed analogous seeding experiments on the amyloidogenic peptides IAPP and amyloid β_{1-40}. Addition of preformed curli nuclei had a complex effect on the aggregation (Figure 7.6 and Figure 7.7).

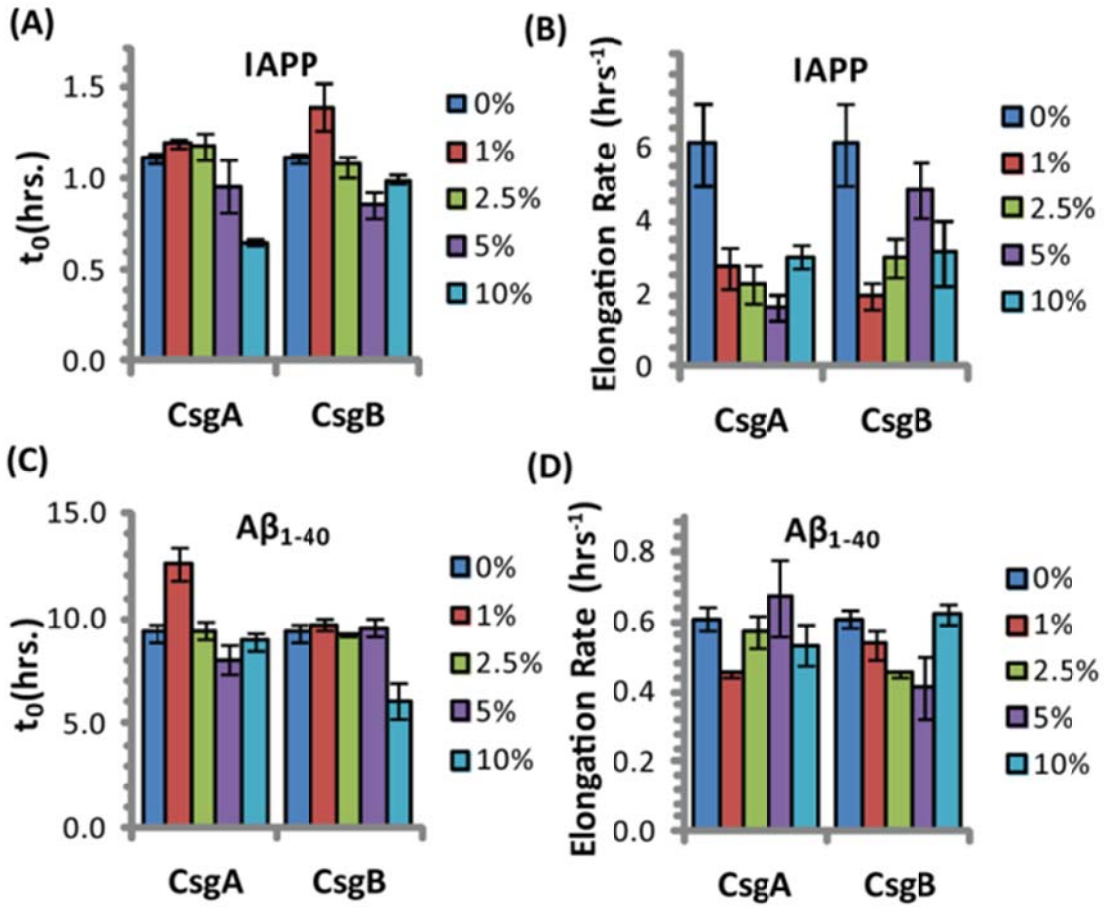

Figure 7.6 Curli's ability to influence amyloid formation is not limited to $PAP_{248-286}$. Impact of preformed csgA and csgB fibers on the lag time (A and C) and elongation time (B and D) of amyloid formation from 2.5 μM IAPP (top) and 5 μM Amyloid β_{1-40} (bottom) as molar fractions of the IAPP and Amyloid β_{1-40} concentrations.

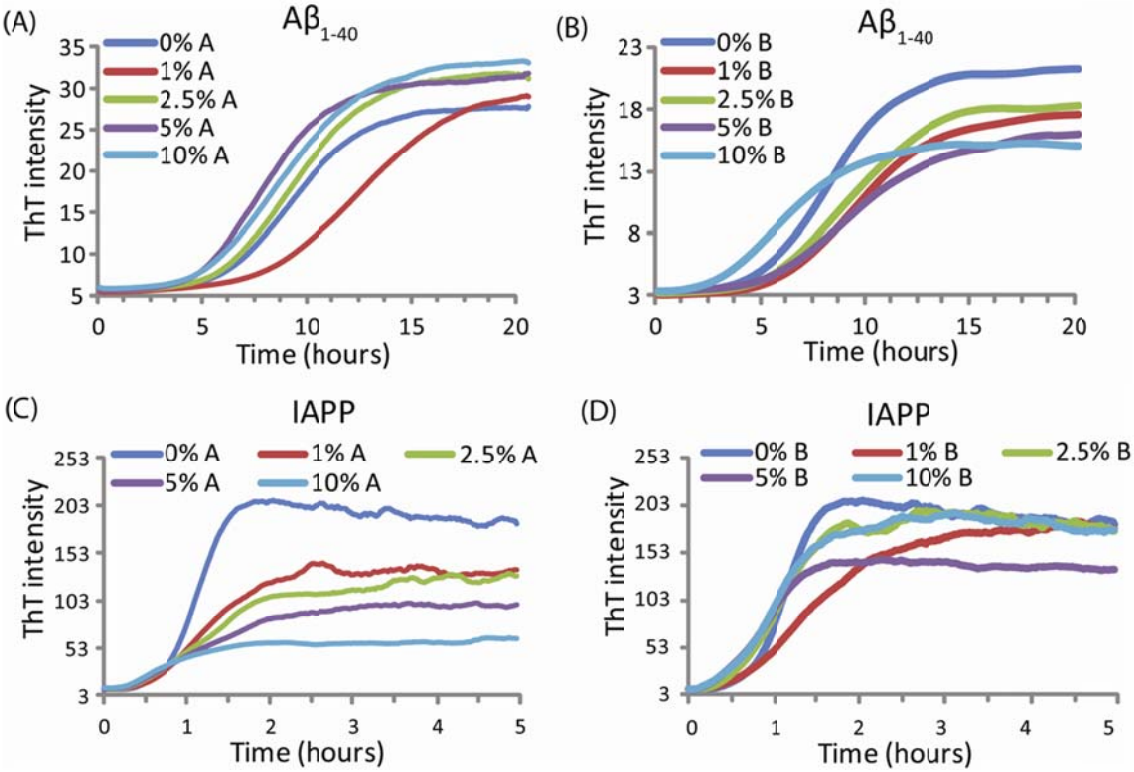

Figure 7.7. Kinetics of Amyloid $\beta_{1\text{-}40}$ and IAPP amyloid fiber formation in the presence of preformed fibers of CsgA and CsgB. ThT fluorescence measurements of Amyloid β1-40 (Top) and IAPP (Bottom) as a function of CsgA (left) and CsgB (right) seeding concentration, expressed as a mole percentage of the Amyloid $\beta_{1\text{-}40}$ and IAPP concentrations (5 μM and 2.5 μM respectively). Curves are averages for 3 measurements.

The fibrillization rate of IAPP was strongly decreased by low concentrations of both CsgA and Csg B (1% of the IAPP concentration or 25 nM) (Figure 7.6). Addition of CsgA, but not CsgB, to IAPP also lowered the total ThT fluorescence, suggesting either fewer or shorter fibers are produced in the presence of CsgA. The effect of Csg A and CsgB on the fibrillization rate of Amyloid $\beta_{1\text{-}40}$ was more modest, and showed a more complex dependence on the concentration with the fibrillization rate slightly decreasing

at lower concentrations and slightly increasing at higher concentrations of both Csg A and CsgB (Figure 7.6). The lag time of both peptides decreased by approximately 50% after addition of 10 mole % of the oppositely charged Csg protein (Csg B for IAPP and CsgA for Amyloid $\beta_{1\text{-}40}$), smaller amounts had little effect. Addition of 1% of the similarly charged Csg protein increased the lag time of both peptides, surprisingly, larger amounts had little effect on the lag time. By comparison, addition of equivalent amounts of preformed Amyloid $\beta_{1\text{-}40}$ fibril seeds led to a linear decrease in induction time but had little effect on the fibrillization rate (Figure 7.8). Although a complete characterization of Curli with IAPP and Amyloid $\beta_{1\text{-}40}$ lies outside the scope of this study, it can be seen from these experiments that both the effect of Curli nucleation on amyloid fibrillogenesis is not limited to $PAP_{248\text{-}286}$ and that Curli can serve as both an inhibitor and enhancer of fibrillization.

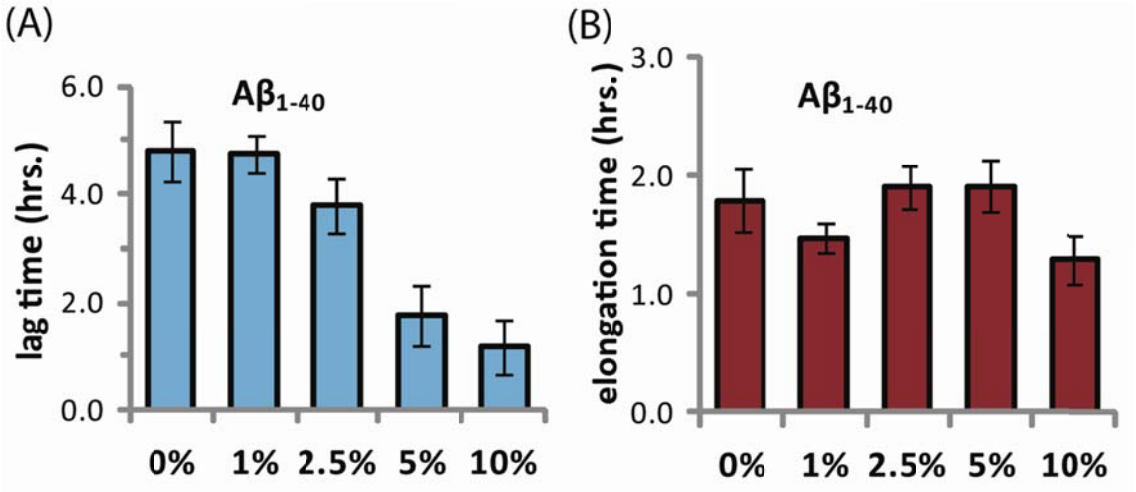

Figure 7.8. Seeding Amyloid $\beta_{1\text{-}40}$ amyloid formation with preformed Amyloid β1-40 significantly affects the lag-time but has less impact on the elongation rate. Impact of preformed Amyloid $\beta_{1\text{-}40}$ fibers on the lag time (A) and elongation time (B) of amyloid formation 5 μM Amyloid $\beta_{1\text{-}40}$ (bottom) as molar percentage of the Amyloid $\beta_{1\text{-}40}$ concentration.

7.5 Conclusions Regarding the Induction of SEVI Fibers by Bacterial Curli Protein

In this study, we characterized the kinetics of $PAP_{248-286}$ cross-seeded by the Curli proteins CsgA and CsgB in comparison to the analogous cross-seeding interactions with the more amyloidogenic proteins hIAPP and Amyloid β_{1-40}. The purpose of this experiment is two-fold. First, $PAP_{248-286}$ is only biologically active in the SEVI amyloid fiber form. The production of these fibers is ultimately controlled by the rate of amyloidogenesis, as $PAP_{248-286}$ is subject to inactivating proteolysis in its monomeric but not in its amyloid form *(4).* Since SEVI fibers have been detected in semen under conditions that would apparently not easily allow aggregation *in vitro* of SEVI alone *(1, 6),* extrinsic factors are a likely source to look for influences on $PAP_{248-286}$ aggregation. Second, amyloid cross-seeding as a general phenomenom is not well understood, as apparently contradictory results regarding the efficiency and specificity of cross-seeding have been obtained *(14-22).* In performing the cross-seeding of $PAP_{248-286}$, we found that while the lag-time for amyloid formation is moderately affected by Curli seeding the elongation rate is greatly increased.

An understanding of this result requires some knowledge of the basic mechanism of the cross-seeding reaction. In contrast to homonucleation by fibrillar seeds of the same protein, cross-seeding can occur by a variety of mechanisms. In epitaxial heteronucleation, growth occurs by specific structural matching of the seeding nucleus with the protein being seeded (Figure 7.9) *(13, 40).* A greater understanding of this process can be made by considering the structural constraints for amyloid formation. The cross β-sheet structure common to all amyloids is built by the intermolecular association of β sheets that are stabilized by hydrogen bonds between amide backbone atoms of

adjacent sheets. Since the amide backbone, in contrast to the side-chain residues, is similar in all proteins, any unfolded or partially folded protein should theoretically be able to associate with preformed seeds of another to formed mixed fibers. However, amyloid fibers apparently derive much of their energy from the formation of a "steric zipper", in which the sidechains from adjacent sheets from an interlocking dry surface *(13, 41-43).* It can be seen from this requirement that epitaxial heteronucleation is unlikely to occur if the seeding nucleus is structurally different then the protein being seeded *(13, 40, 44),* consistent with the observation that cross-seeding between amyloid proteins is most efficient when the two proteins have homologous sequences *(45).* For most amyloidogenic proteins this requirement is quite strict and even single point mutations can eliminate the ability of one amyloidogenic protein to cross-seed another. For others, the best studied being α-synuclein which seeds of a variety of non-homologous proteins, this requirement is relaxed, possibly because the disorder present in the α-synuclein's fiber structure can accommodate multiple fiber polymorphs and different fiber interfaces *(14).*

In the simplest model of epitaxially nucleated amyloidogenesis, the lag-time decreases linearly with the concentration of the seed but the elongation rate is independent of the seed concentration *(46).* Such behavior was seen with the Amyloid β_{1-40} protein (see Figure 7.8). Although the exact dependence for more complicated models varies, in general the sensitivity of the lag-time and insensitivity of the elongation rate to the seeding concentration holds for current models of epitaxially nucleated amyloidogenesis *(46).*

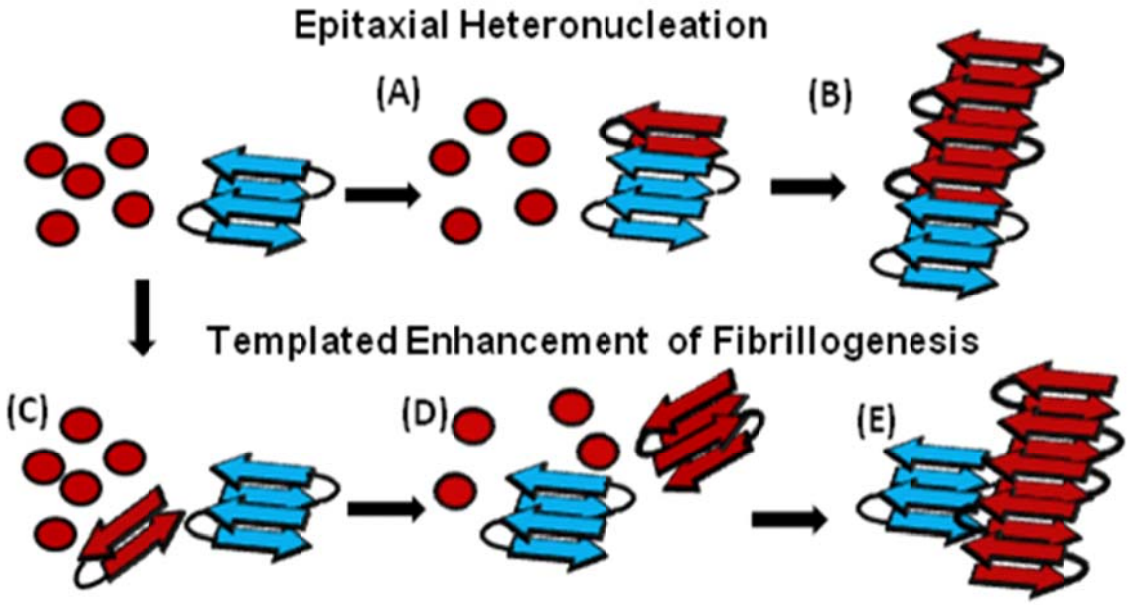

Figure 7.9 Cartoon models of possible cross-seeding reactions Top: Epitaxial Heteronucleation (A) Binding of the $PAP_{248-286}$ monomer to the Curli seed induces formation of the β-sheet conformation of $PAP_{248-286}$ (B) Fiber growth proceeds epitaxially from the seeding nucleus Bottom: Possible mechanism for non-epitaxial heteronucleation (C) A nucleus for the SEVI fiber forms independently of the Curli fiber (D) Growth of the SEVI fiber initially proceeds slowly due to unfavorable interactions between subunits of the fiber (E) Lateral attachment of the nascent SEVI fiber to Curli reduces repulsion between fiber subunits thereby enhancing the rate of fibrillogenesis. The Curli seed may be incorporated into the final SEVI fiber or may detach to catalyze further fiber extension events.

However, epitaxial heteronucleation is not the only possible mechanism by which cross-seeding can occur. In contrast to epitaxial heteronucleation, non-specific heteronucleation can affect both the lag-time and the elongation rate by affecting the stability of different species along the aggregation pathway or by lowering the surface tension associated with forming clusters of the protein. In these mechanisms, the seed is not necessarily incorporated into the new amyloid fiber. Non-specific heteronucleation

has been proposed for surfaces and non-protein ligands *(47-49)*, but not to our knowledge for cross-seeding reactions with other amyloidogenic proteins. Experiments with Lys to Ala $PAP_{248-286}$ mutants show that charge repulsion between monomer units destabilizes the amyloid fiber *(39)*. Lateral association of the Curli fiber with the nascent $PAP_{248-286}$ fiber can reduce this repulsion between monomer subunits, increasing the elongation rate but not affecting the lag-time. In this case, it is expected that the electrostatic differences between CsgA and CsgB (-6 overall charge for CsgA and +5 for CsgB, $PAP_{248-286}$ carries a charge of +6) are primarily responsible for the difference in cross-seeding efficiencies.

The interaction of Curli with IAPP and Amyloid β_{1-40} is less clear. Electrostatics plays a role in cross-seeding nucleation, as the oppositely charged Curli protein reduces the lag-time of both IAPP and Amyloid β_{1-40} but the similarly charged Curli protein has less effect. Both Csg A and Csg B decrease the elongation rate of IAPP, most likely by binding to and blocking reactive fibril ends. The effect of CsgA and CsgB on the elongation rate of Amyloid β_{1-40} displays a complex concentration dependence, likely the result of a mixture of stimulatory and inhibitory effects.

Although the effects of Curli on Amyloid β_{1-40} were moderate, cross-seeding between other bacterial functional amyloids and Amyloid β_{1-40} may have greater clinical significance. For example, the bacteria *Borrelia burgdorferi* produces a curli-like amyloid protein that colocalizes with Amyloid β amyloid deposits in Alzheimer's patients *(50, 51)*. Similarly, inoculation with *Chlamydia pneumoniae* stimulates the production of Amyloid β_{1-42} amyloid plaques *(52, 53)*, although to our knowledge a curli-like amyloid protein has not been found yet for *Chlamydia pneumonia*. Although a definitive link between bacterial infection and amyloid-associated neurodegenerative

diseases has been elusive due to the difficulties in firmly establishing bacterial infection considering the low levels of bacteria typical of chronic long-term infections *(54)*, the identification of new amyloidogenic proteins in bacteria and mammals is increasing rapidly *(24)*, opening up the possibility of an increasing role for bacterial and viral infections in poorly understood amyloidogenic diseases.

This study was supported by research funds from NIH (GM095640 to A.R., AI089282, to A.O., and AI073847 to M.R.C.). The following reagent was obtained through the AIDS Research and Reference Reagent Program, Division of AIDS, NIAID, NIH: CEM-GFP from Jacques Corbeil. Jeffery Brender helped in preparation of the manuscript. Kazuaki Monde preformed the infection assays. Nataliya Popovych expressed the CsgB protein, Margery Evans expressed the CsgA protein.

7.6 Bibliography

1. Munch, J., Rucker, E., Standker, L., Adermann, K., Goffinet, C., ., Schindler, M., Wildum, S., Chinnadurai, R., Rajan, D., Specht, A., Gimenez-Gallego, G., Sanchez, P.C., Fowler, D.M., Koulov, A., Kelly, J.W., Mothes, W., Grivel, J.C., Margolis, L., Keppler, O.T., Forssmann, W.G., Kirchhoff, F., (2007) Semen-derived amyloid fibrils drastically enhance HIV infection. *Cell 131,* 1059–1071.

2. Hong S.H., Klein E.A., Das Gupta J., Hanke K., Weight C.J., Nguyen C., Gaughan C., Kim K.A., Bannert N., Kirchhoff F., Munch, J., and Silverman, R.H., (2009) Fibrils of Prostatic Acid Phosphatase Fragments Boost Infections with XMRV (Xenotropic Murine Leukemia Virus-Related Virus), a Human Retrovirus Associated with Prostate Cancer. *Journal of Virology 83,* 6995-7003.

3. Wurm M., Schambach A., Lindemann D., Hanenberg H., Standker L., Forssmann W.G., Blasczyk R. and Horn P.A. (2010) The influence of semen-derived enhancer of virus infection on the efficiency of retroviral gene transfer. *Journal of Gene Medicine 12,* 137-146.

4. Martellini J.A., Cole A.L., Svoboda P., Stuchlik O., Chen L.M., Chai K.X., Gangrade B.K., Sorensen O.E., Pohl J. and Cole A.M. (2011) HIV-1 Enhancing Effect of Prostatic Acid Phosphatase Peptides Is Reduced in Human Seminal Plasma. *Plos One 6* e16285.

5. Ye Z.Q., French K.C., Popova L.A., Lednev I.K., Lopez M.M. and Makhatadze G.I. (2009) Mechanism of Fibril Formation by a 39-Residue Peptide (PAPf39) from Human Prostatic Acidic Phosphatase. *Biochemistry 48,* 11582-11591.

6. Kim K.A., Yolamanova M., Zirafi O., Roan N.R., Standker L., Forssmann W.G., Burgener A., Dejucq-Rainsford N., Hahn B.H., Shaw G.M., Greene, W.C., Kirchhoff, F., and Munch, J., (2010) Semen-mediated enhancement of HIV infection is donor-dependent and correlates with the levels of SEVI. *Retrovirology 7,* 55-67.

7. Olzscha H., Schermann S.M., Woerner A.C., Pinkert S., Hecht M.H., Tartaglia G.G., Vendruscolo M., Hayer-Hartl M., Hartl F.U. and Vabulas R.M. (2011) Amyloid-like Aggregates Sequester Numerous Metastable Proteins with Essential Cellular Functions. *Cell 144,* 67-78.

8. Manzoni C., Colombo L., Bigini P., Diana V., Cagnotto A., Messa M., Lupi M., Bonetto V., Pignataro M., Airoldi C., Sironi, E., Williams, A., and Salmona, M., (2011) The Molecular Assembly of Amyloid A beta Controls Its Neurotoxicity and Binding to Cellular Proteins. *PloS one 6* e24909.

9. Dzwolak W., Jansen R., Smirnovas V., Loksztejn A., Porowski S. and Winter R. (2005) Template-controlled conformational patterns of insulin fibrillar self-assembly reflect history of solvation of the amyloid nuclei. *Physical Chemistry Chemical Physics 7,* 1349-1351.

10. Foo C.K., Ohhashi Y., Kelly M.J.S., Tanaka M. and Weissman J.S. (2011) Radically Different Amyloid Conformations Dictate the Seeding Specificity of a Chimeric Sup35 Prion. *Journal of Molecular Biology 408,* 1-8.

11. Cloe A.L., Orgel J.P.R.O., Sachleben J.R., Tycko R. and Meredith S.C. (2011) The Japanese Mutant A beta (Delta E22-A beta(1-39)) Forms Fibrils Instantaneously, with Low-Thioflavin T Fluorescence: Seeding of Wild-Type A beta(1-40) into Atypical Fibrils by Delta E22-A beta(1-39). *Biochemistry 50,* 2026-2039.

12. Chien P., Weissman J.S. and DePace A.H. (2004) Emerging principles of conformation based prion inheritance. *Annual Reviews in Biochemistry 73,* 617-656.

13. Apostol M.I., Wiltzius J.J.W., Sawaya M.R., Cascio D. and Eisenberg D. (2011) Atomic Structures Suggest Determinants of Transmission Barriers in Mammalian Prion Disease. *Biochemistry 50,* 2456-2463.

14. Yagi H., Kusaka E., Hongo K., Mizobata T. and Kawata Y. (2005) Amyloid fibril formation of alpha-synuclein is accelerated by preformed amyloid seeds of other proteins - Implications for the mechanism of transmissible conformational diseases. *Journal of Biological Chemistry 280,* 38609-38616.

15. Han H.Y., Weinreb P.H. and Lansbury P.T. (1995) The Core Alzheimers Peptide Nac Forms Amyloid Fibrils Which Seed and Are Seeded by Beta-Amyloid - Is Nac a Common Trigger or Target in Neurodegenerative Disease. *Chemical Biology 2,* 163-169.

16. Westermark P., Lundmark K. and Westermark G.T. (2009) Fibrils from Designed Non-Amyloid-Related Synthetic Peptides Induce AA-Amyloidosis during Inflammation in an Animal Model. *Plos One 4* e6041.

17. Morales R., Estrada L.D., Diaz-Espinoza R., Morales-Scheihing D., Jara M.C., Castilla J. and Soto C. (2010) Molecular Cross Talk between Misfolded Proteins in Animal Models of Alzheimer's and Prion Diseases. *Journal of Neuroscience 30,* 4528-4535.

18. O'Nuallain B., Williams A.D., Westermark P. and Wetzel R. (2004) Seeding specificity in amyloid growth induced by heterologous fibrils. *Journal of Biological Chemistry 279,* 17490-17499.

19. MacPhee C.E. and Dobson C.M. (2000) Formation of mixed fibrils demonstrates the generic nature and potential utility of amyloid nanostructures. *Journal of the American Chemical Society 122,* 12707-12713.

20. Jarrett J.T. and Lansbury P.T. (1992) Amyloid Fibril Formation Requires a Chemically Discriminating Nucleation Event - Studies of an Amyloidogenic Sequence from the Bacterial Protein Osmb. *Biochemistry 31,* 12345-12352.

21. Hinz J., Gierasch L.M. and Ignatova Z. (2008) Orthogonal cross-seeding: An approach to explore protein aggregates in living cells. *Biochemistry 47,* 4196-4200.

22. Rajan R.S., Illing M.E., Bence N.F. and Kopito R.R. (2001) Specificity in intracellular protein aggregation and inclusion body formation. *Proceedings of the National Academy of Sciences 98,* 13060-13065.

23. Thurman A.R. and Doncel G.F. (2011) Innate Immunity and Inflammatory Response to Trichomonas vaginalis and Bacterial Vaginosis: Relationship to HIV Acquisition. *American Journal of Reproductive Immunology 65,* 89-98.

24. Jordal P.B., Dueholm M.S., Larsen P., Petersen S.V., Enghild J.J., Christiansen G., Hojrup P., Nielsen P.H. and Otzen D.E. (2009) Widespread Abundance of Functional Bacterial Amyloid in Mycolata and Other Gram-Positive Bacteria. *Applied and Environmental Microbiology 75,* 4101-4110.

25. Barnhart M.M. and Chapman M.R. (2006) Curli biogenesis and function. *Annual Reviews of Microbiology 60,* 131-147.

26. Cegelski L., Pinkner J.S., Hammer N.D., Cusumano C.K., Hung C.S., Chorell E., Aberg V., Walker J.N., Seed P.C., Almqvist F., Chapman, M.R., and Hultgren, S.J., (2009) Small-molecule inhibitors target Escherichia coli amyloid biogenesis and biofilm formation. *Nature chemical biology 5,* 913-919.

27. Tukel C., Wilson R.P., Nishimori J.H., Pezeshki M., Chromy B.A. and Baumler A.J. (2009) Responses to Amyloids of Microbial and Host Origin Are Mediated through Toll-like Receptor 2. *Cell Host Microbe 6,* 45-53.

28. Hammer N.D., Schmidt J.C. and Chapman M.R. (2007) The curli nucleator protein, CsgB, contains an amyloidogenic domain that directs CsgA polymerization. *Proceedings of the National Academy of Sciences 104,* 12494-12499.

29. Wang X.A., Smith D.R., Jones J.W. and Chapman M.R. (2007) In vitro polymerization of a functional Escherichia coli amyloid protein. *Journal of Biological Chemistry 282,* 3713-3719.

30. Giehm L. and Otzen D.E. (2010) Strategies to increase the reproducibility of protein fibrillization in plate reader assays. *Analytical Biochemistry 400,* 270-281.

31. Naiki H., Higuchi K., Nakakuki K. and Takeda T. (1991) Kinetic analysis of amyloid fibril polymerization in vitro. *Laboratory investigation; a journal of technical methods and pathology 65,* 104-110.

32. Gervaix A., West D., Leoni L.M., Richman D.D., WongStaal F. and Corbeil J. (1997) A new reporter cell line to monitor HIV infection and drug susceptibility in vitro. *Proceedings of the National Academy of Sciences 94,* 4653-4658.

33. Ono A., Monde K. and Chukkapalli V. (2011) Assembly and Replication of HIV-1 in T Cells with Low Levels of Phosphatidylinositol-(4,5)-Bisphosphate. *Journal of Virology 85,* 3584-3595.

34. Romling U., Bian Z., Hammar M., Sierralta W.D. and Normark S. (1998) Curli fibers are highly conserved between Salmonella typhimurium and Escherichia coli with respect to operon structure and regulation. *Journal of Bacteriology 180,* 722-731.

35. Wang X. and Chapman M.R. (2008) Curli provide the template for understanding controlled amyloid propagation. *Prion 2,* 57-60.

36. Wang X., Hammer N.D. and Chapman M.R. (2008) The molecular basis of functional bacterial amyloid polymerization and nucleation. *Journal of Biological Chemistry 283,* 21530-21539.

37. Hauber I., Hohenberg H., Holstermann B., Hunstein W. and Hauber J. (2009) The main green tea polyphenol epigallocatechin-3-gallate counteracts semen-mediated enhancement of HIV infection. *Proceedings of the National Academy of Sciences 106,* 9033-9038.

38. Roan N.R., Sowinski S., Munch J., Kirchhoff F. and Greene W.C. (2010) Aminoquinoline Surfen Inhibits the Action of SEVI (Semen-derived Enhancer of Viral Infection). *Journal of Biological Chemistry 285,* 1861-1869.

39. Roan N.R., Munch J., Arhel N., Mothes W., Neidleman J., Kobayashi A., Smith-McCune K., Kirchhoff F. and Greene W.C. (2009) The Cationic Properties of SEVI Underlie Its Ability To Enhance Human Immunodeficiency Virus Infection. *Journal of Virology 83,* 73-80.

40. Wasmer C., Zimmer A., Sabate R., Soragni A., Saupe S.J., Ritter C. and Meier B.H. (2010) Structural Similarity between the Prion Domain of HET-s and a Homologue Can Explain Amyloid Cross-Seeding in Spite of Limited Sequence Identity. *Journal of Molecular Biology 402,* 311-325.

41. Sawaya M.R., Sambashivan S., Nelson R., Ivanova M.I., Sievers S.A., Apostol M.I., Thompson M.J., Balbirnie M., Wiltzius J.J.W., McFarlane H.T., Madsen, A.O., Riekel, C., and Eisenberg, D., (2007) Atomic structures of amyloid cross-beta spines reveal varied steric zippers. *Nature 447,* 453-457.

42. Eisenberg D., Sievers S.A., Karanicolas J., Chang H.W., Zhao A., Jiang L., Zirafi O., Stevens J.T., Munch J. and Baker D. (2011) Structure-based design of non-natural amino-acid inhibitors of amyloid fibril formation. *Nature 475,* 96-U117.

43. Colletier J.P., Laganowsky A., Landau M., Zhao M.L., Soriaga A.B., Goldschmidt L., Flot D., Cascio D., Sawaya M.R. and Eisenberg D. (2011) Molecular basis for amyloid-beta polymorphism. *Proceedings of the National Academy of Sciences 108,* 16938-16943.

44. Wiltzius J.J.W., Landau M., Nelson R., Sawaya M.R., Apostol M.I., Goldschmidt L., Soriaga A.B., Cascio D., Rajashankar K. and Eisenberg D. (2009) Molecular mechanisms for protein-encoded inheritance. *Nature Structural and Molecular Biology 16,* 973-U998.

45. Krebs M.R., Morozova-Roche L.A., Daniel K., Robinson C.V. and Dobson C.M. (2004) Observation of sequence specificity in the seeding of protein amyloid fibrils. *Protein Science 13,* 1933-1938.

46. Cohen S.I.A., Vendruscolo M., Dobson C.M. and Knowles T.P.J. (2011) Nucleated Polymerisation in the Presence of Pre-Formed Seed Filaments. *International Journal of Molecular Sciences 12,* 5844-5852.

47. Pronchik J., He X.L., Giurleo J.T. and Talaga D.S. (2010) In Vitro Formation of Amyloid from alpha-Synuclein Is Dominated by Reactions at Hydrophobic Interfaces. *Journal of the American Chemical Society 132,* 9797-9803.

48. Auer S., Trovato A. and Vendruscolo M. (2009) A Condensation-Ordering Mechanism in Nanoparticle-Catalyzed Peptide Aggregation. *Plos Computational Biology 5,* e1000458.

49. Yin J., Chen R.Z. and Liu C.L. (2009) Nucleic acid induced protein aggregation and its role in biology and pathology. *Frontiers in Bioscience 14,* 5084-5106.

50. Miklossy J. (2008) Chronic inflammation and amyloidogenesis in Alzheimer's disease - Role of spirochetes. *Journal of Alzheimers Disease 13,* 381-391.

51. Miklossy J., Khalili K., Gern L., Ericson R.L., Darekar P., Bolle L., Hurlimann J. and Paster B.J. (2004) Borrelia burgdorferi persists in the brain in chronic lyme neuroborreliosis and may be associated with Alzheimer disease. *Journal of Alzheimers Disease 6,* 639-649.

52. Gerard H.C., Dreses-Werringloer U., Wildt K.S., Deka S., Oszust C., Balin B.J., Frey W.H., Bordayo E.Z., Whittum-Hudson J.A. and Hudson A.P. (2006) Chlamydophila (Chlamydia) pneumoniae in the Alzheimer's brain. *Federation of European Microbiological Societies: Immunology and Medical Microbiology 48,* 355-366.

53. Little C.S., Hammond C.J., MacIntyre A., Balin B.J. and Appelt D.M. (2004) Chlamydia pneumoniae induces Alzheimer-like amyloid plaques in brains of BALB/c mice. *Neurobiolgy of Aging 25,* 419-429.

54. Dobson C.B., Wozniak M.A. and Itzhaki R.F. (2003) Do infectious agents play a role in dementia? *Trends in Microbiology 11,* 312-317.

CHAPTER 8

CONCLUSIONS REGARDING THE MEMBRANE INTERACTIONS AND FIBRILLIZATION OF THE AMYLIN AND PAP$_{248-286}$ PEPTIDES

8.1 Amylin Conclusions

8.1.1 Summary of Studies

The diabetes related amylin peptide is one that is known to cause membrane disruption and amyloidogenic fiber growth *in vitro* as well as *in vivo* thereby progressing the development of type II diabetes *(1-3)*. The peptide however, is stored in the body in the secretory granule of the β-cells in the islets of Langerhans in the pancreas at very high concentrations (mM range), which have proved very disruptive and amyloidogenic *in vitro*. The specific conditions within the granule seem to inhibit the negative effects that the amylin peptide has on membranes, and are able to contain the peptide at high concentrations under these conditions. Specifically within the granule, there is a very low pH of ~6.0, a very high concentration of zinc (~14mM) and a concentration of insulin that is four times greater than that of the amylin peptide *(4-8)*. It is these specific conditions that were looked at separately to determine their individual effects on the membrane disruptive ability and fiber formation of the amylin peptide.

After determining that amyloidogenic fiber formation is not a requirement of the amylin peptide to display its membrane disruptive ability *(1)*, a comparison study was

done with the membrane binding region (residues 1-19) of amylin, which does not undergo fibrillization. The study looked at the membrane binding region of both the human variant of the peptide hIAPP1-19 and the rat variant of the peptide rIAPP1-19. Both the rat and human variants of the peptide share a large amount of homology, and within the membrane binding region, only differ by a single residue substitution at position 18, where the histidine present in the hIAPP is replaced with an arginine. Despite the large similarity of the peptides, the rat variant does not form fibers and is not membrane disruptive. In looking at how the membrane binding regions of the two peptides interact with model membranes and live rat islets, it was found that while the hIAPP1-19 is still membrane disruptive, its rat counterpart rIAPP1-19 was only minimally disruptive *(9)*. It was presumed that this was due to the electrostatic interactions of the peptide and the model membrane system, where the protonated arginine residue on rIAPP1-19 was unable to penetrate into the hydrophobic core of the membrane and therefore only bound to the surface of the lipids and did not induce disruption. Upon lowering the pH of the system to pH 6.0 and protonating the histidine residue of hIAPP1-19, it was seen that the two peptides then behave identically indicating that specific side chains of residue 18 are not playing as much of a role in the membrane binding region's ability to induce membrane disruption, as much as the charge distribution across the peptide *(9)*. With these findings, it was seen that the low pH of the secretory granule environment would play a role in inhibiting the membrane disruptive ability of the amylin peptide by reducing its interaction with the hydrophobic core of the lipids.

In addition to the low pH of the granule system, there is also a very high concentration of zinc at ~14mM, and is the highest concentration physiological concentration of zinc present in the body *(4, 5)*. To determine the effects this high concentration of zinc has on the amylin peptide, both the kinetics and membrane disruptive ability of the peptide was looked at in the presence of varying zinc concentrations. It was found that even small amounts of zinc would bind to the amylin peptide with a binding constant in the micromolar range *(10)*, and thereby inhibited the ability of the peptide to cause membrane disruption. Zinc is very well known to bind to histidine residues, and upon binding the amylin's His-18 residue, the overall charge distribution is then changed where the membrane binding region cannot penetrate into the lipid hydrophobic core to cause disruption of the membrane integrity. There is also a drastic effect by zinc to inhibit the formation of amyloid fibers. The presence of zinc has a threefold effect on the kinetics of fiber formation of the amylin peptide. The induction time where the nucleus forms, from which fibers elongate and grow, is reduced. However, the elongation rate (the rate at which the fibers themselves form by monomer addition to the nucleus) is also reduced. *(11).* In addition the overall quantity of fibers was also reduced. The combined effects of these kinetic data and the membrane disruption data, would indicate that the presence of zinc is stabilizing an intermediate state of the peptide which is not disruptive to membrane systems.

The last piece of data pertaining to the conditions of the secretory granule and their effect on the amylin peptide is the high concentration of insulin present in the granule. The concentration of insulin is approximately four times greater than that of amylin. In looking at how this relationship with insulin impacts amylin's membrane

disruptive and fibrillogenic abilities, it was seen that the presence of insulin will hinder the growth of amylin fibers, but also will eliminate the membrane disruption associated with fiber formation. The membrane disruptive ability of amylin is biphasic, where there is an initial disruption associated with monomer and small oligomer interaction with the membrane *(12)*, but then there is also continued disruption correlated with the formation of amyloid fibers. While the presence of insulin does not appear to inhibit the initial disruption of membranes by amylin, it hinders the growth of amyloid fibers and completely eliminates the disruption associated with their formation.

8.1.2 Implications of Studies

As was seen with these studies, the effects of low pH *(9)*, high zinc concentrations *(11)*, and high insulin concentrations *(12)*, are shown to reduce the impact of membrane disruption on model membranes by the amylin peptide as well as reduce the peptide's overall ability to undergo fibrillization. Each of these components individually are able to inhibit the negative effects of the amylin peptide, and each of these components are found within the secretory granule. It is very likely that the combination of these conditions, low pH, high zinc, and high insulin, are nessicary for the safe containment of such high concentrations of amylin within the granule. In addition, upon exocytosis of the granule to release the contents into the body, each of these components would protect the exterior membrane from damage by the amylin peptide.

During exocytosis, the protons within the granule causing the low pH would be the first to exit, and cause a pH gradient and a localized low pH to prevent the high amylin concentrations from disrupting the cellular membrane just upon exiting. The

second component that would help to inhibit the membrane disruptive ability of amylin would be the high concentration of zinc present within the granule. As with the pH, the high concentration of zinc upon exocytosis would create a localized higher concentration at the point of opening on the outer membrane. This higher concentration of zinc, already bound to the amylin peptide, would help in preventing the spontaneous formation of amyloid fibers, as well as inhibit the peptide's membrane disruptive ability. As the peptide is released, and is bound to zinc, the concentration gradient of the zinc is acting as a shield for the membranes, binding to the histidine *(10, 11)* and creating a charge distribution that would prevent the peptide from penetrating into the hydrophobic core of the membrane to induce disruption. In the outer limit of the gradient, where the zinc concentration has lowered to normal levels (~pM) and would not be sufficient to inhibit the effects that the amylin peptide has on membrane systems, the amylin peptide would also now be at sufficiently low enough concentrations to no longer be disruptive to membranes, nor to fibrillize. The final component of the granular system would be the high concentration of insulin. This high insulin concentration is stored as a protein crystal and would be the last component of the granule to leave during exocytosis. The insulin remaining behind would then be able to hinder the growth of any amylin fibers, as the pH and zinc concentrations come into equilibrium with the extracellular fluid concentrations. It is these three components of the secretory granule that are able to keep and stabilize the high concentrations of the amylin peptide, and prevent its destructive abilities. Any changes to these components could prove detrimental to the progression of type II diabetes as amylin compromises the integrity of the membranes of the insulin producing β-cells.

8.2 Future Directions of the Amylin Project

With the three components of the granule having been individually studied, it would prove very useful and more physiologically relevant to study the three components simultaneously. There is already work looking at the interaction of zinc and insulin, where it is shown that the presence of zinc stabilizes tetramers and hexamers of insulin *(13)*. However, how these interactions play a role in amylin storage and exocytosis is not known. While the role of zinc is critical inside the secretory granule, and the overall concentration is known to be ~14mM *(4, 5)* the concentration of free zinc is not known. The amount of zinc that is available to interact with the amylin peptide and hinder its membrane disruptive abilities is dependant on the amount of free zinc, as well as the zinc bound to both amylin and insulin. To determine the exact physiological relevance of these components of the granule and how they affect the amylin peptide, they must be studied together in order to determine the complicated relationship between zinc, insulin and amylin.

In addition to studying the effects of the granule components on the amylin peptide, it is also of importance to determine the effects of the granule itself on the amylin peptide. The lipid membrane of the granule and the β-cells in general are very complicated systems. *In vitro* studies have shown amylin is membrane disruptive, and while zinc, low pH and insulin are all effective at inhibiting this ability, there are also components on a cellular membrane that reduce the overall disruption caused by the amylin peptide. The membrane systems contain a number of different lipid types, as well as gangliosides, sphingomeylin, membrane proteins, cholesterol, and other components. To determine the biophysical characteristics of how these components play a role in

membrane stability would give insight to what components may be lacking, when the amylin peptide is able to disrupt cells *in vivo*.

Also, there is a great deal of interest in the curvature of the membrane system and how this affects the ability of the amylin peptide to interact. Many of the vesicles used in membrane disruption assays have greater curvature than a physiological membrane, compared to the inside of a granule which would have negative curvature. Determining both how curvature affects the interaction of amylin, and how amylin affects the curvature of a membrane would be important in determining preferential binding sites on the membrane, as well as the mechanism of how amylin is able to disrupt the membrane of vesicles and physiological cellular membranes.

8.3 $PAP_{248-286}$ Conclusions

8.3.1 Summary of the $PAP_{248-286}$ Project

With the global pandemic of AIDS spreading, indicating a very infectious disease *in vivo*, the question of why HIV is not very infectious *in vitro* is one that needs answering in order to determine the specific causes to the spread of the disease. As determined by Munch et. al. *(14)* the existence of amyloidogenic fibers of a fragment of prostatic acid phosphatase ($PAP_{248-286}$) in human semen was shown to increase the infection of HIV *in vitro* by several orders of magnitude. These amyloid fibers, SEVI (Semen-derived Enhancer of Viral Infection) which can be present at the time of HIV transmission *in vivo*, are a possible cofactor which has lead to the global spread of a virus with low infection rates. The interaction of the $PAP_{248-286}$ peptide, as well as its SEVI

fibers with membrane systems would give rise to how the peptide enhances HIV infectivity.

In dealing with the interaction of the monomeric form of $PAP_{248-286}$ in model membranes it was seen that the large distribution of highly cationic resides would most likely play a role in the peptides strong interaction with lipid systems. The primary interaction with model membrane systems is seen in the promotion of lipid aggregation. The $PAP_{248-286}$ peptide is able to facilitate the aggregation of lipids to enough of an extent that precipitation occurs. There was a large amount of indicative evidence that the $PAP_{248-286}$ peptide also promotes lipid vesicle fusion. These lipid aggregation and lipid fusion effects were studied on different lipid systems, including one comprised of a standard zwitterionic / anionic mixture, as well as model membrane systems mimicking a host cellular membrane and that of the HIV viral envelope. In all cases it seemed that the $PAP_{248-286}$ peptide as able to induce some change on the lipid system. The induction of negative curvature, aggregation of lipid vesicles, lipid diffusion, and membrane disruption are all effects which $PAP_{248-286}$ is able to induce upon lipid vesicle systems *(15)*. However, the monomer itself is not physiologically active, and is shown to not induce the enhancement of HIV transmission *(14)*. The study of the final fiber form of SEVI, and journey from monomer to fiber is important so that the enhancing effects of the SEVI amyloidogenic fiber, can themselves be inhibited.

While the $PAP_{248-286}$ monomer is able to show indications of vesicle fusion *(15)* it is not as physiologically active as the SEVI fibers, which are the conformation needed for enhanced HIV infection *(14).* As a result, finding a way to inhibit or eliminate the growth of these fibers would prove very useful as a way to prevent SEVI's enhancement effects

on HIV transmission. With the SEVI fibers being amyloidogenic in nature, a compound such as epigallocatechin gallate (EGCG) which is a know inhibitor of other amyloids *(16-19)* could prove very beneficial. It was seen that the incubation of the $PAP_{248-286}$ monomer with EGCG was able to prevent the formation of amyloidogenic SEVI fibers, both at pH 7.3 and at an acidic pH of 6.0. What was also able to be shown with the EGCG compound was its ability to disrupt the preformed SEVI amyloid fibers into smaller aggregates. The related compound GC however, was not able to break apart the existing fibers, indicating that the inhibition of amyloid fibers and the disruption of preformed amyloid fibers is specific to EGCG and not its related compounds. The EGCG was generally thought to bind to these amyloidogenic peptides by non-specific binding, however it is seen here that upon blocking the lysine residues and eliminating the positive charge distribution the EGCG is not able to bind as well to the peptide and its inhibitory effects are lessened. While the inhibition of these SEVI fibers is critical to determining how to prevent its HIV enhancing ability, what prompts the $PAP_{248-286}$ to fibrillize initially is also of importance to see how this peptide undergoes its conformational change.

It is currently unknown how the $PAP_{248-286}$ peptide fragment is cleaved from PAP, as well as what triggers the fibrillization *in vivo*. *In vitro* studies show that the $PAP_{248-286}$ fragment requires relatively harsh conditions in which to aggregate into its amyloidogenic SEVI form. High concentrations, and tremendous agitation are required for the peptide to undergo fibrillization *in vitro (14, 20-22)*. With such specific and harsh conditions required for the fibrillization of SEVI which in turn causes the enhancement of HIV infection, any additional cofactors present that could facilitate the formation of

fibers would also be indirectly facilitating the enhancement of HIV infection. In studying the formation of SEVI fibers in the presence of preformed CsgA and CsgB curlin fibers produced extracellularly by E. coli and other bacteria which would be ubiquitous at the primary site of HIV transmission, seemed to trigger the formation of SEVI fibers. This result was unusual, as amyloid peptides and proteins of very different sequence are not known to cross seed the formation of fibers *(23, 24)*. What was seen however is that the presence of either CsgA or CsgB protein fibers was able to induce the formation of SEVI fibers by primarily affecting the elongation rate of SEVI as opposed to the induction time. Physiologically the fibers produced by incubation with the CsgA or CsgB proteins were as effective, if not more so, in the enhancement effect of HIV transmission. A bacterial infection in the area of HIV transmission would produce curlin protein fibers which can induce the fiber formation of SEVI and therefore cause an increase in the infection rate of HIV. A cofactor such as SEVI could be what has turned a very poor pathogen *in vitro*, into a global pandemic.

8.3.2 Implications of the $PAP_{248-286}$ Project

With the discovery of the $PAP_{248-286}$ peptide and its HIV transmission enhancement effects only recently *(14)*, there is still a great deal to study about this peptide in general, as well as its interaction with membrane systems to determine how this enhancement occurs, and what would be required to eliminate it. The peptides overall cationic charge distribution seems to play a key role in both binding to the EGCG inhibitory compound, as well as being the mechanism for interaction with membrane systems. The charge distribution of both the $PAP_{248-286}$ peptide and the SEVI fibers are

able to bring the membranes of host and virus together in order to work synergistically with the GP41 fusion protein on HIV in order to increase the efficiency of infection.

Determining how the $PAP_{248-286}$ monomer aggregates into SEVI fibers, would be effective to develop a way to inhibit this, and indirectly inhibit its HIV transmission enhancing ability. The hydrophobic and electrostatic interactions in the formation of SEVI and other amyloid fibers are able to be utilized to change the kinetics of fiber formation. Slight modifications, either the addition of charge, or the modification of the peptide to increase hydrophobic regions, can either inhibit, or enhance the formation of amyloid fiber. In using the CsgA and CsgB protein fibers, there are some electrostatic interactions with the formation of the SEVI fibers, however their overall hydrophobic interactions seem to be much more effective at accelerating the formation of amyloid fibers. Inhibition of fiber formation by binding and blocking addition of monomer subunits by EGCG or other compounds can prove very useful not only in the elimination of SEVI fiber formation, but also in the disaggregation of preformed fibers. It is only in studying the kinetics of the formation of these HIV enhancing fibers, where potentially useful inhibitors can be developed to eliminate SEVI fiber formation, and decrease the spread of the global AIDS pandemic.

8.4 Future Directions of the $PAP_{248-286}$ Project

There is still a great deal of research to be done in regards to the $PAP_{248-286}$ peptide and the resulting SEVI fibers. The SEVI fibers facilitate the fusion of host and virus membrane, and is only active in its fiber form. The two areas of focus would therefore be on the formation of these fibers, and the interaction of the peptide with

membrane systems. In focusing on the formation of the SEVI fibers, current research is observing the interaction with metal ions, in particular zinc. Zinc is present at relatively high concentrations in human semen (~2mM) *(25)*, where the $PAP_{248-286}$ peptide is found. Metals have been shown in a number of instances to affect the kinetics of fiber formation of amyloid peptides *(26, 27)*, by both inhibiting and initiating the growth of amyloid fibers. Given how metals can affect amyloid fibers, and the high zinc concentration found in human semen, it would be beneficial to determine its effects on SEVI fiber formation, as well as other metal ions which could be used as possible inhibitors of SEVI fiber growth.

In addition to studying the formation of the SEVI fibers, and their fibrillization kinetics, it would also be very beneficial to study the interaction of the fiber and monomeric peptide with membrane systems. Preliminary results show that the $PAP_{248-286}$ peptide induces lipid aggregation and fusion *(15)*. This was done by determining the amount of lipid exchange between model membrane vesicles and while this does indicate membrane fusion, the mixing of the vesicle contents required for virus infection was not determined. A content mixing assay to much more quantitatively determine the amount of content mixing and vesicle fusion of both the $PAP_{248-286}$ monomer and the SEVI fibers on different vesicles would give further insight into how the enhancement of HIV infection takes place. In using monomeric and fiber forms of the peptide, as well as membrane types mimicking host cell and viral envelope membrane systems, the fusiogenic effect can be determined on much more physiological systems. In addition, use of the GP41 fusion peptide located on the membrane of the HIV viral envelope would

serve as a control of fusion, as well as the possibility of a synergistic effect between it and the $PAP_{248-286}$ or SEVI fibers.

1.5 Bibliography

1. Brender, J.R., Lee, E.L., Cavitt, M.A., Gafni, A., Steel, D.G., and Ramamoorthy, A. (2008) Amyloid fiber formation and membrane disruption are separate processes localized in two distinct regions of IAPP, the type-2-diabetes-related peptide. *Journal of the American Chemical Society 130*, 6424-6429.

2. Janson, J., Ashley, R.H., Harrison, D., McIntyre, S., and Butler, P.C., (1999) The mechanism of islet amyloid polypeptide toxicity is membrane disruption by intermediate-sized toxic amyloid particles. *Diabetes 48,* 491–498.

3. Anguiano, M., Nowak, R.J., and Lansbury Jr. P.T., (2002) Protofibrillar islet amyloid polypeptide permeabilizes synthetic vesicles by a pore-like mechanism that may be relevant to type II diabetes. *Biochemistry 41,* 11338–11343.

4. Foster, M.C., Leapman, R.D., Li, M.X., and Atwater, I. (1993) Elemental composition of secretory granules in pancreatic islets of Langerhans. *Biophysical Journal 64*, 525–532.

5. Taylor, C.G. (2005) Zinc, the pancreas, and diabetes: insights from rodent studies and future directions. *BioMetals 18*, 305–312.

6. Wei, L., Jiang, P., Yau, Y.H., Summer, H., Shochat, S.G., Mu, Y., and K. Pervushin. (2009) Residual structure in islet amyloid polypeptide mediates its interactions with soluble insulin. *Biochemistry 48,* 2368–2376.

7. Larson, J.L., and Miranker A.D., (2004) The mechanism of insulin action on islet amyloid polypeptide fiber formation. *Journal of Molecular Biology 335,* 221–231.

8. Jaikaran, E.T., Nilsson, M.R., and Clark, A., (2004) Pancreatic β-cell granule peptides form heteromolecular complexes which inhibit islet amyloid polypeptide fibril formation. *Biochemical Journal 377,* 709–716.

9. Brender, J.R., Hartman, K., Reid, K.R., Kennedy, R.T., and Ramamoorthy, A., (2008) A Single Mutation in the Nonamyloidogenic Region of Islet Amyloid Polypeptide Greatly Reduces Toxicity. *Biochemistry 47*, 12680-12688.

10. Salamekh, S., Brender, J.R., Hyung, S., Nanga, R.P., Vivekanandan, S., Ruotolo, B.T., and Ramamoorthy, A., (2011) A Two-Site Mechanism for the Inhibition of IAPP Amyloidogenesis by Zinc. *Journal of Molecular Biology 410,* 294-306.

11. Brender, J.R., Hartman, K., Nanga, R.P., Popovych, N., Salud Bea, R., Vivekanandan, S., Marsh, E.N., and Ramamoorthy, A., (2010) Role of Zinc in

Human Islet Amyloid Polypeptide Aggregation. *Journal of the American Chemical Society 132,* 8973-8983.

12. Brender, J.R., Lee, E.L., Hartman, K., Wong, P.T., Ramamoorthy, A., Steel, D.G., and Gafni, A., (2011) Biphasic Effects of Insulin on Islet Amyloid Polypeptide Membrane Disruption. *Biophysical Journal 100,* 685-692.

13. Lemaire, K., Ravier, M.A., Schraenen, A., Creemers, J.W., Van de Plas, R., Granvik, M., Van Lommel, L., Waelkens, E., Chimienti, F., Rutter, G.A., Gilon, P., in't Veld, P.A., and Schuit, F.C (2009) Insulin crystallization depends on zinc transporter ZnT8 expression, but is not required for normal glucose homeostasis in mice. *Proceedings of the National Academy of Science 106*, 14872–14877.

14. Munch, J., Rucker, E., Standker, L., Adermann, K., Goffinet, C., Schindler, M., Wildum, S., Chinnadurai, R., Rajan, D., Specht, A., Gimenez-Gallego, G., Sanchez, P.C., Fowler, D.M., Koulov, A., Kelly, J. W., Mothes, W., Grivel, J.C., Margolis, L., Keppler, O.T., Forssmann, W.G., and Kirchhoff, F. (2007) Semen-derived amyloid fibrils drastically enhance HIV infection. *Cell 131*, 1059-1071.

15. Brender, J.R., Hartman, K., Gottler, L.M., Cavitt, M.E., Youngstrom, D.W., and Ramamoorthy, A., (2009) Helical Conformation of the SEVI Precursor Peptide PAP248-286, a Dramatic Enhancer of HIV Infectivity, Promotes Lipid Aggregation and Fusion. *Biophysical Journal 97,* 2474-2483.

16. Hauber, I., Hohenberg, H., Holstermann, B., Hunstein, W. and Hauber, J. (2009). The main green tea polyphenol epigallocatechin-3-gallate counteracts semen-mediated enhancement of HIV infection. *Proceedings of the National Academy of Science 106,* 9033-9038.

17. Porat, Y., Abramowitz, A. and Gazit, E. (2006). Inhibition of amyloid fibril formation by polyphenols: Structural similarity and aromatic interactions as a common inhibition mechanism. *Chemical Biology and Drug Design 67*, 27-37.

18. Ehrnhoefer, D. E., Bieschke, J., Boeddrich, A., Herbst, M., Masino, L., Lurz, R., Engemann, S., Pastore, A. & Wanker, E. E. (2008). EGCG redirects amyloidogenic polypeptides into unstructured, off-pathway oligomers. *Nat. Struct. Mol. Biol. 15,* 558-566.

19. Bieschke, J., Russ, J., Friedrich, R.P., Ehrnhoefer, D.E., Wobst, H., Neugebauer, K. and Wanker, E.E. (2010). EGCG remodels mature alpha-synuclein and amyloid-beta fibrils and reduces cellular toxicity. *Proceedings of the National Academy of Science 107*, 7710-7715.

20. Roan, N.R., Munch, J., Arhel, N., Mothes, W., Neidleman, J., Kobayashi, A., Smith-McCune, K., Kirchhoff, F. and Greene, W. C. (2009). The cationic properties of SEVI underlie its ability to enhance human immunodeficiency virus infection. *Journal of Virology 83,* 73-80.

21. Kim, K.A., Yolamanova, M., Zirafi, O., Roan, N.R., Staendker, L., Forssmann, W.G., Burgener, A., Dejucq-Rainsford, N., Hahn, B.H., Shaw, G.M., Greene, W.C., Kirchhoff, F. and Munch, J. (2010). Semen-mediated enhancement of HIV infection is donor-dependent and correlates with the levels of SEVI. *Retrovirology 7*, 55-67.

22. Wurm, M., Schambach, A., Lindemann, D., Hanenberg, H., Standker, L., Forssmann, W.G., Blasczyk, R. and Horn, P.A. (2010). The influence of semen-derived enhancer of virus infection on the efficiency of retroviral gene transfer. *Journal of Gene Medicine 12*, 137-146.

23. Chien P., Weissman J.S. and DePace A.H. (2004) Emerging principles of conformation based prion inheritance. *Annual Reviews in Biochemistry 73,* 617-656.

24. Apostol M.I., Wiltzius J.J.W., Sawaya M.R., Cascio D. and Eisenberg D. (2011) Atomic Structures Suggest Determinants of Transmission Barriers in Mammalian Prion Disease. *Biochemistry 50,* 2456-2463.

25. Sorensen, M.B., Bergdahl, I.A., Hjollund, N.H., Bonde, J.P., Stoltenberg, M., and Ernst, E., (1999) Zinc, magnesium and calcium in human seminal fluid: relations to other semen parameters and fertility, *Molecular Human Reproduction 5,* 331-337.

26. Eakin, C.M., Knight, J.D., Morgan, C.J., Gelfand, M.A., and Miranker, A.D. (2002) Formation of a copper specific binding site in non-native states of beta-2-microglobulin. *Biochemistry 41*, 10646–10656.

27. Talmard, C., Yona, R.L., and Faller, P. (2009) Mechanism of zinc (II) promoted amyloid formation: zinc (II) binding facilitates the transition from the partially alpha helical conformer to aggregates of amyloid beta protein(1-28). *Journal of Biological Inorganic Chemistry 14*, 449–455.